UNIVERSITY OF SOUTHAMPTON

FACULTY OF ENGINEERING, SCIENCE AND MATHEMATICS

School of Electronics and Computer Science

Minimum Bit Error Rate Multiuser Detection for Multiple Antenna Aided Uplink OFDM

by

Mohamad Yusoff Alias

BEngSc

A doctoral thesis submitted in partial fulfilment of the requirements for the award of Doctor of Philosophy at the University of Southampton

September 2004

SUPERVISORS:

Professor Lajos Hanzo

Dip Ing, MSc, PhD, DSc, FIEEE

Chair of Telecommunications

School of Electronics and Computer Science

University of Southampton

Southampton SO17 1BJ

United Kingdom

Dr. Sheng Chen

BEng, MSc, PhD, SMIEEE

Reader

School of Electronics and Computer Science

University of Southampton

Southampton SO17 1BJ

United Kingdom

UNIVERSITY OF SOUTHAMPTON

ABSTRACT

Faculty of Engineering, Science and Mathematics

School of Electronics and Computer Science

Doctor of Philosophy

Minimum Bit Error Rate Multiuser Detection for Multiple Antenna Aided Uplink OFDM

by Mohamad Yusoff Alias

In this treatise, we employed the so-called Space Division Multiple Access (SDMA) principle in the context of Orthogonal Frequency Division Multiplexing (OFDM) for multiuser transmission by exploiting the system's capability of differentiating multiple users by their unique, user-specific spatial signatures constituted by their different impulse responses between the different transmit and receiver antennas. The classic method of detecting the different users is by using the well-known Minimum Mean Squared Error (MMSE) linear multiuser detector (MUD). However, the MMSE MUD family does not necessarily minimise the achievable Bit Error Rate (BER) of a system, although achieving the minimum BER is our ultimate aim. Therefore, we propose a novel Minimum Bit Error Rate (MBER) type MUD that is capable of directly minimising the BER cost function of a given system. We have demonstrated that the MBER MUD performs better than the MMSE MUD in the scenarios investigated. In the case of the MMSE MUD, different users will achieve a different BER performance and as the amount of multiuser interference increases, the MMSE MUD performs more poorly in distinguishing the different users. This is due to the fact that the performance of the MMSE MUD relies on the system matrix constituted by the different users' channel transfer functions in determining the detected user's BER performance. By contrast, all users employing the MBER MUD experience a fairly similar BER. Moreover, we showed that the MBER MUD is capable of supporting more users than the number of receiver antennas, because it will aim for finding the minimum point on the BER cost function, regardless of the system matrix. We have also employed the Genetic Algorithm (GA) search method in solving for the weight values of the MBER MUD, as an alternative to the normal conjugate gradient search method. In the case where the channel is unknown, adaptive MBER methods can be used to search for the weight values of the MBER MUD.

Acknowledgement

First and foremost, I would like to extend my greatest gratitude toward my supervisor, Professor Lajos Hanzo, for accepting me as one of his students. I am really grateful for his financial assistance, but most of all for his patience, guidance and motivation throughout my PhD years. I would also like to thank my second supervisor, Dr. Sheng Chen for his ideas and insightful thoughts. Many thanks also to Dr. Stephan Weiss for his suggestions on the improvement of the report.

I would also like to extend my appreciation to Majlis Amanah Rakyat (MARA) of the Malaysian Government for their financial support, and to Multimedia University of Malaysia for approving my study leave in order for me to pursue for this degree.

I also wish to express my sincere gratitude to Dennis Harvey and Rebecca Earl for their assistance in the administrative work. Many thanks also to Dr. Bee Leong Yeap and Dr. Soon Xi Ng for their help with the computer system, Dr. Ahmad Kamsani Samingan, Nurul Nadia Ahmad and Andreas Wolfgang for the insightful discussions on MBER, Jos Akhtman for introducing IT++, Feng Guo for the LDPC assistance, Dr. Jin Yee Chung for the collaborations on video coding, Dr. Thong Hoi Liew for sharing the information on STBC, and Dr. Byoung Jo Choi for the inspiration on multiuser detection. I would also like to say thank you to the rest of all the past and present colleagues at the Communication Research Group, too numerous to mention here, for their wonderful friendship.

Special thanks goes to Dr. Hafizal Mohamad and his family for their assistance during my PhD infancy stages here. I would also like to thank Dr. Fazly Salleh Abas, Mohd. Ridzuan Mokhtar, Dr. Mohammad Faizal Ahmad Fauzi and Zulfadzli Yusoff for being able to withstand my 'grouchiness', and for being such outstanding housemates for the three long years under the same roof. To the rest of the Malaysian and Singaporean community in Southampton, thank you for making it feel like home.

Not forgetting my family members and close friends in Malaysia, who have always been supportive throughout the tough years, especially my beloved parents who have brought me up with their unconditional love, and for being understanding with all the decisions that I have made. Last but not least, I would like to thank God for giving me the strength to endure this challenging four years of my life.

List of Publications

1. M. Y. Alias, F. Guo, S. X. Ng, T. H. Liew and Lajos Hanzo, "LDPC and Turbo Coding Assisted Space-Time Block Coded OFDM," *in Proceedings of the IEEE Vehicular Technology Conference (VTC Spring)*, vol. 4, (Jeju, Korea), pp. 2309–2313, 22-25 April 2003.

2. J. Y. Chung, M. Y. Alias, F. Guo and L. Hanzo, "LDPC and Turbo Coding Assisted Space-Time Block Coded OFDM for H.26L Coded Wireless Video Telephony," *Proceedings of the 14th IEEE International Symposium on Personal, Indoor and Mobile Radio Communications (PIMRC)*, (Beijing, China), pp. 2702–2706, 7-10 September 2003.

3. M. Y. Alias, A. K. Samingan, S. Chen and L. Hanzo, "Minimum Bit Error Rate Multiuser Detection in Multiple Antenna Aided OFDM," *8th International OFDM-Workshop*, (Hamburg, Germany) pp. 16–20, 24-25 September 2003.

4. M. Y. Alias, A. K. Samingan, S. Chen and L. Hanzo, "Multiple Antenna Aided OFDM Employing Minimum Bit Error Rate Multiuser Detection," *The IEE Electronics Letters*, vol. 39, no. 24, pp. 1769–1770, 27 November 2003.

5. M. Y. Alias, S. Chen and L. Hanzo, "Genetic Algorithm Assisted Minimum Bit Error Rate Multiuser Detection in Multiple Antenna Aided OFDM," *Accepted for publication for the IEEE Vehicular Technology Conference (VTC Fall)*, (Los Angeles, USA), 26-29 September 2004.

6. M. Y. Alias, S. Chen and L. Hanzo, "Multiple Antenna Aided OFDM Employing Genetic Algorithm Assisted Minimum Bit Error Rate Multiuser Detection," *Submitted for publication to the IEEE Transactions on Vehicular Technology.*

Contents

Abstract ii

Acknowledgement iv

List of Publications v

Preface 1

1 OFDM Overview 3

1.1 Historical background 4

1.2 Basic OFDM system 6

1.2.1 OFDM concepts 6

1.2.2 OFDM transmission over Gaussian channels 10

1.2.3 Wideband channel models 11

1.2.3.1 Two-path Rayleigh fading channel 11

1.2.3.2 Wireless asynchronous transfer mode channel 12

1.2.4 Channel transfer function estimation 14

1.2.4.1 Perfect channel estimation 16

1.2.4.2 Pilot symbol assisted channel estimation 17

1.2.4.2.1 Linear interpolation for PSAM 17

1.2.4.2.2 Lowpass interpolation for PSAM 19

1.2.4.3 Decision-directed channel estimation 21
1.2.4.4 Blind channel estimation 21
1.2.5 OFDM signal amplitude statistics 24
1.2.5.1 Clipping amplifier performance 27
1.2.5.2 BER performance using clipping amplifiers 27
1.3 Advanced OFDM systems 28
1.3.1 Adaptive single-user OFDM techniques 29
1.3.1.1 Fixed threshold adaptation algorithm 30
1.3.1.2 Subband-BER estimator based adaptation algorithm . . . 32
1.3.1.3 Constant-throughput adaptive OFDM 33
1.3.2 Forward error correction coding 34
1.3.2.1 Turbo convolutional codes 34
1.3.2.2 Low-density parity-check codes 36
1.3.3 Space-time block coded OFDM 37
1.3.3.1 Introduction to STBC OFDM 38
1.3.3.2 LDPC-based space-time coded OFDM 42
1.3.3.2.1 Effects of various coding rates 43
1.3.3.2.2 Effects of the code length 47
1.3.3.2.3 Effects of the number of iterations 48
1.3.3.3 Decoding complexity 49
1.4 Chapter conclusion 51

2 Minimum Bit Error Rate Multiuser Detection in Space Division Multiple Access Aided OFDM Systems 54

2.1 Introduction to smart antennas 55
2.2 Space division multiple access 57

2.2.1 SDMA system model 57
2.2.2 Comparison between SDMA and CDMA 60
2.3 Linear multiuser detection techniques for SDMA 60
2.3.1 Minimum mean-square error multiuser detector 63
2.3.2 Soft-output generation for channel decoding 65
2.4 Minimum bit error rate multiuser detector 66
2.4.1 Error probability in BPSK system 67
2.4.2 Exact MBER multiuser detection 69
2.4.3 Simulation results 73
2.4.3.1 Employing two receiver antennas 76
2.4.3.2 Employing four receiver antennas 79
2.4.3.3 Employing eight receiver antennas 93
2.4.3.4 Effects of different number of receiver antennas 93
2.4.4 Effects of varying the CG algorithm parameters 94
2.4.4.1 Step size, μ 95
2.4.4.2 Maximum iterations 96
2.4.4.3 Termination scalar, β 97
2.4.5 LDPC coded MBER multiuser detector 98
2.5 Chapter conclusion 99

3 Genetic Algorithm Assisted MBER MUD 102

3.1 A brief overview of GA 103
3.1.1 GA basics 103
3.1.2 GA operating principles 105
3.1.3 Difference of GA-aided and traditional optimisation methods 106
3.2 GA-aided MBER MUD 108

3.3 Simulation results 109
3.3.1 BER performance for the different users 109
3.3.2 Effects of varying the GA's parameters 112
3.3.2.1 Termination criterion 112
3.3.2.1.1 Termination after a fixed number of generations . 112
3.3.2.1.2 Termination based on quality of convergence . . . 114
3.3.2.1.3 Termination based upon the population's average variance 116
3.3.2.2 Representation of the MUD weights 116
3.3.2.2.1 Binary encoding 117
3.3.2.2.2 Gray encoding 118
3.3.2.3 The effects of the population size 119
3.3.2.4 The effects of different crossovers 120
3.3.2.4.1 Single-point crossover 121
3.3.2.4.2 Two-point crossover 122
3.3.2.4.3 Uniform crossover 122
3.3.2.5 The effects of the mutation probability 123
3.4 Complexity comparisons 125
3.5 Overloaded scenario 126
3.6 Conclusion 127

4 Adaptive MBER MUD **130**

4.1 Introduction 130
4.1.1 Estimated BER for BPSK 131
4.2 Block adaptive MBER algorithm 133
4.2.1 Block adaptive conjugate gradient MBER algorithm 133

4.2.1.1 The effects of varying the step-size 136
4.2.1.2 The effects of varying the kernel-width 138
4.2.1.3 The effects of varying the training block size 140
4.3 Stochastic adaptive MBER algorithm 142
4.3.1 The least bit error rate algorithm 143
4.3.1.1 The effects of varying the step-size 145
4.3.1.2 The effects of varying the kernel-width 147
4.4 GA assisted block adaptive MBER algorithm 147
4.4.1 GA-aided block adaptive implementation 149
4.4.2 Simulation results 150
4.4.2.1 The effects of varying the kernel-width 151
4.4.2.2 The effects of varying the training block size 151
4.5 Chapter conclusion 154

5 Conclusions and Future Research 156

5.1 Summary and conclusion 156
5.2 Suggestions for future research 162
5.2.1 Advanced research on MBER MUD 162
5.2.1.1 Joint channel estimation and multiuser detection employing the MBER criterion 163
5.2.1.2 Iterative LDPC-coded MBER MUD 164
5.2.2 Other MIMO-OFDM systems 165
5.2.2.1 Layered space-time OFDM 165
5.2.2.2 Adaptive beamforming OFDM 167

List of Symbols 169

Glossary **176**

Bibliography **180**

Index **208**

Author Index **211**

Preface

Organisation of the thesis

The layout of this thesis is as follows:

Chapter 1: A brief overview of the underlying orthogonal frequency division multiplexing (OFDM) principles will be presented, complemented by a study of single-user space-time block coded (STBC) OFDM, employing a low-density parity check (LDPC) channel codec as well as turbo codec.

Chapter 2: We will propose the novel minimum bit error rate (MBER)[1] criterion based multiuser detector (MUD) designed for a space division multiple access (SDMA) aided multiuser OFDM system. Firstly, we will describe the SDMA OFDM system and the MBER MUD, which will be characterised with the aid of our simulation results. We will demonstrate that the proposed MBER MUD is capable of achieving a lower BER in comparison to the classic minimum mean-square error (MMSE) MUD in almost all the scenarios investigated. Unlike the MMSE MUD, the MBER MUD is capable of supporting more users than the number of receiver antennas employed at the base station.

Chapter 3: The objective of this chapter is that of implementing a genetic algorithm (GA)-aided exact MBER MUD as a design-alternative to the conjugate gradient method introduced in Chapter 3. The GA-aided search method is shown to require a lower number of iterations compared to the CG method for reaching the MBER solution. We will also study the effects of the different GA parameters.

[1]The MBER MUD explained in this treatise was originally developed by S. Chen for the BPSK signalling, and then further enhanced for the CDMA multiuser case by A. K. Samingan

Chapter 4: This chapter is dedicated to the investigation of some of the well-known adaptive search methods invoked in the context of the MBER MUD, namely the block adaptive conjugate gradient (BACG) algorithm and the least bit error rate (LBER) method. Additionally, we will also introduce a GA-aided block adaptive method.

Chapter 5: Finally, in this chapter we will summarise the findings of the thesis and present our conclusions in this chapter. We will also provide suggestions for future work.

Contributions of this work

Below, we present the novel contributions of this thesis:

- An MBER multiuser detector was designed for the uplink of a multiuser OFDM SDMA system, which is capable of supporting more users than both the number of receiver antennas and the classical MMSE MUD [1, 2].
- Employing the GA-aided search method as an alternative to the conjugate gradient method for the exact MBER MUD required a lower number of iterations than the conjugate gradient algorithm [3].
- Adaptive MBER MUDs, namely the block adaptive conjugate gradient (BACG) and the least bit error rate (LBER) adaptive MBER SDMA MUDs were contrived and studied.
- The GA-based search method was also used for assisting the block adaptive MBER MUD's operation.

Chapter 1

OFDM Overview

Over the past decade, the popularity of mobile communications has been increasing right across the globe. Researchers have now turned their attention to the next generation of wireless broadband multimedia communications systems. The voice-related teletraffic has now reached saturation, but there is a growing demand for wireless Internet type services. While the family of the aforementioned communications systems was primarily designed for voice communications, there is a growing demand for multimedia services requiring high information rates exceeding 2 Mbps. Supporting such high data rates at a sufficiently high robustness against radio channel impairments requires careful system optimisation. Orthogonal frequency division multiplexing (OFDM) [4–6] has emerged as a promising choice of modulation for numerous applications, exhibiting the following key advantages [6]:

- OFDM constitutes an efficient technique of mitigating the effects of multipath propagation; for a given delay spread, its implementation complexity is significantly lower than that of a single-carrier system using a channel equaliser.
- In relatively slowly-varying channels it is possible to significantly enhance the achievable capacity by adapting the data rate per subcarrier according to the signal-to-noise ratio (SNR) experienced by that particular subcarrier.
- OFDM is capable of tolerating a lower Nyquist excess bandwidth than typical single-carrier systems.

- When combined with Walsh-Hadamard code based frequency-domain and/or time-domain spreading, OFDM retains all the flexibility and robustness benefits of MC-CDMA.

On the other hand, OFDM also has some drawbacks compared to single-carrier modulation:

- OFDM is more sensitive to frequency offset and phase noise.
- OFDM has a relatively high peak-to-average power ratio, which tends to reduce the power efficiency of the RF amplifier used.

Section 1.1 will provide a brief overview of OFDM history. In Section 1.2, a basic OFDM system is presented, while Section 1.3 describes a range of more advanced OFDM systems. Finally, we conclude the chapter in Section 1.4. For details of the basic principles of OFDM systems, the readers might like to refer to Hanzo *et al.* [4,5], or Prasad and van Nee [6].

1.1 Historical background

The concept of using parallel data transmission and frequency division multiplexing was proposed as early as the mid-1960s [7–9], while a US patent was issued in January, 1970 [10]. In a classic parallel data system, the signal frequency band is divided into K non-overlapping frequency-domain subchannels. Each subchannel's carrier is modulated by a separate symbol and then the K subchannels are frequency-multiplexed. Inter-subcarrier interference is avoided with the aid of sinc-shaped frequency-domain pulses, having equidistant zero-crossing at all but one subcarrier.

In 1971, Weinstein and Ebert applied the Discrete Fourier Transform (DFT) [11] for the efficient implementation of the modulation and demodulation process. More explicitly, instead of carrying out the modulation and Nyquist filtering of all subchannels individually, as it was proposed by Hirosaki in 1980s [22, 23], all subcarriers are modulated in a single step by the DFT, which uses a set of harmonically related complex-valued exponential subcarrier functions [4,5]. Hence, by using the DFT, the transmitted data of all subchannels can be recovered without any crosstalk. Additionally, using the DFT-based multicarrier

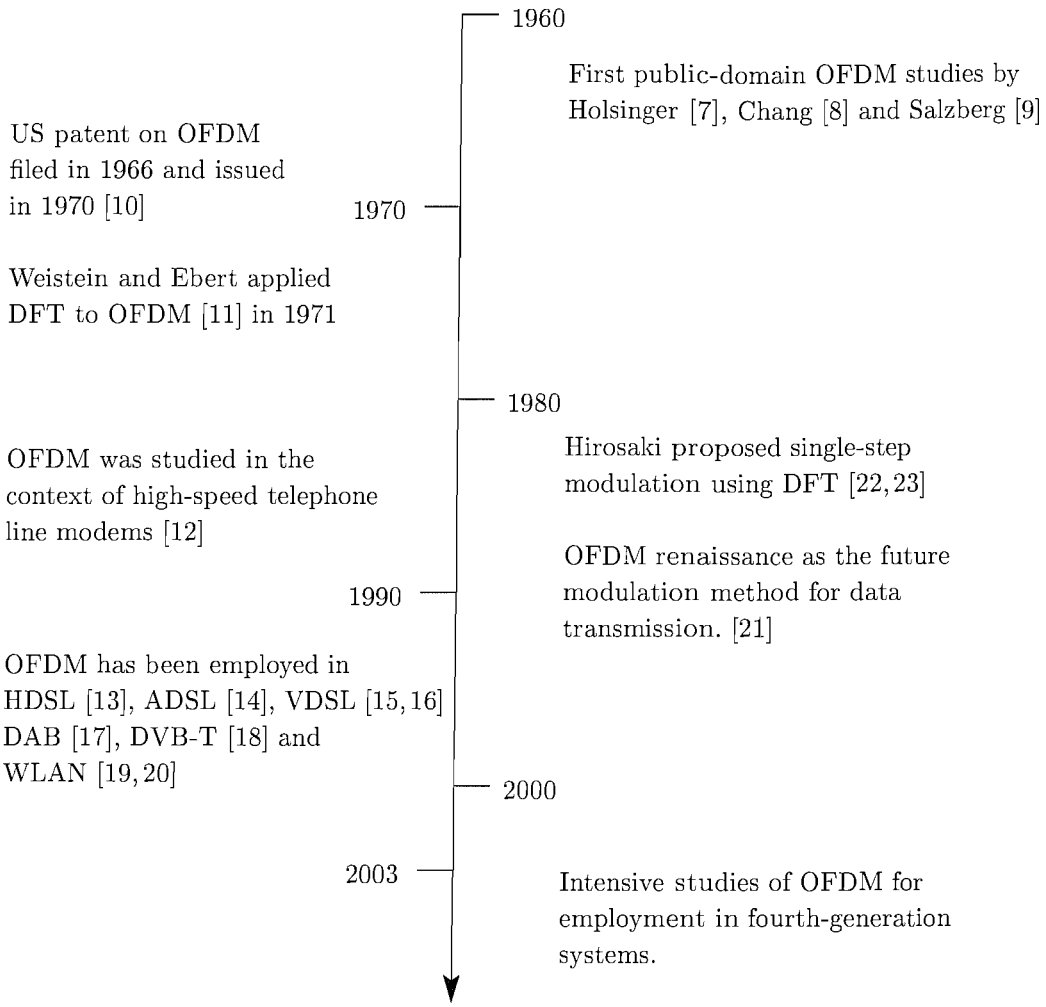

Figure 1.1: Important events in the history of OFDM.

modulation technique, frequency division multiplexing is achieved without invoking a bank of bandpass filters. A more efficient implementation of the DFT is based on the Fast Fourier Transform (FFT), when the number of subcarriers is high. With the recent advances in very-large scale integration (VLSI) technology, high-speed FFT chips are readily available and commercially affordable.

In the 1960s, the OFDM technique was used in several high-frequency military systems. In the 1980s, OFDM was studied in the context of high-speed telephone-line modems [12] and digital mobile communications [21]. In the 1990s, OFDM was invoked for high-bit-rate digital subscriber lines (HDSL) [13], asymmetric digital subscriber lines (ADSL) [14], very-high-speed digital subscriber lines (VDSL) [15, 16], digital audio broadcasting (DAB) [17], and high-definition television (HDTV) [18] terrestrial broadcasting [24, 25]. OFDM has also

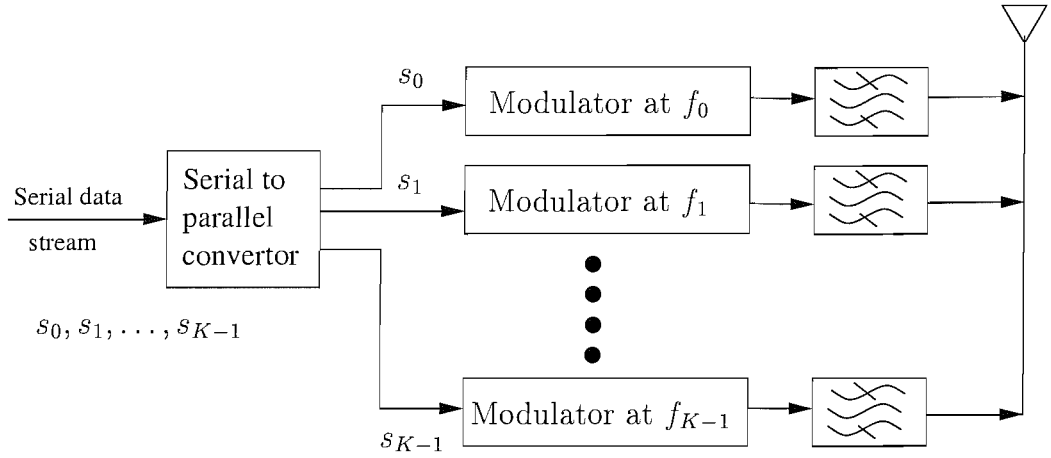

Figure 1.2: Basic OFDM transmitter.

been adopted in wireless local area networks (WLAN) standardised as IEEE 802.11 [19] in the US, ETSI HIPERLAN [20] in Europe and by the Multimedia Mobile Access Communication (MMAC) standard body in Japan. The timeline of the important events that occurred in the history of OFDM is summarised in Figure 1.1, while some of the main contributions to the state-of-the-art of OFDM systems are summarised in Table 1.1.

1.2 Basic OFDM system

In this section, we will commence our discourse on a basic OFDM system. The fundamental concepts of OFDM will be presented in Section 1.2.1, outlining the basic transmitter and receiver structures. The performance of OFDM systems over Gaussian channels is characterised in Section 1.2.2, while the wideband channels used throughout the report are briefly discussed in Section 1.2.3. In Section 1.2.4, rudimentary channel transfer function estimation methods are presented, which is followed by a brief characterisation of the OFDM signal's amplitude statistics in Section 1.2.5.

1.2.1 OFDM concepts

The fundamental principle of OFDM is to split the signal to be transmitted into K parallel streams, each of which modulates a carrier using an arbitrary modulation technique. Figure 1.2 shows the basic transmitter of an OFDM modem. The frequency spacing between the adjacent carriers is Δf, resulting in a total signal bandwidth of $K \cdot \Delta f$. The resultant

Year	Author	Contribution
'66	Holzinger [7]	Early research on digital communications over fixed time-continuous dispersive channels having memory.
	Chang [8]	First known study of multichannel data transmission.
'67	Salzberg [9]	Investigated the performance of an efficient parallel data transmission system.
'70	Chang [10]	A US patent that Chang filed in November 1966 was issued in January 1970.
'71	Weistein and Ebert [11]	Applied the DFT for the efficient implementation of the modulation and demodulation process.
'81	Hirosaki [22]	Implemented an orthogonally multiplexed QAM system using the DFT.
'86	Hirosaki, Hasegawa and Sabato [23]	Introduced an advanced group-band modem using an orthogonally multiplexed QAM technique.
'90s onward	Bingham [21]	Contributed a tutorial article that initiated the surge of OFDM research in the 1990s.
	Cioffi [14,15]	Introduced ADSL [14] and VDSL [15].
	Blum, Cimini, Sollenberger, Winters and Geoffrey Li [26–30]	Extensive research studies in the field of OFDM especially in channel estimation [26], peak-to-average power ratio [27], forward error correction [28] and multiple antenna systems [29,30].
	Letaief, Murch and Cheng [31–35]	Conducting studies on the multiple antenna and multiuser OFDM system.
	Rohling [36,37]	Exploiting channel coding in conjunction with OFDM signals [36] and ICI cancellation [37].
	Bölcskei, Gesbert and Pulraj [38]	Invoked spatial multiplexing in OFDM.
	Necker and Stüber [39]	Proposed totally blind channel estimation in OFDM.
	Prasad and van Nee [6]	Produced a compilation of OFDM topics.
	Lu and Wang [40–42]	Advocated iterative receivers for space-time block coded OFDM.
	Hanzo, Münster, Choi and Keller [5]	Studies on adaptive modulation, channel estimation, peak-to-average power ratio reduction and Space Division Multiple Access (SDMA) in OFDM.
	Lindner [43,44]	Employing time, frequency and spatial spreading in OFDM.
	Kammeyer [45–47]	Exploring methods to reduce the peak-to-average power ratio [45], iterative decoding [46] and channel estimation [47]

Table 1.1: Main contributions on OFDM.

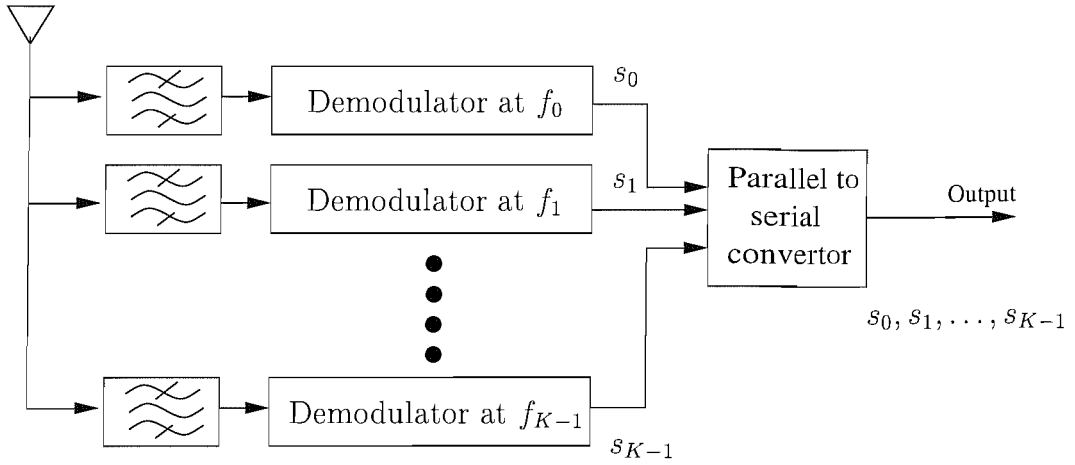

Figure 1.3: Basic OFDM receiver.

K number of modulated and multiplexed signals are transmitted over the channel and at the receiver K parallel receiver branches assist in recovering the information. A multiplexer then recombines the K parallel signal streams into a high-rate serial stream, as seen in Figure 1.3. For the complex QAM symbols, an OFDM symbol starting at $t = t_s$ may be written as [5]:

$$s(t) = \begin{cases} Re\left\{\sum_{i=-\frac{K}{2}}^{\frac{K}{2}-1} d_{i+K/2} \exp(j2\pi(f_c - \frac{i+0.5}{T})(t-t_s))\right\}, & t_s \leq t \leq t_s + T \\ 0, \quad t < t_s \quad \wedge \quad t > t_s + T, \end{cases} \tag{1.1}$$

where K is the number of subcarriers, T is the OFDM symbol duration and f_c is the carrier frequency.

In the literature, often the equivalent complex baseband representation is used [5]. In this representation, the real and imaginary parts correspond to the in-phase and quadrature components of the OFDM signal, which modulate a cosinusoidal and sinusoidal carrier frequency for the sake of producing the OFDM modulated signal in the form of [5]:

$$s(t) = \begin{cases} \sum_{i=-\frac{K}{2}}^{\frac{K}{2}-1} d_{i+K/2} \exp(j2\pi \frac{i}{T}(t-t_s)), & t_s \leq t \leq t_s + T \\ 0, \quad t < t_s \quad \wedge \quad t > t_s + T. \end{cases} \tag{1.2}$$

It may be readily shown that the complex baseband OFDM signal defined by Equation 1.2 is the inverse Fourier Transform of K number of QAM input symbols [5, 11]. The corresponding discrete-time equivalent is the inverse discrete Fourier transform (IDFT), which

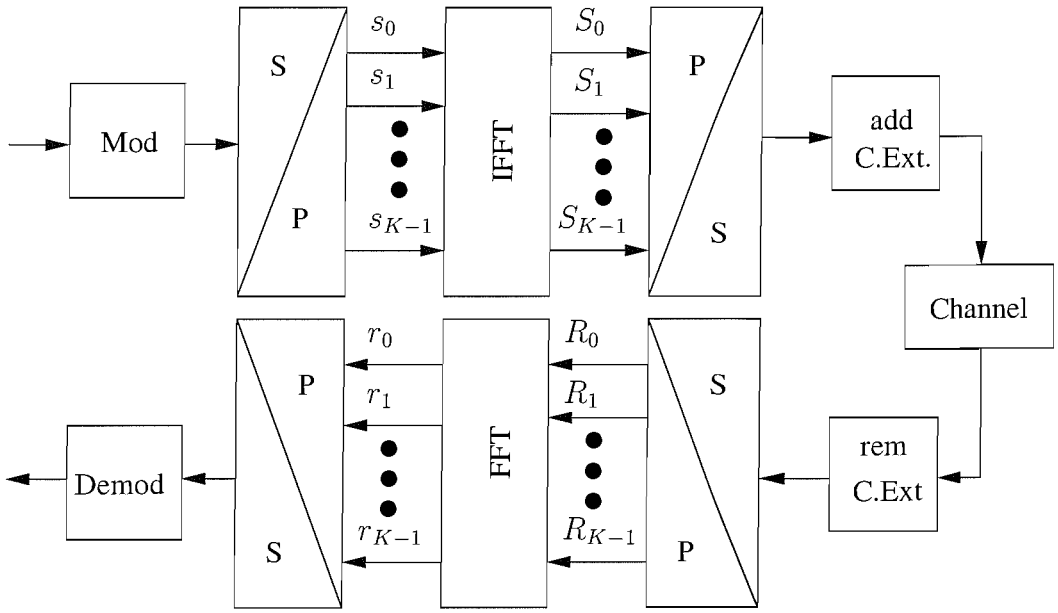

Figure 1.4: Schematic of K-subcarrier OFDM transmission system using IFFT and FFT.

can be expressed as:

$$s(n) = \sum_{i=0}^{K-1} d_i \exp(j2\pi \frac{in}{K}), \tag{1.3}$$

where the time t was replaced by the sample-index n and d_i represents either the *phase shift keying* (PSK) or *quadrature amplitude modulated* (QAM) symbols. In practice, this transform can be more efficiently implemented by the Inverse Fast Fourier Transform (IFFT), when the number of subcarriers is sufficiently high. Figure 1.4 shows the schematic of the OFDM system implemented using the IFFT at the transmitter and the FFT at the receiver.

One of the most important reasons of employing OFDM is its efficiency in dealing with multipath-induced delay spread. When mapping the input datastream to K subcarriers, the associated symbol duration becomes K times longer, which reduces the relative multipath delay spread, relative to the symbol duration by the same factor. In order to eliminate intersymbol interference (ISI) between the consecutive OFDM symbols, a quasi-periodic extension also termed as cyclic prefix is introduced for each OFDM symbol. The cyclic prefix duration is chosen to be longer than the expected delay spread of the channel, such that dispersed multipath components of one symbol cannot interfere with the next symbol. For a detailed discourse on OFDM the interested reader is referred to [5].

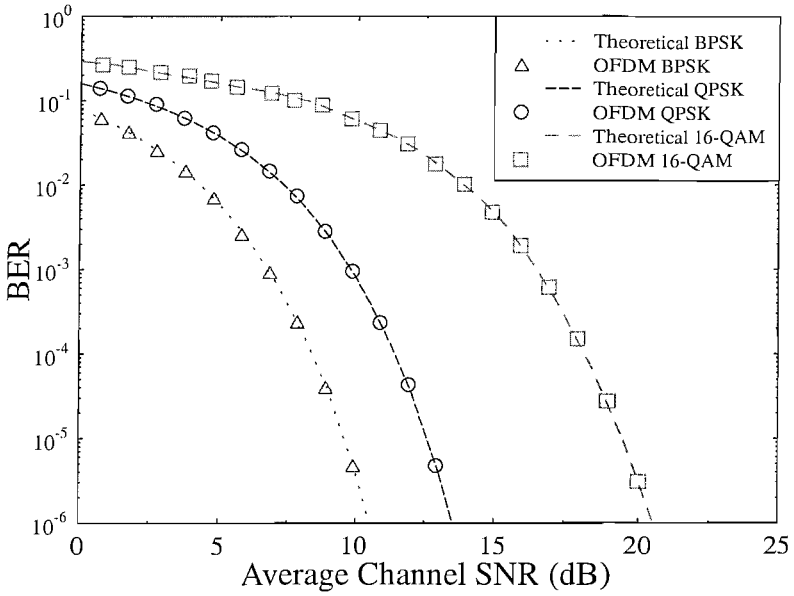

Figure 1.5: BER versus SNR curves for the OFDM modem in AWGN channels using BPSK, QPSK and 16-QAM. The lines indicate the theoretical performance of the coherently detected modulation schemes of a serial modem over AWGN channels.

1.2.2 OFDM transmission over Gaussian channels

The OFDM modem's performance is expected to be identical to the performance of a classic serial modem based on the fact that the average power of the additive white Gaussian noise (AWGN) is the same in both the time domain and the frequency domain [48]. Similar to a serial system, the bit error rate (BER) versus signal-to-noise ratio (SNR) characteristics of the OFDM modem are determined by the modulation scheme used. Figure 1.5 displays the simulated BER versus SNR curves for binary phase shift keying (BPSK), quaternary phase shift keying (QPSK) and 16-level quadrature amplitude modulation (16-QAM) together with the corresponding theoretical BER curves of serial modems in an AWGN channel, as derived in [49]:

$$p_{e,BPSK}(\gamma) = Q(\sqrt{2\gamma}), \tag{1.4}$$

$$p_{e,QPSK}(\gamma) = Q(\sqrt{\gamma}), \tag{1.5}$$

$$p_{e,16-QAM}(\gamma) = \frac{3}{4}Q(\sqrt{\gamma}) + \frac{1}{2}Q(3\sqrt{\gamma}) - \frac{1}{4}Q(5\sqrt{\gamma}), \tag{1.6}$$

where γ is the SNR and the Gaussian $Q(\cdot)$-function is defined as:

$$Q(y) = \frac{1}{\sqrt{2\pi}} \int_y^\infty e^{-x^2/2} dx = erfc\left(\frac{y}{\sqrt{2}}\right). \quad (1.7)$$

It can be seen from the figure that the experimentally evaluated BER performance of the OFDM modem is in good agreement with the theoretical BER curves of conventional serial modems in AWGN channels. At a BER value of 10^{-4}, BPSK requires 3 dB and 10 dB lower SNR than QPSK and 16-QAM in terms of the average channel SNR, respectively.

1.2.3 Wideband channel models

One of the main advantages of using OFDM is its resilience against time dispersive or frequency selective fading channels which is achieved without employing a high-complexity time-domain channel equaliser [4]. The channel model assumed is that of a finite impulse response (FIR) filter having time-varying tap values. Every propagation path n is characterised by a fixed delay τ_n and a complex-valued Rayleigh fading process $g_n(t)$. The Rayleigh processes g_n are independent from each other, but they all exhibit the same normalised Doppler frequency f'_d, depending on the parameters of the simulated channel [4].

The ensemble of the p propagation paths constitutes the channel impulse response (CIR) expressed as:

$$h(t,\tau) = \sum_{n=1}^{p} g_n(t) \cdot \delta(\tau - \tau_n), \quad (1.8)$$

which is convolved with the transmitted signal. Most of the investigations carried out were based on the channel models characterised in this section.

1.2.3.1 Two-path Rayleigh fading channel

The simplest model of a dispersive multipath channel is the equal-power two-path channel model. This simple model will be invoked for demonstrating the advantages of using an OFDM system in a multipath channel. For this kind of channel model, 128 subcarriers will be used for the OFDM symbol. Each OFDM symbol has a duration of 120 μs and a cyclic prefix of 40 μs duration. The Jake model is adapted for modelling the fading channels [50] and the taps are separated by 5 μs. The maximum Doppler frequency is set to 200 Hz and

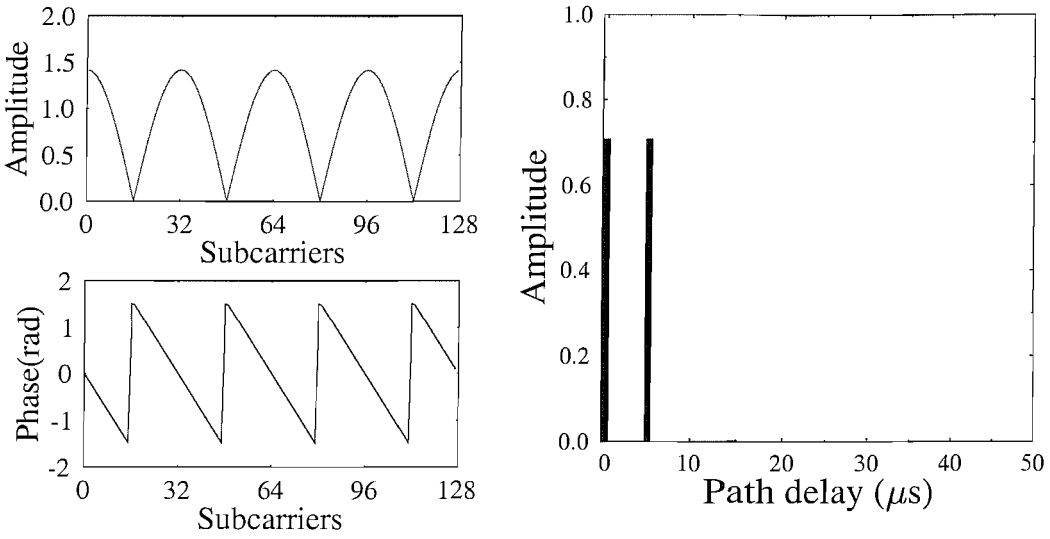

(a) channel transfer function

(b) channel impulse response

Figure 1.6: 2-path Rayleigh fading channel: (a) unfaded frequency domain channel transfer function $H(n)$, (b) impulse response.

both paths undergo independent Rayleigh fading. The channel impulse response and the channel transfer function for this particular channel is depicted in Figure 1.6.

1.2.3.2 Wireless asynchronous transfer mode channel

In our wideband simulations we will also use an indoor channel model, which we refer to as the wireless asynchronous transfer mode (WATM) channel. The associated OFDM FFT length is 512 and each symbol is padded with a cyclic prefix of length 64. The sampling rate of the corresponding WATM system is 225 Msamples/s, and the carrier frequency is 60 GHz. The uncoded target data rate of the system is 155 Mbps. The associated static frequency domain channel transfer function (FDCHTF) is depicted in Figure 1.7(a). This channel transfer function was derived by taking the Fourier transform of the impulse response shown in Figure 1.7(b). Since the WATM channel model of Figure 1.7 may be viewed as the worst-case scenario for a high data rate indoor network, Hanzo *et al.* [4] has introduced a truncated version of the original WATM channel impulse response as depicted in Figure 1.8, which retains the first three lower-delay CIR taps. This reduces the total length of the impulse response, with the last path arriving at a delay of 48.9 ns and hence

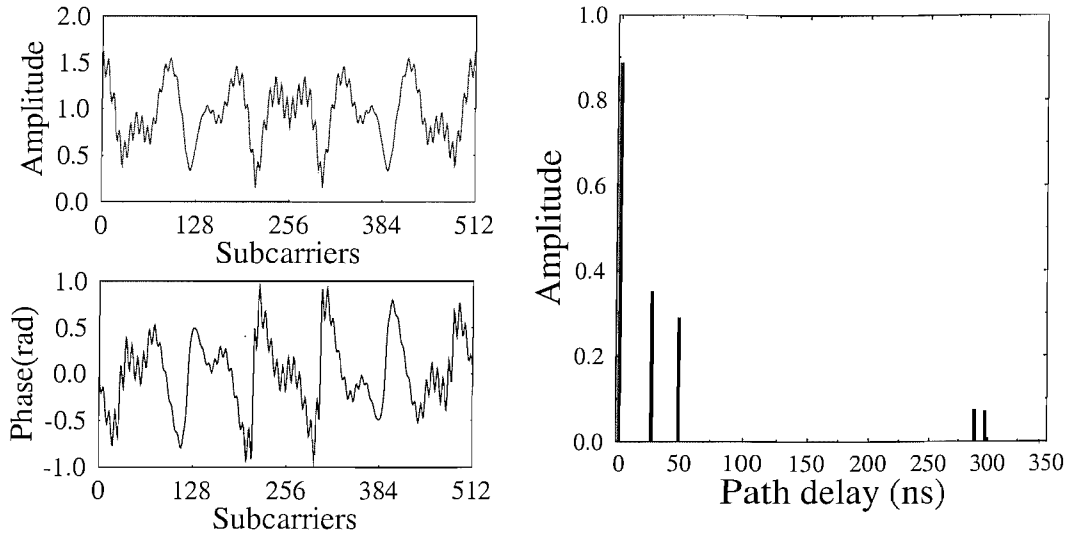

(a) channel transfer function

(b) channel impulse response

Figure 1.7: WATM channel: (a) unfaded frequency domain channel transfer function $H(n)$, (b) impulse response.

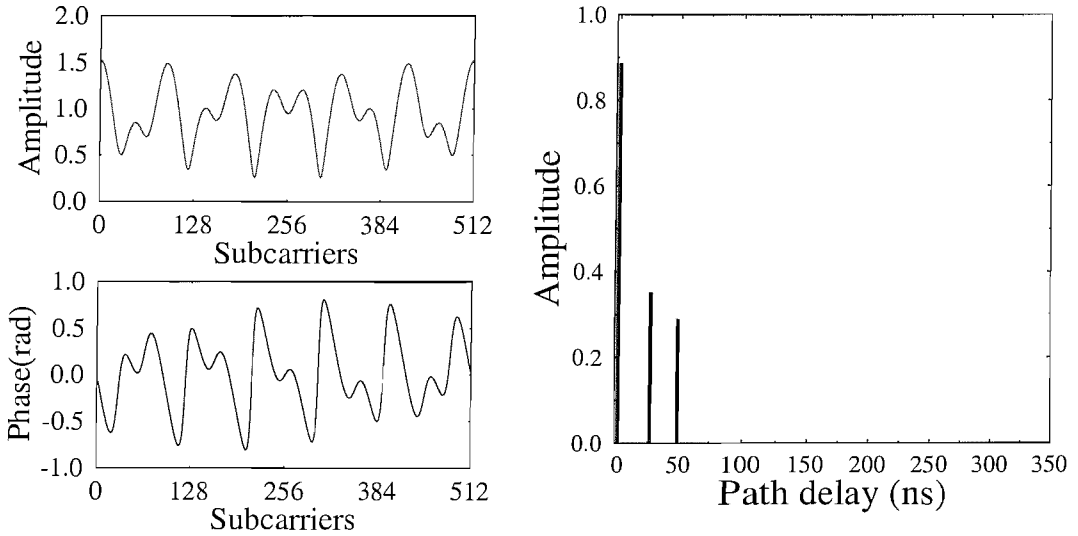

(a) channel transfer function

(b) channel impulse response

Figure 1.8: SWATM channel: (a) unfaded frequency domain channel transfer function $H(n)$, (b) impulse response.

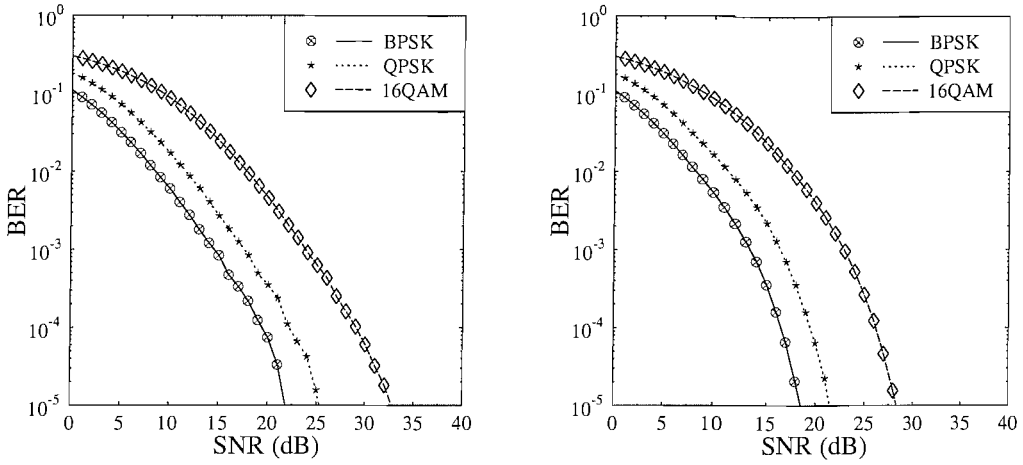

(a) WATM (b) SWATM

Figure 1.9: BER versus average channel SNR for unfaded a) WATM and b) SWATM channel using perfect channel estimation and coherent detection.

may be viewed as representative of a smaller indoor cell, which exhibits a lower delay-spread.

1.2.4 Channel transfer function estimation

The time-variant propagation conditions of the wireless communication channel render channel estimation for OFDM a demanding task at the receiver. In order to support coherent detection, the channel transfer function must be estimated. FDCHTF estimation algorithms [5] generate the channel transfer function estimates $\hat{H}(n)$, where n is the subcarrier index, before demodulation of the received symbols takes place. The accuracy of the FDCHTF estimation will influence the system's performance to a great extent, especially for systems employing multilevel modulation and coherent detection. The following subsections will briefly highlight the philosophy of FD pilot-aided channel estimation techniques that are normally used in estimating the channel transfer function of wideband channels in OFDM systems. More specifically, we will briefly study the effects of perfect channel estimation in Section 1.2.4.1, pilot symbol assisted channel estimation in Section 1.2.4.2, decision-directed channel estimation in Section 1.2.4.3 and blind channel estimation in Section 1.2.4.4.

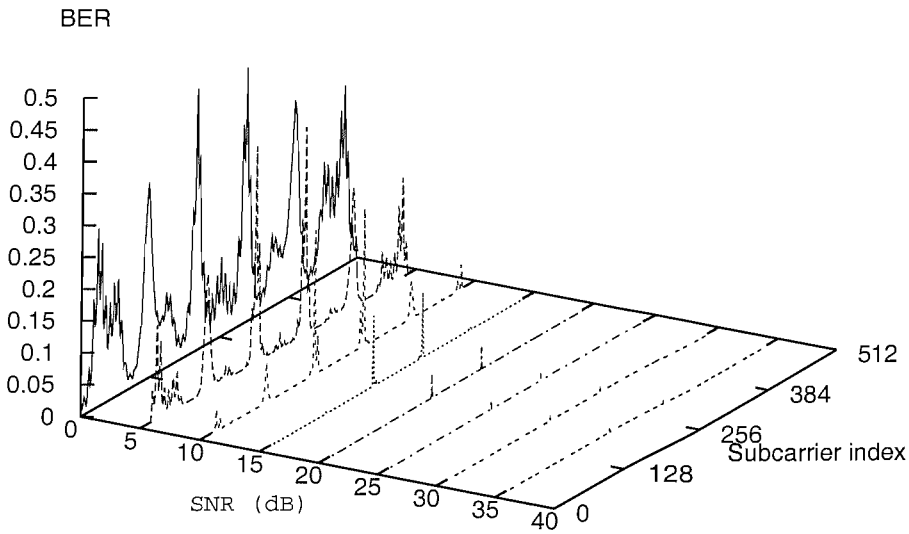

(a) BPSK

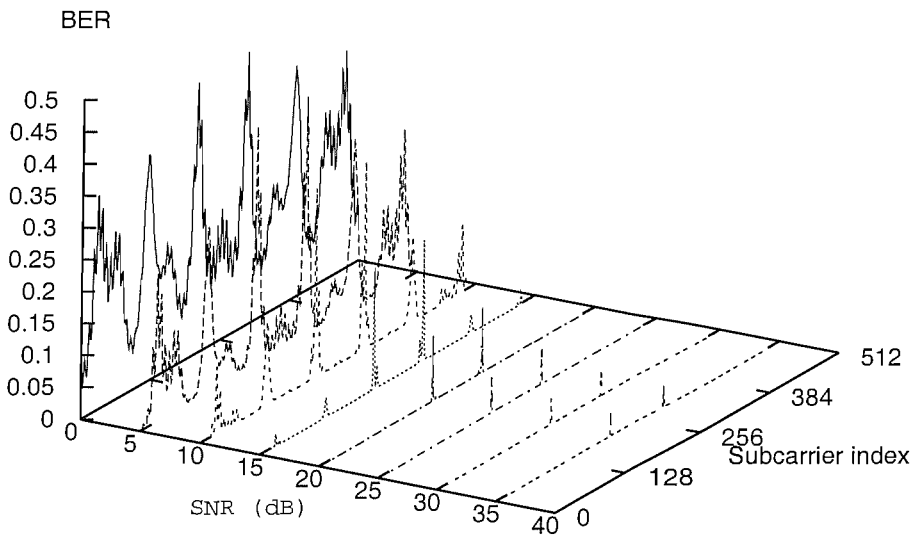

(b) QPSK

Figure 1.10: Simulated BER per subcarrier when communicating over the time-invariant WATM channel using perfect channel estimation for (a) coherent BPSK transmission, and (b) coherent QPSK transmission. The symmetry of the BER curves with respect to the subcarrier in the centre of the frequency band indicates that the unfaded CIR was real.

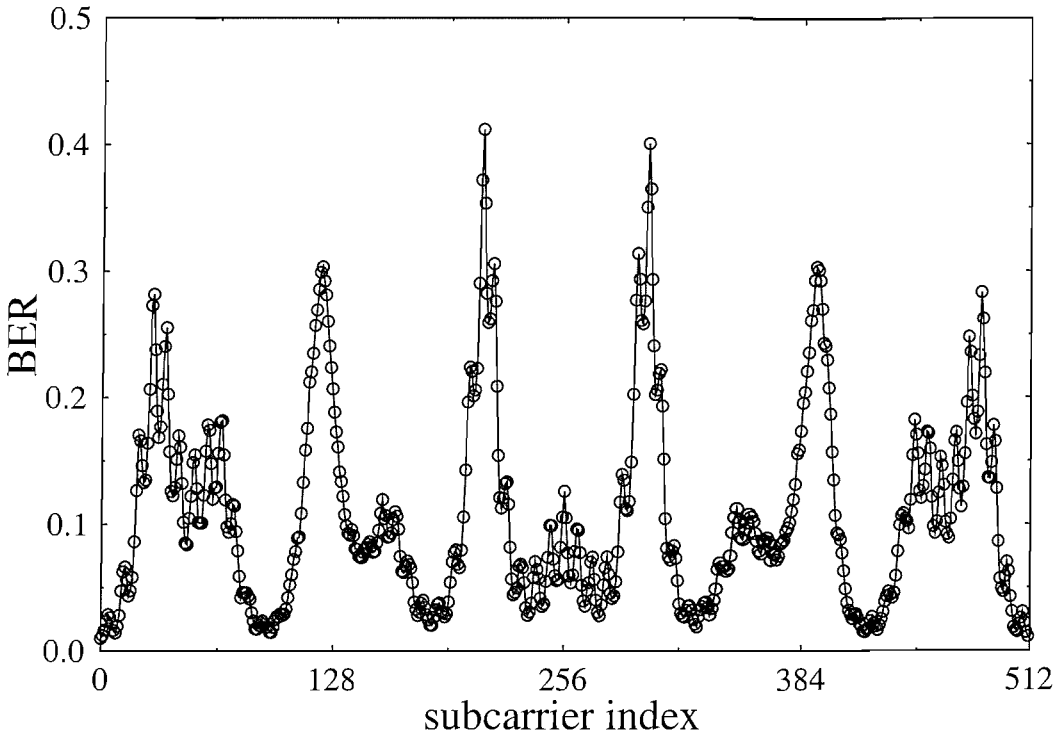

Figure 1.11: Simulated BER per subcarrier for coherently detected BPSK transmission using perfect channel estimation for transmission over the unfaded WATM channel in Figure 1.7 at an average channel SNR of 0 dB.

1.2.4.1 Perfect channel estimation

The best-case scenario for OFDM transmissions over time dispersive channels, such as the WATM channel of Figure 1.7 is based on exploiting perfect channel estimation. The performance results corresponding to using perfect channel estimation and coherent detection for the WATM and SWATM channels are depicted in Figure 1.9. On the other hand, Figure 1.10 shows the BER per subcarrier for different levels of average OFDM SNR for the simulated 512-subcarrier modem communicating over the WATM channel employing coherently detected BPSK in the subcarriers. As observed in Figure 1.11, it can be seen that the bit error probability varies significantly between different subcarriers, from about 2% in high-quality sub-channels, up to 40% in the deep fades of the channel transfer function $H(n)$ at an average OFDM SNR of 0 dB. At an average SNR of 5 dB, groups of virtually error-free subcarriers can be observed, interspersed with bundles of carriers exhibiting high bit error probabilities. At 15 dB, only a low number of subcarriers experience measurable

non-zero transmission error rates.

1.2.4.2 Pilot symbol assisted channel estimation

Pilot symbols can be used for estimating the channel transfer function at the receiver so that coherent detection can be performed. This system of incorporating pilot symbols in the transmission is termed as *pilot symbol assisted modulation* (PSAM) [51]. In this scheme, known pilot symbols are inserted among the transmitting symbols. For each received pilot symbol the instantaneous channel fading value is estimated as the quotient of the received and expected symbol, and the channel estimate for the data symbols is derived from these pilot-based fading estimates by means of interpolation between them [5]. For example, n_p pilot symbols having values of P_i are transmitted in the subcarriers associated with indeces p_i, $i = 1, \ldots, n_p$ within the total OFDM symbol bandwidth hosting K subcarriers. At the receiver, the estimated channel transfer factor value $\hat{H}(p_i)$ can be calculated from the received samples $y(p_i)$ by $\hat{H}(p_i) = y(p_i)/P_i$. Again, the values of the FDCHTF between the pilots can then be estimated from the resultant pilot-based values using interpolation. There are a number of interpolation methods in the literature [5] but only two of these will be introduced in the next subsection, namely linear interpolation in Section 1.2.4.2.1 and lowpass interpolation in Section 1.2.4.2.2.

1.2.4.2.1 Linear interpolation for PSAM The simplest interpolation technique that can be used for estimating the channel transfer function for the data subcarriers between two neighbouring channel estimation pilot samples $\hat{H}(p_i)$ and $\hat{H}(p_{i+1})$ is a linear function formulated as follows:

$$\hat{H}(n) = \hat{H}(p_i) + \frac{\hat{H}(p_{i+1}) - \hat{H}(p_i)}{p_{i+1} - p_i} \cdot (n - p_i) \qquad for \qquad p_i \leq n \leq p_{i+1}. \tag{1.9}$$

Figure 1.12 shows the amplitude and the phase of the stationary WATM channel's frequency domain transfer function $H(n)$ for different numbers of equidistant pilot symbols in the frequency domain in an ideal noiseless environment. It can be seen that the channel estimation accuracy improves upon increasing the number of pilot tones in the spectrum. The number of pilot tones in the OFDM spectrum necessary for sampling the channel transfer function can be determined on the basis of the sampling theorem as follows.

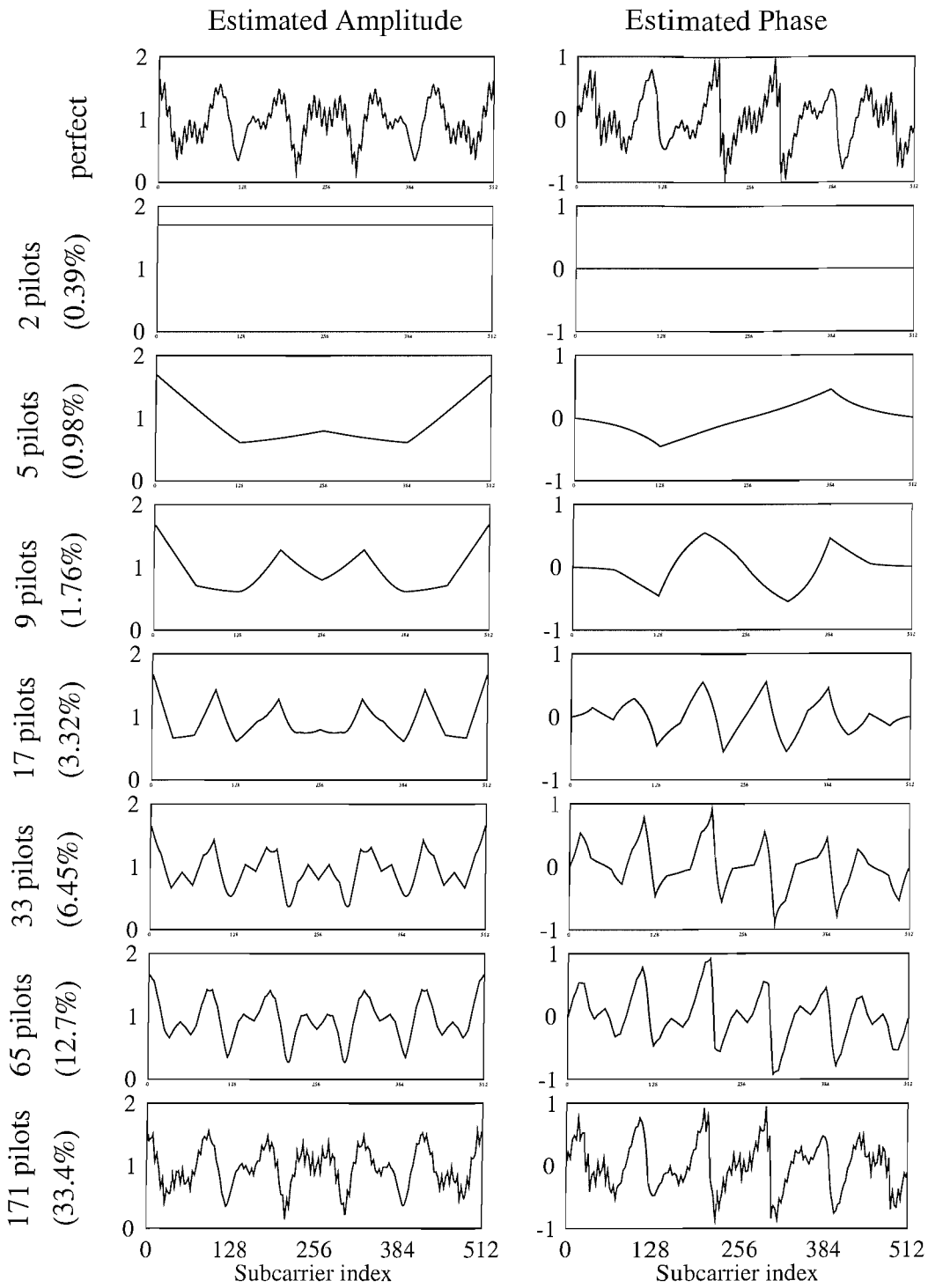

Figure 1.12: Estimation of the unfaded WATM channel in a noiseless environment using linear interpolation in a 512-subcarrier OFDM symbol.

The FDCHTF, $H(f)$ is the Fourier transform of the channel impulse response $h(t)$. Each of the impulses in the impulse response will result in a complex exponential function of $e^{-(j2\pi\tau/T_s)f}$ in the frequency domain, depending on its time delay τ. In order to sample its contribution to the FDCHTF $H(f)$ according to the sampling theorem [4], the maximum pilot spacing Δp in the OFDM symbol has to satisfy:

$$\Delta p \leq \frac{K}{2\tau/T_s}\Delta f. \tag{1.10}$$

Inspection of Figure 1.12 underlines these points. In order to resolve the full spectral-domain detail of the original transfer function, as depicted at the top of the figure, 171 pilots must be used. Even when using 171 pilots in the OFDM symbol, the estimated FDCHTF is not an exact match of the original. This is due to the inaccuracy of the linear interpolation algorithm used.

1.2.4.2.2 Lowpass interpolation for PSAM Another type of interpolation technique that can be used for estimating the channel transfer function from the pilot symbols is constituted by lowpass interpolation. According to this method, an ideal lowpass filter having a cut-off frequency of $1/\Delta p$ has to be used, where Δp is the spectral distance between consecutive pilot subcarriers. Unlike in linear interpolation, this technique requires equidistant pilot placement within the OFDM symbol. A detailed discourse on this method can be found in [4].

Figure 1.13 provides an informal characterisation of the estimation accuracy of the PSAM scheme combined with lowpass interpolation in a noiseless environment. The resolution of the FDCHTF estimation depends heavily on the number of pilots per OFDM symbol. If a perfect lowpass interpolation scheme was to be used over the WATM channel, then a pilot distance of $\Delta p = 2\Delta f$ would have to be employed, resulting in 256 pilot subcarriers per 512-subcarrier OFDM symbol.

Figure 1.14 and Figure 1.15 show the achievable BER performance for transmission over the unfaded WATM channel using linear interpolation and lowpass interpolation employing PSAM-BPSK and PSAM-16QAM, respectively. It can be seen that the WATM system encounters a high residual bit error rate when using less that 128 pilots. In these pilot sets, the channel transfer function is inadequately sampled in the frequency domain and the resultant channel estimation is of insufficient accuracy for coherently detecting 16-QAM.

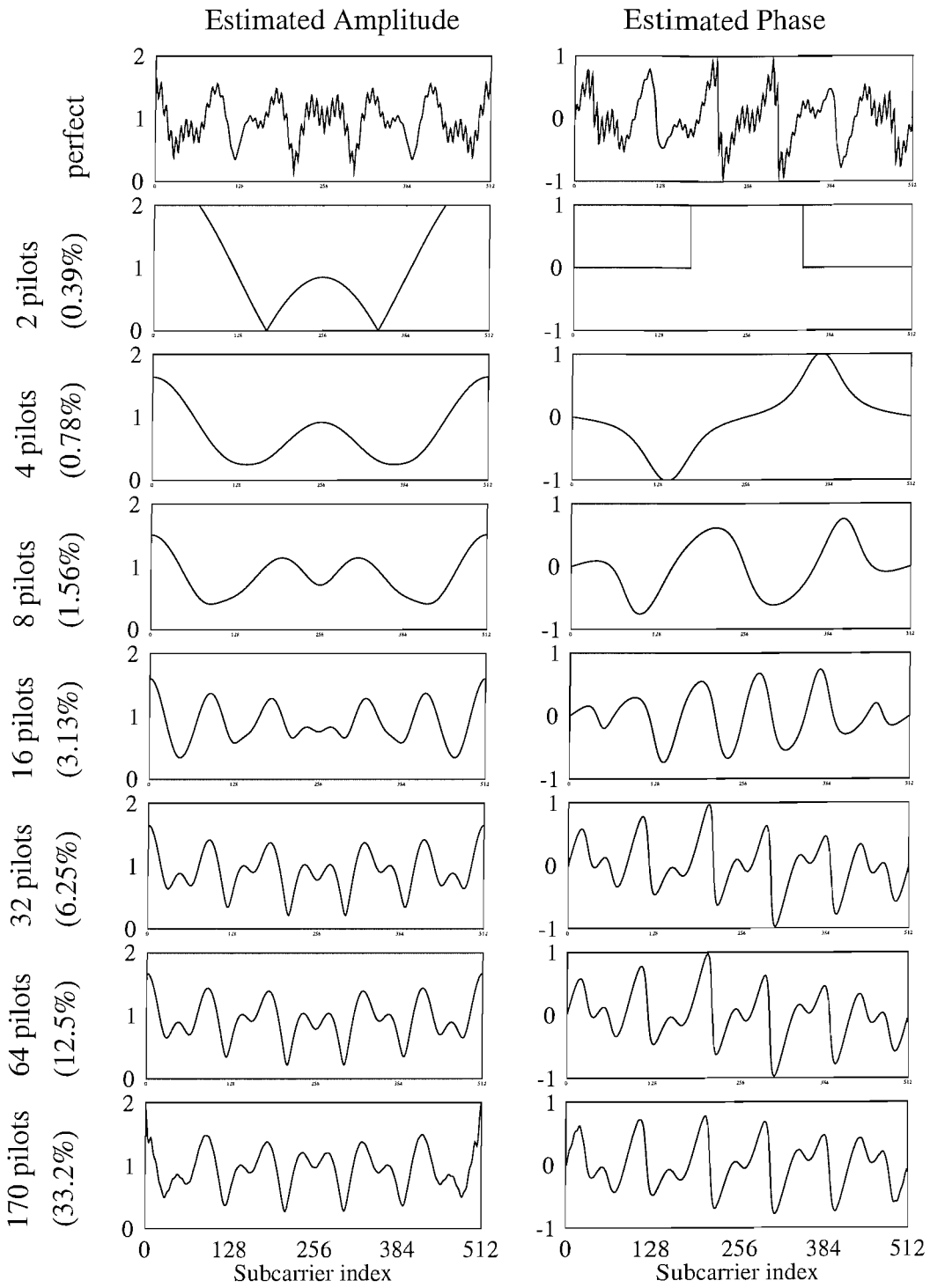

Figure 1.13: Estimation of the unfaded WATM channel in a noiseless environment using lowpass interpolation in a 512-subcarrier OFDM symbol.

We may also notice from Figure 1.14 that the performance of the BPSK system for the lowpass interpolation with the 16 pilot symbols actually outperforms the system using 32 and 64 pilots, which is not as expected. This phenomenon may be explained by the effects of the associated phase estimation error, as depicted in Figure 1.16. We can see that although the average of the phase estimation error for the case of 32 and 64 pilots is quite small, the peak values observed in Figures 1.16(c) and 1.16(d) representing the 32 and 64 pilots, respectively, are closer to the decision boundary for the BPSK system, i.e. to the phase value of $\pm\pi/2$, compared to the maximum phase error of the 16-pilot scenario [5]. Therefore, at high SNRs, these peak values will dominate the BER and result in a worse achievable BER for both the 32- and 64-pilot assisted system. Similar arguments are valid also for employing linear interpolation.

1.2.4.3 Decision-directed channel estimation

The disadvantage of using pilot symbols is that they absorb a certain percentage of the useful bandwidth. An alternative solution for avoiding this bandwidth loss is to use decision-directed channel estimation [5]. For this method, instead of using pilot symbols, data estimates are used for predicting the channel transfer function for the next OFDM symbol [52]. Naturally in order to initiate the decision-directed channel estimation process, at least one known OFDM symbol must be transmitted at the commencement of communications. This enables the receiver to attain initial channel estimates for all subcarriers, which are then used for detecting the data in the following OFDM symbol. However, the setback of using this channel estimation method is that the erroneous results of the previous detections will affect the following detections. This kind of error propagation can be minimised by regularly transmitting known training sequences, while sacrificing some of the useful transmitted power.

1.2.4.4 Blind channel estimation

Another method of estimating the channel transfer function is referred to as blind channel estimation. In this context, the terminology blind implies that no pilot symbols or training blocks are required for performing channel estimation. Blind channel estimation does not 'waste' power and does not sacrifice useful data throughput for pilots, hence contributing to

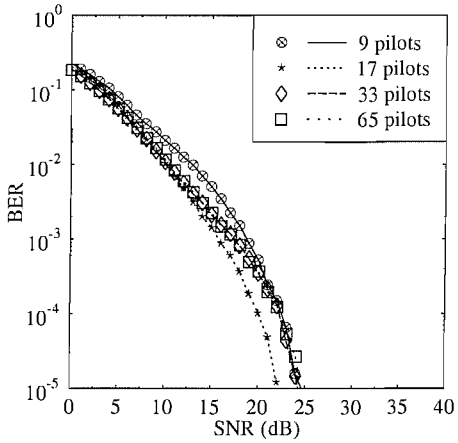

(a) WATM linear interpolation

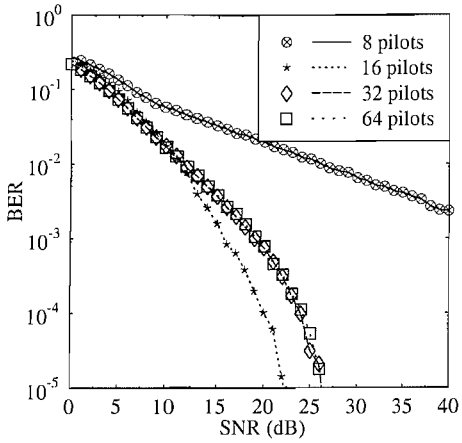

(b) WATM lowpass interpolation

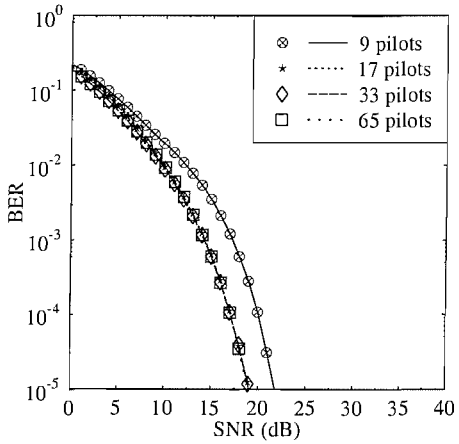

(c) SWATM linear interpolation

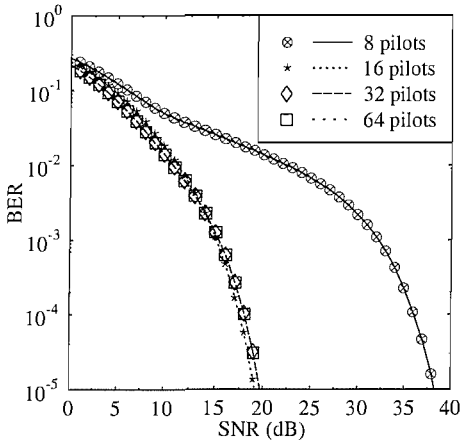

(d) SWATM lowpass interpolation

Figure 1.14: BER versus average channel SNR for PSAM-BPSK when communicating over the unfaded WATM channel in conjunction with a) linear and b) lowpass interpolation, as well as in the unfaded SWATM channel with c) linear and d) lowpass interpolation.

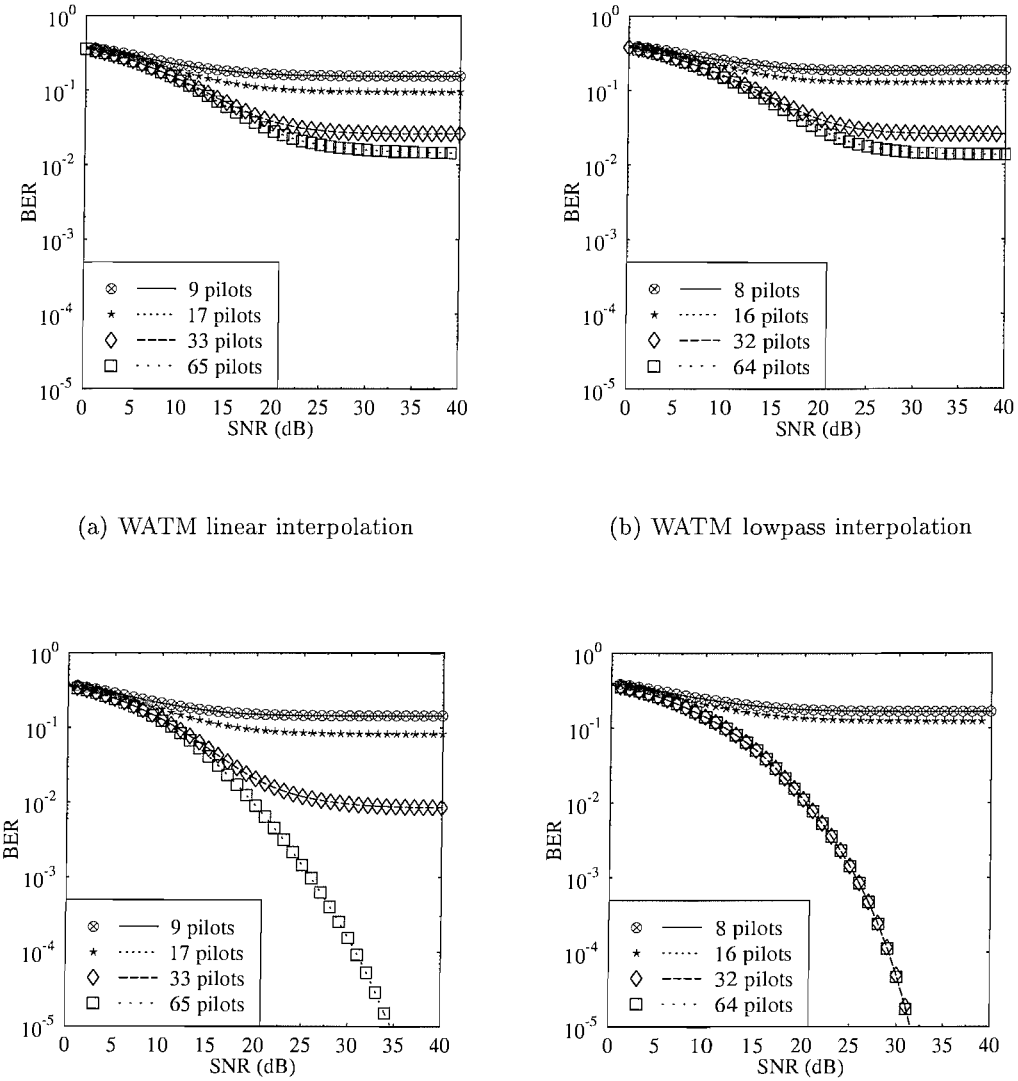

(a) WATM linear interpolation

(b) WATM lowpass interpolation

(c) SWATM linear interpolation

(d) SWATM lowpass interpolation

Figure 1.15: BER versus average channel SNR for PSAM-16QAM when communicating over the unfaded WATM channel in conjunction with a) linear and b) lowpass interpolation, as well as in the unfaded SWATM channel with c) linear and d) lowpass interpolation.

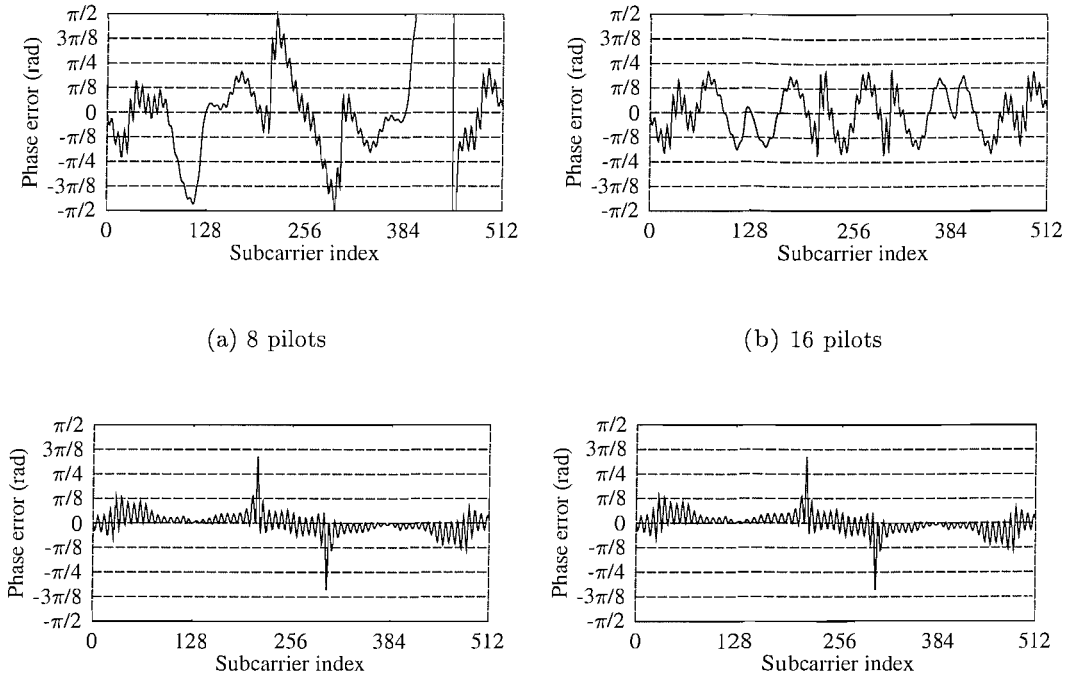

(a) 8 pilots

(b) 16 pilots

(c) 32 pilots

(d) 64 pilots

Figure 1.16: Phase estimation error of the channel transfer function for the WATM channel of Figure 1.7 while implementing the lowpass filter interpolator for pilot symbol equals to (a) 8, (b) 16, (c) 32 and, (d) 64.

the enhancement of system's throughput. However, in a mobile radio environment, where significant FDCHTF variations may be experienced between two consecutive training blocks, blind channel estimation is prone to error propagation. There are various ways of carrying out blind channel estimation, and some of the techniques used in single carrier schemes can also be applied to OFDM [39, 53, 54].

1.2.5 OFDM signal amplitude statistics

In order to briefly characterise the amplifier linearity requirements of OFDM modems, in this section we briefly review the amplitude distribution of OFDM modulated signals [5]. The time domain OFDM signal is constituted by the sum of complex exponential functions, whose amplitudes and phases are determined by the data symbols transmitted over the different carriers. For the sake of demonstrating that the resultant time domain signal

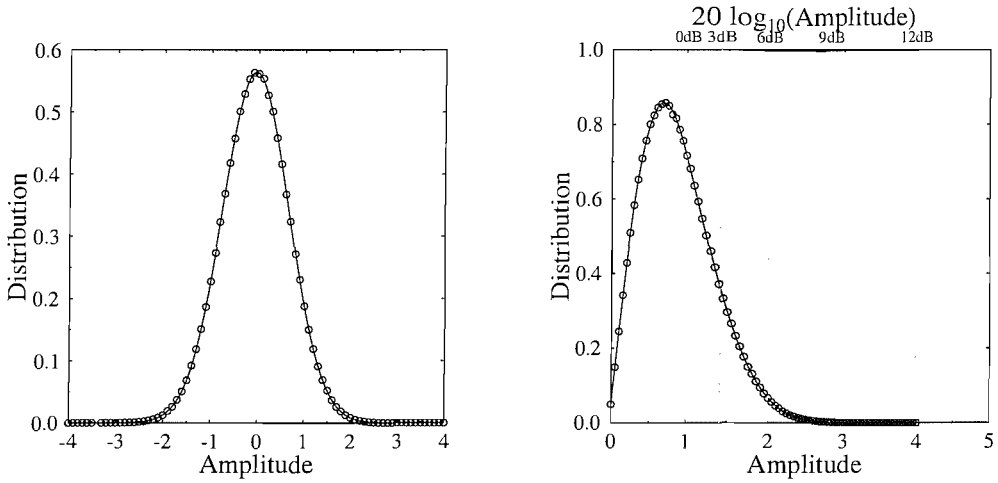

(a) I/Q PDF (b) Amplitude PDF

Figure 1.17: Two-dimensional amplitude histogram of the time-domain OFDM signal following a Rayleigh PDF.

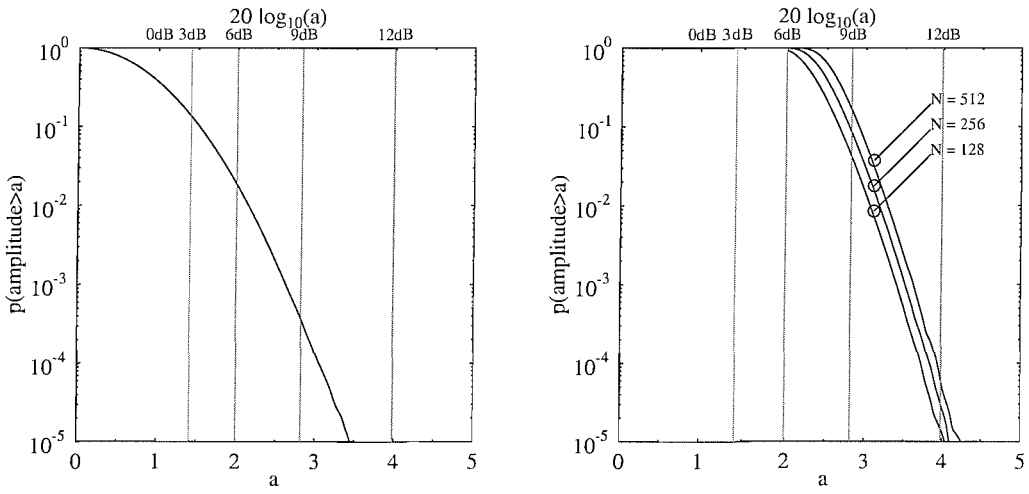

(a) Signal CDF (b) Peak CDF

Figure 1.18: Cumulative distribution function (CDF) of the (a) instantaneous signal amplitude, and (b) peak amplitude per OFDM symbol exceeding a given threshold value.

exhibits an amplitude probability density function (PDF) similar to the complex Gaussian distribution in conjunction with a high number of subcarriers, random data symbols were collected. The resultant PDF portrayed in Figure 1.17(a), which explicitly shows that the amplitude histogram of both the in-phase (I) and quadrature (Q) component of a 256-subcarrier OFDM signal closely matches a Gaussian distribution having a standard deviation of $\sigma = 1/\sqrt{2}$. The mean power of the signal is $2\sigma^2 = 1$. Hence the corresponding magnitude histogram follows a complex-valued Gaussian, or synonymously, a Rayleigh distribution having the same standard deviation, since both the in-phase (I) and the quadrature-phase (Q) component is Gaussian. This histogram is shown in Figure 1.17(b) for the previously used 256-subcarrier OFDM signal along with the corresponding Rayleigh probability density function. The vertical grid lines in the figure indicate the relative amplitude above the mean value expressed in decibels. It can be seen that unlike full-response single-carrier modulation schemes - which have a more limited range of possible output amplitudes - the OFDM modulated output signal exhibits substantial amplitude fluctuations. We have investigated this phenomenon in conjunction with different number of subcarriers, but all the scenarios considered resulted in a similar histogram to that of Figure 1.17(a). This is because the standard deviation σ associated with the PDF is independent of the number of subcarriers employed, since the mean of the signal power is normalised to unity.

In order to quantify the probability of the instantaneous signal amplitude exceeding a given threshold, the corresponding cumulative distribution function (CDF) was plotted in Figure 1.18(a). From this figure, it can be seen that the signal exceeds the 3 dB mark with a probability of about 0.15, while the probability of the signal amplitude exceeding the 6 dB mark is about 0.02. On the other hand, the 9 dB mark is exceeded with the probability of about 3.5×10^{-4}. Since signal peaks substantially higher than the average are encountered with a high probability, OFDM modulation requires high-linearity class-A amplifiers for the sake of preventing the dramatic BER performance degradation imposed by the amplifier-induced peak-clipping [5]. Hence, in the next section we briefly characterise the effects of peak clipping.

1.2.5.1 Clipping amplifier performance

Simulations have been conducted employing a simple clipping amplifier model in order to evaluate the effect of non-linear power amplifiers on the achievable BER performance of an OFDM system. This clipping amplifier limits the amplitude of the transmitted signal to a given level, without perturbing the phase information. This amplitude limitation of the time domain signal affects both the BER of all subcarriers in the OFDM symbol, as well as the frequency domain out-of-band emissions, and therefore increases the interference inflicted on adjacent carriers.

In Figure 1.18(a) the probability of the instantaneous signal amplitude exceeding a given level was shown. Since the amplitude limitation imposed in the time domain affects all the subcarriers of the OFDM symbol, the probability of the time domain peak amplitude per OFDM symbol period being clipped by the amplifier corresponds to the probability of at least one of the N time domain samples exceeding a given amplitude limit. This clipping probability recorded for a given maximal amplifier amplitude a is displayed in Figure 1.18(b). It can be observed that the clipping probability per OFDM symbol is dependent on the number of subcarriers employed because in the case of a higher number of subcarriers the peak amplitude might become higher for an inconvenient coincidence of the subcarrier signals.

Given the peak-clipping probabilities of Figure 1.18(b), the necessary amplifier back-off for an OFDM transmitter can be determined. If, for example, the acceptable clipping probability per OFDM symbol is 10^{-5}, then the necessary amplifier back-off values would be 12.1 dB, 12.3 dB and 12.5 dB for a 128-, 256- and 512-subcarrier OFDM modem, respectively. If a clipping probability of 10^{-4} is acceptable, then these back-off values can be reduced by about 0.6 dB.

1.2.5.2 BER performance using clipping amplifiers

If lower amplifier back-off values are chosen and no peak power reduction techniques are employed in the OFDM transmission system, then the clipping amplifier will influence both the BER performance of the OFDM link as well as the out-of-band emissions. The effects of the amplifier back-off value on the BER performance experienced in an AWGN channel

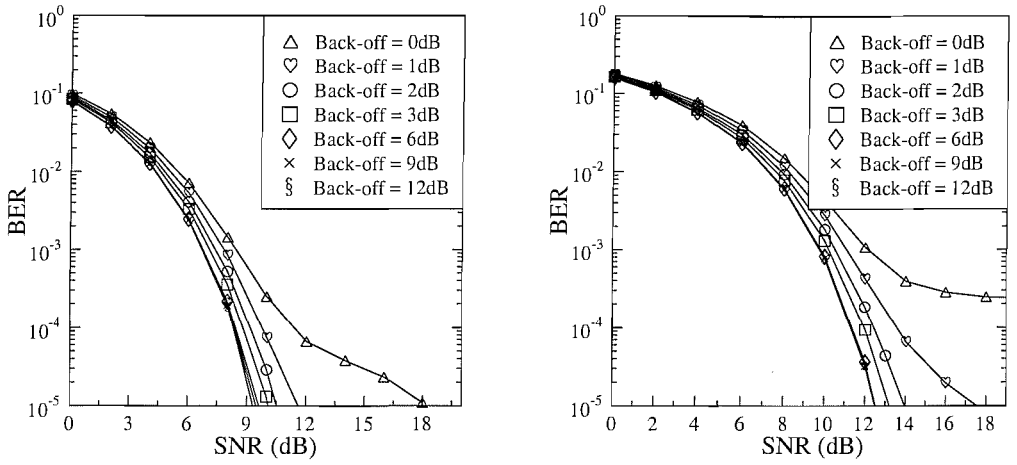

(a) BPSK (b) QPSK

Figure 1.19: Influence of amplifier-induced amplitude clipping on the BER performance of an OFDM modem using (a) BPSK, and (b) QPSK modulation.

for the coherently detected 512-subcarrier BPSK and QPSK OFDM transmission schemes are depicted in Figure 1.19(a) and Figure 1.19(b), respectively.

The back-off values investigated range from 9 dB down to 0 dB. According to Figure 1.18(b), an amplifier back-off of 9 dB results in a clipping probability per OFDM symbol of about 17%, while an amplifier back-off of 0 dB results in nearly certain clipping of every transmitted OFDM symbol.

1.3 Advanced OFDM systems

To further enhance a communication system, OFDM can be combined with other powerful performance enhancement schemes. In this section, we will outline some of the systems that have been studied by other researchers. We will commence this section by highlighting the philosophy of adaptive single-user OFDM techniques in Section 1.3.1. Then we will continue our discourse with the employment of forward error correction coding in Section 1.3.2. Finally, we will discuss the advantages of space and time diversity in an OFDM system in Section 1.3.3.

1.3.1 Adaptive single-user OFDM techniques

Adaptive modulation was first proposed by Steele and Webb [55] for accommodating the time-variant Shannonian channel capacity variations of fading narrowband channels. Among others Wong *et. al* [31, 35] and Keller [56] have conducted research in exploiting adaptive techniques in an OFDM environment. The motivation of this research arose from the fact that the bit error probability of different OFDM subcarriers transmitted in time dispersive channels depends on the frequency domain channel transfer function, as seen in Figure 1.10 and Figure 1.11. Most of the bit errors occurred in the set of severely faded subcarriers. If the subcarriers that are affected by the deep fades can be identified, the overall BER can be improved by introducing a modulation scheme that will minimise the number of errors. The badly faded subcarriers may also be excluded from transmission.

The most convenient setting for an adaptive OFDM (AOFDM) system is a time division duplex (TDD) scheme operating in a slowly varying channel while the duplex directions exhibit a similar FDCHTF allowing open-loop adaptation of the modulation scheme [5]. Both stations transmit an OFDM symbol in turn, and at each station the most recent received symbol is used for estimating the channel quality to be experienced, which is then used for determining the modulation mode to be used for the next transmitted OFDM symbol. The modulation modes were chosen from the set of BPSK, QPSK, 16-QAM and "no transmission", which assumes that no signal is transmitted. These modulation modes are denoted by M_m, where $m(0, 1, 2, 4)$ is the number of data bits associated with the subcarrier data symbol of each mode.

In order to keep the system's complexity low, the modulation mode is not varied on a subcarrier-by-subcarrier basis, but instead the total OFDM bandwidth of 512 subcarriers is split into blocks of similar-quality adjacent subcarriers, referred to as subbands, and this substantially simplifies the task of signalling the modem modes. Three different modulation mode allocation algorithms were investigated in [56], which are highlighted in Section 1.3.1.1 for the fixed-threshold adaptive algorithm, in Section 1.3.1.2 for the subband-BER estimator based algorithm and in Section 1.3.1.3 for the constant-throughput adaptive algorithm.

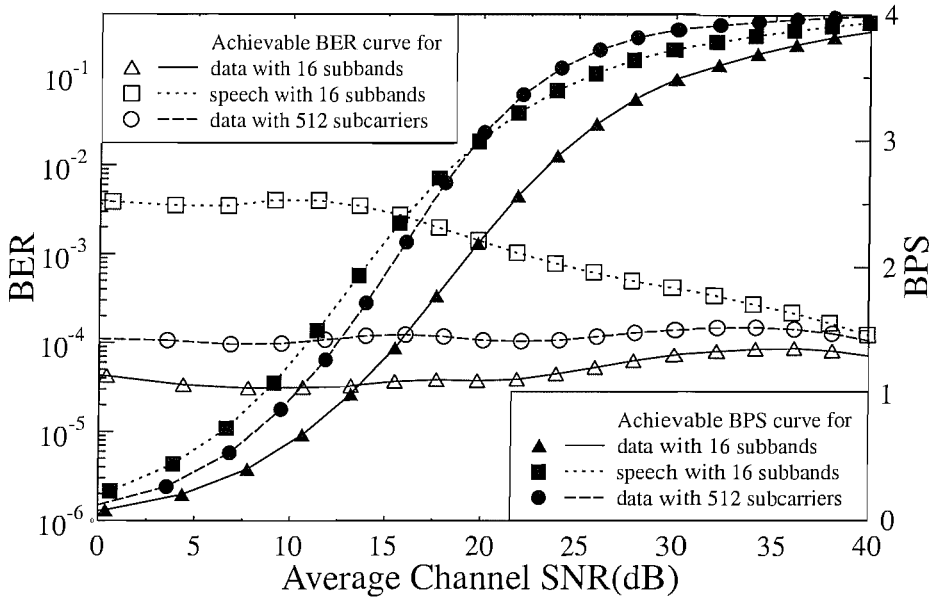

Figure 1.20: BER and BPS throughput performance of the 16-subband, 512-subcarrier switching level adaptive OFDM modem employing "no transmission", BPSK, QPSK and 16-QAM communicating over the Rayleigh fading time dispersive channel model of Figure 1.8 using the switching thresholds of Table 1.2.

	l_0	l_1	l_2	l_3
BER = 10^{-2}	$-\infty$	3.31 dB	6.48 dB	11.61 dB
BER = 10^{-4}	$-\infty$	7.98 dB	10.42 dB	16.76 dB

Table 1.2: Optimised switching levels for adaptive modulation communicating over Rayleigh fading channels at BER = 10^{-2} and 10^{-4} [58].

1.3.1.1 Fixed threshold adaptation algorithm

The fixed threshold algorithm was derived from the adaptation algorithm proposed by Torrance for serial modems [57]. The original algorithm assumed encountering a constant SNR over all of the transmission block's symbols, but in the case of an OFDM system communicating over a frequency selective channel the channel quality varies across the different subcarriers. The SNR thresholds derived for a given long-term target BER were determined by Powell optimisation [58]. The resultant SNR thresholds l_m invoked for activating a given modulation mode M_m in a slowly Rayleigh fading narrowband channel in order to achieve the uncoded target bit error rate of 10^{-2} and 10^{-4} are given in Table 1.2 [58].

In the case of an OFDM system operating in a frequency selective channel, the channel

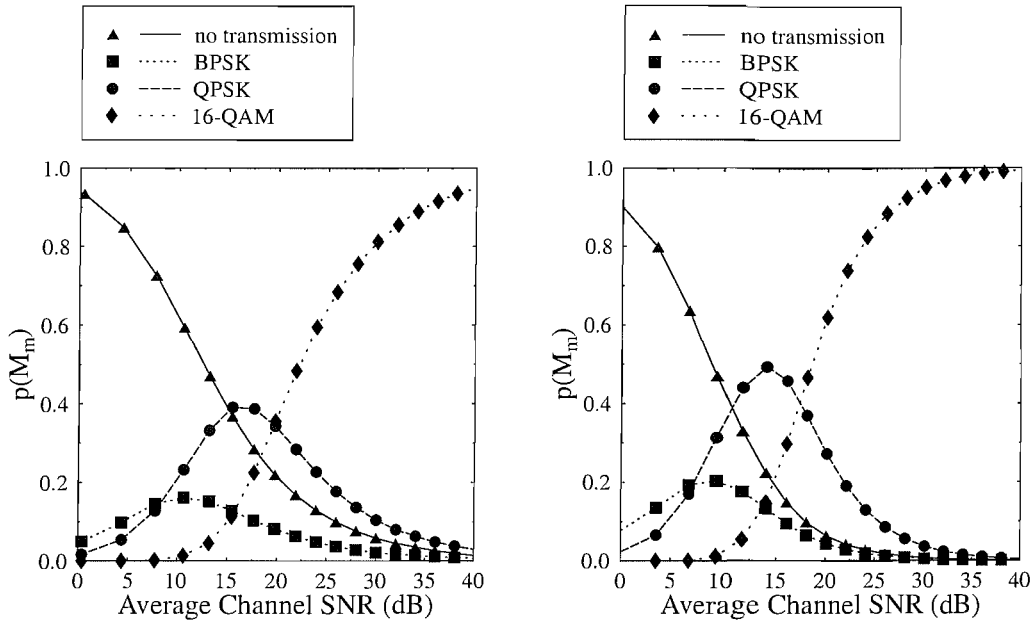

(a) 16 subbands

(b) subcarrier-by-subcarrier

Figure 1.21: Histograms of various AOFDM modulation modes versus channel SNR for the 10^{-4} target BER employing the (a) 16-subband, and (b) subcarrier-by-subcarrier for the 512-subcarrier AOFDM modem communicating over the Rayleigh fading time dispersive channel model of Figure 1.8 using the switching thresholds of Table 1.2.

quality varies across the different subcarriers. For subband adaptive OFDM, the lowest quality subcarrier in the subband is chosen for determining the modulation scheme for the particular subband. The performance of the 16 subband adaptive system communicating over the shortened WATM Rayleigh fading channel of Figure 1.8 is shown in Figure 1.20. The results show the typical behaviour of a variable throughput adaptive OFDM system, which strikes a trade-off between the best achievable BER and the highest throughput performance. For low SNRs, the system transmits a number of bits only when the channel conditions allow the modem to achieve a low BER. However, as the SNR increases, the achievable throughput also increases without significant change in the BER encountered. Finally, at high SNRs the BER drops, as the throughput approaches its modem-mode dependant maximum determined by the BER of the highest throughput modem mode.

Figure 1.21 shows the long-term modulation mode histograms for a range of channel SNR values using the modem-mode switching level set derived for BER = 10^{-4} in both the 16 subband and the subcarrier-by-subcarrier adaptive modems using the switching

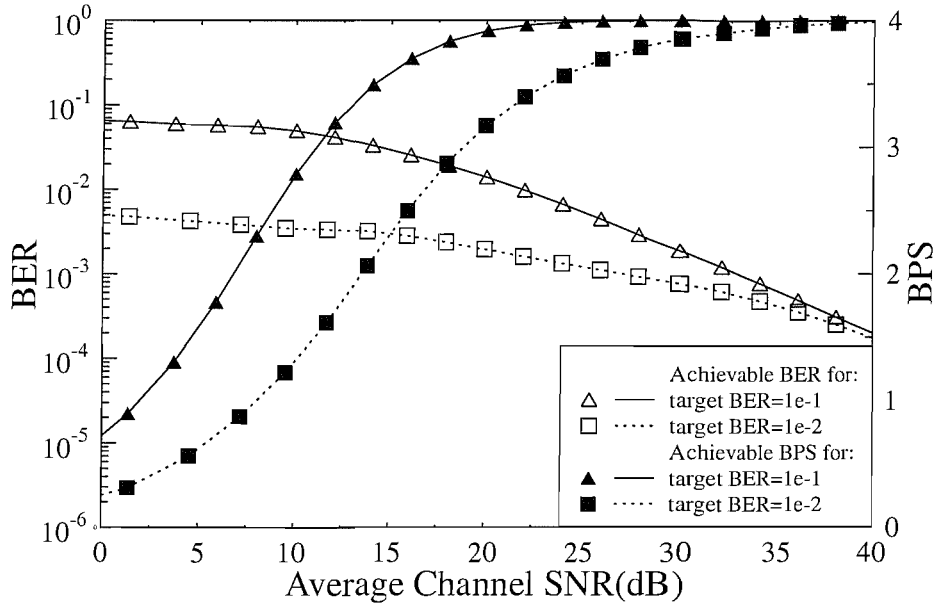

Figure 1.22: BER and BPS throughput performance of 512-subcarrier employing the subband-BER estimator based adaptive algorithm communicating over the Rayleigh fading time dispersive channel model of Figure 1.8.

thresholds of Table 1.2. Comparison of the graphs shows that the higher-order modulation modes are used more frequently by the subcarrier-by-subcarrier adaptation algorithm. The throughput penalty imposed by employing subband adaptation depends on the rate of frequency domain variation of the channel transfer function, because the more rapid the channel quality fluctuations, the higher the number of subbands required for avoiding a substantial channel quality variation within the subbands. Let us continue our discourse by considering the subband-BER estimation based adaptation algorithm.

1.3.1.2 Subband-BER estimator based adaptation algorithm

In the previous subsection we have seen that the employment of the fixed switching level based algorithm leads to a throughput performance penalty, if used in a subband adaptive OFDM modem. This is due to the fact that we choose the lowest-quality subcarrier in the subband for determining the modem modes in an effort not to exceed the target BER. An alternative scheme is to take into account the variation of the SNR values across the subcarriers, although this was not investigated here. For each subband, the modulation mode having the highest throughput, whose estimated BER is lower than a given target

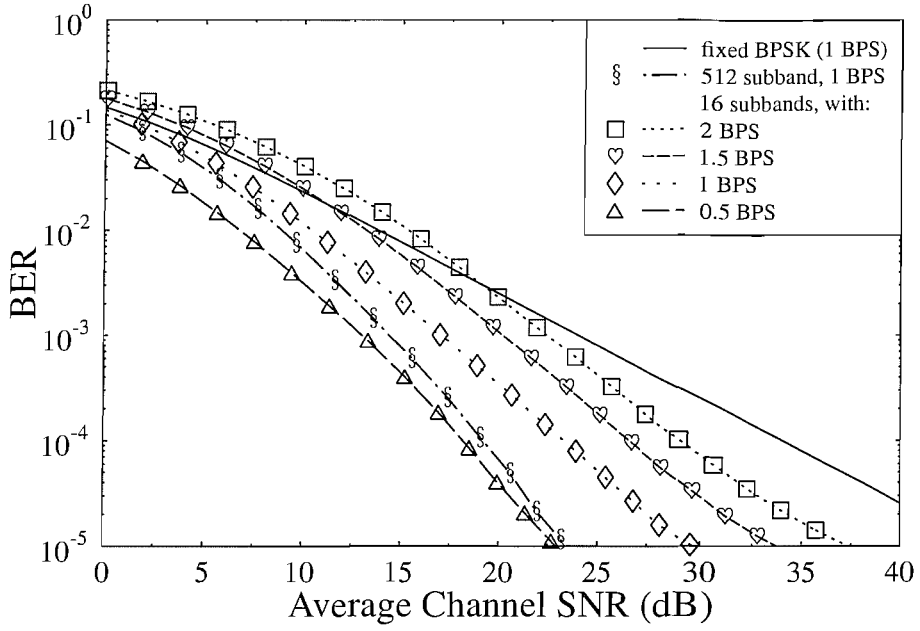

Figure 1.23: BER versus SNR performance for the 512-subcarrier, 16-subband constant-throughput adaptive OFDM modem employing "no transmission", BPSK, QPSK and 16-QAM communicating over the Rayleigh fading time dispersive channel model of Figure 1.8 for 0.5, 1, 1.5 and 2 BPS effective target throughput.

BER threshold is then chosen. Figure 1.22 shows the BER and throughput performance for the 16-subband adaptive OFDM scheme employing the BER estimator algorithm of [5] for the Rayleigh fading time dispersive channel model of Figure 1.8. Let us now review the constant-throughput adaptive OFDM (AOFDM) philosophy.

1.3.1.3 Constant-throughput adaptive OFDM

The constant-throughput adaptive OFDM scheme exploits the frequency selectivity of the channel, while endeavouring to maintain a constant bit rate. The modulation mode allocation of the subbands is performed on the basis of a cost function, which is explained in detail in [4]. This cost function is based on the expected number of bit errors in each subband. Figure 1.23 gives an overview of the BER performance of the fixed throughput 512-subcarrier OFDM modem communicating over the time dispersive channel model of Figure 1.8 for a range of target bit error rates. The curve without symbols represents the performance of a fixed-mode BPSK OFDM modem transmitting over the same channel, i.e where the modem transmits 1 bit using each data subcarrier in the OFDM symbol.

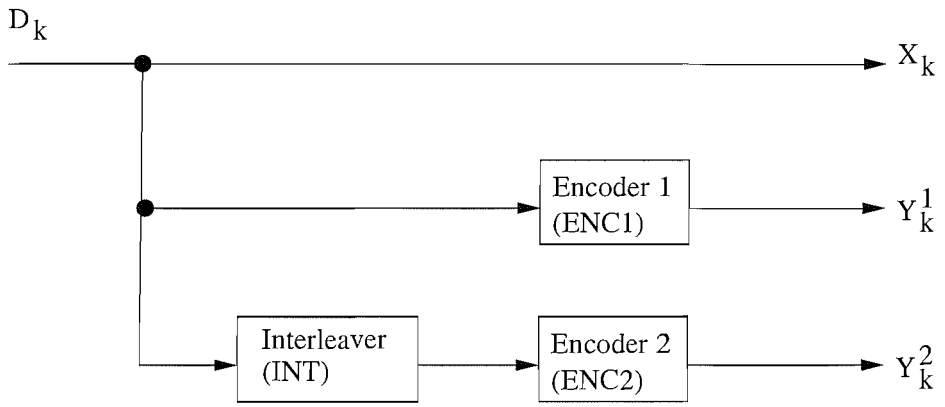

Figure 1.24: Generic turbo convolutional encoder.

We will now consider another scheme that is capable of enhancing the performance of an OFDM system, namely by the employment of forward error correction coding.

1.3.2 Forward error correction coding

In an OFDM system, the problem of intersymbol interference between consecutive OFDM symbols can be avoided by incorporating a cyclic prefix. However, in a dispersive multipath fading channel, exemplified by the WATM FDCHTF of Figure 1.7(a) some subcarriers of an OFDM signal may be completely obliterated owing to deep frequency-domain fades. Hence, even though most subcarriers may be detected without errors, the overall average BER is likely to be largely dominated by the subcarriers having the smallest amplitudes. In order to avoid this detrimental effect of the weakest subcarriers, the employment of forward error correction coding is essential in OFDM modems. Numerous error-correcting codes had been applied to OFDM, such as convolutional codes [28, 59], Reed-Solomon codes [60, 61], Turbo Convolutional (TC) codes [62, 63], and so on. Recently, Low-density Parity Check (LDPC) codes also enjoyed a renaissance as attractive forward-error correction coding techniques. Next we will briefly review two of the most powerful codes, namely TC codes in Section 1.3.2.1 and LDPC codes in Section 1.3.2.2.

1.3.2.1 Turbo convolutional codes

Turbo codes were proposed in [64], which are constituted by the parallel concatenation of two recursive systematic convolutional codes. Since then, the term "turbo codes" has been extended to different iteratively detected concatenated schemes.

Code	Code Rate	Puncturing Pattern
TC(2,1,4)	0.50	10,01
TC(2,1,4)	0.67	1000,0001
TC(2,1,4)	0.75	100000,000001
TC(2,1,4)	0.83	1000000000,0000000001

Table 1.3: Puncturing pattern for the TC(2,1,4) turbo code [66].

An example of the TC encoder is shown in Figure 1.24. The first block of data will be encoded by the ENC1 block, which represents a half-rate recursive systematic encoder [65]. The same block of bits is interleaved by the interleaver INT, and encoded by the second encoder, ENC2 which is also a half-rate systematic recursive encoder. The main purpose of using an interleaver is to increase the minimum distance of the turbo code.

Ignoring the encoding delay of each block, we may assume that both encoders will produce the output data simultaneously, resulting in a rate 1/3 turbo code. The two encoders do not have to be identical. The parity bits can be punctured, in order to arrive at higher coding rates. Various puncturing patterns are as shown in Table 1.3, which are based on the puncturing approach proposed by Acikel *et al.* in [66].

The optimum decoding of TCs is the maximum likelihood decoding algorithm applied to the turbo codes trellis structure [67]. However, due to the interleaver embedded in the turbo encoder, the turbo code trellis will have an extremely high number of states. This fact renders the employment of the maximum likelihood decoding process unrealistic practice for large interleaver sizes [65]. A more practical approach is constituted by the employment of an iterative decoding approach, where the maximum likelihood decoding algorithm is applied to the constituent convolutional codes of the TC [67].

It has been shown that TC codes are capable of achieving a low BER and approach the Shannonian limit [65]. Their performance is always better than that of convolutional codes having a similar complexity [65]. Various TCs have been applied to OFDM for example in [62,63]. For more details on TC codes the motivated reader is referred for example to [67].

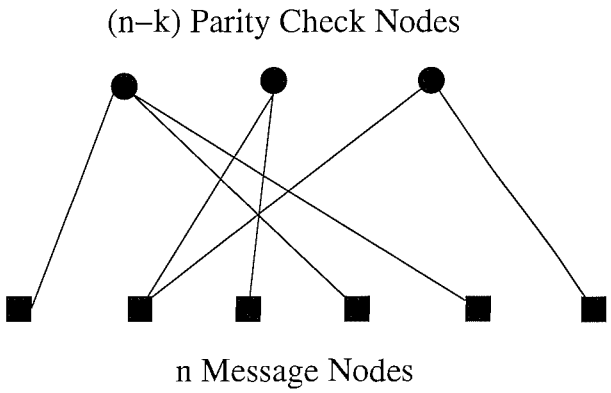

Figure 1.25: Factor graph representation of the LDPC code's parity-check matrix.

1.3.2.2 Low-density parity-check codes

Low-density parity-check (LDPC) codes were proposed by Gallagher as early as 1962 [68]. In spite of their excellent properties, LDPC codes have been dormant for about thirty years. It was demonstrated that the performance of LDPC codes is close to the Shannon limit, while maintaining a decoding complexity, which may be lower than that of TCs, as it will be argued in Section 1.3.3.3. Moreover, the performance of TC codes is highly dependent on the interleaver size, the interleaver design, the constituent codes, and on the number of iterations [65], which motivates the study of LDPC codes.

LDPC codes are defined as codes using a sparse parity-check matrix having a fixed number of logical ones per column (column weight) and similarly a fixed number of logical ones per row (row weight), both of which are low compared to the block length. LDPC codes can be defined by an $m \times n$-dimensional parity-check matrix, encoding k information bits by concatenating $m = n - k$ parity bits. The resultant code rate is $R = k/n$ [68–70].

Representatives of the family of LDPC codes can be decoded by using the decoding algorithm referred to as the sum-product algorithm (SPA) or belief propagation decoder [68, 69]. Another decoding method, namely the Parity Likelihood Ratio Algorithm (PLRA) was introduced by Ping *et al.* in [71]. Both, the performance of the SPA and PLRA methods is similar, when using a perfect arithmetic, but the latter is less sensitive to the quantisation effects imposed by finite word length implementations.

These codes have been shown to exhibit a better codeword error performance than turbo codes, because the minimum distance of an LDPC code tends to increase proportionally to the codeword length. At the same time, a longer erroneous codeword typically inflicts a

higher number of bit errors than shorter LDPC codes. Nonetheless, the lower codeword error probability is advantageous in many applications. An example of a parity-check matrix, $\mathbf{C}$, is shown below:

$$\mathbf{C} = \begin{array}{c} \overset{\longleftarrow \quad n \quad \longrightarrow}{\left[\begin{array}{cccccccccc} 0 & 1 & 1 & 0 & 0 & 0 & 1 & 0 & 0 & 1 \\ 1 & 0 & 0 & 0 & 1 & 1 & 0 & 1 & 0 & 0 \\ 0 & 0 & 0 & 1 & 0 & 1 & 0 & 1 & 1 & 0 \\ 0 & 1 & 0 & 1 & 0 & 0 & 1 & 0 & 0 & 1 \\ 1 & 0 & 1 & 0 & 1 & 0 & 0 & 0 & 1 & 0 \end{array}\right]} \begin{array}{l} \uparrow \\ \\ \\ n-k \\ \downarrow \end{array} \end{array} \tag{1.11}$$

Many researchers have explored the inclusion of LDPC codes in OFDM systems. For example in [70, 72, 73], Futaki and Ohtsuki have proposed LDPC coded OFDM (LDPC-COFDM) systems for improving the achievable BER of OFDM systems communicating in multipath fading channels. Other experiments have also been conducted by Lu *et. al* [42], Gruenbacher *et. al* [74, 75], Li *et. al* [76], Yoshimochi *et. al* [77], Niu *et. al* [78] and Mannoni *et. al* [79]. Further details on LDPC-coded OFDM may be found in [70].

Let us now continue by considering another way of enhancing the performance of an OFDM system, namely by exploiting the benefits of having space and time diversity in the following section.

1.3.3 Space-time block coded OFDM

In an effort to support high data rate transmissions in mobile communications environments, the bit per symbol capacity of band-limited wireless channels can be increased by employing multiple transmitter and receiver antennas [80]. In the past different transmit diversity techniques have been proposed in the literature for example in [30, 81–83]. One of the most remarkable advancement in this area is constituted by space-time block coding (STBC) proposed by Alamouti in [81], a philosophy which was further generalised by Tarokh *et al.* in [82]. A specific limitation of STBC schemes is however that their performance gain erodes, if the channel becomes dispersive. This deficiency has been circumvented by embedding STBC codes into OFDM modems upon mapping the two consecutive time-slots of the original STBC scheme [82] to two adjacent subcarriers, which typically experience narrowband fading [67].

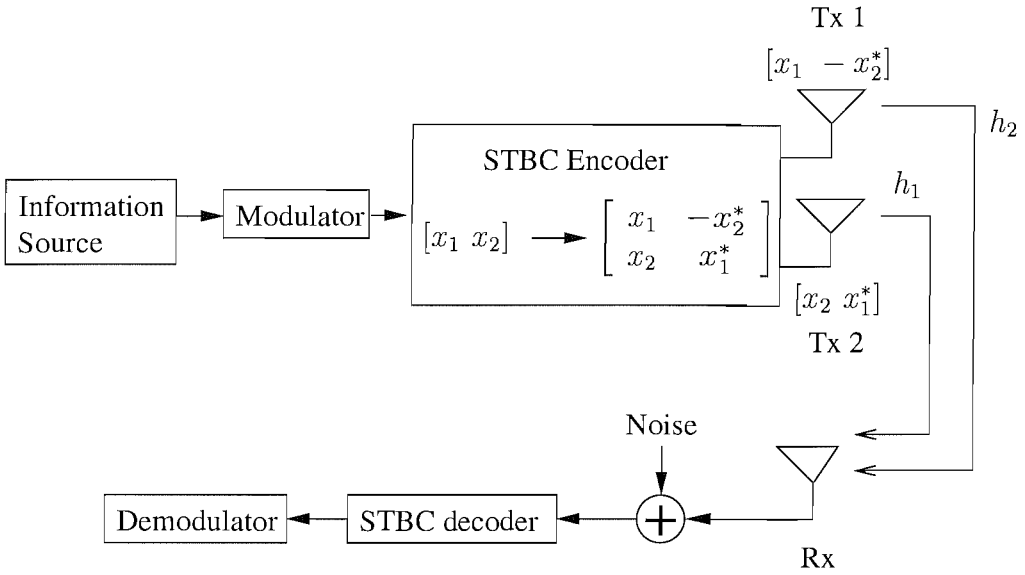

Figure 1.26: The encoding and decoding part of the STBC system.

In this section, we will investigate the benefits of space-time block codes, especially those of Alamouti's G_2 STBC in an OFDM environment. We will begin with an introduction of STBC OFDM in Section 1.3.3.1. We will then demonstrate the advantages of incorporating both the G_2 STBC and LDPC codes in an OFDM system in Section 1.3.3.2. Finally, we will estimate the decoding complexity of LDPC-based STBC OFDM in Section 1.3.3.3.

1.3.3.1 Introduction to STBC OFDM

Space-time block coded (STBC) OFDM constitutes a promising scheme for employment in future wideband multimedia wireless communications systems, which integrate channel coding, modulation and multiple antennas for the sake of achieving a high performance in fading channels [32,81,82]. Since OFDM is capable of effectively mitigating the ISI induced by multipath fading channels, the combination of STBC and OFDM promises an enhanced performance in terms of reduced SNR requirements, when communicating in wideband wireless channels. Table 1.4 shows the history of STBC and the evolution of STBC research in OFDM environments.

Again, the simplest form of space-time block codes was proposed by Alamouti in [81], which is a simple twin-transmitter-based scheme. This scheme is the first space-time block code contrived for providing full transmit diversity for systems equipped with two transmit

Year	Author	Contribution
'98	Alamouti [81]	A simple transmit diversity technique designed for wireless communications, where the STBC G_2 is one of the proposed techniques.
	Agrawal, Tarokh, Naguib and Seshadri [82]	Space-time coded OFDM for high data-rate wireless communication over wideband channels.
'99	Tarokh, Jafarkhani and Calderbank [84–86]	Performance results of space-time block coding for wireless communications.
'01	Uysal, Al-Dhahir and Georghiades [83]	A space-time block-coded OFDM scheme for unknown frequency selective fading channels.
	Blum, Yan, Li and Winters [30, 87]	Improved techniques for 4 transmit and 4 receive antenna aided MIMO-OFDM for wireless communications. A pair of two transmitter antennas is used in parallel for space-time block coding.
	Li, Winters and Sollenberger [88]	Signal detection for MIMO-OFDM wireless communications using the classical MMSE and ZF.
	Liew and Hanzo [89]	Space-time block coding aided by adaptive modulation in an OFDM environment.
'02	Hanzo, Liew and Yeap [67]	A comprehensive book compiling information on turbo coding, turbo equalisation as well as space-time coding.
	Lu, Wang and Li [41]	Iterative receivers for space-time block-coded OFDM systems operating in dispersive fading channels.
	Lee and Williams [90]	Bandwidth efficient OFDM transmitter diversity techniques.
	Yue and Gibson [91]	Performance of a space-time block coded OFDM system.
	Suto and Ohtsuki [92]	Performance evaluation of space-time-frequency block codes over frequency selective fading channels.
	Panayirci and Cirpan [93]	Channel estimation for space-time block-coded OFDM systems in the presence of multipath fading.
'03	Vucetic and Yuan [94]	An exhaustive treatise on space-time coding.
	Liang and Wu [95]	Channel estimation based on pilot subcarriers in space-time block-coded OFDM systems.
	Torabi and Soleymani [96]	Adaptive bit allocation for space-time block coded OFDM systems.
	Paulraj, Nabar and Gore [80]	Another textbook on space-time wireless communications.

Table 1.4: Contributions on STBC-OFDM

Time slot, T	antenna Tx 1	antenna Tx 2
1	x_1	x_2
2	$-x_2^*$	x_1^*

Table 1.5: The encoding and transmission process for the G_2 space-time block code.

antennas. The transmission matrix is defined as [81]:

$$G_2 = \begin{pmatrix} x_1 & x_2 \\ -x_2^* & x_1^* \end{pmatrix} \tag{1.12}$$

We can see from the matrix of Equation 1.12 that there are two columns, which represent the number of transmitters, p. There are also $k = 2$ input symbols, namely x_1 and x_2, and the code spans over $n = 2$ time slots corresponding to the number of rows. The signals x_1^* and x_2^* represent the complex conjugate of x_1 and x_2, respectively. Since k and n are equal, the code rate, $R = k/n$ is unity. The associated encoding and transmission process is depicted in Figure 1.26 and in Table 1.5. For further details on the encoding and decoding processes of the G_2 STBC, the users are referred to [67, 81, 94].

Figure 1.27 portrays the BER performance of a 512-subcarrier OFDM modem using a G_2 STBC employing multiple receive antennas, when communicating over an equal-power two-path channel, where the Channel Impulse Response (CIR) taps are separated by a delay spread of $5\mu s$. The maximum Doppler frequency was 200 Hz. All multipath components undergo independent Rayleigh fading and the receiver has a perfect knowledge of the CIR. We can see from the figure that upon increasing the number of receivers we can significantly improve the achievable BER performance. However, this BER improvement is achieved at an increased complexity.

In [97], Liew *et al.* has carried out a comparative study of concatenated TCs and STBCs as well as Space-Time Trellis coded (STTC) OFDM. The schematic of the system is shown in Figure 1.28. At the transmitter, the information source generates random information data bits. The information bits are then encoded by TC codes [64], Reed Solomon (RS) codes [60] or left uncoded. Only the TC coded bits are channel interleaved and the output bits are then passed to the STBC or STTC encoder. At the receiver, the signal of each receive antenna is OFDM demodulated. The demodulated signals are then fed to the STTC or STBC decoder. The space-time decoders apply the Logarithmic Maximum

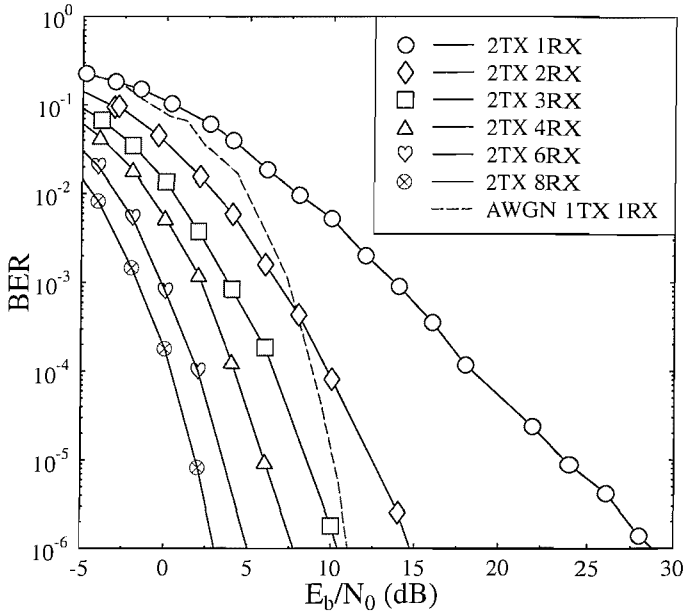

Figure 1.27: BER performance of the space-time block code G_2 in conjunction with various numbers of receivers. The transmitted framelength of all schemes was 512 bits and a channel having a CIR characterised by two equal-power rays separated by a delay spread of 5μs was used. The maximum Doppler frequency was 200Hz.

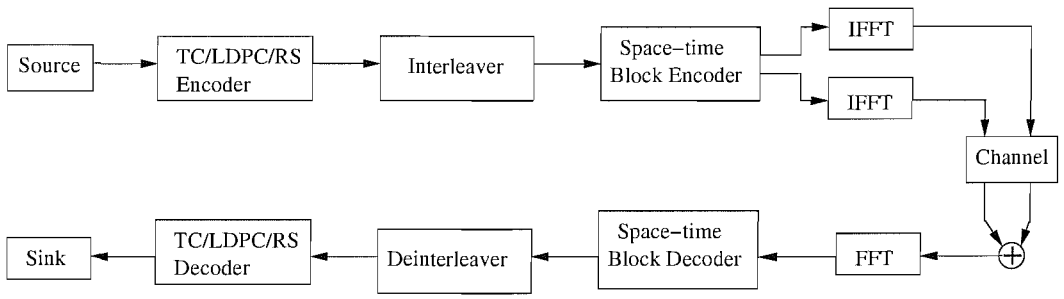

Figure 1.28: Schematic of the concatenated forward error correction coding and STBC aided OFDM system.

Code	TC(2, 1, 4)
Octal Generator polynomial	13,15
No. of trellis states	8
Decoding algorithm	Log-MAP

Table 1.6: Parameters of the TC(2, 1, 4) codec.

A-Posteriori (Log-MAP) decoding algorithms for providing soft-outputs to the channel decoder. If no channel codecs are employed by the system, the space-time decoders apply the Viterbi Algorithm (VA), which provides a slightly lower performance compared to the MAP decoder, but at a lower complexity.

The results of these performance comparisons are as shown in Figure 1.29 and Figure 1.30 for the effective throughputs of 2 and 3 Bits per Symbol (BPS), respectively, using the space-time block code G_2 in conjunction with one receiver antenna. We can see that in both cases the space-time block code G_2 concatenated with TC coding performs better than the unprotected space-time trellis codes. The associated performance difference can be clearly seen in terms of the FER, especially in the context of the 3 BPS effective throughput, where the STBC G_2 concatenated with TC coding outperforms the nearest competitor by almost 10 dB at an FER of 10^{-3}.

1.3.3.2 LDPC-based space-time coded OFDM

In this section, we provide our simulation results for the various space-time coded QPSK modulated OFDM schemes [67] protected by both TC and LDPC coding, while using 128 subcarriers. We employed the TC(2,1,4) code [67] using the parameters shown in Table 1.6. Each OFDM symbol has a duration of $160\mu s$ and a cyclic prefix of $40\mu s$ duration. In these simulations, the Jakes model was adopted for modelling the fading channels [50]. Again, we assume an equal-power two-path Channel Impulse Response (CIR), where the CIR taps are separated by a delay spread of $5\mu s$. The maximum Doppler frequency was 200 Hz. All multipath components undergo independent Rayleigh fading and the receiver has a perfect knowledge of the CIR. The simulation results will be shown in terms of the effect of varying the coding rates in Section 1.3.3.2.1, the influence of the code length in Section 1.3.3.2.2 and the effect of the number of iterations in Section 1.3.3.2.3.

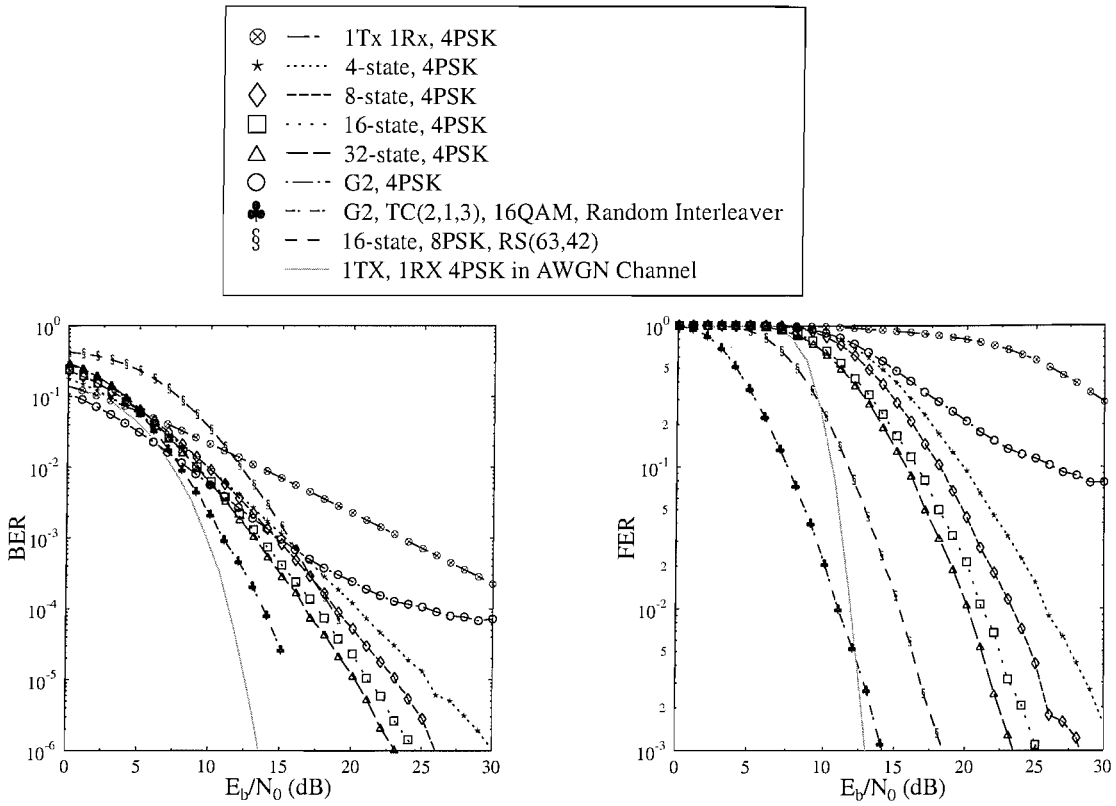

(a) BER against Eb/N

(b) FER against Eb/No

Figure 1.29: BER and FER performance of various 4PSK space-time trellis codes and the space-time block code G_2 concatenated with the TC(2,1,3) code using one receiver, while maintaining an effective throughput of 2 BPS. The transmitted framelength of all schemes was 512 bits and a channel having a CIR characterised by two equal-power rays separated by a delay spread of $5\mu s$ was used. The maximum Doppler frequency was 200Hz. The OFDM scheme has 512-subcarriers [67].

1.3.3.2.1 Effects of various coding rates Let us now compare the achievable performance of the LDPC and TC channel coding schemes at different coding rates. As mentioned in Section 1.3.2.2, the code rate R of the LDPC codes can be calculated as $R = k/n$, where k is the difference between the number of columns and rows of the parity check matrix, and n is the number of columns of the matrix determining the block length of the code. Different LDPC code rates can be readily created by adjusting the value of k and n.

On the other hand, for TC we have to specify the correct puncturing pattern in order to produce the required code rates. The puncturing patterns used in our simulations are shown in Table 1.3, which are based on the puncturing approach proposed by Acikel *et al.*

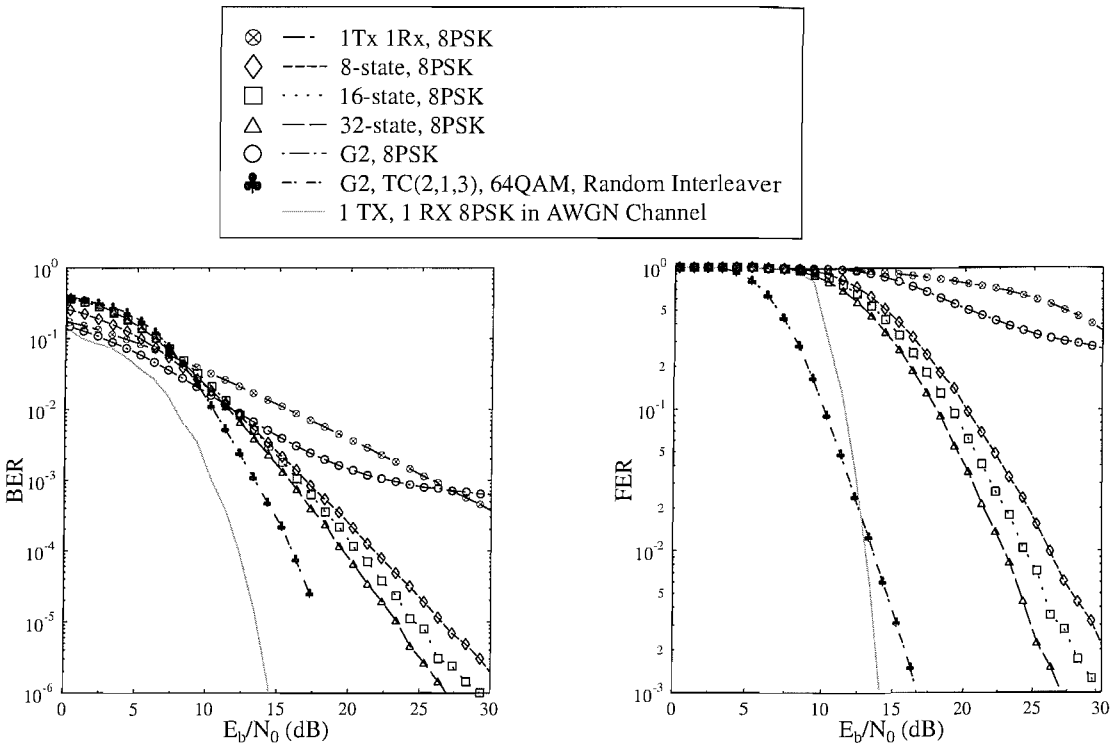

(a) BER against Eb/N

(b) FER against Eb/No

Figure 1.30: BER and FER performance of various 8PSK space-time trellis codes and the space-time block code G_2 concatenated with the TC(2,1,3) code using one receiver, while maintaining an effective throughput of 3 BPS. The transmitted framelength of all schemes was 512 bits and a channel having a CIR characterised by two equal-power rays separated by a delay spread of $5\mu s$ was used. The maximum Doppler frequency was 200Hz. The OFDM modem had 512 subcarriers [67].

in [66]. Clearly, it is more straightforward to produce arbitrary code rates for LDPC codes compared to TCs.

The results of our simulations using QPSK and 16-QAM are shown in Figure 1.31 and Figure 1.32 in terms of the achievable BER and FER, respectively. We can see from these figures that the LDPC code has a similar BER performance to the TC, but slightly outperforms the TC in terms of the achievable FER, as the coding rate increases. From Figure 1.31 we can infer the effective Bits per Symbol (BPS) versus E_b/N_0 performance at BER = 10^{-6}. The corresponding results are shown in Figure 1.33. We observe that the performance of the LDPC code surpasses that of the TCs, when the effective BPS throughput becomes higher than approximately 1.5 in conjunction with QPSK and 3.2 for 16-QAM, respectively.

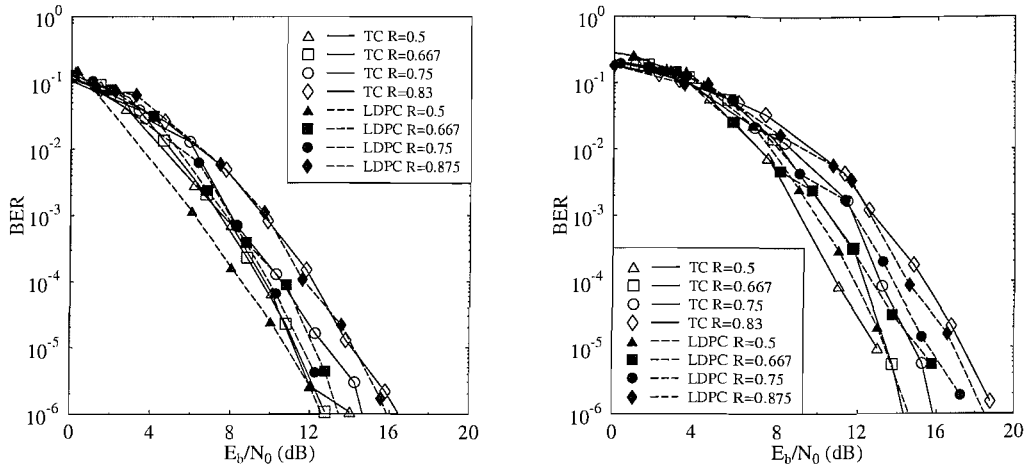

(a) QPSK (b) 16-QAM

Figure 1.31: BER versus E_b/N_0 performance using TC and LDPC codes having various coding rates using G_2 space-time block coded (STBC) OFDM and one receiver antenna for a) QPSK and b) 16-QAM. The transmission frame length of all schemes was 512 bits and a channel having a CIR characterised by two equal-power rays separated by a delay spread of 5μs. The maximum Doppler frequency was 200Hz.

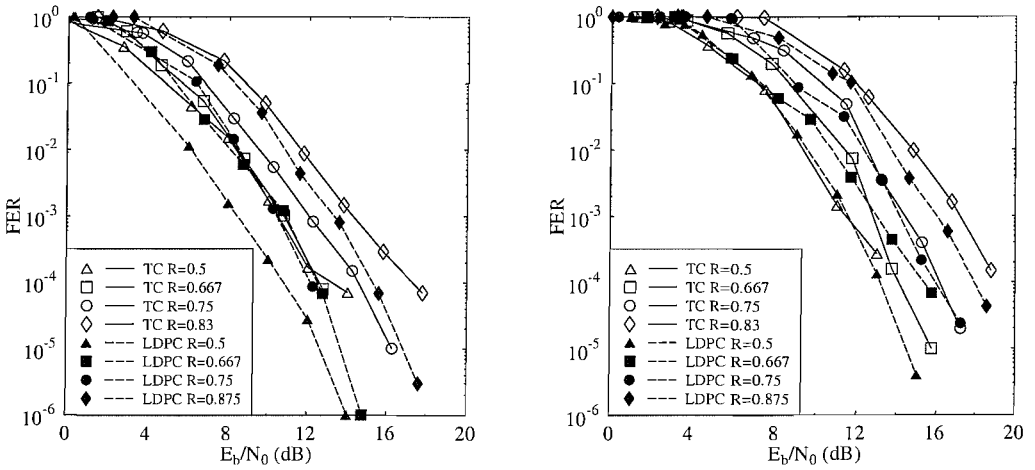

(a) QPSK (b) 16-QAM

Figure 1.32: FER versus E_b/N_0 performance using TC and LDPC codes at various coding rates using G_2 space-time block code (STBC) OFDM and one receiver antenna for a) QPSK and b) 16-QAM. The transmission frame length of all schemes was 512 bits and a channel having a CIR characterised by two equal-power rays separated by a delay spread of 5μs. The maximum Doppler frequency was 200Hz.

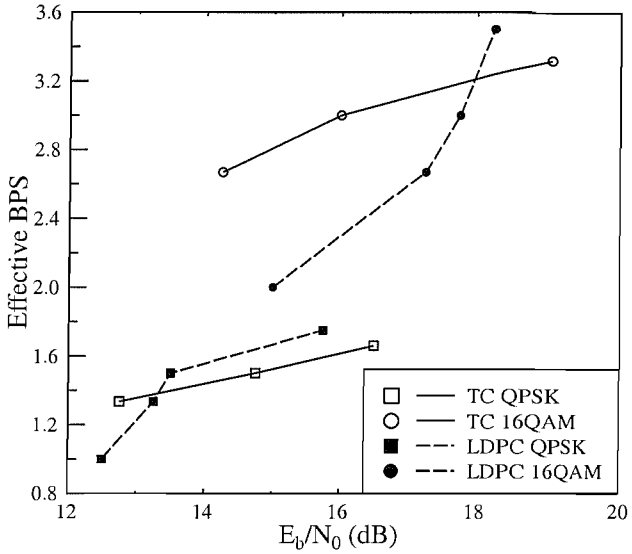

Figure 1.33: Effective BPS throughput versus E_b/N_0 using TC and LDPC codes having various coding rates employing the STBC G_2 and one receiver antenna in an OFDM system at BER $= 10^{-6}$. A channel having a CIR characterised by two equal-power rays separated by a delay spread of 5μs was used. The maximum Doppler frequency was 200Hz.

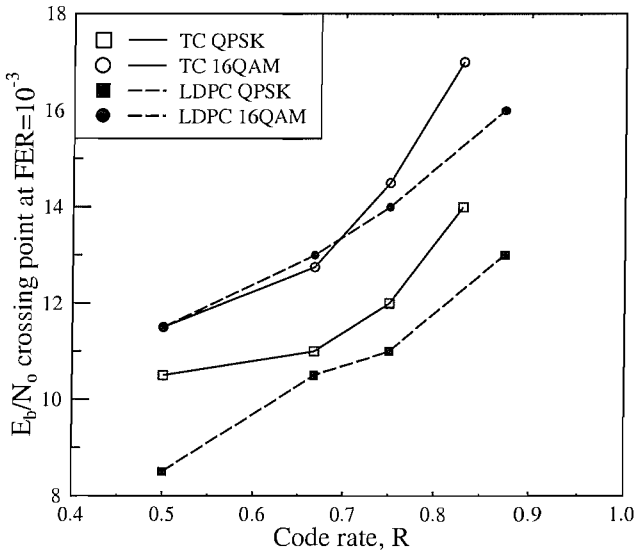

Figure 1.34: E_b/N_0 crossing point at FER $= 10^{-3}$ versus the coding rate for TC and LDPC coding using the STBC G_2 and one receiver antenna in a QPSK and 16-QAM OFDM system. A channel having a CIR characterised by two equal-power rays separated by a delay spread of 5μs was used. The maximum Doppler frequency was 200Hz.

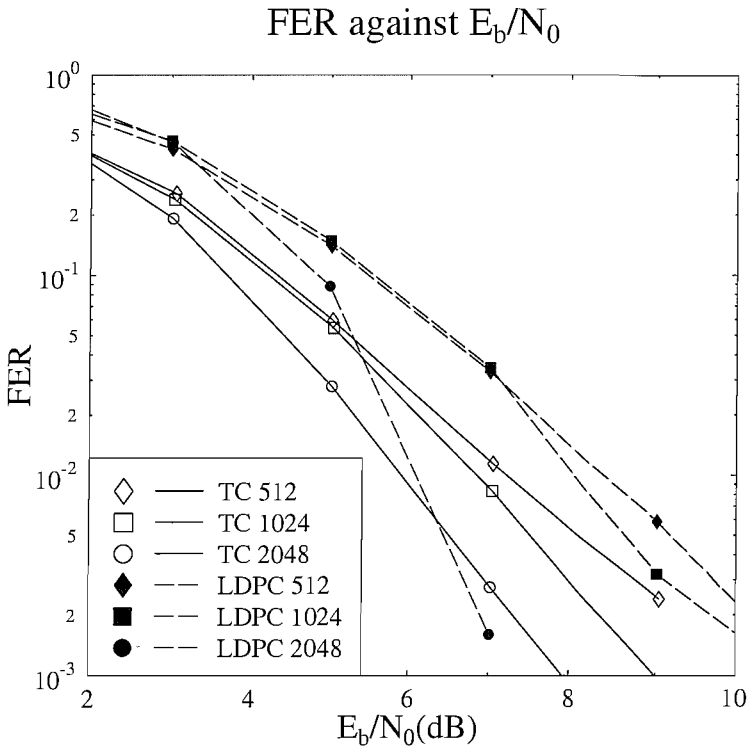

Figure 1.35: FER versus E_b/N_0 performance in conjunction with different input block lengths for both the half-rate TC and LDPC codes employing eight iterations concatenated with the STBC G_2 using one receiver and a 128-subcarrier QPSK modulated OFDM modem. The CIR was characterised by two equal-power rays separated by a delay spread of $5\mu s$. The maximum Doppler frequency was 200Hz. The length of the turbo interleaver was half of the channel interleaver, which resulted in the same overall system latency or delay.

From Figure 1.32 we can also extract a plot of the E_b/N_0 values required for maintaining FER = 10^{-3} versus the code rate. The corresponding plot is featured in Figure 1.34. This plot shows that LDPC codes may require lower values of E_b/N_0 for reaching an FER value of 10^{-3} compared to TCs.

1.3.3.2.2 Effects of the code length The codeword length of the codes was also varied for the sake of investigating the effects of various coding delays on the performance of the system. In these investigations the number of iterations used by both the TC and LDPC codes was fixed to eight, the modulation scheme used was QPSK, and the code rate was 0.5 for both the TC and LDPC codes. In Figure 1.35 we can see that the FER of the LDPC code becomes lower than that of the TC code, when we increase the input block length.

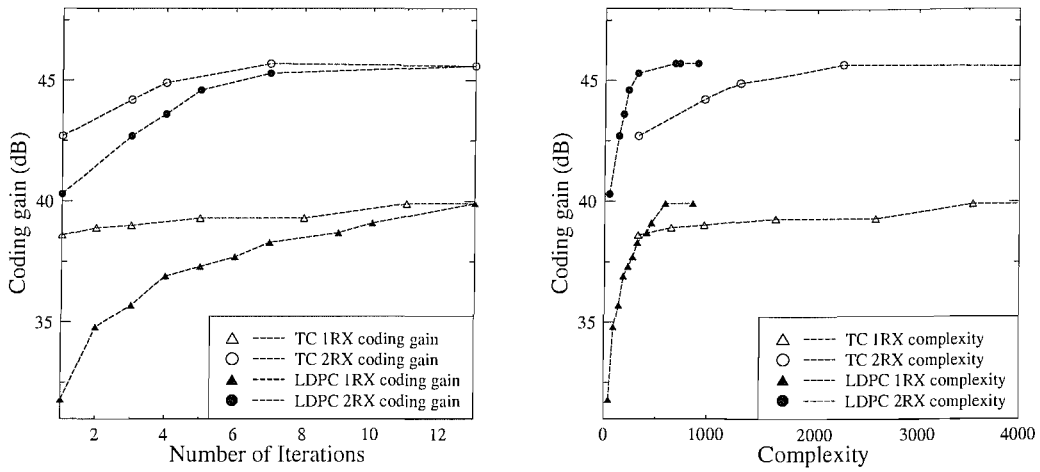

(a) (b)

Figure 1.36: Coding gain extracted from the FER versus E_b/N_0 curves at FER = 10^{-3} as a function of (a) the number of iterations and (b) versus estimated complexity for the half-rate TC and LDPC coded STBC G_2 OFDM scheme using one or two receiver antennas and a 128-subcarrier QPSK OFDM modem for transmission over a channel having a CIR characterised by two equal-power rays separated by a delay spread of 5μs. The maximum Doppler frequency was 200Hz.

1.3.3.2.3 Effects of the number of iterations In Figure 1.36(a), we characterise the achievable coding gain of both LDPC codes and TCs, when different number of iterations are used. The achievable coding gain was defined here as the E_b/N_0 difference — expressed in decibels (dB) at FER= 10^{-3} — between the proposed schemes and the uncoded single-transmitter, single-receiver system having the same effective throughput. In the case of Figure 1.36(a) the TC and LDPC codeword length has been fixed at 512 bits, the modulation scheme used is QPSK and the code rate is fixed at 0.5. We can see from the figure that for a single receiver antenna based system the LDPC code performs less well at a low number of iterations, although its performance eventually reaches that of the TC after about 12 iterations. It also has to be mentioned that an LDPC iteration is typically less complex than a TC iteration, as it will be shown in quantitative terms in Section 1.3.3.3 and argued with reference to Figure 1.36(b).

1.3.3.3 Decoding complexity

TC(n,k,K) Complexity: Let us now consider the decoding complexity of the TC(2,1,4) scheme utilising the binary Log-MAP decoder [67]. Briefly, the *a posteriori* probability of a binary information bit u_t, $t \in \{0, \ldots, N-1\}$, given the received coded bit sequence of $\mathbf{y} = \{y_0, \ldots, y_{Nn-1}\}$, where N is the number of n-bit coded symbols, can be computed as follows [67]:

$$\mathbf{Pr}\{u_t = \pm 1|\mathbf{y}\} = \sum_{\substack{(\grave{s},s)\Rightarrow \\ u_t=\pm 1}} \beta_t(s) \cdot \alpha_{t-1}(\grave{s}) \cdot \gamma_t(\grave{s}, s), \tag{1.13}$$

where $(\grave{s}, s) \Rightarrow u_t = \pm 1$ indicates the specific set of trellis transitions emerging from the previous trellis state $S_{t-1} = \grave{s}$ to the present state $S_t = s$ that can be encountered, when the information bit is $u_t = \pm 1$. Furthermore, $\alpha_t(s)$, $\beta_{t-1}(\grave{s})$ and $\gamma_t(\grave{s}, s)$ are the forward recursion, backward recursion and branch transition metric, respectively [67]. The Log Likelihood Ratio (LLR) of $\mathbf{Pr}\{u_t = \pm 1|\mathbf{y}\}$ can be computed as [67]:

$$L(u_t|\mathbf{y}) = \ln\left(\frac{\mathbf{Pr}\{u_t = +1|\mathbf{y}\}}{\mathbf{Pr}\{u_t = -1|\mathbf{y}\}}\right). \tag{1.14}$$

Explicitly, we have

$$\alpha_t(s) = \sum_{\text{all } \grave{s}} \gamma_t(\grave{s}, s) \cdot \alpha_{t-1}(\grave{s}) \tag{1.15}$$

$$\beta_{t-1}(\grave{s}) = \sum_{\text{all } s} \beta_t(s) \cdot \gamma_t(\grave{s}, s) \tag{1.16}$$

$$\text{and} \quad \gamma_t(\grave{s}, s) = \Pi_{t,u_t} \cdot \eta_t(\grave{s}, s). \tag{1.17}$$

Specifically, Π_{t,u_t} is the *a priori* information regarding the information bit u_t and

$$\eta_t(\grave{s}, s) = \exp\left(\frac{1}{2}\sum_{l=1}^{n} L(x_{nt+l}|\mathbf{y})x_{nt+l}\right), \tag{1.18}$$

where $x_{nt+1}, \ldots, x_{nt+n}$ are the legitimate transmitted coded bits corresponding to the information bit u_t, when a state transition from the previous trellis state $\grave{s}$ to the present state s occurred. Furthermore, $L(x_{nt+l}|\mathbf{y})$ is the LLR of x_{nt+l}, given the received coded bit sequence $\mathbf{y}$, which is obtained at the demodulator.

Let us now determine the complexity of the MAP decoder associated with evaluating $\mathbf{Pr}\{u_t = +1|\mathbf{y}\}$ based on Equation 1.13. In order to compute the term $\eta_t(\grave{s}, s)$ given $L(x_{nt+l}|\mathbf{y})$, we need $n+1$ multiplications and $n-1$ additions. Note that the exponential

function in the expression of $\eta_t(\grave{s}, s)$ is cancelled out, when the Log-MAP decoder is employed. When evaluating the term $\gamma_t(\grave{s}, s)$ using $\Pi_{t,a}$ and η_t, we need only one multiplication since there is only one trellis transition emerging from the previous trellis state $\grave{s}$ to the present state s that can be encountered, when the information bit is $u_t = +1$. As for α_t and β_t, each term requires S number of multiplications and $S-1$ number of additions, where we have $S = 2^{K-1}$ and K is the constraint length of the code. Finally, the evaluation of the term $\mathbf{Pr}\{u_t = +1|\mathbf{y}\}$ requires $2S$ number of multiplications and $S-1$ number of additions. Therefore, a total of $(n+1)+1+4S = 4S+n+2$ number of multiplications and $(n-1)+3(S-1) = 3S+n-4$ number of additions are required for computing $\mathbf{Pr}\{u_t = +1|\mathbf{y}\}$. However, we also have to calculate $\mathbf{Pr}\{u_t = -1|\mathbf{y}\}$ and compute the corresponding ratio in order to evaluate the LLR of Equation 1.14. Therefore, a total of $2(4S+n+2)+1 = 8S+2n+5$ number of multiplications/divisions and $2(3S+n-4)$ number of additions are required by one MAP decoder for decoding the binary information bit u_t. Since two MAP decoders are required in the TC decoder, which performs T number of turbo iterations for decoding a block of N information bits, the estimated complexity of the TC scheme per information bit per iteration is $2(8S+2n+5)$ multiplications/divisions plus $4(3S+n-4)$ number of additions.

When the log-MAP decoder is employed for the sake of reducing the computational complexity imposed, the multiplication/division operations are substituted by addition/subtraction operations in the logarithmic domain. Furthermore, the addition operation is substituted by the Jacobian sum operation [98], when it is carried out in the logarithmic domain. More specifically, each Jacobian sum consists of an addition, a subtraction, a table look-up and a maximum evaluation operation [98]. However, we can ignore the table lookup and max operations due to their comparably low complexity. As a result, the total complexity of the TC scheme per information bit per iteration in terms of the number of additions and subtractions is:

$$\begin{aligned} comp\{TC(n,1,K)\} &= 2(8S+2n+5)+4(3S+n-4) \\ &= 32(2^{K-1})+8n-6 \qquad (1.19) \\ &\quad \text{where} \quad S = 2^{K-1}. \end{aligned}$$

LDPC(j,k) Complexity: The decoding complexity per information bit per iteration of LDPC codes in conjunction with a parity check matrix having a column weight of j and a

Number of Iterations	TC(2,1,4)	LDPC
1	266	45
2	532	90
4	1064	180
8	2128	360

Table 1.7: Comparisons of decoding complexity for TC(2,1,4) and LDPC with column weight, k and row weight, j equals to 3.

row weight of k can be approximated in terms of the number of additions and subtractions, when operating in the logarithmic domain [99] as:

$$comp\{LDPC\} = (4k + j)j. \tag{1.20}$$

From Equation 1.19 and Equation 1.20, we can see that the complexity of decoding one bit in one iteration is lower in LDPC codes compared to TC codes. For the systems used in our simulations, the estimated complexity of a TC(2,1,4) code is calculated to be 322 using Equation 1.19. However, from Equation 1.20, the corresponding complexity of the LDPC code is just 45, since the column weight, k and row weight, j used were 3. As an example, a single TC(2,1,4) iteration has a similar complexity to about 7 LDPC iterations. Hence Figure 1.36(b) shows the achievable coding gain versus the estimated complexity of the TC(2,1,4) and LDPC codes for the same codelength. Similarly, Table 1.7 shows the complexity comparison of the TC(2,1,4) and LDPC codes for 1, 2, 4 and 8 iterations.

1.4 Chapter conclusion

In this chapter, we have provided a brief overview of OFDM systems. We commenced the chapter with a brief historical background on OFDM systems in Section 1.1. This was followed by a discussion on the basic OFDM system components in Section 1.2. The underlying basic OFDM concepts were presented in Section 1.2.1, followed by the performance characterisation of OFDM transmissions over Gaussian channels in Section 1.2.2. From the simulation results portrayed in Figure 1.5, it can be seen that these results closely match the theoretical BER performance of classic serial systems. We introduced the wideband channels that were used throughout the report in Section 1.2.3. Specifically, the two wideband channels that were used are the two-path Rayleigh fading channel and the wireless asynchronous transfer mode (WATM) channel, which were highlighted in Section 1.2.3.1 and

Section 1.2.3.2. In Section 1.2.4, a number of channel transfer function estimation techniques were presented, namely the perfect channel estimation scenario of Section 1.2.4.1, pilot symbol assisted channel estimation in Section 1.2.4.2, decision-directed channel estimation in Section 1.2.4.3 and blind channel estimation in Section 1.2.4.4. Another issue discussed was that of the OFDM signal amplitude PDFs in Section 1.2.5. We have briefly characterised the performance of the clipping amplifier in Section 1.2.5.1, focusing on its BER performance in Section 1.2.5.2.

We then continued with a discussion on some advanced OFDM systems that have been studied by other researchers in Section 1.3. The first advanced system of interest was the adaptive single-user OFDM scheme of Section 1.3.1. This adaptive algorithm can be implemented by using either the fixed threshold adaptation algorithm, the subband-BER estimator based algorithm or the constant-throughput adaptive algorithm of Section 1.3.1.1, Section 1.3.1.2 and Section 1.3.1.3, respectively. Another scheme capable of enhancing an OFDM system was channel coding. In Section 1.3.2, two of the most powerful FECs were highlighted, namely the turbo convolutional codes of Section 1.3.2.1 and the low-density parity-check codes of Section 1.3.2.2. The final advanced system that was discussed was based on exploiting both space and time diversity in Section 1.3.3. After introducing the STBC OFDM system in Section 1.3.3.1, we continued our discourse with the characterisation of an LDPC-based STBC OFDM system in Section 1.3.3.2. In particular, we investigated the effects of various coding rates, the impact of the code length and the influence of the number of iterations in Section 1.3.3.2.1, Section 1.3.3.2.2 and Section 1.3.3.2.3, respectively. We also estimated the decoding complexity of an LDPC-based STBC OFDM system and compared it to the TC-based STBC OFDM system in Section 1.3.3.3. It was shown that the LDPC assisted system is capable of performing as well as the TC-based system in terms of the achievable BER and FER, at a potentially lower implementational complexity.

In this chapter, we have restricted our attention to a single-user OFDM environment. However, in a multiuser mobile communication system, the effect of interference imposed by the other users will also have to be taken into account. There are other single-user topics that may be found in the literature such as frequency offset synchronisation [100–108], frequency domain equalisation [109–114], filterbank theory [115–117], interleaving [118,119], advanced modulation methods [120–127], spreading [128–130], interference cancellation [131–133]

and implementation issues [134–142]. Further discussions on peak-to-average power reduction [143–154], pilot-symbol assisted system [155–158], forward error correction coding [159–166], channel estimation [167–177] and multiple antenna implementation [178–198] are also among the popular topics that have been published in recent years. In the next chapter we will focus our attention on using a multiple-antenna aided system, namely Space Division Multiple Access (SDMA) for supporting multiple OFDM users. We will also investigate the novel family of minimum bit error rate SDMA MUDs designed for these multiuser OFDM systems.

Chapter 2

Minimum Bit Error Rate Multiuser Detection in Space Division Multiple Access Aided OFDM Systems

In Chapter 1, we have provided an overview of recent OFDM research. However, the systems discussed in Chapter 1 support only a single user. In a mobile communication system, a multiplicity of users has to be supported thus imposing interference on each other's signals. In this chapter we will consider the employment of multiple base station receiver antennas invoked for supporting multiple users. We will commence our discourse with a brief introduction to smart antennas in Section 2.1, followed by an overview of the so-called space division multiple access principle applied for supporting multiple users in the uplink by employing multiple antennas at the base-station. This is the topic of Section 2.2. The chapter will then proceed in Section 2.3 with the description of classical linear multiuser detectors employed in the SDMA system. Finally, in Section 2.4, we will propose a novel minimum bit error rate (MBER) multiuser detector for employment in an SDMA OFDM system.

Beamforming [199]	Typically $\lambda/2$-spaced antenna elements are used for the sake of creating a spatially selective transmitter/receiver beam. Smart antennas using beamforming have been employed for mitigating the effects of cochannel interfering signals and for providing beamforming gain.
Spatial Diversity [67] and Space-Time Spreading	In contrast to the $\lambda/2$-spaced phased array elements, in spatial diversity schemes, such as space-time block or trellis codes [67] the multiple antennas are positioned as far apart as possible, so that the transmitted signals of the different antennas experience independent fading, resulting in the maximum achievable diversity gain.
Space Division Multiple Access [5]	SDMA exploits the unique, user-specific "spatial signature" of the individual users for differentiating amongst them. This allows the system to support multiple users within the same frequency band and/or time slot.
Multiple Input Multiple Output Systems [200]	MIMO systems also employ multiple antennas, but in contrast to SDMA arrangements, not for the sake of supporting multiple users. Instead, they aim for increasing the throughput of a wireless system in terms of the number of bits per symbol that can be transmitted by a given user in a given bandwidth at a given integrity.

Table 2.1: Applications of multiple antennas in wireless communications.

2.1 Introduction to smart antennas

In recent years various smart antenna designs have emerged, which have found application in diverse scenarios, as seen in Table 2.1. The main objective of employing smart antennas is that of combating the effects of multipath fading on the desired signal and suppressing interfering signals, thereby increasing both the performance and capacity of wireless systems [201]. Specifically, in smart antenna assisted systems multiple antennas may be invoked at the transmitter and/or the receiver, where the antennas may be arranged for achieving spatial diversity, directional beamforming or for attaining both diversity and beamforming. In smart antenna systems the achievable performance improvements are usually a function of the antenna spacing and that of the algorithms invoked for processing the signals received by the antenna elements.

In beamforming arrangements [199] typically $\lambda/2$-spaced antenna elements are used for the sake of creating a spatially selective transmitter/receiver beam. Smart antennas using beamforming have widely been employed for mitigating the effects of various interfering signals and for providing beamforming gain. Furthermore, the beamforming arrangement is capable of suppressing co-channel interference, which allows the system to support multiple users within the same bandwidth and/or same time-slot by separating them spatially. This spatial separation, however, becomes only feasible, if the corresponding users are separable in terms of the angle of arrival of their beams. These beamforming schemes, which employ appropriately phased antenna array elements that are spaced at distances of $\lambda/2$ typically result in an improved SINR distribution and enhanced network capacity [199].

In contrast to the $\lambda/2$-spaced phased array elements, *in spatial diversity schemes* the multiple antennas are positioned as far apart as possible, using a typical spacing of 10λ [201], so that the transmitted signals of the different antennas experience independent fading, when they reach the receiver. This is because the maximum diversity gain can be achieved, when the signal replicas experience independent fading. Although spatial diversity can be achieved by employing multiple antennas at either the base station, mobile station, or both, it is more cost effective and practical to employ multiple antennas at the base station. A system having multiple receiver antennas has the potential of achieving receiver diversity, while that employing multiple transmit antennas exhibits transmit diversity.

Recently, the family of transmit diversity schemes based on space-time coding, either space-time block codes or space-time trellis codes, has received wide attention and has been invoked in the third-generation systems [202]. The aim of using spatial diversity is to provide both transmit as well as receive diversity and hence enhance the system's integrity/robustness. This typically results in a better physical-layer performance and hence a better network-layer performance, hence space-time codes indirectly increase not only the transmission integrity, but also the achievable spectral efficiency. One of the applications of space-time block code is as discussed in Section 1.3.3.

A third application of smart antennas is often referred to as *Space Division Multiple Access* [5] (SDMA), which exploits the unique, user-specific "spatial signature" of the individual users for differentiating amongst them. In simple conceptual terms one could argue that both a conventional CDMA spreading code and the Channel Impulse Response (CIR)

affect the transmitted signal similarly - they are namely convolved with it. Hence, provided that the CIR is accurately estimated, it becomes known and certainly unique, although - as opposed to orthogonal Walsh-Hadamard spreading codes, for example - not orthogonal to the other CIRs. Nonetheless, it may be used for uniquely identifying users after channel estimation and hence for supporting several users within the same bandwidth. Provided that a powerful multi-user detector is available, one can support even more users than the number of antennas. Hence this method enhances the achievable spectral efficiency directly. We will further investigate the family of SDMA techniques in Section 2.2.

Finally, Multiple Input Multiple Output (MIMO) systems [200] also employ multiple antennas, but in contrast to SDMA arrangements, not for the sake of supporting multiple users. Instead, they aim for increasing the throughput of a wireless system in terms of the number of bits per symbol that can be transmitted by a given user in a given bandwidth at a given integrity.

2.2 Space division multiple access

In an effort to increase the achievable system capacity of an OFDM system, antenna arrays can be employed for supporting multiple users in a Space Division Multiple Access (SDMA) communications scenario [38,203,204]. The benefit of this system is that in case of employing a sufficiently high number of receiver antennas at the base station, the degree of freedom provided by the P number of base station receiver antennas and L number of transmit antennas is higher than necessary for supporting L number of simultaneous users. Hence, the remaining degrees of freedom allow us to increase the achievable receiver diversity gain of the system and therefore contributes toward improving the system's transmission integrity. In this section, we will look into details of the SDMA system. Firstly, SDMA system model will be presented in Section 2.2.1. This is followed by a comparison of the SDMA model to the well-known Code Division Multiple Access (CDMA) system in Section 2.2.2.

2.2.1 SDMA system model

The so-called SDMA system is capable of differentiating L users' transmitted signals at the base-station (BS) invoking their unique, user-specific spatial signature created by the

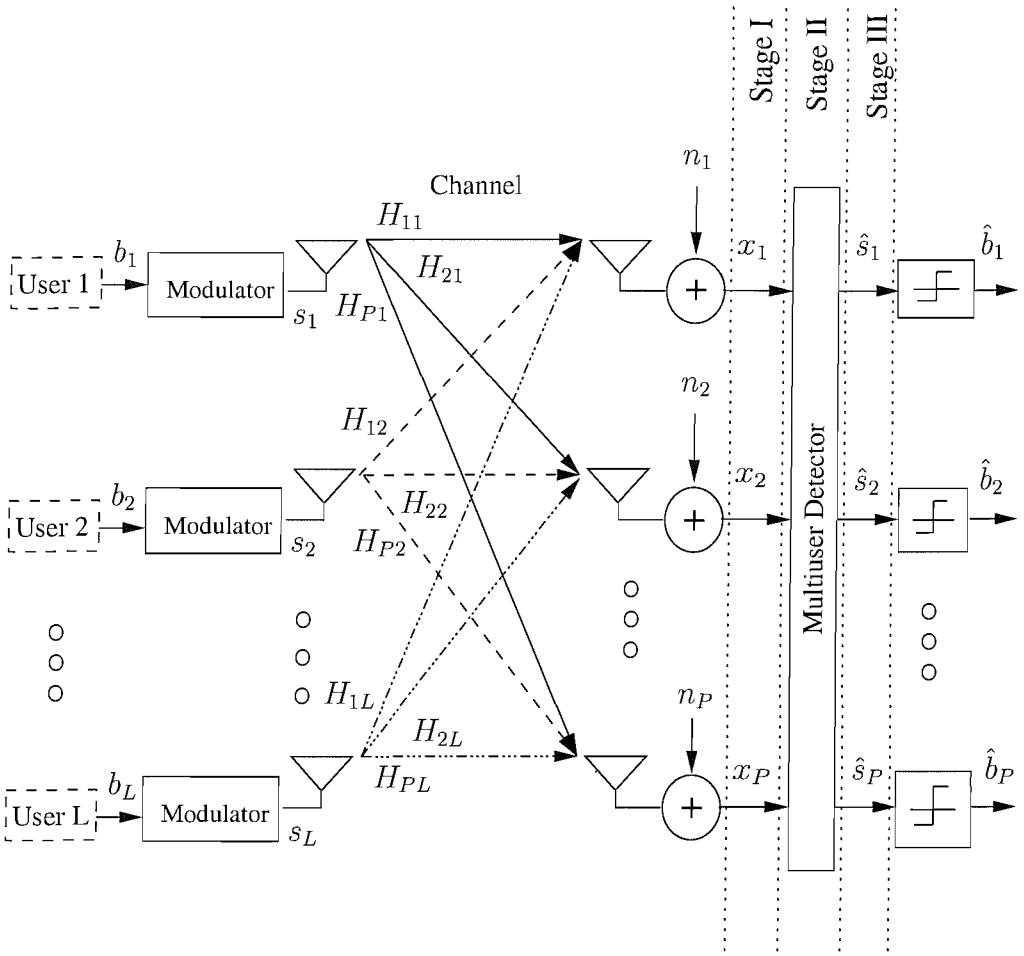

Figure 2.1: Schematic of an antenna array uplink scenario as observed on an OFDM basis, where each of the L users is equipped with a single transmit antenna and the receiver is assisted by a P-element antenna front-end.

different channel transfer functions or channel impulse responses (CIR) between the users' single transmit antenna and the P different receiver antennas at the BS [5, 203].

Figure 2.1 portrays the antenna array aided uplink transmission scenario considered. In this figure, each of the L simultaneous users is equipped with a single transmission antenna, while the receiver capitalises on a P-element antenna front-end [205]. The set of complex signals, $x_p[n,k], p \in 1,\ldots,P$ received by the P-element antenna array in the k-th subcarrier of the n-th OFDM symbol is constituted by the superposition of the independently faded signals associated with the L users sharing the same space-frequency resource [5]. The received signal was corrupted by the Gaussian noise at the array elements, and can be written as:

$$\mathbf{x}[n,k] = \mathbf{H}[n,k] * \mathbf{s}[n,k] + \mathbf{n}[n,k] = \bar{\mathbf{x}}[n,k] + \mathbf{n}[n,k], \quad (2.1)$$

where the $(P \times 1)$-dimensional vector $\mathbf{x}$ of the received signals, the vector of transmitted signals $\mathbf{s}$ and the array noise vector $\mathbf{n}$, respectively, are given by:

$$\mathbf{x} = (x_1, x_2, \ldots, x_P)^T, \tag{2.2}$$

$$\mathbf{s} = (s_1, s_2, \ldots, s_L)^T, \tag{2.3}$$

$$\mathbf{n} = (n_1, n_2, \ldots, n_P)^T. \tag{2.4}$$

The indices $[n, k]$ have been omitted for notational convenience during our forthcoming discourse, yielding [5]:

$$\mathbf{x} = \mathbf{H}\mathbf{s} + \mathbf{n} = \bar{\mathbf{x}} + \mathbf{n}. \tag{2.5}$$

Furthermore, $\bar{\mathbf{x}}$ represents the noiseless component of $\mathbf{x}$. The frequency domain channel transfer function (FDCHTF) matrix $\mathbf{H}$ of dimension $P \times L$ is constituted by the set of channel transfer function vectors of the L users:

$$\mathbf{H} = (\mathbf{H}_1, \mathbf{H}_2, \ldots, \mathbf{H}_L), \tag{2.6}$$

each of which describes the frequency domain channel transfer factor between the single transmitter antenna associated with a particular user l and the reception array elements $p \in 1, \ldots, P$:

$$\mathbf{H}_l = (H_{1l}, H_{2l}, \ldots, H_{Pl})^T. \tag{2.7}$$

The complex data signal, s_l, transmitted by the l-th user, $l \in 1, \ldots, L$ and the AWGN noise process, n_p, at any antenna array element p, $p \in 1, \ldots, P$ are assumed to exhibit a zero mean and a variance of σ_l^2 and $2\sigma_n^2$ for the data signal and AWGN noise process, respectively. The frequency domain channel transfer functions, H_{pl} of the different array elements $p \in 1, \ldots, P$ for users $l \in 1, \ldots, L$ are independent, stationary and complex-valued Gaussian distributed processes with zero-mean and unit variance. Rewriting Equation 2.5 more explicitly yields:

$$\underbrace{\begin{bmatrix} x_1 \\ x_2 \\ \vdots \\ x_P \end{bmatrix}}_{\mathbf{x}} = \underbrace{\begin{bmatrix} H_{11} & H_{12} & \ldots & H_{1L} \\ H_{21} & H_{22} & \ldots & H_{2L} \\ \vdots & & \ddots & \vdots \\ H_{P1} & H_{P2} & \ldots & H_{PL} \end{bmatrix}}_{\mathbf{H}} \cdot \underbrace{\begin{bmatrix} s_1 \\ s_2 \\ \vdots \\ s_L \end{bmatrix}}_{\mathbf{s}} + \underbrace{\begin{bmatrix} n_1 \\ n_2 \\ \vdots \\ n_P \end{bmatrix}}_{\mathbf{n}} \tag{2.8}$$

2.2.2 Comparison between SDMA and CDMA

In multiple access communications several transmitters share a common channel. One of the most widespread multiple access systems is CDMA [206]. In a CDMA system different spreading codes are employed by different users for distinguishing them. The schematic of a CDMA system is depicted in Figure 2.2(b).

As mentioned in Section 2.1, an SDMA system can also be used for multiple access, where the different FDCHTFs or CIRs associated with the multiple antennas can be employed for distinguishing the different users. Hence, an SDMA system can be visualised similarly to a CDMA system. The 'fictitious' spreading codes of the SDMA system are constituted by the dispersive CIRs between the transmitter antenna and the receiver antenna, as depicted in Figure 2.2. However, unlike the spreading codes, the CIRs are not known apriori, they must be estimated and their shape is beyond the control of the users or the base-station. Therefore, it is 'highly unlikely' that the CIRs or the corresponding channel transfer functions may become orthogonal.

2.3 Linear multiuser detection techniques for SDMA

One of the key issues in SDMA systems is the separation of the signals transmitted by the different users, which can be performed based on their unique, user-specific spatial signature, assuming the knowledge of the CIR. A multiplicity of algorithms has been proposed for performing the task of MUD. Most of these algorithms are based on the multiuser detection techniques previously investigated in the context of CDMA communications [207].

Representatives of the first group of detectors that we investigated in this study are referred to as linear detectors. The employment of this type of detectors is motivated by the fact that by using the optimum Maximum Likelihood (ML) detector, a potentially large number of symbol combinations has to be tested in order to determine the most likely transmitted symbol on the basis of the Euclidean distance measured between the received and the legitimate channel output phasors. A better approach is therefore to generate the estimates of the different users' transmitted symbols with the aid of lower-complexity multiuser detectors. The estimated signals of the individual users will then be demodulated

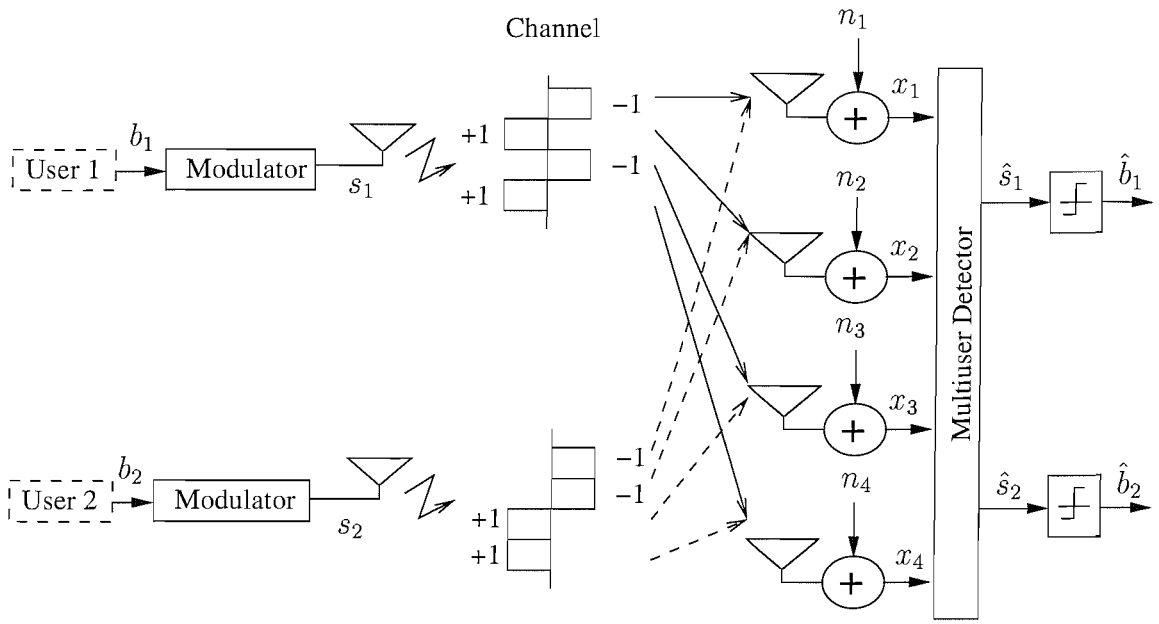

(a) SDMA

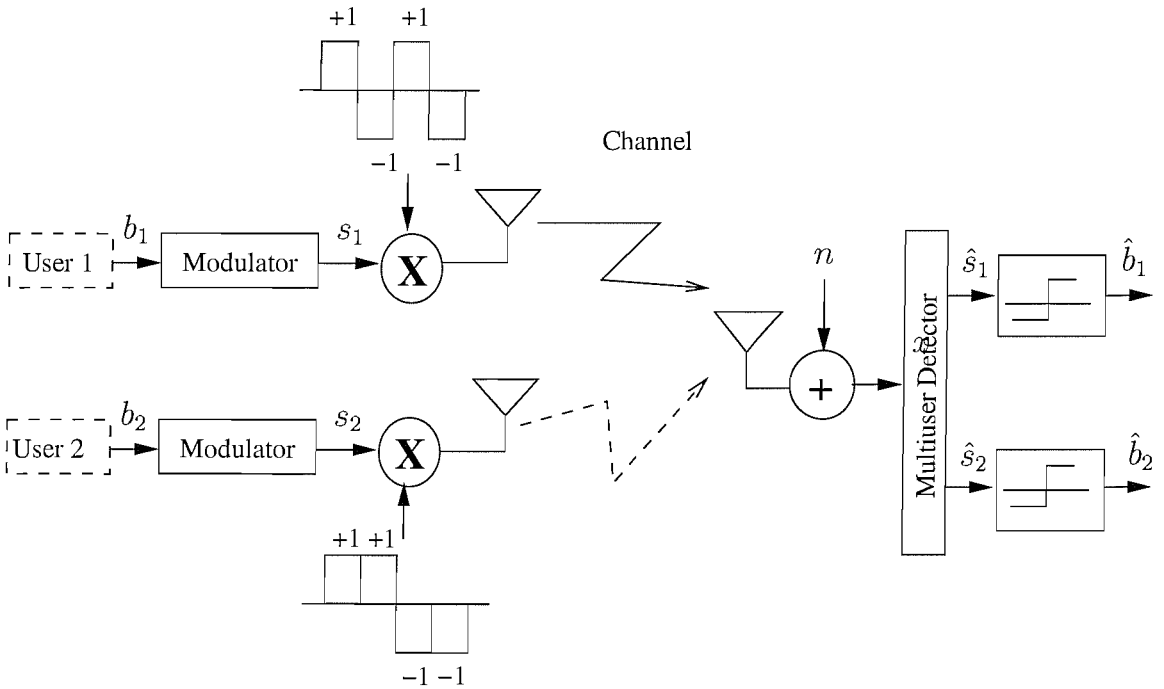

(b) CDMA

Figure 2.2: Stylised-comparison of an SDMA system and a CDMA system. The spreading codes used are $\{+1, -1, +1, -1\}$ for User 1 and $\{+1, +1, -1, -1\}$ for User 2.

separately. Thus the total detection complexity is reduced from that of determining the Euclidean distance for all users' symbols at the same time to the less-complex problem of detecting the signals of the individual users.

Before we continue our discourse by investigating a range of multiuser detectors [5], let us characterise the linear detector's output signal. An estimate $\hat{\mathbf{s}}$ of the vector of transmitted signals $\mathbf{s}$ is generated for the L simultaneous users by linearly combining the signals received by the P different antenna elements at the BS with the aid of the MUD's weight matrix $\mathbf{W}$, resulting in:

$$\hat{\mathbf{s}} = \mathbf{W}^H \mathbf{x}. \tag{2.9}$$

By substituting Equation 2.5 into Equation 2.9 and considering the l-th user's associated vector component, we will arrive at:

$$\begin{aligned} \hat{s}_l &= \mathbf{w}_l^H \mathbf{x}, \\ &= \mathbf{w}_l^H \mathbf{H}\mathbf{s} + \mathbf{w}_l^H \mathbf{n} \\ &= \bar{\mathbf{s}}_l + \mathbf{w}_l^H \mathbf{n}, \\ &= \underbrace{\mathbf{w}_l^H \mathbf{H}_l s_l}_{\hat{s}_{l(S)}} + \underbrace{\mathbf{w}_l^H \sum_{i=1, i\neq l}^{L} \mathbf{H}_i s_i}_{\hat{s}_{l(I)}} + \underbrace{\mathbf{w}_l^H \mathbf{n}}_{\hat{s}_{l(N)}}, \end{aligned} \tag{2.10}$$

where the MUD weight vector $\mathbf{w}_l$ is the l-th column of the weight matrix $\mathbf{W}$. The first term of Equation 2.10, namely $\hat{s}_{l(S)}$, refers to the desired user's contribution, while the second term and third term, namely $\hat{s}_{l(I)}$ and $\hat{s}_{l(N)}$ respectively, corresponds to the interfering users' contributions and to the Gaussian noise, respectively.

The variance of the desired user's contribution can be calculated as [5]:

$$\begin{aligned} \sigma_{l(S)}^2 &= E\{\hat{s}_{l(S)}^H \hat{s}_{l(S)}\} \\ &= \mathbf{w}_l^H \mathbf{R}_{l(a,S)} \mathbf{w}_l, \end{aligned} \tag{2.11}$$

where $\mathbf{R}_{l(a,S)} = \sigma_l^2 \mathbf{H}_l \mathbf{H}_l^H$ is the $(P \times P)$-dimensional auto-correlation matrix of the desired user's signal. Analogously, the variance of the interfering users' signals can be calculated as [5]:

$$\begin{aligned} \sigma_{l(I)}^2 &= E\{\hat{s}_{l(I)}^H \hat{s}_{l(I)}\} \\ &= \mathbf{w}_l^H \mathbf{R}_{l(a,I)} \mathbf{w}_l, \end{aligned} \tag{2.12}$$

where $\mathbf{R}_{l(a,I)} = \sum_{i=1,i\neq l}^{L} \sigma_i^2 \mathbf{H}_l \mathbf{H}_l^H$ is the $(P \times P)$-dimensional auto-correlation matrix of the interfering users' contribution. On the other hand, the contribution imposed by the residual AWGN can be calculated as [5]:

$$\begin{aligned} \sigma_{l(N)}^2 &= E\{\hat{s}_{l(N)}^H \hat{s}_{l(N)}\} \\ &= \mathbf{w}_l^H \mathbf{R}_{l(a,N)} \mathbf{w}_l, \end{aligned} \tag{2.13}$$

where $\mathbf{R}_{l(a,N)} = 2\sigma_n^2 \mathbf{I}$ is the $(P \times P)$-dimensional diagonal noise correlation matrix. Therefore, the undesired signal's auto-correlation matrix can be expressed as

$$\mathbf{R}_{l(a,I+N)} = \mathbf{R}_{l(a,I)} + \mathbf{R}_{l(a,N)}, \tag{2.14}$$

where the undesired signal is given by the sum of the interference and residual AWGN.

The variances of the desired user's contribution $\sigma_{l(S)}^2$, the interfering users' signals $\sigma_{l(I)}^2$ and the residual AWGN $\sigma_{l(N)}^2$ shown in Equations 2.11, 2.12 and 2.13, respectively, are particularly useful for characterising the performance of the linear MUD [5]. The recorded Signal-to-Noise Ratio (SNR) at the output of the MUD can be expressed as:

$$\mathrm{SNR}_l = \frac{\sigma_{l(S)}^2}{\sigma_{l(N)}^2} = \frac{\mathbf{w}_l^H \mathbf{R}_{l(a,S)} \mathbf{w}_l}{\mathbf{w}_l^H \mathbf{R}_{l(a,N)} \mathbf{w}_l}, \tag{2.15}$$

which is of salient importance in terms of characterising the MUD. By the same token, the advantage of the desired user's signal over the interfering users' contributions or the Signal-to-Interference-Ratio (SIR) can be expressed as:

$$\mathrm{SIR}_l = \frac{\sigma_{l(S)}^2}{\sigma_{l(I)}^2} = \frac{\mathbf{w}_l^H \mathbf{R}_{l(a,S)} \mathbf{w}_l}{\mathbf{w}_l^H \mathbf{R}_{l(a,I)} \mathbf{w}_l}. \tag{2.16}$$

In the following sections we will investigate the classic Minimum Mean-Square Error (MMSE) MUD, which is perhaps the most widely known multiuser detector. We will briefly discuss the derivation of the MMSE MUD in Section 2.3.1. This is followed by the calculation of the MUD's soft-outputs in the SDMA system to be used for channel decoding, when forward error correction coding is applied in the system of Section 2.3.2.

2.3.1 Minimum mean-square error multiuser detector

We will now embark on a brief overview of the classic MMSE MUD. The MMSE detector exploits the availability of the statistical knowledge of the transmitted signals as well as that

of the Gaussian noise generated at the receiver antennas. The aim of the MMSE detector is to minimise the MSE between the estimated signals and the actual signals, which is expressed as:

$$\begin{aligned}
\text{MSE}(\hat{\mathbf{s}}) &= E[(\mathbf{s}-\hat{\mathbf{s}})(\mathbf{s}-\hat{\mathbf{s}})^H] \\
&= E[(\mathbf{s}-\mathbf{W}^H\mathbf{x})(\mathbf{s}-\mathbf{W}^H\mathbf{x})^H] \\
&= E[\mathbf{s}\mathbf{s}^H - \mathbf{s}\mathbf{x}^H\mathbf{W} - \mathbf{W}^H\mathbf{x}\mathbf{s}^H + \mathbf{W}^H\mathbf{x}\mathbf{x}^H\mathbf{W}] \\
&= E[\mathbf{s}\mathbf{s}^H] - E[\mathbf{s}\mathbf{x}^H\mathbf{W}] - E[\mathbf{W}^H\mathbf{x}\mathbf{s}^H] + E[\mathbf{W}^H\mathbf{x}\mathbf{x}^H\mathbf{W}] \\
&= \mathbf{R}_s - \mathbf{R}_{sx}\mathbf{W} - \mathbf{W}^H\mathbf{R}_{xs} + \mathbf{W}^H\mathbf{R}_x\mathbf{W}, \qquad (2.17)
\end{aligned}$$

where $\mathbf{R}_s = E[\mathbf{s}\mathbf{s}^H]$, $\mathbf{R}_{sx} = E[\mathbf{s}\mathbf{x}^H]$, $\mathbf{R}_{xs} = E[\mathbf{x}\mathbf{s}^H]$ and $\mathbf{R}_x = E[\mathbf{x}\mathbf{x}^H]$. Expanding these terms using the expression $\mathbf{x} = \mathbf{H}\mathbf{s} + \mathbf{n}$ of Equation 2.5 yields:

$$\begin{aligned}
\mathbf{R}_{sx} &= E[\mathbf{s}(\mathbf{H}\mathbf{s}+\mathbf{n})^H] \\
&= E[\mathbf{s}\mathbf{s}^H(\mathbf{H})^H] + E[\mathbf{s}\mathbf{n}^H] \\
&= \mathbf{R}_s(\mathbf{H})^H, \qquad (2.18)
\end{aligned}$$

$$\begin{aligned}
\mathbf{R}_{xs} &= E[(\mathbf{H}\mathbf{s}+\mathbf{n})\mathbf{s}^H] \\
&= E[\mathbf{H}\mathbf{s}\mathbf{s}] + E[\mathbf{n}\mathbf{s}^H] \\
&= \mathbf{H}\mathbf{R}_s, \qquad (2.19)
\end{aligned}$$

and

$$\begin{aligned}
\mathbf{R}_x &= E[(\mathbf{H}\mathbf{s}+\mathbf{n})(\mathbf{H}\mathbf{s}+\mathbf{n})^H] \\
&= E[\mathbf{H}\mathbf{s}\mathbf{s}^H(\mathbf{H})^H + \mathbf{n}\mathbf{n}^H] \\
&= E[\mathbf{H}\mathbf{s}\mathbf{s}^H(\mathbf{H})^H] + E[\mathbf{n}\mathbf{n}^H] \\
&= \mathbf{H}\mathbf{R}_s(\mathbf{H})^H + \mathbf{R}_n, \qquad (2.20)
\end{aligned}$$

where we have $\mathbf{R}_n = E[\mathbf{n}\mathbf{n}^H]$. Note that $E[\mathbf{s}\mathbf{n}^H] = E[\mathbf{n}\mathbf{s}^H] = 0$, since we assumed that the transmitted data and the noise are uncorrelated with each other. For the specific case of $\mathbf{R}_s = \sigma_s^2\mathbf{I}$ and $\mathbf{R}_n = 2\sigma_n^2\mathbf{I}$, which implies that the transmitted signal and noise samples are uncorrelated, the MMSE detector's quadratic form, which has to be minimised, will become:

$$\begin{aligned}
\text{MSE}(\hat{\mathbf{s}}) &= \sigma_s^2\mathbf{I} - \sigma_s^2(\mathbf{H})^H\mathbf{W} - \sigma_s^2\mathbf{W}^H(\mathbf{H}) \\
&\quad + \mathbf{W}^H(\sigma_s^2(\mathbf{H})(\mathbf{H})^H + 2\sigma_n^2\mathbf{I})\mathbf{W}. \qquad (2.21)
\end{aligned}$$

Using the orthogonality principle [5], for minimising the MSE, the error vector $\mathbf{e} = \mathbf{s} - \hat{\mathbf{s}}$ has to be rendered orthogonal to the detector's input vector $\mathbf{x}$ [5]. This implies that:

$$E[(\mathbf{s} - \hat{\mathbf{s}})\mathbf{x}^H] = \mathbf{0}, \tag{2.22}$$

where $\mathbf{0}$ is a matrix with all its elements being zero. If we let $\hat{\mathbf{s}} = \mathbf{W}^H\mathbf{x}$, then,

$$\begin{aligned} E[(\mathbf{s} - \mathbf{W}^H\mathbf{x})\mathbf{x}^H] &= \mathbf{0} \\ E[\mathbf{s}\mathbf{x}^H - \mathbf{W}^H\mathbf{x}\mathbf{x}^H] &= \mathbf{0} \\ E[\mathbf{s}\mathbf{x}^H] - E[\mathbf{W}^H\mathbf{x}\mathbf{x}^H] &= \mathbf{0} \\ \mathbf{R}_{sx} - \mathbf{W}^H\mathbf{R}_x &= \mathbf{0} \\ \mathbf{W}^H &= \mathbf{R}_{sx}\mathbf{R}_x^{-1}. \end{aligned} \tag{2.23}$$

Upon substituting Equation 2.18 and Equation 2.20 into Equation 2.23, we get:

$$\begin{aligned} \mathbf{W}^H &= \mathbf{R}_s(\mathbf{H})^H(\mathbf{H}\mathbf{R}_s(\mathbf{H})^H + \mathbf{R}_n)^{-1} \\ \mathbf{W} &= (\mathbf{H}\mathbf{R}_s(\mathbf{H})^H + \mathbf{R}_n)^{-1}\mathbf{H}\mathbf{R}_s, \end{aligned} \tag{2.24}$$

If we assume that $\mathbf{R}_n = 2\sigma_n\mathbf{I}$ and $\mathbf{R}_s = \mathbf{I}$, which is the case when the noise samples are uncorrelated and have a variance of σ_n^2, as well as assuming furthermore that the transmitted data are also uncorrelated and normalised to a variance of unity, then the expression of the MMSE weight matrix of Equation 2.24 will become:

$$\mathbf{W}_{MMSE} = (\mathbf{H}\mathbf{H}^H + 2\sigma_n^2\mathbf{I})^{-1}\mathbf{H}. \tag{2.25}$$

It becomes explicit in Equation 2.25 that the MMSE weight vector attempts to reduce the effects of noise. Therefore, the MMSE solution can be viewed as a compromise solution that takes into account the relative importance of each interfering user as well as that of the background noise.

2.3.2 Soft-output generation for channel decoding

Channel coding is a powerful means of enhancing the performance of the system. This is achieved at the expense of lower effective throughput and additional computational complexity. We have shown in Section 1.3.3.2 that LDPC has emerged as an attractive, low

complexity channel code, capable of achieving a near-Shannonian performance. In order to employ soft-output channel decoding, the detector's soft-output has to be generated.

It can be observed from Equation 2.10 that the l-th user's combiner output signal $\hat{s}_l$ is constituted by a superposition of the desired user's signal $H_{l(\text{eff})}s_l$ and of the undesired signal $n_{l(\text{eff})}$, which is expressed as:

$$\hat{s}_l = H_{l(\text{eff})}s_l + n_{l(\text{eff})}, \tag{2.26}$$

where the desired user's effective transfer factor, $H_{l(\text{eff})}$ is given by $H_{l(\text{eff})} = \mathbf{w}_l^H \mathbf{H}_l$, and the effective undesired signal, $n_{l(\text{eff})}$, is the sum of the $L-1$ interfering signals and the residual Gaussian noise given by $n_{l(\text{eff})} = \hat{s}_{l(I)} + \hat{s}_{l(N)}$.

From Equation 2.26, we can then obtain the soft-bit value using the log-likelihood ratio $L_{l(m)}$ associated with the l-th user at the m-th bit position as [5]:

$$L_{l(m)}\left(b_{l(m)}|\hat{s}_l, H_{l(\text{eff})}\right) = \ln\left(\frac{\mathbf{Pr}\{b_{l(m)}=1|\hat{s}_l, H_{l(\text{eff})}\}}{\mathbf{Pr}\{b_{l(m)}=0|\hat{s}_l, H_{l(\text{eff})}\}}\right), \tag{2.27}$$

which is the natural logarithm of the quotient of two *a posteriori* probabilities, namely that of the m-th bit transmitted by the l-th user having a logical value of $b_{l(m)}=1$ or $b_{l(m)}=0$.

In the following section, we will introduce the minimum bit error rate multiuser detector, which will directly minimise the achievable BER, unlike the MMSE MUD that minimises the MSE.

2.4 Minimum bit error rate multiuser detector

A variety of linear multiuser detectors have been proposed in the literature for performing the SDMA-based separation of OFDM users upon exploiting their unique, user-specific, spatial signature, provided that their channel impulse response was accurately estimated [5, 204]. The most popular design strategy is constituted by the MMSE MUD of Section 2.3.1. However, as recognised in [208–211], a better strategy is to choose the linear MUD's coefficients so as to directly minimise the bit error-probability or bit-error rate (BER), rather than the mean-squared error (MSE). This is because minimising the MSE does not necessarily guarantee that the BER of the system is also minimised. The family of detectors that

directly minimises the BER is referred to as the class of minimum bit-error rate (MBER) detectors [212,213]. The range of past contributions on the design of various MBER detectors is summarised in Table 2.2.

In this section, we will investigate the performance of the proposed MBER linear MUD in the context of an uplink SDMA/OFDM system. We will commence with a discussion on the error probability of a BPSK system in Section 2.4.1. This is followed by presenting our exact MBER MUD proposed for the OFDM SDMA system in Section 2.4.2. In Section 2.4.3, we will provide simulation results for characterising the performance of the MBER MUD. Then, we will present our results concerning the effects of varying the different parameters of the simplified conjugate gradient (CG) method in Section 2.4.4. Finally, we will also investigate the employment of LDPC codes in conjunction with the MBER MUD in Section 2.4.5.

2.4.1 Error probability in BPSK system

In this treatise, the term BER and probability of error P_E are used interchangeably. The BER encountered at the output of the SDMA MUD characterised by the combiner weight vector $\mathbf{w}_l$ of user l may be expressed as [226]:

$$\begin{aligned} P(\mathbf{w}_l) &= Pr[\mathrm{sgn}(b_l) \cdot \bar{s}_l(\mathbf{w}_l) < 0], \\ &= Pr[z_l < 0], \end{aligned} \tag{2.28}$$

where z_l is the signed decision variable given by:

$$z_l = \mathrm{sgn}(b_l) \cdot \bar{s}_l(\mathbf{w}_l), \tag{2.29}$$

while as before, b_l represents the transmitted bit of user l and $\bar{s}_l$ is the noiseless signal at the output of the MUD related to the l-th user.

The Probability Density Function (PDF) of the decision variable z_l is constituted by a mixture of the Gaussian distribution associated with each possible combination of the transmitted data symbols of all users. Under the assumption that all the noise-free signal states are equiprobable, the PDF of z_l is given by [226]:

$$p_{z_l}(z_l; \mathbf{w}_l) = \frac{1}{N_b\sqrt{2\pi}\sigma_n\sqrt{\mathbf{w}_l^H\mathbf{w}_l}} \sum_{j=1}^{N_b} \exp\left(-\frac{(z_l - \mathrm{sgn}(b_l^{(j)})\bar{s}_l^{(j)})^2}{2\sigma_n^2\mathbf{w}_l^H\mathbf{w}_l}\right), \tag{2.30}$$

Year	Author	Contribution
'66	Aaron and Tufts [214]	Establishing the interrelationship of intersymbol interference and error probability.
'74	Shamash and Yao [215]	Outlining the structure and characterising the performance of a linear decision feedback equaliser (DFE) based on the minimum error probability criterion.
'96	Chen, Chng, Mulgrew and Gibson [216]	Deriving an MBER solution for the DFE that employs a linear combination of the channel observations and the past decision.
'97	Yeh and Barry [217]	Proposing algorithms for approximating MBER linear and decision-feedback equalisers for binary signalling.
	Mandayam and Aazhang [218]	A non-adaptive MBER linear multiuser detector based on gradient optimisation for CDMA communicating over narrow-band Gaussian channels which do not introduce ISI.
'98	Yeh and Barry [219]	Approximate MBER equalisation for pulse-amplitude and quadrature amplitude modulation.
	Yeh, Lopes and Barry [220]	Approximate MBER multiuser detection.
	Chen, Mulgrew, Chng and Gibson [221]	Space translation properties and the MBER linear combiner DFE.
'99	Chen and Mulgrew [222]	The minimum-SER linear-combiner decision feedback equaliser.
	Psaromiligkos, Batalama and Pados [223]	Adaptive MBER receivers using linear filters in the context of DS-CDMA.
'00	Yeh and Barry [213]	Adaptive MBER equalisation for binary signalling.
	Mulgrew and Chen [224]	Stochastic gradient MBER DFEs.
	Wang, Lu and Antoniou [209]	Design of a constrained MBER MUD.
'01	Chen, Samingan, Mulgrew and Hanzo [225, 226]	Adaptive MBER linear MUD for DS-CDMA signals transmitted over multipath fading channels.
	Mulgrew and Chen [212]	Adaptive MBER DFEs for binary signalling.
	Samingan, Chen and Hanzo [227]	Adaptive MBER linear MUD for CDMA signals transmitted over multipath channels using 4-QAM.
'03	Chen, Mulgrew and Hanzo [228]	Least bit-error rate adaptive nonlinear equalisers for binary signalling.
	de Lamare and Sampaio-Neto [210]	Adaptive MBER decision feedback multiuser receivers for frequency selective fading channels.
	Chen, Hanzo and Ahmad [211]	Adaptive MBER beamforming assisted receiver for wireless communications.
	Gesbert [229]	A minimum error-rate approach for robust linear MIMO receivers.
	Alias, Samingan, Chen and Hanzo [2]	SDMA OFDM employing MBER MUD.

Table 2.2: Contributions on MBER receivers.

where N_b is the number of equiprobable combinations of the binary vectors of the L users, i.e. we have $N_b = 2^L$. Furthermore, $\bar{s}_l^{(j)}$, $j \in 1, \ldots, N_b$, denotes the noiseless signal at the output of the MUD related to the l-th user, while $b_l^{(j)}$, $j \in 1, \ldots, N_b$, is the transmitted bit of user l.

The erroneous decision events are associated with the area under the PDF curve in the interval $(-\infty, 0)$, which is quantified as:

$$P_E(\mathbf{w}_l) = \int_{-\infty}^{0} p_z(z_l; \mathbf{w}_l) dz_l. \tag{2.31}$$

Upon using the integration by substitution technique and introducing the shorthand of

$$y_j = \frac{(z_l - \mathrm{sgn}(b_l^{(j)})\bar{s}_l^{(j)})}{\sigma_n \sqrt{\mathbf{w}_l^H \mathbf{w}_l}}, \tag{2.32}$$

the probability of error in Equation 2.31 becomes:

$$\begin{aligned} P_E(\mathbf{w}_l) &= \frac{1}{N_b\sqrt{2\pi}} \sum_{j=1}^{N_b} \int_{-\infty}^{c_j(\mathbf{w}_l)} \exp\left(-\frac{(y_j)^2}{2}\right) dy_j \\ &= \frac{1}{N_b} \sum_{j=1}^{N_b} Q[c_j(\mathbf{w}_l)], \end{aligned} \tag{2.33}$$

where $c_j(\mathbf{w}_l)$ is given by:

$$c_j(\mathbf{w}_l) = \frac{\mathrm{sgn}(b_l^{(j)}) \cdot \bar{s}_l^{(j)}}{\sigma_n \sqrt{\mathbf{w}_l^H \mathbf{w}}} = \frac{\mathrm{sgn}(b_l^{(j)}) \cdot \mathbf{w}_l^H \bar{\mathbf{x}}_j}{\sigma_n \sqrt{\mathbf{w}_l^H \mathbf{w}}}, \tag{2.34}$$

and $\bar{\mathbf{x}}_j$, $j \in 1, \ldots, N_b$ constitutes a possible value of $\bar{\mathbf{x}}$ defined in the context of Equation 2.5.

Note that the BER is invariant to a positive scaling of the weight vector $\mathbf{w}_l$, in other words, the BER depends only on the vectorial direction of $\mathbf{w}_l$, but not on its magnitude.

2.4.2 Exact MBER multiuser detection

The MBER solution is defined as [226]:

$$\mathbf{w}_{l(MBER)} = \arg\min_{\mathbf{w}_l} P_E(\mathbf{w}_l). \tag{2.35}$$

The complex, irregular shape of the BER cost function is exemplified in Figure 2.3, which prevents us from deriving a closed-form solution for the MBER MUD weights. Therefore

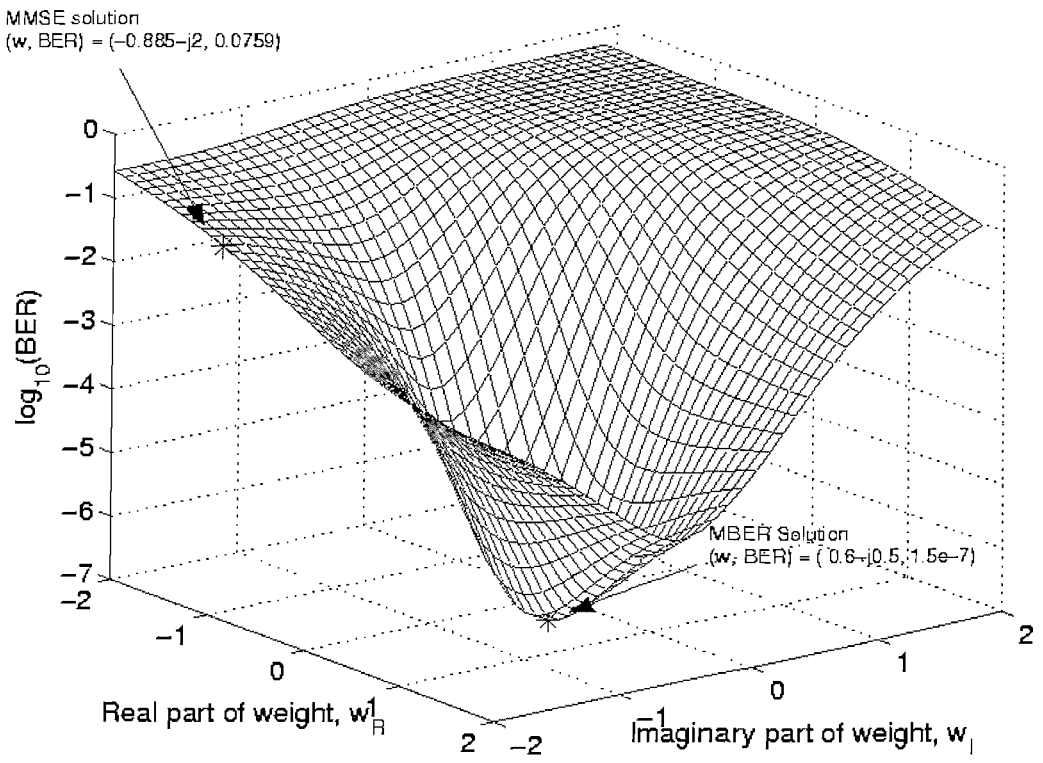

Figure 2.3: An example of the BER cost function surface for subcarrier 62 in the $P = 2, L = 2$ OFDM SDMA system employing 128-subcarrier in the SWATM channel at SNR = 10 dB.

in practice an iterative strategy based on the steepest-descent gradient method can be used for finding the MBER solution [226]. According to this method, the linear MUD's weight vector $\mathbf{w}_l$ is iteratively updated, commencing for example from the MMSE weights of Equation 2.25, until the weight vector that exhibits the lowest BER is arrived at. In each step, the weight vector is updated according to a specific step-size, μ, in the vectorial direction in which the BER cost function decreases most rapidly, namely in the direction opposite to the gradient of the BER cost function given in Equation 2.39. The steepest-descent gradient algorithm that can be used for finding the MBER solution is summarised as follows [226]:

$$\mathbf{w}_l(i+1) = \mathbf{w}_l(i) + \mu \mathbf{d}(i), \tag{2.36}$$

where the step-size is represented by μ, and the update direction vector $\mathbf{d}(i)$ at instance i is given by:

$$\mathbf{d}(i) = -\nabla_{\mathbf{w}_l} P_E[\mathbf{w}_l(i)]. \tag{2.37}$$

In Equation 2.37, $\nabla_{\mathbf{w}_l} P_E[\mathbf{w}_l(i)]$ is the gradient of $P_E[\mathbf{w}_l(i)]$ with respect to $\mathbf{w}_l$ and i indicates the iteration index. By exploiting the following identity [226]:

$$\frac{\partial}{\partial t}\int_{a(t)}^{c(t)} f(y)\,dy = f[c(t)]\frac{\partial c(t)}{\partial t} - f[a(t)]\frac{\partial a(t)}{\partial t}, \tag{2.38}$$

the gradient of $P_E(\mathbf{w}_l)$ with respect to the MUD's weight vector $\mathbf{w}_l$ can then be computed by:

$$\begin{aligned}
\nabla_{\mathbf{w}_l} P_E(\mathbf{w}_l) &= \frac{1}{N_b\sqrt{2\pi}}\sum_{j=1}^{N_b}\exp\left(-\frac{(-\mathrm{sgn}(b_l^{(j)})\cdot\bar{s}_l^{(j)})^2}{2\sigma_n^2\mathbf{w}_l^H\mathbf{w}_l}\right)\frac{\partial c_j(\mathbf{w}_l)}{\partial \mathbf{w}_l} \\
&= \frac{1}{N_b\sqrt{2\pi}\sigma_n}\sum_{j=1}^{N_b}\exp\left(-\frac{(\bar{s}_l^{(j)})^2}{2\sigma_n^2\mathbf{w}_l^H\mathbf{w}_l}\right)\cdot\mathrm{sgn}(b_l^{(j)}) \\
&\quad\cdot\left\{\frac{-\bar{\mathbf{x}}_j}{(\mathbf{w}_l^H\mathbf{w}_l)^{\frac{1}{2}}}+\mathbf{w}_l^H\bar{\mathbf{x}}_j\frac{\mathbf{w}_l}{(\mathbf{w}_l^H\mathbf{w}_l)^{\frac{3}{2}}}\right\} \\
&= \frac{1}{N_b\sqrt{2\pi}\sigma_n}\left(\frac{\mathbf{w}_l\mathbf{w}_l^H-\mathbf{w}_l^H\mathbf{w}_l\mathbf{I}}{(\mathbf{w}_l^H\mathbf{w}_l)^{\frac{3}{2}}}\right) \\
&\quad\cdot\sum_{j=1}^{N_b}\exp\left(-\frac{(\bar{s}_l^{(j)})^2}{2\sigma_n^2\mathbf{w}_l^H\mathbf{w}_l}\right)\cdot\mathrm{sgn}(b_l^{(j)})\cdot\bar{\mathbf{x}}_j.
\end{aligned} \tag{2.39}$$

Again, as it may be observed in Equation 2.34, the BER is independent of the magnitude of the MUD's weight vector, hence the knowledge of the vectorial orientation of the detector's weight vector is sufficient for defining the decision boundary of the linear MBER SDMA detector. Therefore the MBER detector has an infinite number of solutions.

It is, however, desirable in any optimisation problem to have a single global minimum. In the case of the proposed MBER algorithm, the MUD's global BER minimum is found by constraining the detector's weight vector to have a unity magnitude. This is achieved by introducing the normalisation process in each iteration according to:

$$\overline{\mathbf{w}}_l = \frac{\mathbf{w}_l}{\|\,\mathbf{w}_l\,\|} = \frac{\mathbf{w}_l}{\sqrt{\mathbf{w}_l^H\mathbf{w}_l}}. \tag{2.40}$$

With the aid of this normalisation, the gradient expression of Equation 2.39 can be simplified to [226]:

$$\nabla_{\mathbf{w}_l} P_E(\overline{\mathbf{w}}_l) = \frac{1}{N_b\sqrt{2\pi}\sigma_n}\sum_{j=1}^{N_b}\exp\left(-\frac{(\bar{s}_l^{(j)})^2}{2\sigma_n^2}\right)\cdot\mathrm{sgn}(b_l^{(j)})\cdot(\overline{\mathbf{w}}_l\cdot\bar{s}_l^{(j)}-\bar{\mathbf{x}}_j), \tag{2.41}$$

where $\overline{\mathbf{w}}_l$ is the MUD's normalised weight vector evaluated using Equation 2.40. Comparing the gradient expressions of Equation 2.39 and Equation 2.41, we may conclude that the

constraint of Equation 2.40 imposed on the optimisation problem of Equation 2.39 reduces the infinite number of MBER solutions to a single solution.

Unfortunately, the steepest-descent gradient algorithm of Equation 2.36 may converge slowly [226]. In order to circumvent this convergence problem, the computationally more complex Gauss-Newton algorithm [226] can be invoked. Based on optimising the non-linear least-square cost function of Equation 2.41, the Gauss-Newton algorithm updates the detector's weight vector in the direction given by [226]:

$$\mathbf{d}(i+1) = -[\nabla_{\mathbf{w}_l} P_E(\mathbf{w}_l(i))]^{-1}[\nabla^2_{\mathbf{w}_l} P_E(\mathbf{w}_l(i))], \tag{2.42}$$

where $\mathbf{d}(i)$ is the direction of the MUD's weight update for iteration i and $\nabla^2_{\mathbf{w}_l} P_E(\mathbf{w}_l)$ is the second derivative of $P_E(\mathbf{w}_l)$ with respect to $\mathbf{w}_l$. Naturally, extra computations are needed for evaluating the second-derivative of the $P_E(\mathbf{w}_l)$. The compromise solution to this optimisation problem can be arrived at by using the Conjugate Gradient (CG) [226] method. This algorithm searches for the direction of the current MUD weight-vector update that is the conjugate of the previous update. This strategy is different from the Steepest Descent Gradient (SDG) [226] method, which chooses the direction of the current update to be orthogonal to that of the previous update. Furthermore, CG [226] avoids using the same direction twice consecutively and hence improves the efficiency of the SDG method with the advent of using orthogonal consecutive directions. Unlike the SDG method [226], the full-complexity version of the CG [226] technique requires N iterations, where N is the dimension of the SDMA detector's weight vector $\mathbf{w}_l$. This is achieved by calculating the optimal step size for each iteration. However, in our forthcoming discourse we opt for employing a simpler version [226] of the CG MUD weight-update method, which uses a constant step size for all iterations. This algorithm can be summarised as follows [226]:

Initialisation: Choose a step size $\mu > 0$ and a termination scalar $\beta > 0$; given $\mathbf{w}(1)$ and

$$\mathbf{d}(1) = -\nabla_{\mathbf{w}_l} P_E[\mathbf{w}_l(1)]; \tag{2.43}$$

Loop: If $\| \nabla_{\mathbf{w}_l} P_E[\mathbf{w}_l(i)] \| = \sqrt{[\nabla_{\mathbf{w}_l} P_E(\mathbf{w}_l(i))]^T \nabla_{\mathbf{w}_l} P_E[\mathbf{w}_l(i))} < \beta$: goto *Stop*,

Otherwise:

$$\begin{aligned}
\mathbf{w}_l(i+1) &= \mathbf{w}_l(i) + \mu\mathbf{d}(i) \\
&= \frac{\mathbf{w}_l(i+1)}{\| \mathbf{w}_l(i+1) \|} && (2.44) \\
\phi_i &= \frac{\| \nabla_{\mathbf{w}_l} P_E[\mathbf{w}_l(i+1)] \|^2}{\| \nabla_{\mathbf{w}_l} P_E[\mathbf{w}_l(i)] \|^2} && (2.45) \\
\mathbf{d}(i+1) &= \phi_i \mathbf{d}(i) - \nabla_{\mathbf{w}_l} P_E[\mathbf{w}_l(i+1)] && (2.46) \\
i &= i+1, \text{ goto } \textit{Loop}.
\end{aligned}$$

Stop: $\mathbf{w}_l(i)$ is the solution.

Step (2.46) ensures the conjugate relationship between the directions of the successive iterations. The variable ϕ_i of Equation 2.45 quantifies the ratio of the previous and the current BER gradients, which is used for weighting the previous gradient $\mathbf{d}(i)$, as seen in step 2.46. Note that if we have $\phi_i = 0$, we arrive at the SDG algorithm. The MBER solution is arrived at when the gradient $\mathbf{d}(i)$ becomes zero, i.e. when we have $\nabla_{\mathbf{w}_l} P_E(\mathbf{w}_l) = 0$. While achieving this requires numerous iterations, the termination scalar β can be chosen such that the gradient becomes sufficiently small in order to arrive at a near-MBER solution.

2.4.3 Simulation results

In this section we will present our simulation results using the exact MBER MUD and compare its performance to that of the classical MMSE MUD. All the simulations were conducted using the SWATM channel of Section 1.2.3.2. The number of subcarriers used in the simulations is 128 in conjunction with a cyclic prefix of 32 and using a frame-invariant environment. The results of the simulations are shown in Section 2.4.3.1, Section 2.4.3.2 and Section 2.4.3.3 for the two, four and eight receiver antennas scenario, respectively. We had also performed simulation to quantify the effects of varying the number of receiver antennas, while fixing the number of users and the corresponding results are presented in Section 2.4.3.4.

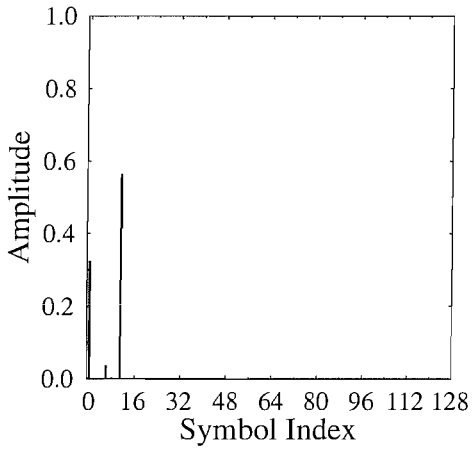

(a) CIR 1: User 1, antenna 1

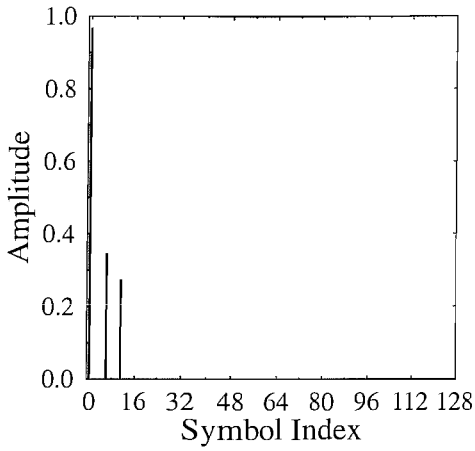

(b) CIR 2: User 1, antenna 2

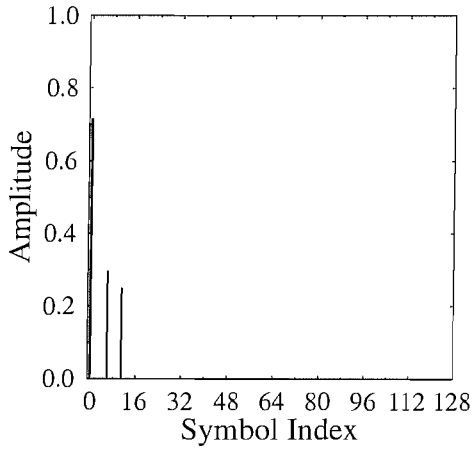

(c) CIR 3: User 2, antenna 1

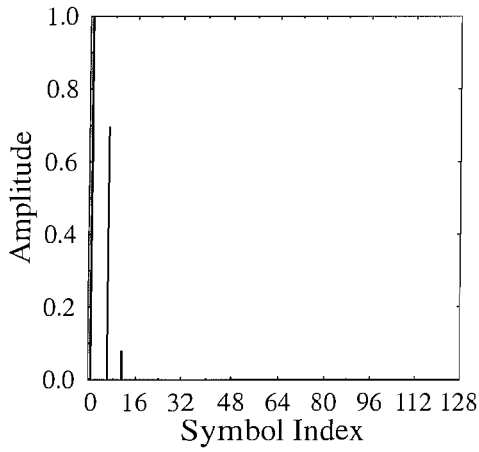

(d) CIR 4: User 2, antenna 2

Figure 2.4: Four different time-invariant channel impulse responses (CIR) recorded at the two receiver antennas, when two users are supported.

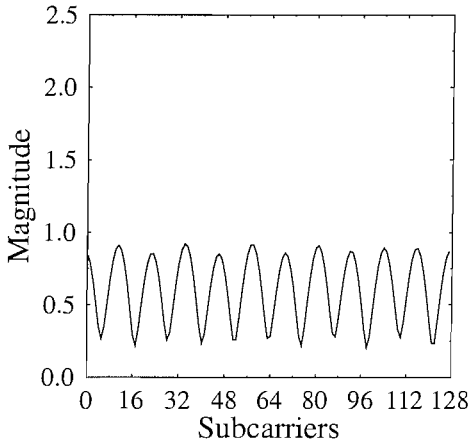

(a) FDCHTF 1: User 1, antenna 1

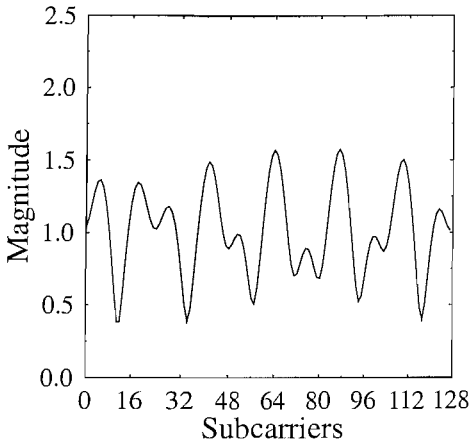

(b) FDCHTF 2: User 1, antenna 2

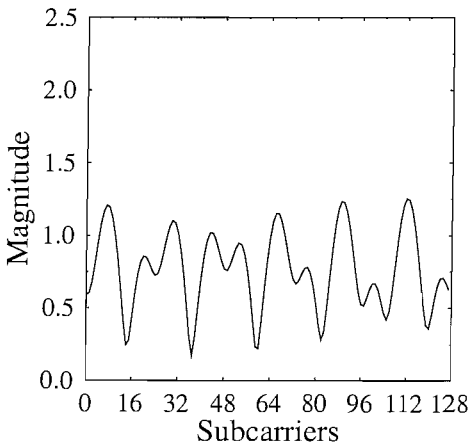

(c) FDCHTF 3: User 2, antenna 1

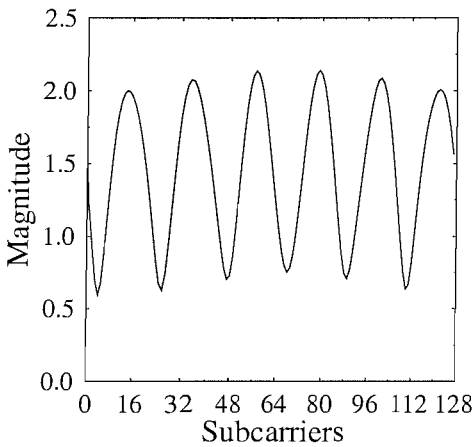

(d) FDCHTF 4: User 2, antenna 2

Figure 2.5: Four time-invariant FDCHTFs for the CIRs seen in Figure 2.4 (a) FDCHTF 1, (b) FDCHTF 2, (c) FDCHTF 3, and (d) FDCHTF 4.

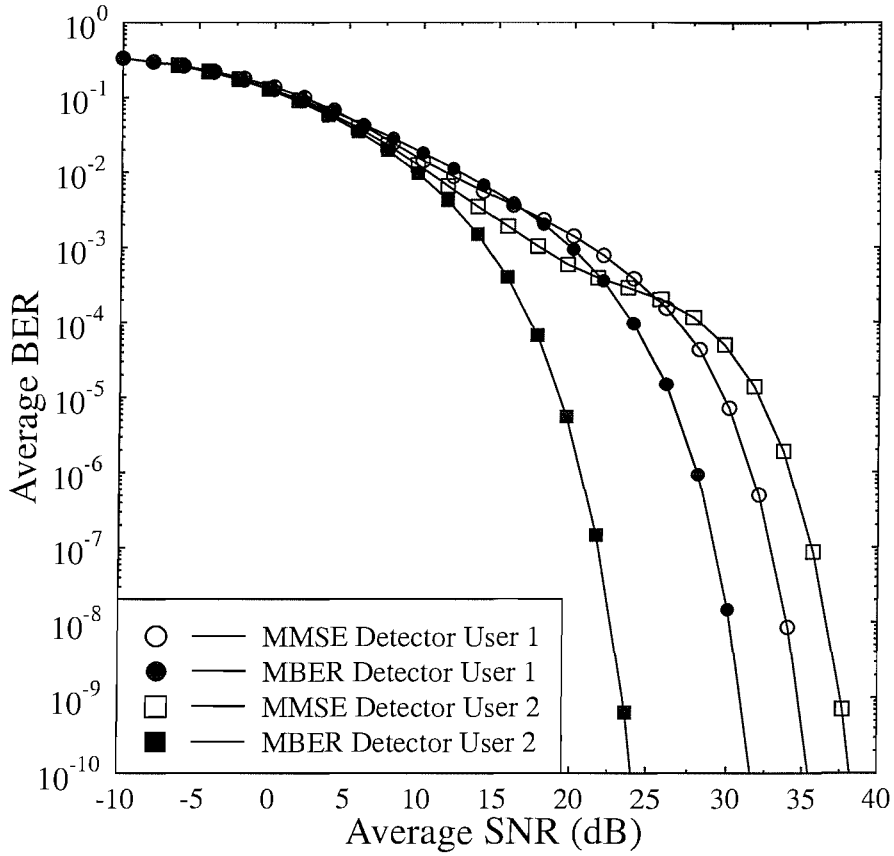

Figure 2.6: Average BER versus the average SNR expressed in dB for the MMSE and the MBER multiuser detectors of User 1 and User 2 supported by two receiver antennas, when using 128-subcarrier OFDM for communicating over the channel characterised by the CIRs and FDCHTFs shown in Figure 2.4 and Figure 2.5, respectively. These curves were evaluated from Equation 2.33.

2.4.3.1 Employing two receiver antennas

In our first quantitative investigation we used the simplest possible SDMA OFDM system supporting two users with the aid of two receiver antennas. As shown in Figure 2.1, each user has a unique FDCHTF with respect to each receiver antenna. The four corresponding CIRs are shown in Figure 2.4 and the resultant FDCHTFs are depicted in Figure 2.5. The CIRs represent a three-path indoor type channel [4], where no fading is experienced. Correspondingly, the time-invariant FDCHTF 1 and FDCHTF 2 are encountered by User 1 at the first and second receiver antenna, respectively. Similarly, FDCHTF 3 is encountered at the first receiver antenna and FDCHTF 4 at the second antenna by User 2. The OFDM

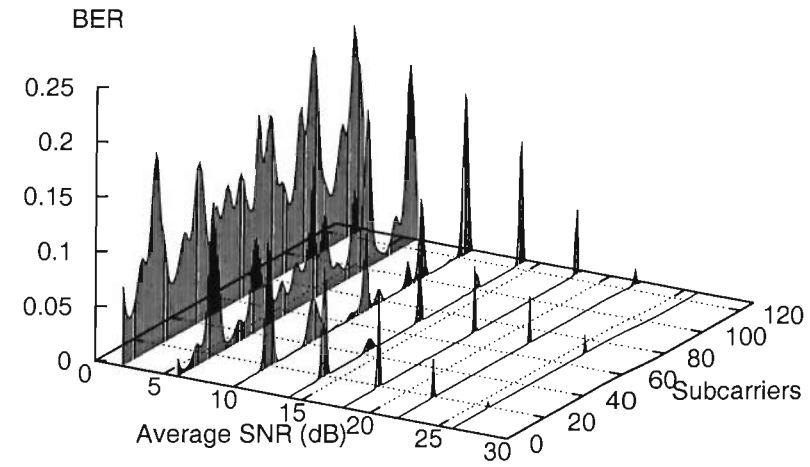

(a) MMSE

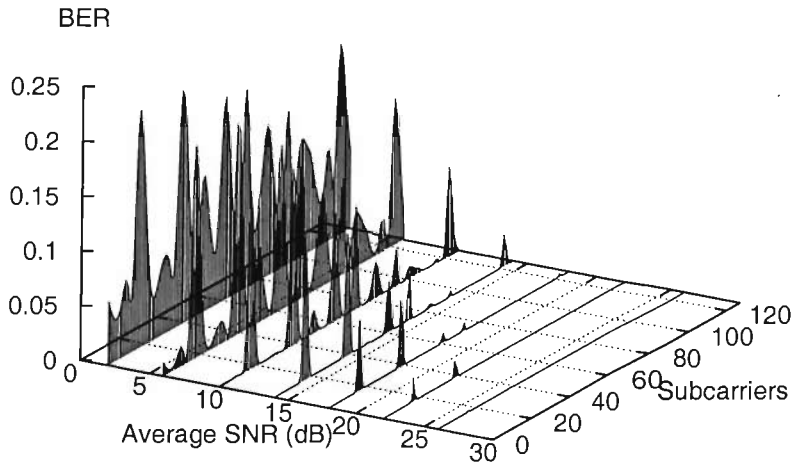

(b) MBER

Figure 2.7: BER versus the average SNR for every OFDM subcarrier for both the (a) MMSE, and (b) MBER multiuser detector of User 1 when supporting two users with the aid of two receiver antennas using 128-subcarrier OFDM for communicating over the channel characterised with the aid of the CIRs and FDCHTFs shown in Figure 2.4 and Figure 2.5, respectively.

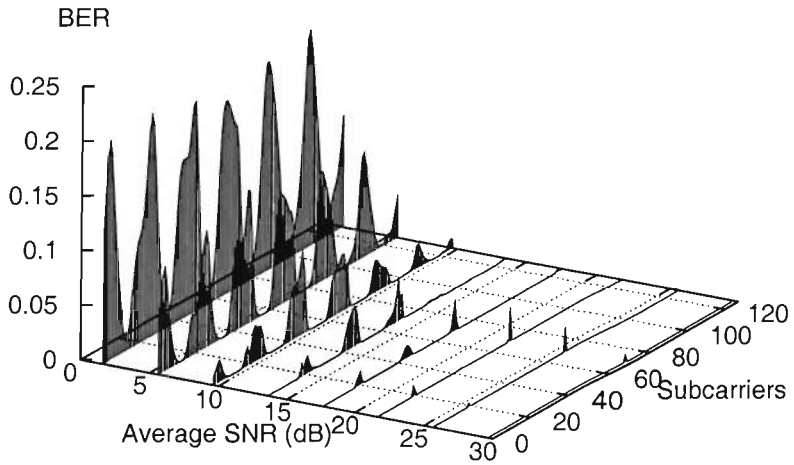

(a) MMSE

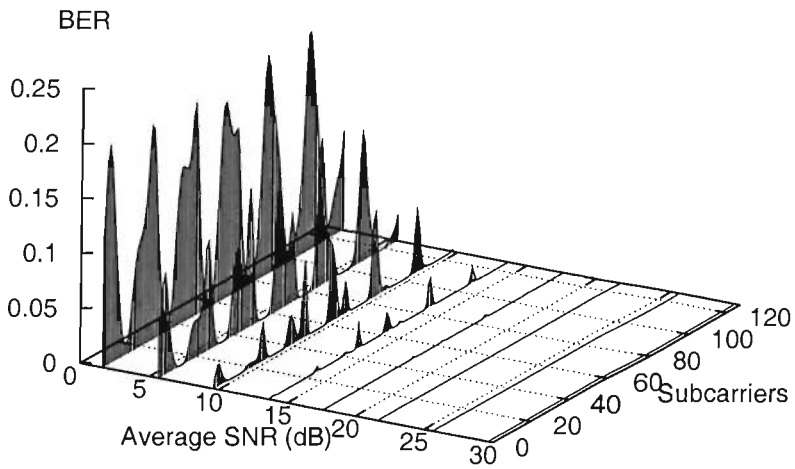

(b) MBER

Figure 2.8: BER versus the average SNR for every OFDM subcarrier for both the (a) MMSE, and (b) MBER multiuser detector of User 2, when supporting two users with the aid of two receiver antennas using 128-subcarrier OFDM for communicating over the channel characterised with the aid of the CIR and FDCHTF shown in Figure 2.4 and Figure 2.5, respectively.

modem had 128 subcarriers. In our simulations, we initialised the iterative MBER algorithm to the MMSE MUD weights given by Equation 2.25.

The results of our simulations are shown in Figures 2.6, 2.7 and 2.8. The average BER of User 1 and User 2 recorded in the context of both the MMSE and MBER MUD is portrayed in Figure 2.6. We can see from this figure that User 1 has a better average BER in conjunction with the MMSE detector compared to User 2 for SNRs in excess of about 25 dB. By contrast, the MBER detector of User 2 outperforms that of User 1 in terms of the average BER. We can also see that the MBER detectors of both users have a substantially lower average BER compared to the MMSE detectors. Again, as expected, this is because the MMSE is directly minimising the MSE and not the BER. We may also note that the average BER difference between the MMSE and MBER detectors is not the same for both users. Specifically, the MBER MUD of User 2 has an SNR advantage of almost 12 dB, while that of User 1 has about 5 dB SNR advantage, when the target BER is 10^{-6}. This is a consequence of the unique combinations of the channel transfer functions of both users, since it can be seen in Figure 2.4 that the CIR of User 1 exhibits a lower ratio between the main and the delayed CIR taps than that of User 2.

In Figure 2.7 and Figure 2.8, we can see that the BER of the MMSE and MBER MUD is different for every OFDM subcarrier. This is because the particular combination of the FDCHTFs is unique for the different OFDM subcarriers. These FDCHTF differences will result in a frequency and time-variant system matrix, $\mathbf{H}$, for each OFDM subcarrier, thus imposing a direct influence on the calculation of the MUD's weight values, as suggested by Equation 2.25 and Equation 2.35 for the MMSE and MBER MUD, respectively. By comparing the BER plots of Figure 2.7 and Figure 2.8 recorded for User 1 and User 2 respectively, we can see that the BER peaks of the dramatically attenuated subcarriers of Figure 2.5 are higher for the MMSE MUD than for the MBER arrangement.

2.4.3.2 Employing four receiver antennas

We will now investigate the achievable performance of the MUDs employing four receiver antennas. As in the two receiver antenna scenario, each user has a different CIR at each receiver antenna. Initially, we support the same number of users as the number of receiver antennas, which is four. The CIR and FDCHTF of User 1 is as shown in Figure 2.9 and

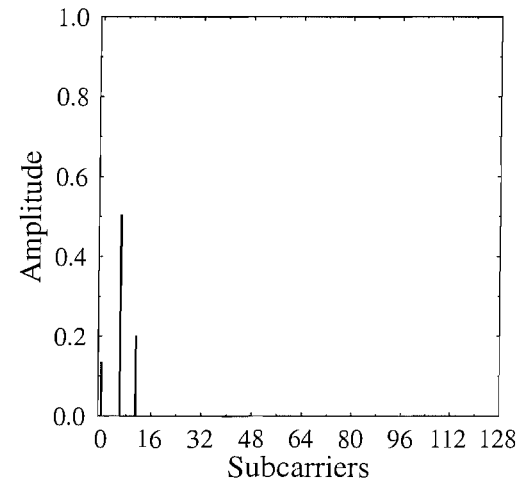

(a) CIR 1: User 1, antenna 1

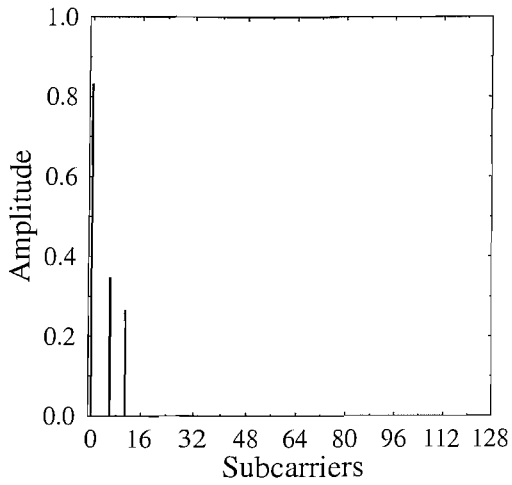

(b) CIR 2: User 1, antenna 2

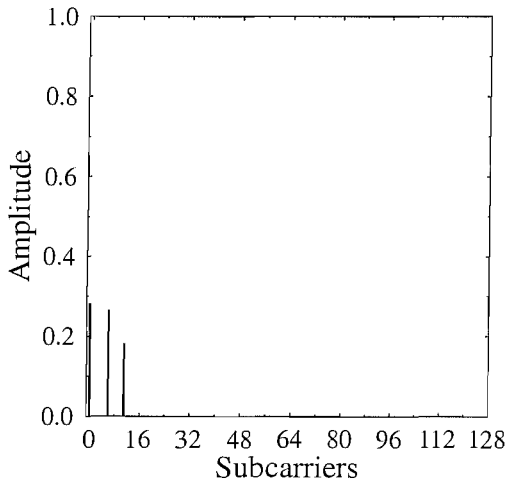

(c) CIR 3: User 1, antenna 3

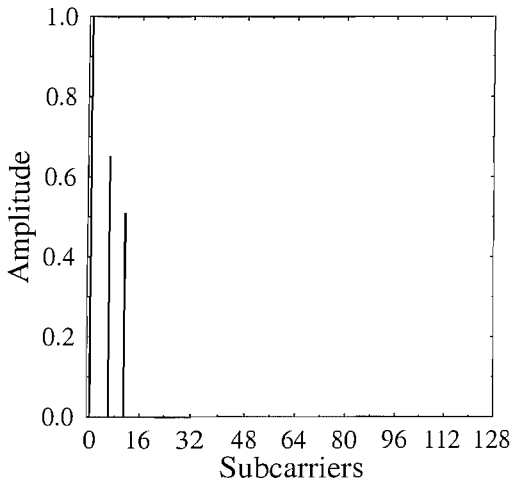

(d) CIR 4: User 1, antenna 4

Figure 2.9: Four different time-invariant channel impulse responses (CIR) recorded at the four receiver antennas for User 1, which benefits from the lowest BER among the four users, as shown in Figure 2.13.

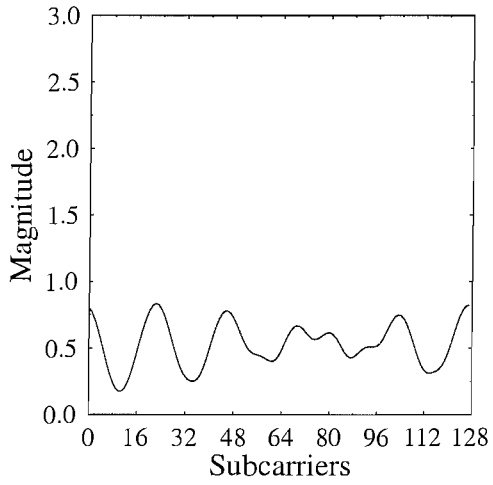

(a) FDCHTF 1: User 1, antenna 1

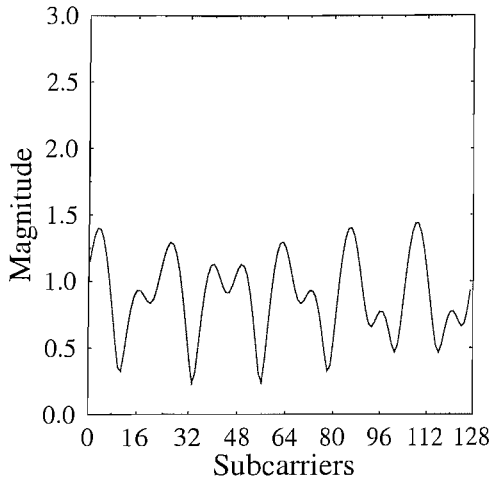

(b) FDCHTF 2: User 1, antenna 2

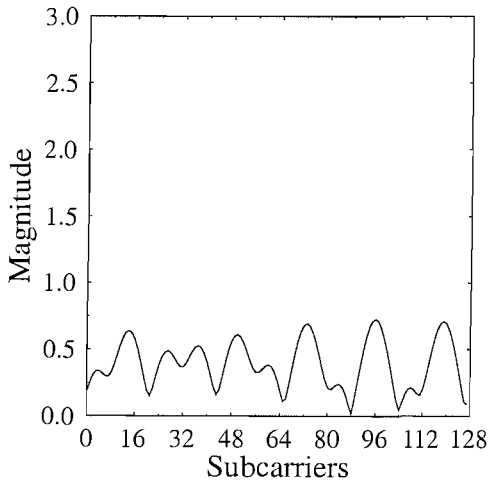

(c) FDCHTF 3: User 1, antenna 3

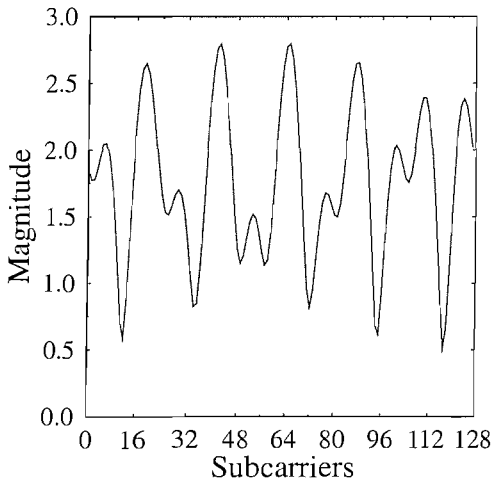

(d) FDCHTF 4: User 1, antenna 4

Figure 2.10: Four time-invariant FDCHTFs for the CIRs seen in Figure 2.9 (a) FDCHTF 1, (b) FDCHTF 2, (c) FDCHTF 3, and (d) FDCHTF 4.

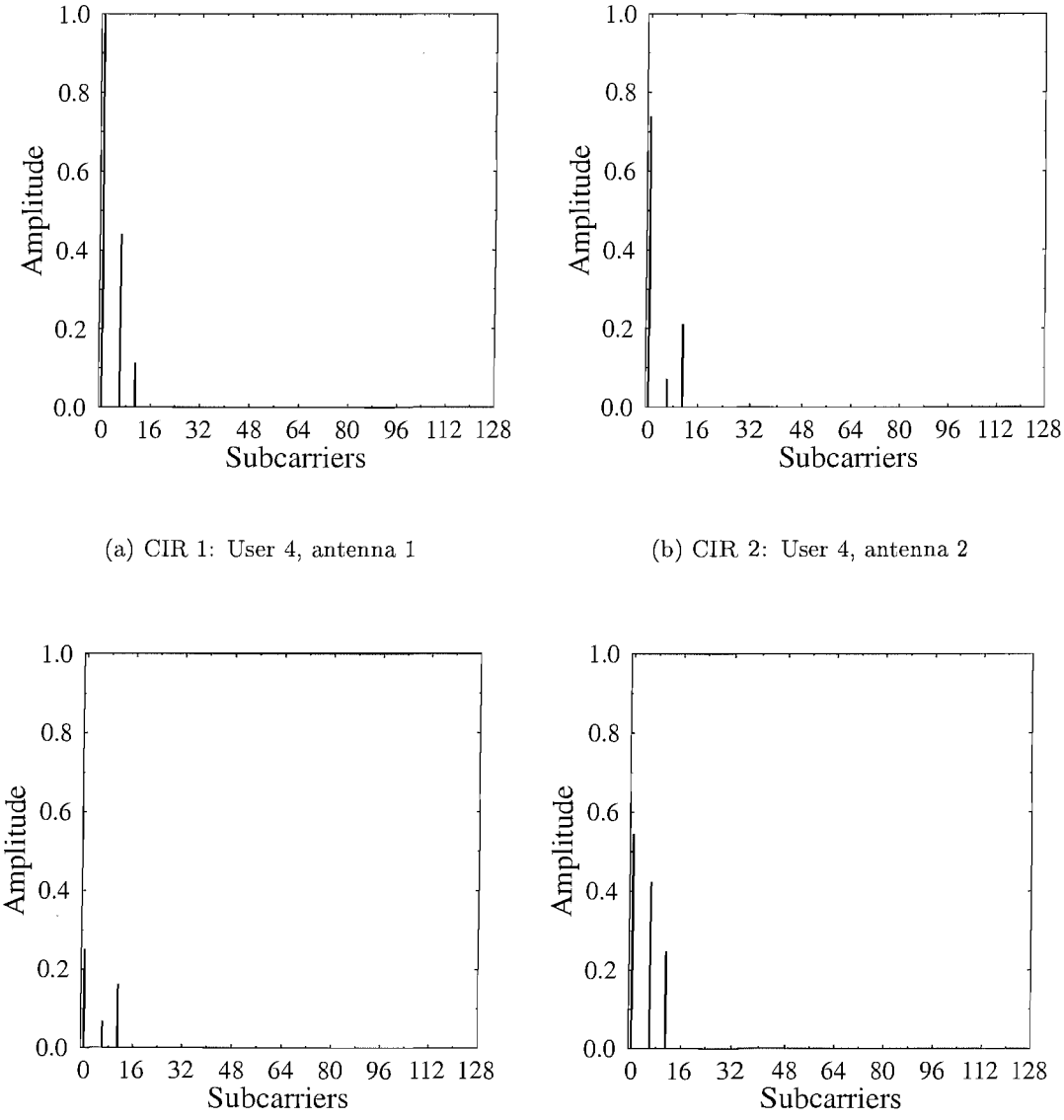

(a) CIR 1: User 4, antenna 1

(b) CIR 2: User 4, antenna 2

(c) CIR 3: User 4, antenna 3

(d) CIR 4: User 4, antenna 4

Figure 2.11: Four different time-invariant channel impulse responses (CIR) recorded at the four receiver antennas for User 4, which experiences the worst-case BER among the four users, as shown in Figure 2.13.

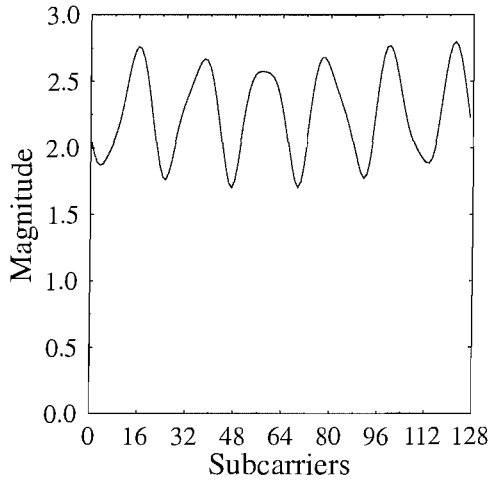

(a) FDCHTF 1: User 4, antenna 1

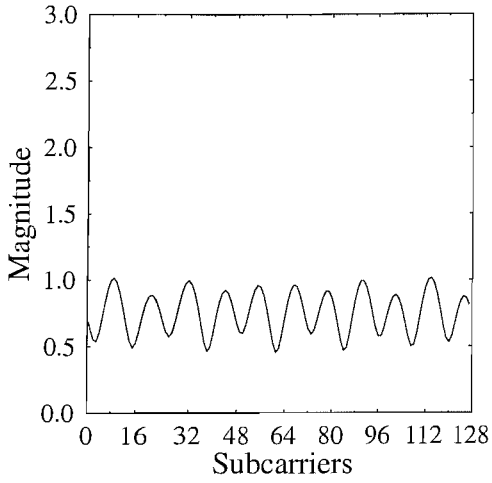

(b) FDCHTF 2: User 4, antenna 2

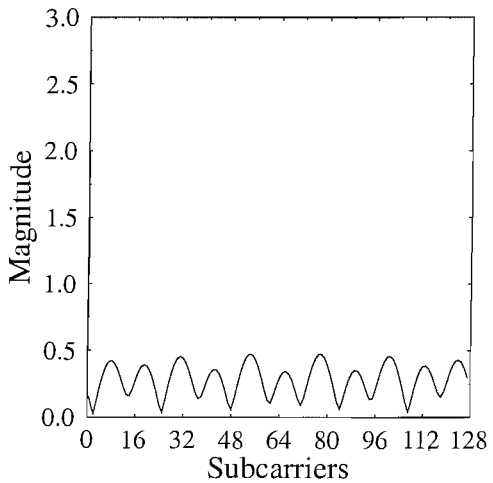

(c) FDCHTF 3: User 4, antenna 3

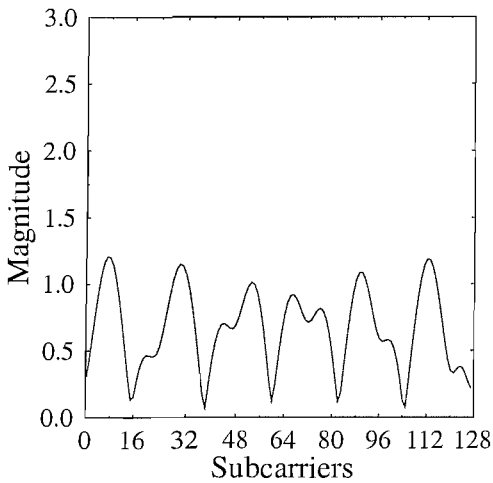

(d) FDCHTF 4: User 4, antenna 4

Figure 2.12: Four time-invariant FDCHTFs for the CIRs seen in Figure 2.11 (a) FDCHTF 1, (b) FDCHTF 2, (c) FDCHTF 3, and (d) FDCHTF 4.

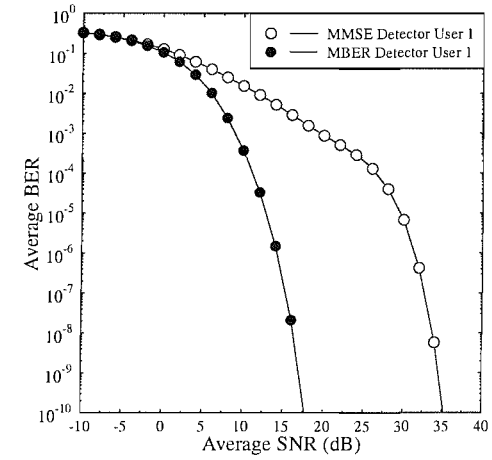

(a) User 1

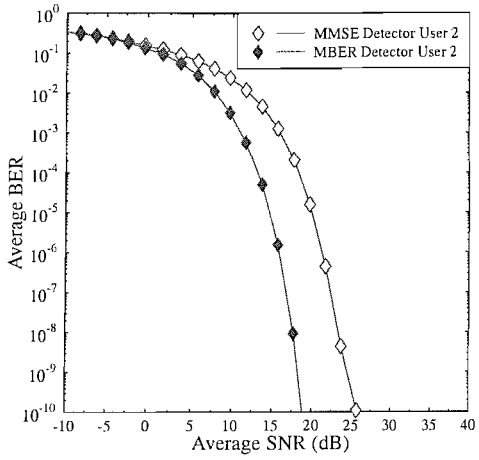

(b) User 2

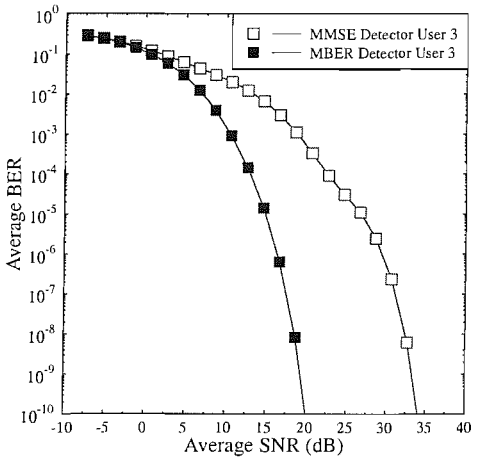

(c) User 3

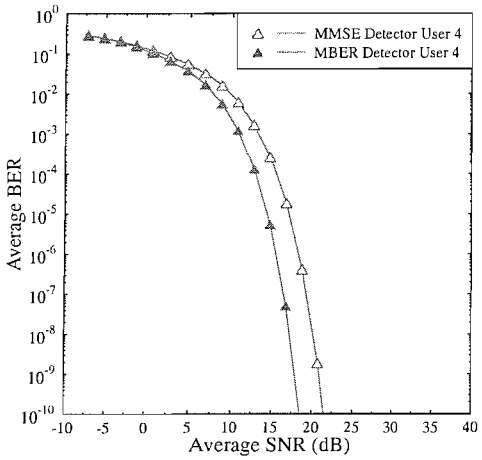

(d) User 4

Figure 2.13: The BER performance of the four different users in an SDMA system employing four receiver antennas and 128-subcarrier OFDM for communicating over the frame-invariant SWATM channel. These curves were evaluated from Equation 2.33.

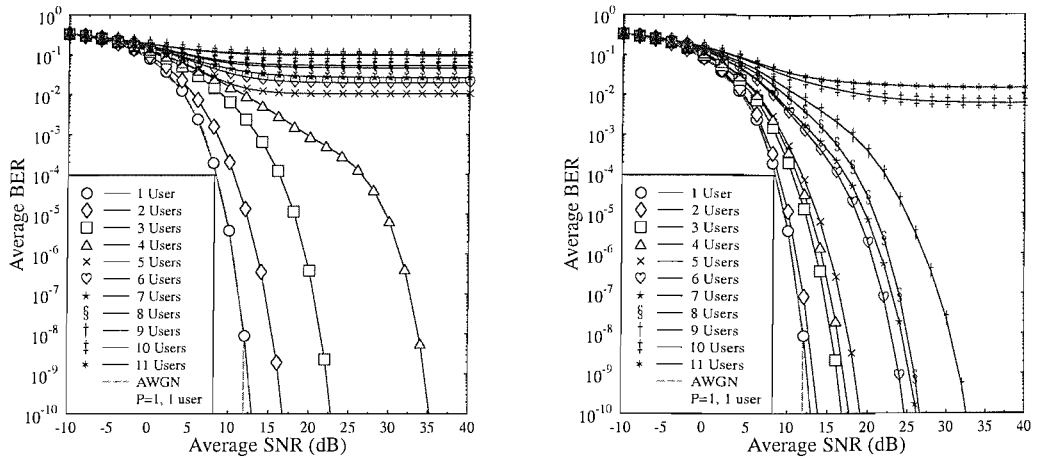

(a) MMSE MUD (b) MBER MUD

Figure 2.14: The BER performance of User 1 employing both the MMSE and MBER MUD in an SDMA system equipped with four receiver antennas for different number of users employing 128-subcarrier OFDM communicating over the frame-invariant SWATM channel. These curves were evaluated from Equation 2.33.

Figure 2.10, respectively. It will be shown in Figure 2.13 that User 1 achieves the biggest difference between the achievable BER of the MBER and MMSE MUDs. By contrast, the smallest difference between the achievable BER of the MBER and MMSE MUDs among the four users is experienced by User 4, which has its CIR and FDCHTF depicted in Figure 2.11 and Figure 2.12, respectively. Again, the corresponding BERs are shown in Figure 2.13.

We can see from Figure 2.13 that each user performs differently in terms of the achievable BER. The argument that was mentioned in Section 2.4.3.1 for the two-user case also applies here, namely that each user has its own unique system matrix as a consequence of the unique combinations of the channel transfer functions of all users. However, in general the MBER MUD performed better than the MMSE MUD in all investigated scenarios. The highest BER difference was experienced by User 1, where the MBER MUD outperformed the MMSE MUD by about 17 dB, while the smallest difference was recorded for User 4, where the corresponding SNR advantage was only about 3 dB, when the target BER was 10^{-6}.

So far, we have been supporting the same number of users as the number of receiver antennas in our simulations. By contrast, Figure 2.14 shows the BER results for User 1 for

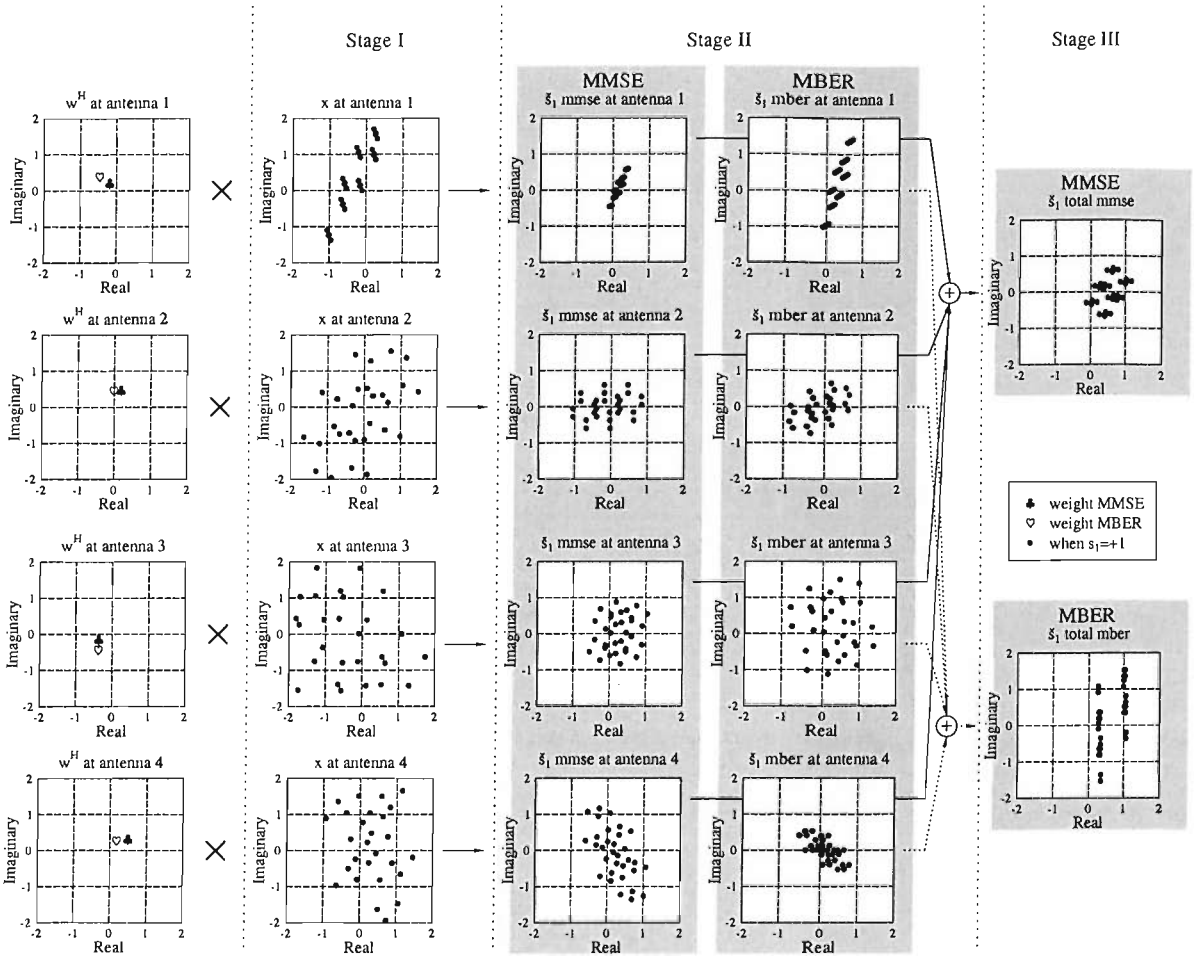

Figure 2.15: An example composition of the probable noiseless received signal for User 1 for the case of $P = 4, L = 6$ when transmitting $s_1 = +1$. The stages is as depicted in Figure 2.1.

supporting different number of users in the four receiver antenna scenario. We can see from the figure that as the number of users increases, the BER performance degrades owing to the increased multiuser interference imposed. In the absence of multiuser interference when only one user is communicating, both MUDs have similar BER curves. As expected, this is because no multiuser interference is inflicted and hence the MMSE MUD is also capable of minimising the BER. However, the MMSE MUDs characterised in Figure 2.14(a) can only support a maximum number of users that is equal to the number of receiver antennas, which is four in this case. Once the number of users exceeds the number of receiver antennas, the MMSE MUD becomes incapable of differentiating the users and this results in the high residual BER seen in Figure 2.14(a).

These performance trends may be more explicitly interpreted with the aid of Figure 2.15,

where the composition of User 1's noiseless received phasors are illustrated, when transmitting $s_1 = +1$ in the six-user scenario employing four receiver antennas. Different processing stages seen in this figure were defined in Figure 2.1.

Stage I represents the received composite multiuser signals, $x_1, \ldots, x_P$, impinging at the different antennas. Let us recall from Equation 2.1 that $x_p, p \in 1, 2, \ldots, P$, is constituted by the superposition of the L number of users, which in this case is $L = 6$. Since we are assuming that User 1 is transmitting $s_1 = +1$, the number of possible combinations at each antenna in Figure 2.15 is $N_b/2 = 2^L/2 = 2^6/2 = 32$. However, some of the points might be overlapping, thus only a lower number of points is observable. It can also be seen that the location of the points varies between the antennas due to the fact that the different antennas will experience different combinations of the FDCHTF.

Stage II shows the outputs from the product of the Hermitian of the MUD's weight value, w_p, $p \in 1, \ldots, P$, of the individual antenna elements and the corresponding x_p, $p \in 1, \ldots, P$, value, i.e. $w^H x$, as seen in Equation 2.9. At this stage, it is the appropriate combination of the individual antennas' combinations at Stage III, which determines the final output of the MUD.

Explicitly, the MMSE MUD attempts to minimise the Euclidean distance between the estimated received symbol, $\hat{s}_1$ and the original transmitted symbol s_1. However, as can be observed at Stage III of Figure 2.15, some of the $\hat{s}_{1,MMSE}$ points are either on the wrong half-plane of the BPSK phasor constellation or exactly on the decision boundary, namely at $y_R = 0$. As a consequence, the associated residual BER experienced in the absence of noise can be calculated by taking into account the relative frequency of these points. On the other hand, since the MBER MUD is directly minimising the BER, the MUD's weight values are adjusted for the sake of ensuring that the estimated phasors are as far away from the decision boundary as possible. Therefore, we can see from Figure 2.15 that the estimated received phasors $\hat{s}_{1,MBER}$ are significantly further from the BPSK decision boundary of $y_R = 0$, than for the MMSE MUD, hence avoiding the MMSE-specific residual BER.

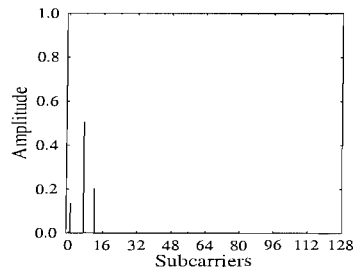

(a) CIR 1: User 1, antenna 1

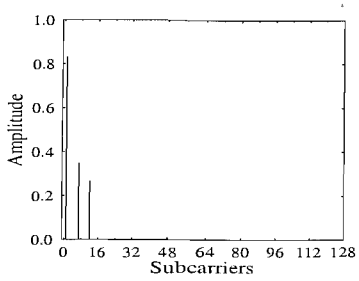

(b) CIR 2: User 1, antenna 2

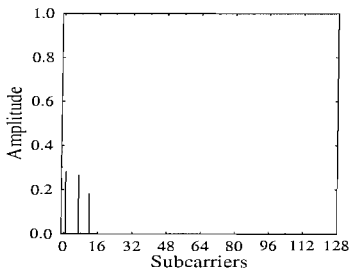

(c) CIR 3: User 1, antenna 3

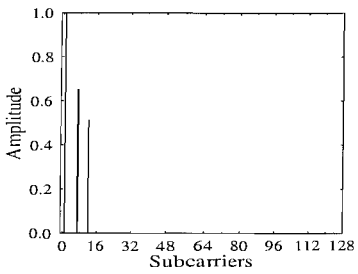

(d) CIR 4: User 1, antenna 4

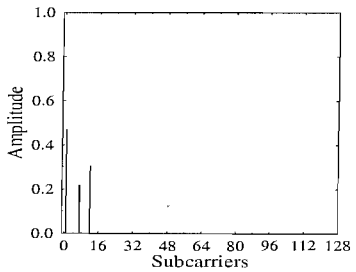

(e) CIR 5: User 1, antenna 5

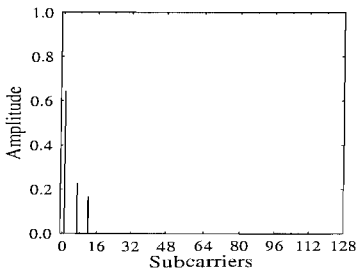

(f) CIR 6: User 1, antenna 6

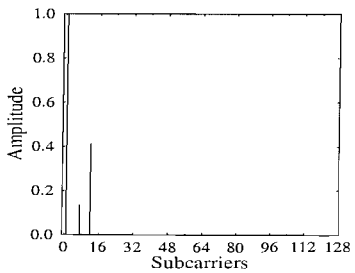

(g) CIR 7: User 1, antenna 7

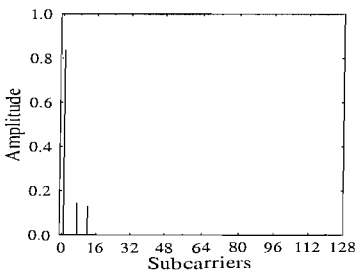

(h) CIR 8: User 1, antenna 8

Figure 2.16: Eight different time-invariant channel impulse responses (CIR) recorded at the eight receiver antennas for User 1, which experiences the best-case BER among the eight users, as shown in Figure 2.20.

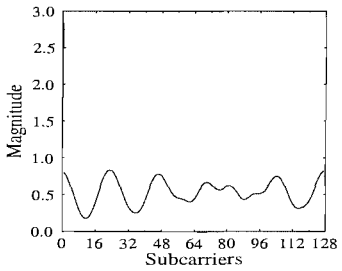

(a) FDCHTF 1: User 1, antenna 1

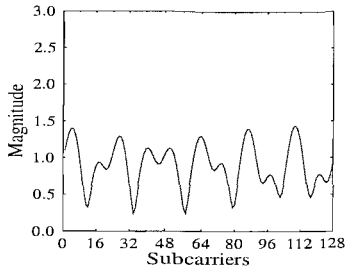

(b) FDCHTF 2: User 1, antenna 2

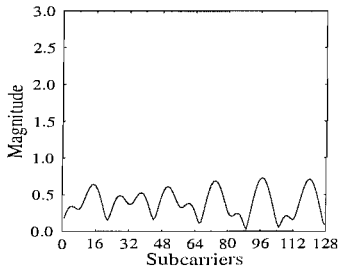

(c) FDCHTF 3: User 1, antenna 3

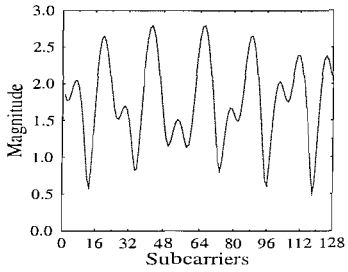

(d) FDCHTF 4: User 1, antenna 4

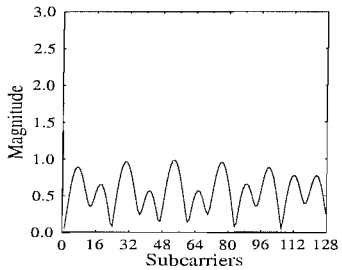

(e) FDCHTF 5: User 1, antenna 5

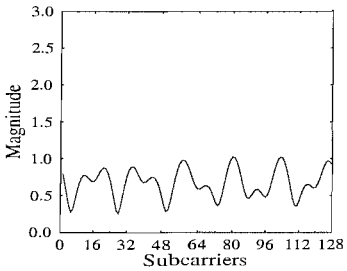

(f) FDCHTF 6: User 1, antenna 6

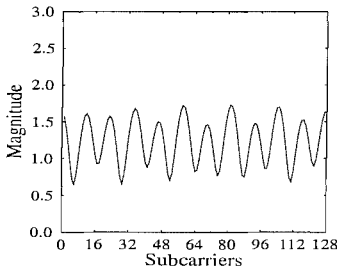

(g) FDCHTF 7: User 1, antenna 7

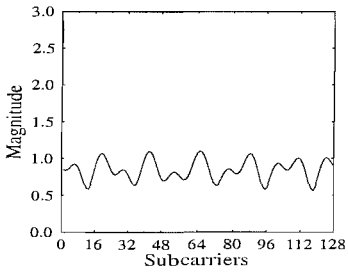

(h) FDCHTF 8: User 1, antenna 8

Figure 2.17: Eight time-invariant FDCHTFs for the CIRs seen in Figure 2.16 (a) FDCHTF 1, (b) FDCHTF 2, (c) FDCHTF 3, and (d) FDCHTF 4 (e) FDCHTF 5, (f) FDCHTF 6, (g) FDCHTF 7, and (h) FDCHTF 8.

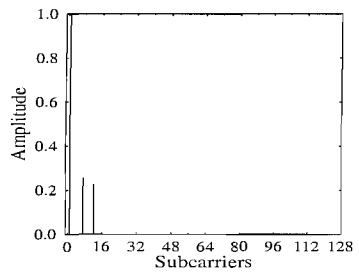

(a) CIR 1: User 5, antenna 1

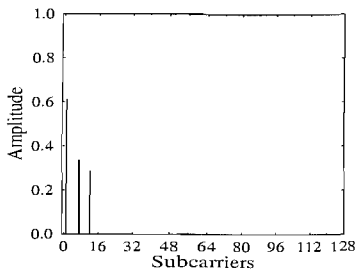

(b) CIR 2: User 5, antenna 2

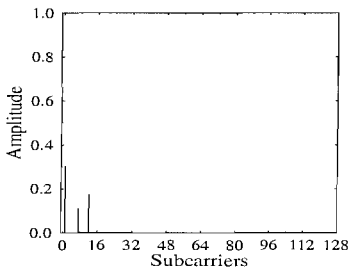

(c) CIR 3: User 5, antenna 3

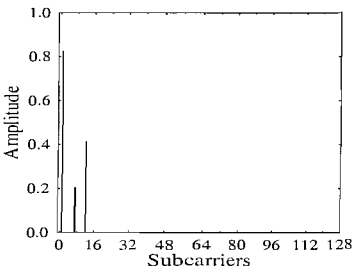

(d) CIR 4: User 5, antenna 4

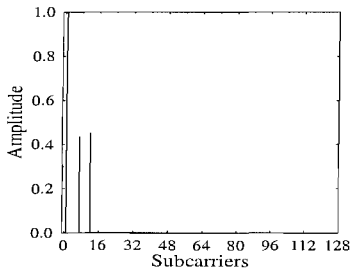

(e) CIR 5: User 5, antenna 5

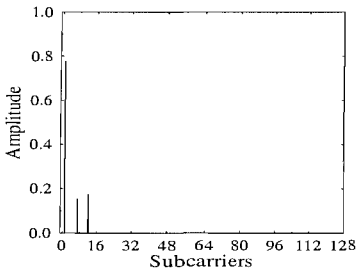

(f) CIR 6: User 5, antenna 6

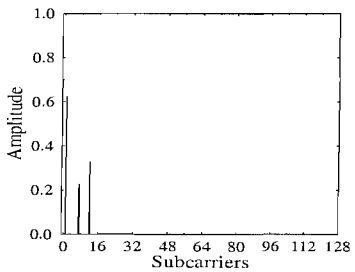

(g) CIR 7: User 5, antenna 7

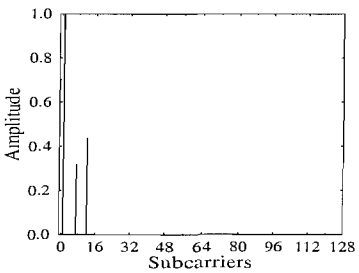

(h) CIR 8: User 5, antenna 8

Figure 2.18: Eight different time-invariant channel impulse responses (CIR) recorded at the eight receiver antennas for User 5, which experiences the worst-case BER among the eight users, as shown in Figure 2.20.

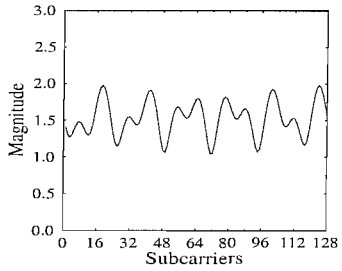

(a) FDCHTF 1: User 5, antenna 1

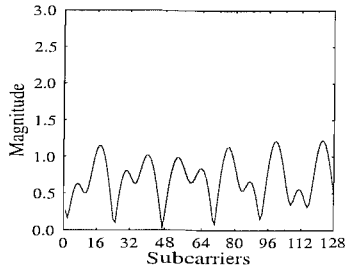

(b) FDCHTF 2: User 5, antenna 2

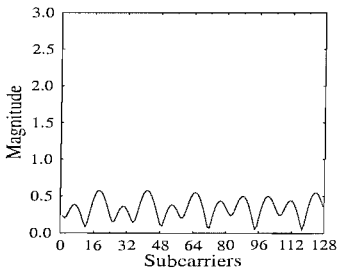

(c) FDCHTF 3: User 5, antenna 3

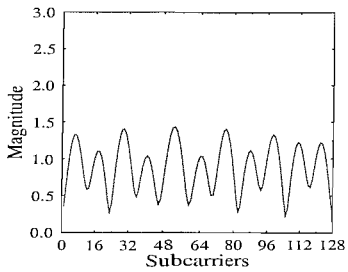

(d) FDCHTF 4: User 5, antenna 4

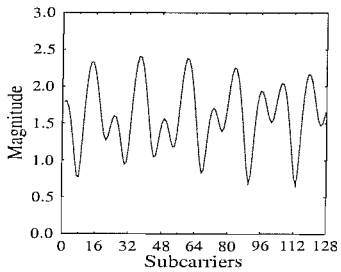

(e) FDCHTF 5: User 5, antenna 5

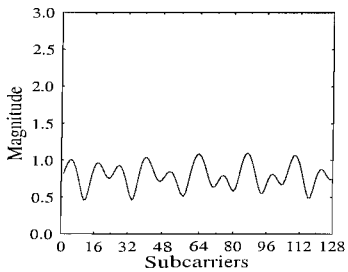

(f) FDCHTF 6: User 5, antenna 6

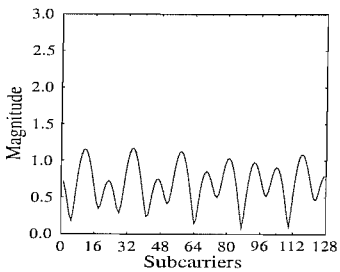

(g) FDCHTF 7: User 5, antenna 7

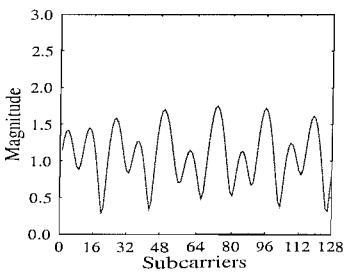

(h) FDCHTF 8: User 5, antenna 8

Figure 2.19: Eight time-invariant FDCHTFs for the CIRs seen in Figure 2.18 (a) FDCHTF 1, (b) FDCHTF 2, (c) FDCHTF 3, and (d) FDCHTF 4 (e) FDCHTF 5, (f) FDCHTF 6, (g) FDCHTF 7, and (h) FDCHTF 8.

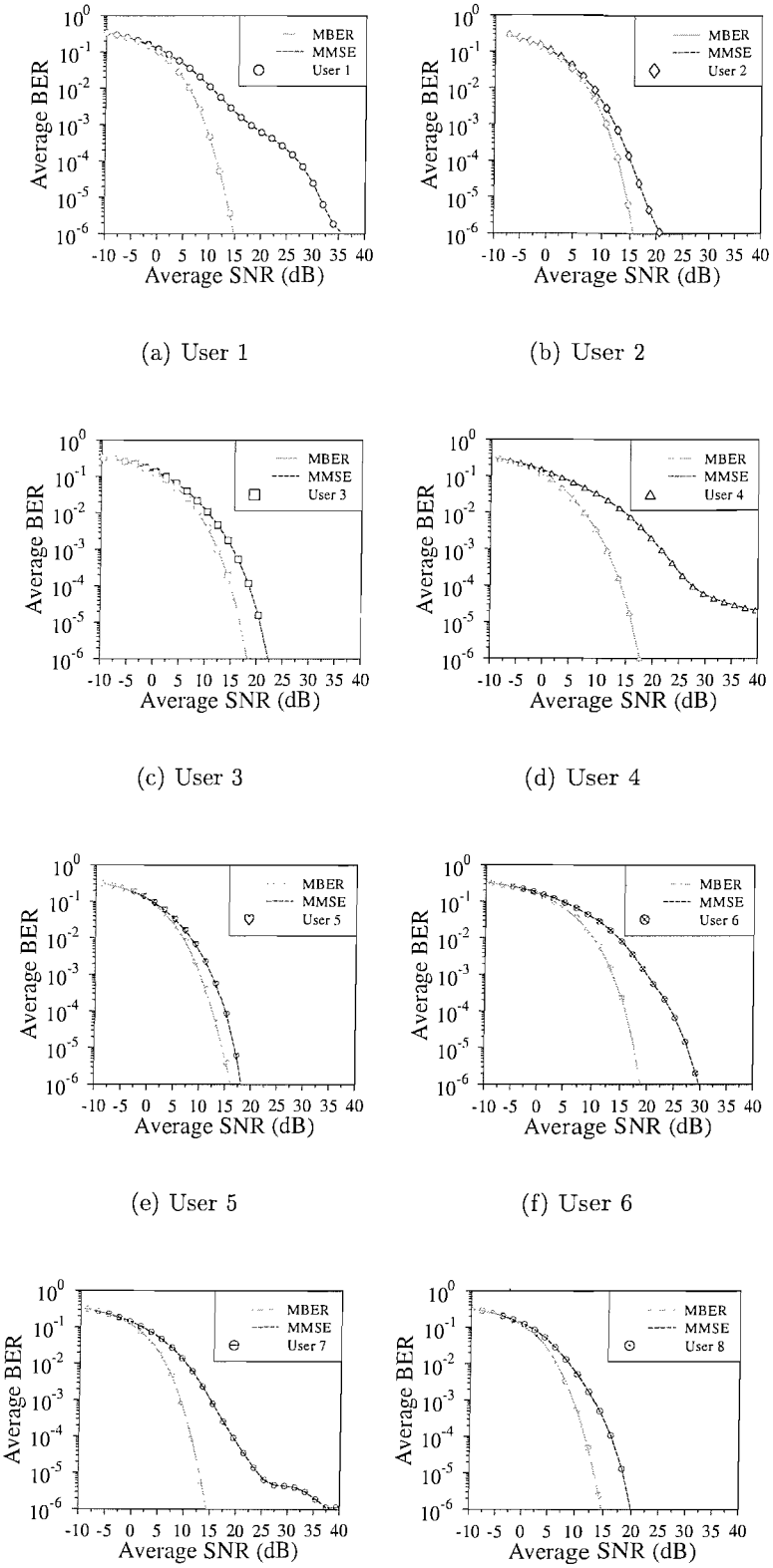

(a) User 1 (b) User 2

(c) User 3 (d) User 4

(e) User 5 (f) User 6

(g) User 7 (h) User 8

Figure 2.20: The BER performance of eight different users in an SDMA system equipped with eight receiver antennas using 128-subcarrier OFDM for communicating over the frame-invariant SWATM channel. These curves were evaluated from Equation 2.33.

2.4.3.3 Employing eight receiver antennas

In this section, we will continue our investigations by using eight antennas at the receiver. The number of users supported is the same as the number of receiver antennas. The CIR and the FDCHTF associated with the highest difference in the achievable average BER of the MBER and MMSE MUDs were encountered by User 1, which were shown in Figure 2.16 and Figure 2.17, respectively. By contrast, the scenario associated with the smallest difference between the achievable BER of the MBER and MMSE MUDs among the eight users was that of User 5, who has his/her CIR and FDCHTF depicted in Figure 2.18 and Figure 2.19, respectively.

The associated simulation results are shown in Figure 2.20. We can see that there are cases when the MMSE MUDs perform poorly, exhibiting a high residual BER as the SNR increases, for example in the case of User 4 and User 7. On the other hand, for User 5 the MMSE MUD performs similarly well to the MBER MUD. The large performance variation experienced by the different users may be owing to the fact that as the number of receiver antennas is increased, there is a high probability of encountering a detrimental combination of desired-user CIR and interfering-user CIR for the different users. Furthermore, when supporting eight users, the multiuser interference becomes high. However, the MBER MUD still performs consistently better than the MMSE MUD for all the users.

2.4.3.4 Effects of different number of receiver antennas

In this section, we will now investigate the effect of varying the number of receiver antennas at the base station, when employing both the MMSE and the MBER MUD. The number of users is fixed to two. The results of these investigations is portrayed in Figure 2.21. Both the MMSE and MBER MUD's BER performance improved, as the number of antennas was increased. This is because as the number of antennas increases, the MUD becomes more efficient in mitigating the effects of multiuser interference. Even when only two receivers antennas are used, the BER performance of the MBER MUD approaches the BER curve of the non-dispersive single-user AWGN channel as can be seen in Figure 2.21(b). On the other hand, the MMSE MUD characterised in Figure 2.21(a) required more than six antennas for achieving a BER performance close to the AWGN benchmarker curve. Therefore we may

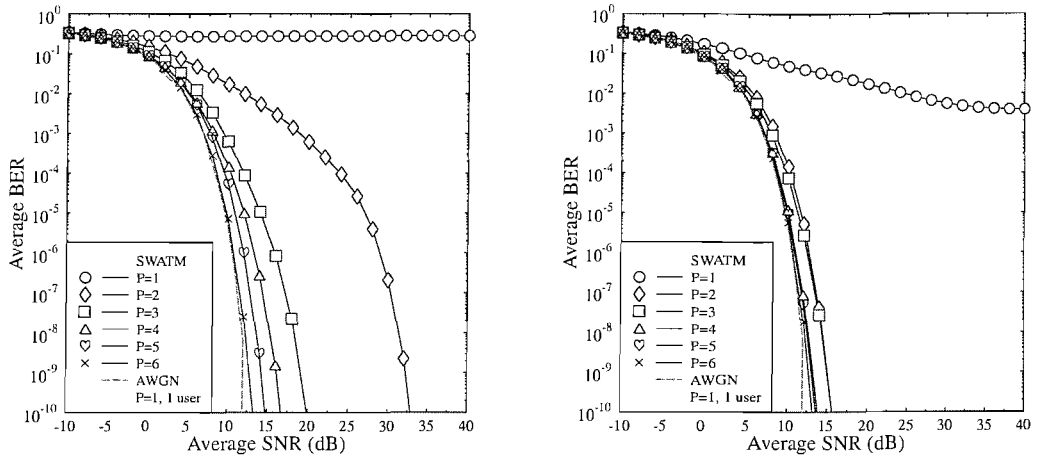

(a) MMSE MUD (b) MBER MUD

Figure 2.21: The BER performance of User 1 encountering a better BER than User 2, when employing both the MMSE and MBER MUD for supporting two users with the aid of different number of receiver antennas employing 128-subcarrier SDMA OFDM for communicating over the frame-invariant SWATM channel. These curves were evaluated from Equation 2.33.

conclude that the MBER MUD typically requires a lower number of receiver antennas compared to the MMSE MUD for the case of reaching the AWGN performance, when the same number of users are supported.

2.4.4 Effects of varying the CG algorithm parameters

Let us now commence our study of the effects of varying the different parameters in the context of the CG method used for finding the optimum MBER MUD weights. We will initially study the effects of using various step-sizes μ in Section 2.4.4.1. This is followed by Section 2.4.4.2, where we will investigate the effects of varying the maximum number of iterations in the search. Finally, we will show the results associated with using different termination scalars β in Section 2.4.4.3.

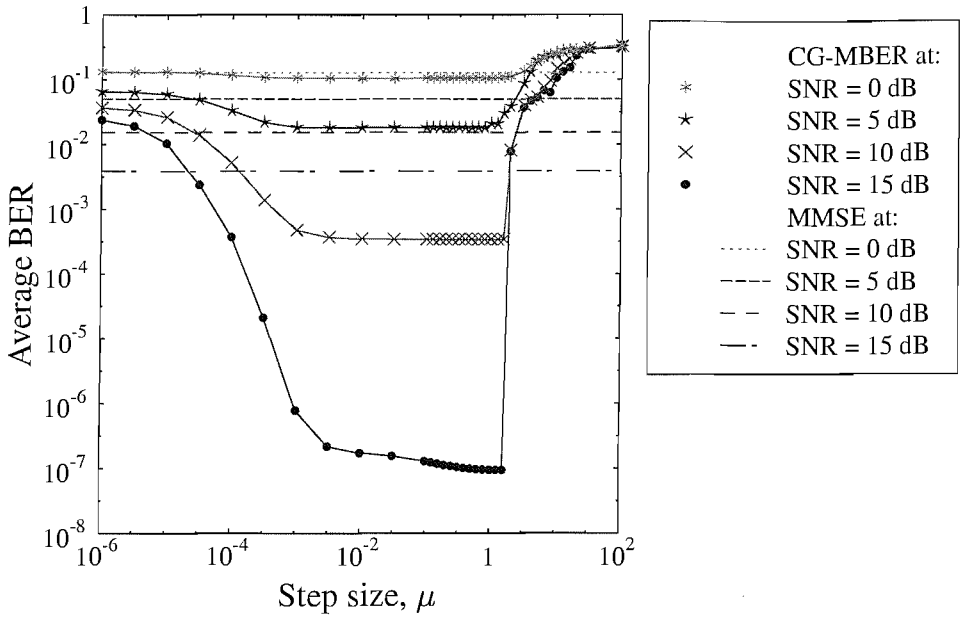

Figure 2.22: The average achievable BER of User 1 in the $P = 4$ and $L = 4$ OFDM SDMA system when varying the step size, μ of the conjugate gradient algorithm while fixing the maximum iterations to 10000 and initialising the MBER weight values to the MMSE weight values and the weight from the previous SNR. These curves were evaluated from Equation 2.33.

2.4.4.1 Step size, μ

One of the most important parameters in the context of the conjugate gradient search algorithm is the step-size μ. Figure 2.22 shows our simulation results when using different fixed values of μ for User 1 in a $P = 4$, $L = 4$ scenario. We can see from the figure that the best fixed value of μ is between 10^{-2} and 1. For a μ value that is too small, the search method might not be able to approach the optimum solution within the given maximum number of iterations. On the other hand, if the value of μ is too high, then the gradient search might miss the optimum solution. Therefore a suitable value of μ must be chosen to ensure that the best solution can be attained. In our case we have chosen the μ value of 10^{-1}. An alternative approach is to use an adaptive μ value, where the μ value varies according to the SNR and as a function of the complexity of the scenario investigated. However, we have opted for employing a simplified approach where a fixed value of μ is used.

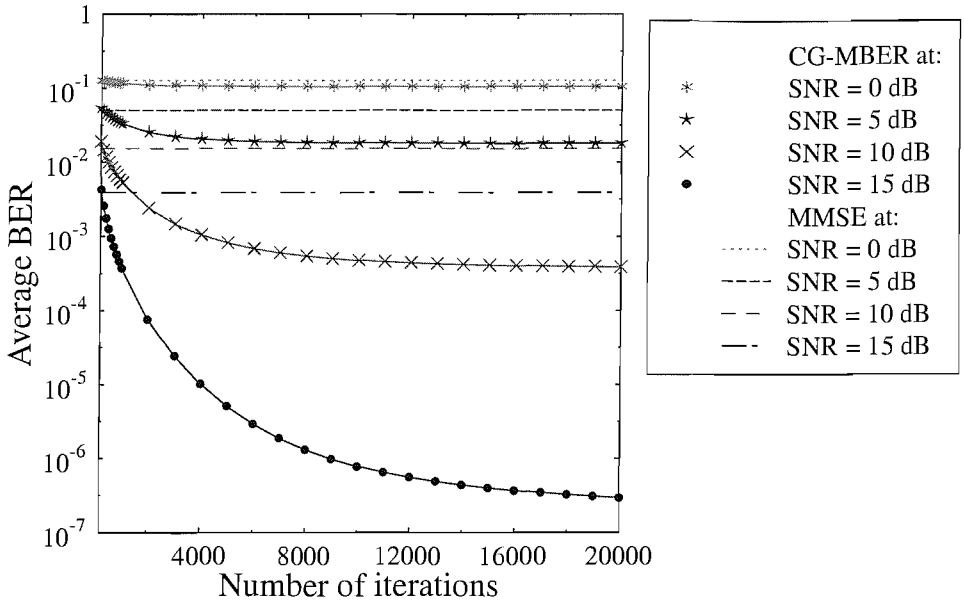

Figure 2.23: The average of the achievable BER of User 1 in the $P = 4$ and $L = 4$ OFDM SDMA system when varying the maximum number of iterations of the conjugate gradient algorithm while fixing the step size, μ to 0.1 and initialising the MBER weight values to the MMSE weight values and the weight from the previous SNR. These curves were evaluated from Equation 2.33.

2.4.4.2 Maximum iterations

Let us now study another factor that determines the performance of the CG search algorithm, namely the maximum number of iterations. The maximum number of iterations is usually fixed so that the complexity of the search becomes constant. However, an insufficiently high number of iterations may result in a premature termination of the search method, before the optimum solution is found. However, setting the maximum number of iterations to a value that is too high may waste battery power, especially when the achievable improvement is only modest, despite using a high number of iterations. Figure 2.23 shows our related simulation results, when the maximum number of iterations is varied. We can see from the figure that at a lower SNR value, a lower number of iterations is required to reach the optimum solution, if the same step-size is employed for all SNRs. This is because at a lower SNR value, the minimum value at the valley of the BER surface, such as the one seen in Figure 2.3, is not as deep as the one found at higher SNRs. Therefore, at high SNRs more iterations are required to reach the minimum BER point.

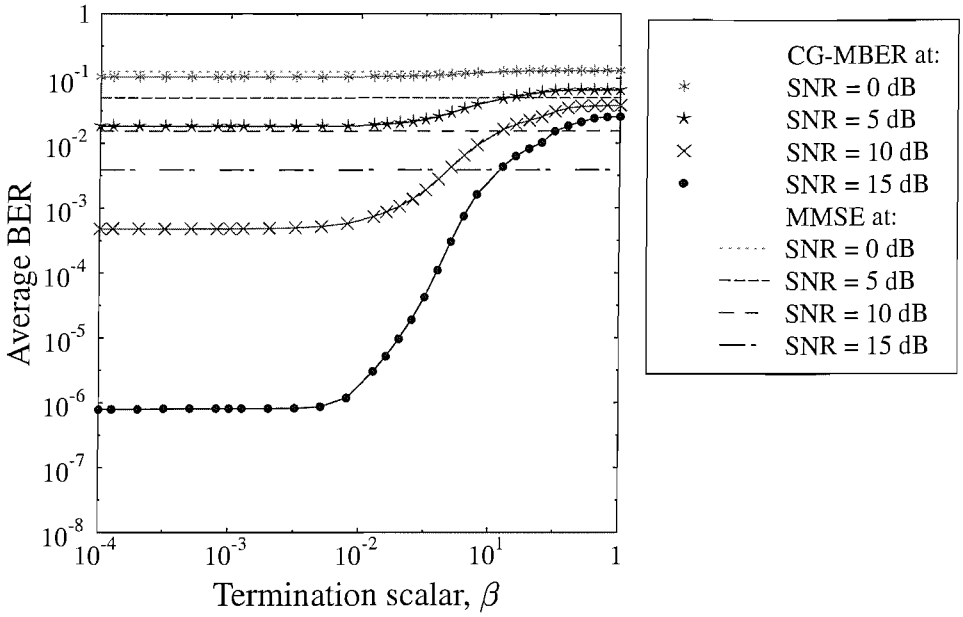

Figure 2.24: The average of the achievable BER of User 1 in the $P = 4$ and $L = 4$ OFDM SDMA system when varying the termination scalar, β of the conjugate gradient algorithm while fixing the step size, μ to 0.1, maximum iterations to 10000 and initialising the MBER weight values to the MMSE weight values and the weight from the previous SNR. These curves were evaluated from Equation 2.33.

2.4.4.3 Termination scalar, β

The final CG parameter that we have investigated is the termination scalar β. As observed on page 72, the termination scalar β is employed for the sake of allowing us to terminate the iterations, when the magnitude of the gradient becomes close to zero. This is because although we originally required the magnitude of the gradient to be zero, this might require an extremely high number of iterations to achieve. Therefore, by invoking a termination scalar we will ensure that the search will approach zero, thus restricting the number of iterations required. However, the specific choice of the termination scalar is quite important, because if β too small, an excessive number of iterations will be required. On the other hand, if a high β value is chosen, the final search result might not be sufficiently close to the optimum solution. Figure 2.24 shows our simulation results for the various values of β, confirming the above-mentioned expectations.

In summary, the choice of all three parameters, namely the step-size μ, the maximum number of iterations and the termination scalar β, is important for the CG algorithm for

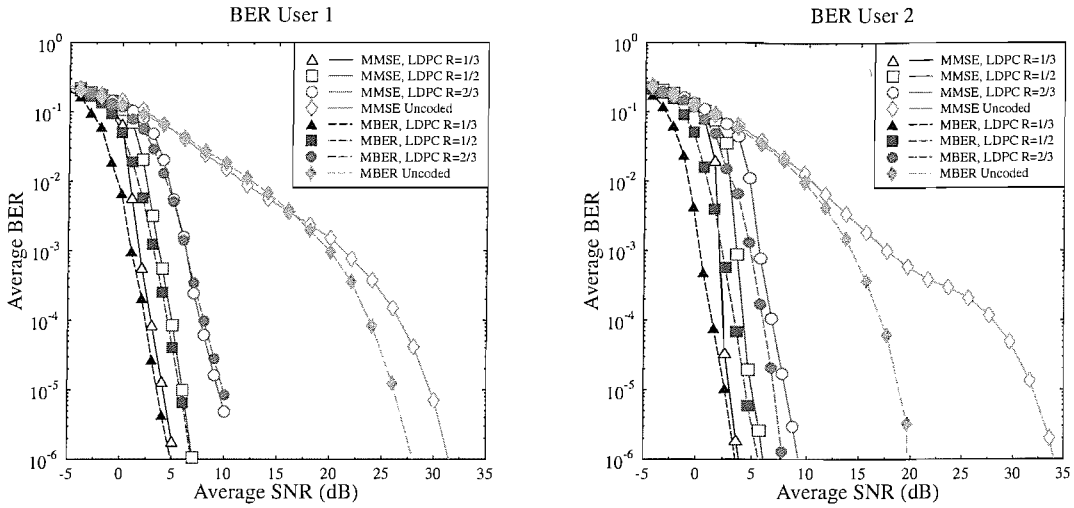

(a) (b)

Figure 2.25: BER versus the average SNR for User 1 and User 2 employing LDPC-coded MMSE and MBER MUDs, when supporting two users with the aid of two receiver antennas using 128-subcarrier OFDM for communicating over the channel characterised with the aid of the CIR and FDCHTF shown in Figure 2.4 and Figure 2.5, respectively.

the sake of approaching the MBER solution, and all of them are inter-related. Let us now embark on investigating the effects of employing an LDPC code for the sake of improving the achievable performance of the MBER MUD in the following section.

2.4.5 LDPC coded MBER multiuser detector

Using the soft-bit generation technique described in Section 2.3.2, we will now compare the performance of the LDPC coded MMSE and MBER MUDs. For this simulation, we first obtained the weight vectors using known reference sequences. The resultant weight vectors were then used to detect the streams of LDPC coded bits. Again, we assumed encountering OFDM symbol-invariant fading, where the fading remains constant during an OFDM symbol. The results of our simulations are shown in Figure 2.25 and Figure 2.26 for the attainable BER and FER, respectively. We can see from Figure 2.25 for both users that the BER of the LDPC assisted MBER MUD is marginally better than that of the MMSE schemes, in particular at lower SNRs. However, as the SNR increases, the performance of the two MUDs becomes indistinguishable. This is because at higher SNRs the LDPC code

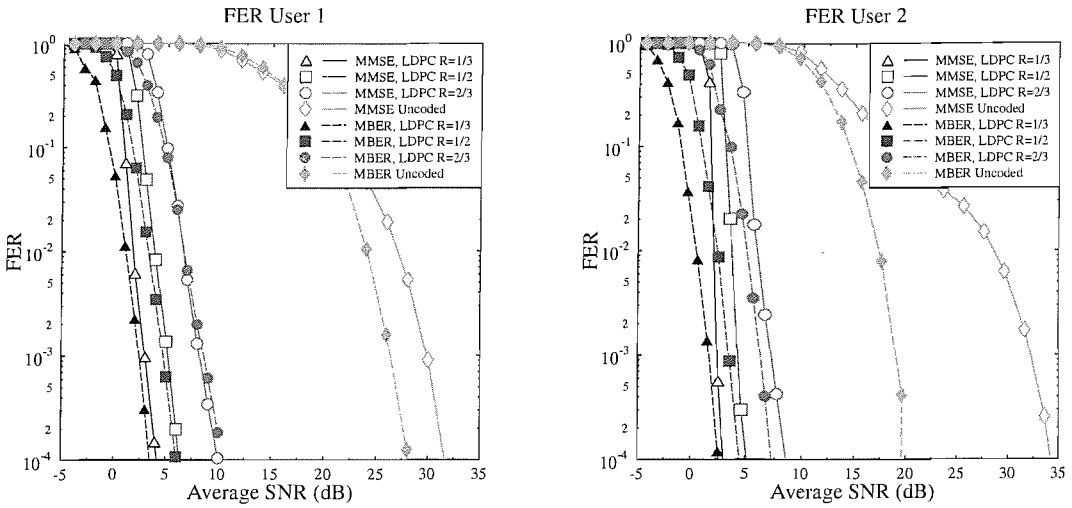

(a) (b)

Figure 2.26: FER versus the average SNR for User 1 and User 2 employing LDPC-coded MMSE and MBER MUDs, when supporting two users with the aid of two receiver antennas using 128-subcarrier OFDM for communicating over the channel characterised with the aid of the CIR and FDCHTF shown in Figure 2.4 and Figure 2.5, respectively.

will improve the performance regardless of the type of detector used, provided that the MUD's uncoded BER is sufficiently low.

It can also be seen in Figure 2.25 that the achievable BER difference between the two detectors was higher for User 2 compared to User 1. This is because even when no channel coding is used, the performance difference advantage of the MBER detector compared to the MMSE MUD of User 2 exceeded that of User 1 by almost 15 dB. This SNR advantage diminishes to a mere 3 dB, 2 dB and 1 dB, when an LDPC code rate of R= 2/3, 1/2 and 1/3 is used, respectively. In terms of the attainable FER, the trends of Figure 2.26 seems to mirror the BER trends, namely that User 2 has a more obvious difference compared to User 1. In general, we may conclude that the MBER MUD performs $2-5$ dB better than the MMSE MUD at low SNRs, when powerful LDPC codes are invoked.

2.5 Chapter conclusion

In Chapter 2, we have investigated the advantages of using multiple antennas for multiuser detection in an OFDM system. The so-called SDMA system exploits the unique user-specific

channel impulse responses for distinguishing the different users, not unlike the spreading codes of a CDMA system differentiate the users.

The chapter commenced with a brief introduction to the various applications of smart antennas in Section 2.1. One of the smart antenna aided systems, namely the SDMA system was further investigated in this chapter. The SDMA system model was presented in Section 2.2.1, followed by a comparison of the SDMA model to the well-known CDMA system model in Section 2.2.2.

In Section 2.3, linear multiuser detection techniques designed for SDMA systems were introduced. We have discussed the derivation of the classic MMSE MUD in Section 2.3.1. We have also described the soft-output calculation procedure designed for the SDMA system, that was used in conjunction with forward error correction coding in Section 2.3.2.

Our discussions continued in Section 2.4 with the proposal of a novel MBER multiuser detector contrived for SDMA systems. We first interpreted the corresponding error probability expressions in the context of BPSK system in Section 2.4.1, followed by the derivation of the exact MBER MUD in Section 2.4.2. We later presented our simulation results in Section 2.4.3. The simulations were conducted in the context of two, four and eight receiver antennas and the corresponding results were discussed in Sections 2.4.3.1, 2.4.3.2 and 2.4.3.3, respectively. Moreover, we showed in Section 2.4.3.2 that unlike the MMSE MUD, the MBER MUD is capable of supporting more users than the number of receiver antennas employed at the base station. We also presented our results characterising the effects of different number of receiver antennas, while fixing the number of users to two in Section 2.4.3.4.

These discussions were then followed by our results concerning the effects of varying the different parameters of the CG algorithm in Section 2.4.4. In particular, we have characterised the effects of varying the step-size μ in Section 2.4.4.1, the effects of varying the maximum number of iterations in Section 2.4.4.2 and the effects of varying the termination scalar β in Section 2.4.4.3. In Section 2.4.5, LDPC channel coding was employed by the OFDM SDMA system, in order to investigate the performance of the MBER MUD with the assistance of the LDPC code.

In summary, the MBER MUD performs better in terms of the attainable BER compared

to the classic MMSE MUD in all investigated cases. This is because the MBER MUD directly minimises the BER, while the MMSE MUD attempts to minimise the MSE. Moreover, it was shown that the MMSE MUD is only capable of supporting the same number of users as the number of receiver antennas, whereas the MBER MUD has the ability to support more users than the number of receiver antennas. However, the advantage of the MBER MUD over the MMSE MUD varies across the different users due to the fact that different users experience different combinations of the CIRs at the receiver antennas, hence resulting in a different system matrix $\mathbf{H}$.

Eventhough the MBER MUD shows substantial advantages over the classic MMSE MUD, the performance of the CG method used in this chapter depends on its initialization and on the effects of the various parameters such as the step-size and the termination scalar. In the next chapter we will introduce a GA-aided search method as a design alternative to the CG search method employed in the context of the exact MBER MUD algorithm.

Chapter 3

Genetic Algorithm Assisted MBER MUD

Even though the MBER detector of Chapter 2 is capable of maintaining a good performance, the convergence of the algorithm is sensitive to the choice of the algorithm's parameters. For example, the choice of the initial condition for the MBER MUD is critical in order for the solution to converge to the minimum of the BER surface seen in Figure 2.3. In Chapter 2, the MMSE SDMA MUD weight solution has been used for initialising the CG algorithm based MUD, which is also exemplified in Figure 2.3. However, this choice of initial conditions does not necessarily guide the algorithm's convergence to the required MBER solution, if the BER surface exhibits local minima, although this is not the case in Figure 2.3. Another parameter that affects the performance of the MBER detector is the step size μ used for updating the array weights in the direction opposite to the BER gradient. The choice of this step size must be based on a compromise, since a step-size that is too high might not allow convergence to the minimum BER point, whereas the opposite scenario will require a high number of iterations for attaining convergence to the MBER solution. An attractive method that might be able to assist the MBER MUD in circumventing the above-mentioned problems is constituted by the family of Genetic Algorithms (GA) [230], which were extensively used in various CDMA and MC-CDMA MUD problems in [206].

Hence, in this chapter, we will embark on designing a GA-based exact MBER MUD. The GA will be invoked for finding the MUD optimum weight values that will minimise the

BER cost function. We will commence our discourse with a brief overview of GA in Section 3.1. This is followed by Section 3.2, demonstrating how GAs may be exploited in the MBER-MUD assisted SDMA-OFDM system. Our simulation results will then be depicted in Section 3.3. In Section 3.4, we will characterise the proposed GA-MBER MUD in comparison to the exact MBER MUD of Chapter 2, outlining the associated implementational complexity calculations. We will also quantify the performance of the GA-MBER MUD in an overloaded scenario in Section 3.5 where the number of users supported is higher than the number of antenna elements. Finally, we will conclude this chapter in Section 3.6.

3.1 A brief overview of GA

In this section we will briefly highlight the operating principles of GAs. For further details on the origin of GAs and its applications, the readers are referred to the impressive compilation of ideas in [230–234]. We will commence with an informal definition of GAs in Section 3.1.1. This is followed by a brief summary of the operating principles of GAs in Section 3.1.2. Lastly, in Section 3.1.3 we will highlight the differences between GAs and the family of traditional optimisation and search methods.

3.1.1 GA basics

The family of GA-aided search methods mimic the rules of evolution and survival in nature. They follow the laws of nature in which a group of the fittest individuals in a population will survive. These fittest individuals will then mutate for the sake of creating a new generation of individuals. Even though the process of evolution is randomised, unlike in conventional random processes, the GAs rely on improving the performance or fitness of the evolving new generation with the aid of information emerging from the previous generations.

GAs were developed by Holland *et al.* at the University of Michigan in the early 1970s [231]. His original aim was that of studying the adaptive process of natural evolution and the adoption of this natural process in an artificial system software. However, his discovery had turned out to be the commencing point of GA-based optimisation. Holland's research was later further developed by one of his students, Goldberg [230]. Since then, GA have been employed in numerous applications, such as machine learning [246–248]

Year	Author	Contribution
'75	Holland [231]	Originally proposed GAs for studying the adaptive process of natural evolution in an artificial system software.
'89	Goldberg [230]	Goldberg further developed GAs in the context of optimisation and machine learning.
'96	Mitchell [232]	A further advancement of GAs in machine learning.
'97	Juntti, Schlosser and Lilleberg [235]	First known study of the application of GAs in MUDs.
'98	Wang, Lu and Antoniou [236]	Proposed a detector for multiuser communications, which is based on the maximum-likelihood decision rule and employs a GA for detecting the user bits sequentially.
'00	Ergun and Hacioglu [237]	Suggested a hybrid approach that combines GAs with a multistage multiuser detector (MSD) in the context of a CDMA system.
'01	Yen and Hanzo [238]	Employed a novel CDMA multiuser receiver based on GAs, for jointly estimating the transmitted symbols and the fading channel coefficients of all users.
	Abedi and Tafazolli [239]	Proposed and characterised a genetic implementation of the optimal MUD.
'02	Ng, Yen and Hanzo [240]	Advocated a turbo trellis coded modulation assisted GA-aided reduced complexity MUD (TTCM-GA-MUD) that is capable of providing a considerable coding gain without any bandwidth expansion, while maintaining a low complexity compared to the optimum MUD.
	Chiang and Chang [241]	Improved the GA and MSD using eugenic[1] population.
'03	Shayesteh, Menhaj and Nobary [242]	Proposed a modified genetic algorithm for multiuser detection in DS/CDMA systems, which attains a performance comparable to that of the optimum detector with at a lower complexity.
	Yen and Hanzo [243]	Advocated a spatial diversity reception assisted CDMA multiuser detector based on GAs.
	Du and Chan [244]	Invoked a GA for sub-optimal detection in space-time block coding (STBC) aided multiuser detection systems.
'04	Wolfgang, Ahmad, Chen and Hanzo [245]	Introduced a novel GA assisted Minimum Bit Error Ratio (MBER) beamforming technique.
	Alias, Chen and Hanzo [3]	Employing GA to solve for the MUD's weight of an SDMA OFDM system based on the MBER criterion.

Table 3.1: Contributions towards the development of GA-aided MUDs.

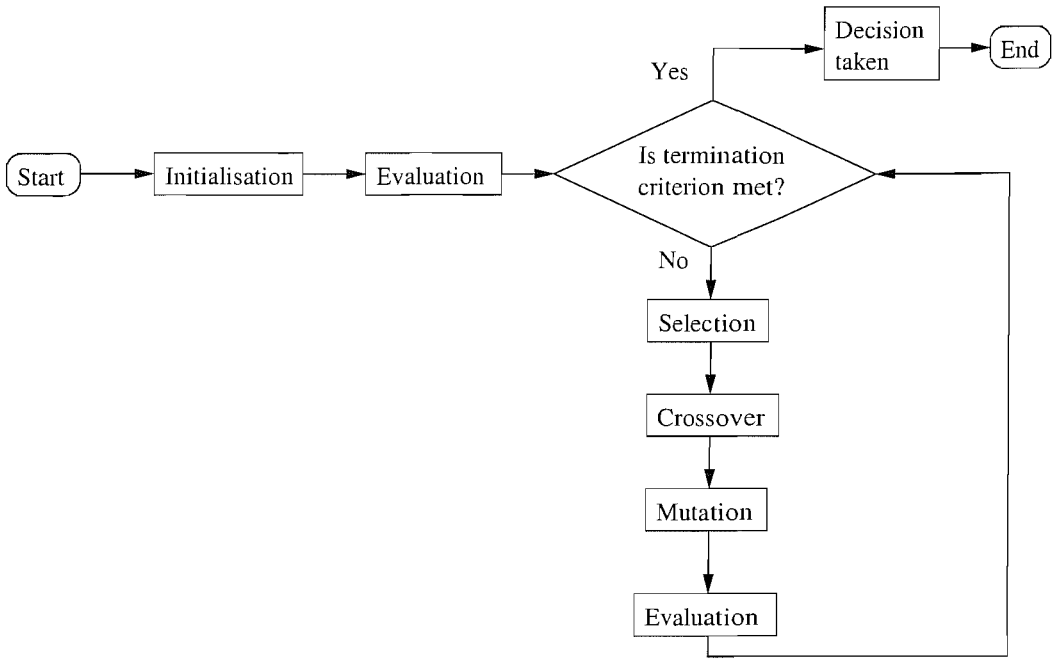

Figure 3.1: Flowchart of function optimisation using GAs.

and the modelling of adaptive processes [249, 250], but by far the widest application field of GAs is found in the domain of function optimisation [230, 231, 251]. In recent years GAs have found their way into a range of wireless applications, such as beamforming [245] and CDMA multiuser detection scenarios [234]. Table 3.1 summarises the history of GAs and the main contributions in the field of using GAs for solving MUD problems.

3.1.2 GA operating principles

Figure 3.1 shows the flow chart of a GA that may be invoked in an optimisation problem. The basic approach of a GA system is appealingly simple [206, 230]. Firstly, an objective function to be optimised by the GA is defined. In order to commence the GA-aided optimisation process, an initial population consisting of Y number of so-called individuals is created in the 'Initialisation' block, where Y is known as the GA's population size. Each individual represents a legitimate solution to the optimisation problem considered. An individual may be considered as a vector consisting of the decision variables of each of the users to be optimised in a multiuser system. Traditionally, the individuals in a GA's population assume the form of binary bit vectors, but they can also be represented by real values. The

initial population is often generated randomly, but the user can also specified any values as well. If some *a-priori* knowledge concerning the choice of the optimum vector is available in advance, then it can be used for expediting the search or for reducing its complexity.

Each individual in the population is evaluated according to the so-called *fitness* value associated with it. This fitness value is calculated by substituting the individual into the objective function in the 'Evaluation' block seen in Figure 3.1. Following the fitness evaluation process, the termination criterion will be checked, which may be either a certain convergence accuracy, a certain number of generations or a range of other criteria. We will further study the effect of the specific termination criterion used in Section 3.3.2.1. If the stopping criterion is not met, a group of the highest-fitness individuals is selected for creating a generation in the 'Selection' block of Figure 3.1. This group of individuals, referred to as *parents*, will be subjected to various genetically-inspired operators, such as the so-called *crossover* and *mutation*, for the sake of creating new individuals. The fitness of these new individuals will then be re-evaluated and the termination criterion is examined again.

This process will continue, until the termination criterion is finally met. After this stage, the best individual having the highest fitness encountered will be chosen as the solution to the optimisation problem.

3.1.3 Difference of GA-aided and traditional optimisation methods

Traditional optimisation and search methods can be basically divided into three main types: *calculus-based*, *enumerative* and *random* [230]. The *calculus-based* method is one of the most widely known method and has been studied by generations of mathematicians. This method seeks the local extrema of a function by either directly solving the equation like the MMSE method in Section 2.3.1, or by using gradient methods, such as the CG or SD techniques introduced in Section 2.4.2 for finding the MBER solution. The latter one is usually employed, when the equations are highly complex and not directly solvable, as exemplified by the BER cost function. This method is adequate, when there is a single extreme point on the cost function surface. However, when there are more than one extreme points, we might only arrive at a local optimum, rather than the desired global extrema. Therefore, we might not be able to arrive at the best solution.

The second technique, referred to as the *enumerative* method [252], compares the objective function values computed for every point in a given finite search space. Although this method is conceptionally simple, it is only efficient when the search space and the number of possibilities is small. However, in most practical problems, for example in the context of the BER cost function problem, the number of possibilities in the search space is vast and hence its exhaustive search becomes excessive for the enumerative method to solve. An example of this method is constituted by the classic Maximum Likelihood Sequence Estimation (MLSE) technique.

The other type of traditional search methods is represented by the *random* method, which is becoming popular among researchers as an alternative to the calculus-based and enumerative schemes. However, this method is incapable of exceeding the performance of the enumerative method.

GAs are different from traditional optimisation algorithms, because they do not directly attempt to optimise the desired decision variable or a set of decision variables itself [230]. Instead, they encode the decision variables into finite-length bit- or symbol-strings referred to as individuals, which are then optimised. In the case of SDMA-MUDs, the MUD's weights have to be represented by a single string for the sake of creating an individual. A GA does not commence its optimisation process from a single point in the search space, but instead from a whole set of individuals, which form the initial population. In other words, GAs may be invoked in robust global search and optimisation procedures that do not require the knowledge of the objective function's derivatives or any gradient-related information concerning the search space. Hence, non-differentiable functions as well as functions having multiple local minima, like the BER surface, represent classes of problems, where GAs can be efficiently applied [233].

Even though a GA also employs random values, it is not a random search but rather a randomised search technique. This simply means that GAs use random choices as a tool for guiding a directed search process through a parameter space [230]. In the following section, we will invoke a GA in the MBER MUD designed for the OFDM SDMA system of Section 2.2.

w_{1R}	1 0 0 1 1 1 0 1 0 1 0 0 1 1 0 1
w_{1I}	1 1 0 0 1 1 0 0 1 1 0 0 1 1 0 0
w_{2R}	0 1 1 1 1 1 1 1 0 0 0 0 1 0 1 0
w_{2I}	0 0 0 1 1 0 0 1 0 1 0 1 1 1 0 0
⋮	⋮
w_{PR}	1 0 0 1 0 0 0 1 1 1 1 0 1 1 0 1
w_{PI}	0 1 0 0 1 1 1 1 0 1 0 0 1 1 0 1

Figure 3.2: An example of an individual in the GA-aided MUD represented by the two-dimensional binary arrays, where P is the number of antennas at the receiver, R is the real part of the weight and I is the imaginary part of the weight.

3.2 GA-aided MBER MUD

In this section we will invoke a GA for finding the MBER MUD's weight values. Firstly, we will set the objective function of the GA to be the probability of error as a function of the weight values. The probability of error formula of Equation 2.31 is rewritten for convenience as:

$$P_E(\mathbf{w}_l) = \frac{1}{N_b}\sum_{j=1}^{N_b} Q\left[\frac{\mathrm{sgn}(b_l^{(j)})\cdot \Re\{\mathbf{w}_l^H \bar{\mathbf{x}}_j\}}{\sigma_n\sqrt{\mathbf{w}_l^H\mathbf{w}_l}}\right], \tag{3.1}$$

where N_b is the number of equiprobable combinations of the binary vectors of the L BPSK users, i.e. we have $N_b = 2^L$, $\mathbf{w}_l$ is the SDMA combiner's weight vector for user l, $b_l^{(j)}$ $j \in 1,\ldots,N_b$ is the transmitted bit of user l, σ_n is the variance of the noise, and $\bar{\mathbf{x}}_j$, $j \in 1,\ldots,N_b$ constitutes a possible value of the noiseless received signal vector $\bar{\mathbf{x}}$.

The real and imaginary parts of the MUD's weight vector, $\mathbf{w}_l$, are represented by binary strings. Therefore, each individual in the population constitutes a two-dimensional binary string, where rows represent the real or imaginary parts of the MUD's weight while the columns cast a number of bits representing the binary-encoded decimal MUD weights. Since we separately represent the real and imaginary parts, the number of rows is twice the number of receiver antennas, P. On the other hand, the number of columns is limited by the number of bits per MUD weight, which predetermines the MUD's implementational complexity and storage requirements. An example of the GA's individuals is shown in

Figure 3.2.

The fitness, f_i of an individual is quantified as:

$$f_i = -\log_{10}(P_E(\mathbf{w}_l)), \tag{3.2}$$

where $P_E(\mathbf{w}_l)$ is the probability of error given by Equation 3.1. The employment of the logarithm of $P_E(\mathbf{w}_l)$ in the objective function has significantly improved the convergence behaviour of the GA since the logarithmic function expands the most-important low-BER range. There are various ways of defining the fitness function but for the context of the MBER MUD the fitness function of Equation 3.2 constitutes a plausible choice. We will now continue our discussions by characterising the achievable performance of the proposed GA-based MBER MUD.

3.3 Simulation results

In this section, we will present our simulation results for the GA MBER MUD outlined in Section 3.2. We will commence by outlining the BER part of the different users investigated employing the default parameters given in Table 3.2. We will then continue our discourse by exploring the effects of varying the different GA parameters in Section 3.3.2.

3.3.1 BER performance for the different users

The parameters used in our simulations are outlined in Table 3.2. The Short Wireless Asynchronous Transfer Mode (SWATM) Channel Impulse Response (CIR) of [5] was used, where the CIR taps were not faded. As a starting point, we used binary type genomes [230] for representing the GA's individuals. Therefore each real and imaginary part of each of the components of the SDMA MUD weight vectors is represented by a 16-bit binary string. The GA's termination criterion is constituted by the maximum affordable number of generations. Following the termination of the GA-aided optimisation process, the best individual encountered is deemed to be the best MBER MUD weight solution and hence it is converted to the corresponding real and imaginary values of the MUD's weight vectors. Our results derived for the four different users supported employing the parameters summarised in Table 3.2 are presented in Figure 3.3. We can see from Figure 3.3 that the achievable

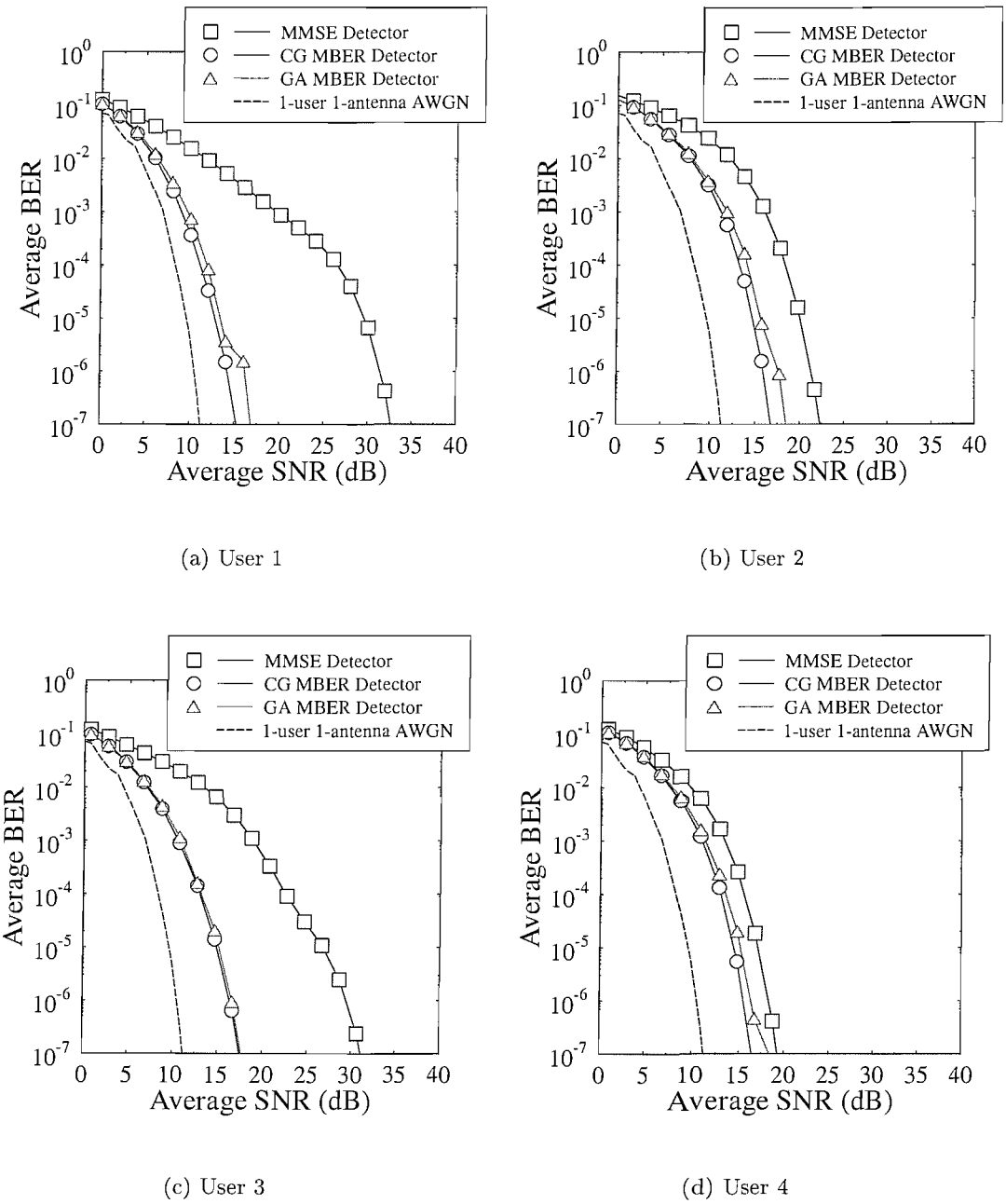

(a) User 1

(b) User 2

(c) User 3

(d) User 4

Figure 3.3: The BER versus SNR performance of the four different users in an SDMA system employing four receiver antennas and 128-subcarrier OFDM for communicating over the unfaded SWATM channel of Figure 2.9. The remaining system parameters were summarised in Table 3.2. These curves were evaluated from Equation 2.33.

Parameter	Value or type
SDMA	
Number of users	4
Number of receiver antennas	4
OFDM	
Number of subcarriers	128
Number of cyclic prefix samples	32
GA	
GA type	Non-overlapping
Population size	30
Number of generations	100
Mutation type	Flip mutator
Probability of mutation	0.01
Crossover type	One-point crossover
Probability of crossover	0.6
Scaling	Sigma truncation
Genome type	Binary string
Initialisation	Uniform
Comparison	Bit comparator
Individual Encoding/decoding	Binary encoding and decoding
Selection	Roulette wheel
Elitism	On
p-convergence	0.99
n-convergence	50
Others	
MBER	Exact MBER
Channel	3-path SWATM frame-invariant

Table 3.2: Default parameters for the GA-aided SDMA MUD simulations.

BER performance of the GA assisted MBER MUD is significantly better than that of the MMSE MUD. More importantly, the GA assisted MBER MUD approaches the BER performance of the exact MBER MUD using the system parameters of Table 3.2, where the true MBER solution was approximated with the aid of the CG algorithm as explained in Section 2.4.2. However, in the following section we will further characterise the effect of the different parameters and demonstrate that further performance improvements may be attained, potentially approaching the CG based MBER MUD's performance more closely.

3.3.2 Effects of varying the GA's parameters

In this section we will quantify the effects of varying the different GA parameters. The section commences by studying the effects of using different termination criteria in Section 3.3.2.1. This is followed by Section 3.3.2.2, where we will consider the effects of the different number of bits per every weight. In Section 3.3.2.3, we will study the impact of the population size, while in Section 3.3.2.4 we will investigate the influence of using various crossover methods. Finally, Section 3.3.2.5 is dedicated to the study of the probability of mutation.

3.3.2.1 Termination criterion

As mentioned in Section 2.4.2, the exact structure of the BER surface is typically unknown and irregular. Hence in searching for the optimised MUD weight values minimising the BER, it is typically difficult to ensure that the optimum solution can be found. More importantly, the search might require a high number of generations thus increasing the complexity imposed and potentially exhausting the available resources. Therefore an appropriate termination criterion must be found for halting the search process. There are numerous ways of determining the termination criterion for GAs. In Section 3.3.2.1.1 we will consider termination after a fixed number of generations. This is followed by considering termination after a sufficiently accurate convergence in Sections 3.3.2.1.2 and 3.3.2.1.3.

3.3.2.1.1 Termination after a fixed number of generations The most straightforward way of terminating the GA is constituted by fixing the number of generations, i.e. when the GA is terminated once the search reached the G-th generation, where G is a value fixed at the beginning of the search. The best individual associated with the highest fitness value during the search encountered will then be selected as the final solution. By specifying the exact number of generations to be used, the computational complexity of the GA can be determined beforehand, as we will argue in Section 3.4. However, the disadvantage of this method of termination is that the value of G must be carefully determined in order to ensure that a high-probability of an adequate solution is obtained. Moreover, the solution found after the termination might not be the optimum solution and the choice of an adequate G value depends on the BER surface.

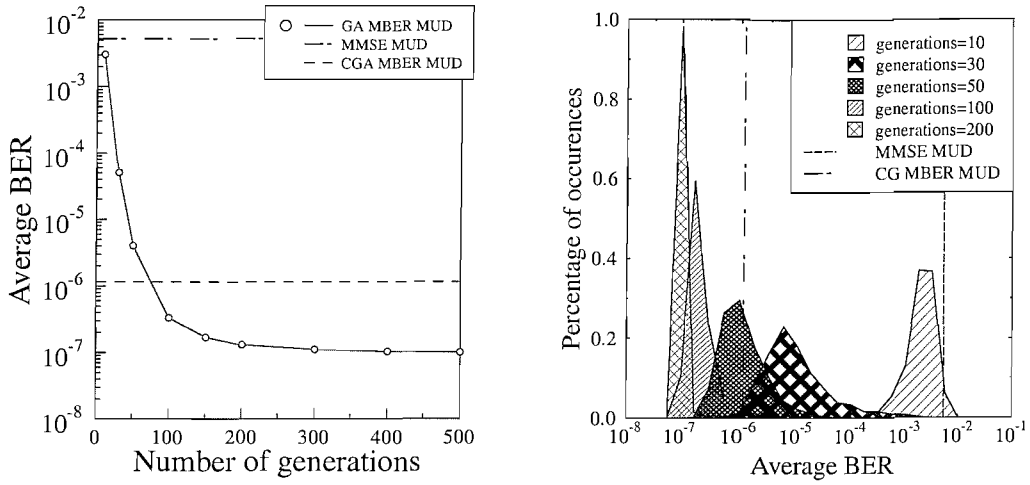

(a) Average BER versus generation

(b) PDF

Figure 3.4: The (a) average BER versus number of generations, and (b) PDF of the average BER for 1000 simulation runs for the termination criterion verified by a fix number of generations for User 1 employing the CIR of Figure 2.9 at SNR = 15 dB. The remaining parameters were specified in Table 3.2. These curves were evaluated from Equation 2.33.

The average BER results associated with varying the number of generations, G are shown in Figure 3.4(a). The remaining system parameters are summarised in Table 3.2. We can see from the figure, that as the number of generations increases, the achievable average BER also improves. However, as it will be explained in detail in Section 3.4, this is achieved at the price of an increased complexity. In Figure 3.4(a) we can see that after 200 generations, the average BER becomes better than that of the CG MBER MUD. This is because for the CG MBER MUD the termination criterion was defined as the maximum number of iterations, which was insufficiently high for the CG MBER MUD to arrive at the optimum solution in this scenario.

To elaborate a little further, Figure 3.4(b) shows the PDF of the achievable BER for 1000 simulation runs using a fixed number of generations as the termination criterion. From the figure we can see that if a low number of generations is used, the probability of achieving a good BER is low. However, as the number of generations is increased, there is a higher probability that we will arrive at the optimum solution. In our scenario, it can be clearly observed that when the termination generation is fixed at 200, the average BER of most of the 1000 simulation runs is close to the optimum solution, which manifests itself in terms of a narrow BER PDF.

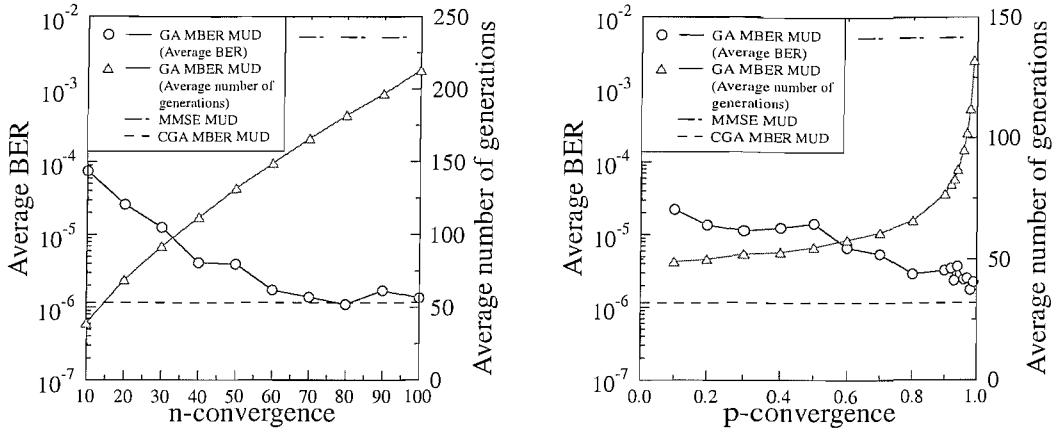

(a) Varying the GA's *n-convergence* parameter while fixing *p-convergence* to 0.99

(b) Varying the GA's *p-convergence* value while fixing *n-convergence* to 50

Figure 3.5: Average BER results for varying the GA's termination parameters (a) *n-convergence* and (b) *p-convergence* for User 1 at SNR = 15dB. The remaining parameters are as in Table 3.2 and the CIR was shown in Figure 2.9. These curves were evaluated from Equation 2.33.

3.3.2.1.2 Termination based on quality of convergence Another method of terminating the GA's search operation is based on detecting that there are no further substantial improvements in the maximum fitness value after a number of consecutive generations. Hence the GA will compare the best individual to that of the previous n number of generations specified by a value we refer to as *n-convergence* [230]. The GA-aided search will then terminate, when the fitness value of the best individual of the current generation is within a certain percentage of the fitness of the best individual of the n-th previous population. This percentage is referred to here as *p-convergence* [230]. For this termination technique, the number of generations required for the GA to reach a decision is uncertain.

Figure 3.5 shows the average BER results achieved upon varying the value of the *n-convergence* and *p-convergence* parameters. We can see from Figure 3.5(a) that as the value of *n-convergence* increases, the achievable BER also improves. However, the average number of generations required for reaching the optimum solution also increases, thus implying an increase in complexity, as it will be argued in detail in Section 3.4. The increase in the number of average generations is needed because the GA will require at least the same number of generations, as the *n-convergence* value in order to be able to carry out the required comparison.

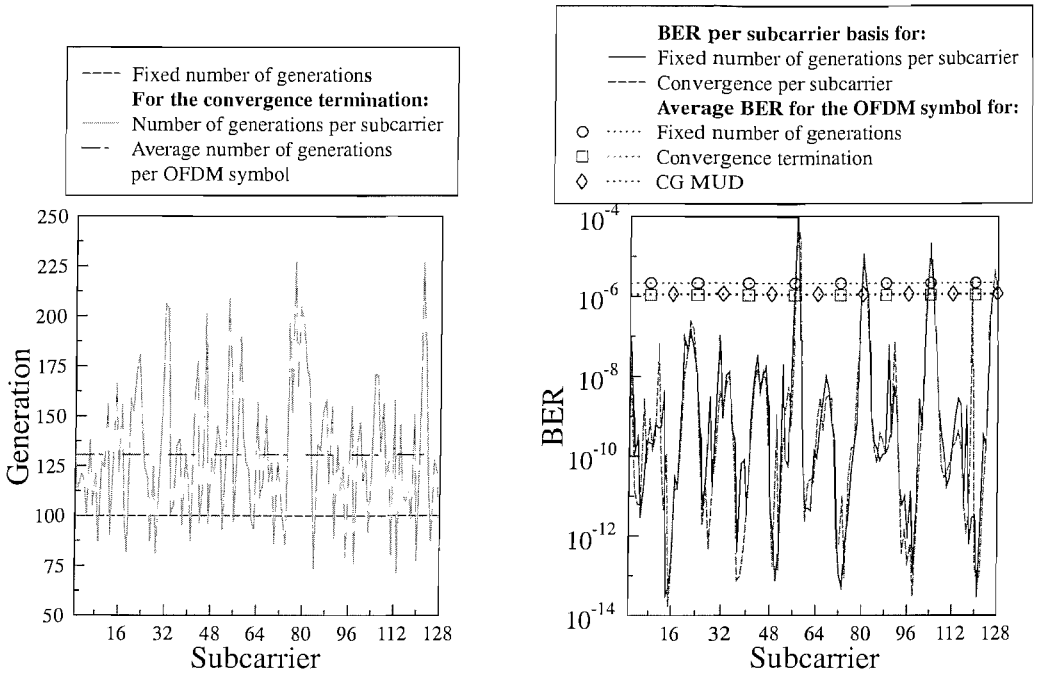

(a) Number of generations required on a per subcarrier basis.

(b) BER on a per subcarrier basis.

Figure 3.6: The required number of generations for User 1 at SNR = 15 dB, when comparing the termination regime using a fixed number of generations and convergence tests on a per subcarrier basis in terms of (a) the number of generations required, and (b) the achievable BER. The remaining parameters are summarised in Table 3.2 and the CIR was shown in Figure 2.9. These curves were evaluated from Equation 2.33.

As for Figure 3.5(b), we can see that the average BER performance also improves, as the *p-convergence* parameter increases although not as drastically as in Figure 3.5(a). However, we can see that the average number of generations required increases exponentially, as a higher *p-convergence* parameter is used. This is because as we increase the value of *p-convergence*, it will become more difficult to reach a solution where the best individual of the n-th previous generation is similar to the best individual of the current generation thus increasing the number of generations required for satisfying this convergence criterion.

Figure 3.6 compares the results of using the termination regime based on a fixed number of generations and the quality of convergence based termination on a subcarrier basis. For the termination regime based on a fixed number of generations, we used a G value of 100 generations. We can see from Figure 3.6(a), that different number of generations will be required for approaching convergence. The required number of generations depends very much on the nature of the BER surface at the particular subcarrier concerned. The average

number of generations required for converging is higher than the fixed number of generations used. It is not surprising that the BER achieved at a specific subcarrier also varies. This is because for certain subcarriers the fixed number of generations, G is sufficiently high for reaching the optimum solution, whereas the rest of the subcarriers may require a higher number of generations, as shown in Figure 3.6(b).

3.3.2.1.3 Termination based upon the population's average variance Convergence can also be evaluated by comparing the population's average fitness to the highest fitness individual in the population. In this case, the GA will terminate, once the population's average fitness is within a certain percentage of the best individual fitness score. However, this type of termination is not particularly suitable for the employment in the MBER MUD since we will only have to find the best individual, rather than the average fitness of the population. Moreover, when the population size is large, it will require a high number of generations, before the above goal is achieved.

Let us now continue our discussions by characterising the effects of using different number of bits for the representation of the binary encoded GA individuals in the following section.

3.3.2.2 Representation of the MUD weights

Traditionally, as defined by Holland [231], the GA's individuals are represented in the form of bit vectors, which are comprised of a combination of binary zeros and ones. The strong preference for using encoded binary representations of the individuals in GAs was justified by Holland [231] using schema theory [231]. It is claimed in [230] that GAs are well suited for handling pseudo-Boolean and combinatorial optimisation problems. For optimisation problems that involve non-binary or real-valued decision variables, these decision variables have to be encoded into binary-valued bit vectors, in order to perform the above-mentioned genetic operations. Similarly, these bit vectors must be converted back to their original real-valued form, in order to evaluate their associated fitness values from the objective function. There are several potential encoding schemes for mapping non-binary decision variables to binary valued vectors [230], but we will investigate only the so-called *binary encoding* in Section 3.3.2.2.1 and *Gray encoding* techniques in Section 3.3.2.2.2.

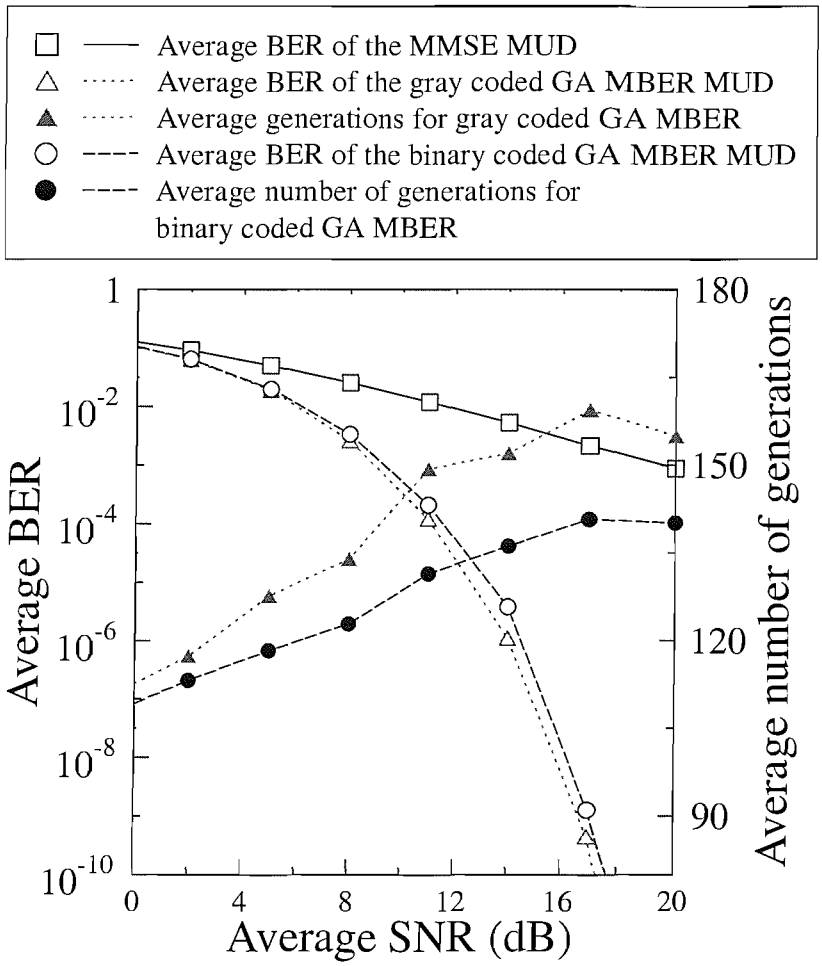

Figure 3.7: The average BER achieved and the number of generations required for User 1 at SNR = 15 dB when employing either binary or Gray-encoded bit representations. The remaining parameters are as specified in Table 3.2. These curves were evaluated from Equation 2.33.

3.3.2.2.1 Binary encoding The so-called *binary encoding* [232] is the simplest and most commonly used individual encoding scheme. Encoding of non-binary integers is quite straightforward. For example, 3 and 10 can be represented in binary form as 11 and 1010, respectively. For real-valued decision variables, the number of bits invoked will determine the resolution of the encoding. Consider a real-valued decision variable x, where $a \leq x \leq b$, is to be encoded to an n-bit vector. Firstly, we can convert x to a non-binary integer y according to:

$$y = \left\lfloor \frac{b-a}{2^n} \times x \right\rfloor. \tag{3.3}$$

We can then encode the integer y according to any non-binary integer encoding. Binary encoding has the drawback that in some cases all the bits must be changed in order to

increase the non-binary number by one. For example, the bit pattern 011 translates to 3 in decimal form, but 4 is represented by 100. This may render it implementationally inconvenient for an individual that is close to the optimum solution to move even closer to the optimum with the aid of the crossover and mutation operation.

3.3.2.2.2 Gray encoding In order to overcome the above-mentioned disadvantage of the binary encoding algorithm, a different kind of encoding scheme, namely Gray coding was proposed [232]. Unlike the above-mentioned binary codes, Gray codes have the property that incrementing or decrementing any integer number by one always involves only a single-bit change. The mapping from the binary encoded n-bit vector to a Gray coded n-bit vector is given by:

$$g_k = \begin{cases} b_1 & \text{if } k = 1, \\ b_{k+1} \oplus b_k & \text{if } k > 1 \end{cases} \tag{3.4}$$

where g_k and b_k are the k-th Gray code bit and binary code bit, respectively, for $k = 1, \ldots, n$ and $\oplus$ denotes a modulo 2 addition. The conversion from Gray encoding to binary encoding is given by:

$$b_k = \sum_{i=1}^{k} g_i. \tag{3.5}$$

In practice, Gray-encoded representations are often more successful in real-valued parameter optimisation applications, than binary-encoded representations.

Figure 3.7 characterises the performance difference between binary and Gray encoding, where we used the termination regime based upon the population's average fitness for determining the number of generations required for both type of individual encoders for approaching optimum. We can see from the figure that the achievable average BER of the Gray encoding is slightly better than that of binary encoding. This is because Gray encoding approached the optimum point more closely than binary encoding. However, the Gray encoding required a higher number of generations for converging thus imposing a higher complexity compared to binary encoding. In summary, we may conclude that in the scenario considered it is more beneficial to invoke binary encoding than the Gray coding since the performance of the two types of encoding schemes was similar, but the binary encoding scheme had the advantage of requiring a lower number of generations for convergence, thus requiring a reduced complexity.

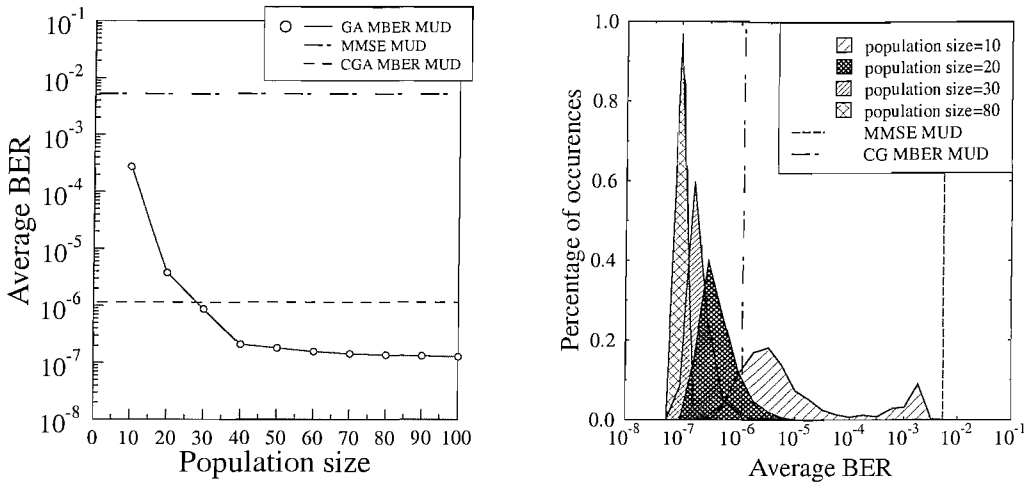

(a) Average BER versus population size

(b) PDF

Figure 3.8: (a) The achievable BER, and (b) PDF of the BER for 1000 simulation runs when employing different population sizes for User 1 at SNR = 15 dB. The remaining parameters are summarised in Table 3.2. These curves were evaluated from Equation 2.33.

Let us now continue our investigations by varying the population size associated with a generation in Section 3.3.2.3.

3.3.2.3 The effects of the population size

In this section, we will characterise the effect of having different population sizes, while fixing the number of generations. The population size refers to the number of individuals in the population. If there are too few individuals in a generation, the GAs will have a limited number of possibilities for performing crossovers, and only a small fraction of the legitimate search space will be explored. On the other hand, if there are too many individuals, the GAs will impose a high complexity. Experimental evidence shows that, which mainly depends on type of the individual encoding and on the problem specified, it is not necessary to increase the population size beyond a certain limit because the algorithm is unlikely to outperform moderate sized populations [253]. The achievable BER associated with employing different population sizes is shown in Figure 3.8(a), while the remaining parameters are summarised in Table 3.2. We can see from Figure 3.8(a) that as the population size increases, the achievable average BER of the GA-assisted MBER MUD becomes lower. This is because when the size of the population is increased, there are more individuals, producing better

offsprings. However, as the number of individual increases, the complexity of the GA also increases, as it will be explained in more detail in Section 3.4. Therefore, increasing the number of individuals in the population beyond about 50 while imposing an increased complexity results in a modest BER improvement.

For the sake of providing further insights, Figure 3.8(b) shows the PDF of the BER for 1000 simulation runs for the different number of individuals in a population. We can see from the figure, that when the population size approaches 90, the probability of approaching the optimum BER is nearly unity. In the following section, we will explore the effects of using different types of crossovers.

3.3.2.4 The effects of different crossovers

Another important element in a GA-assisted search algorithm is the choice of the crossover. In this section, we will describe the effects of different types of crossovers in the context of our problem. The crossover operation is a process in which arbitrary decision variables are exchanged between a pair of selected parents, portraying the process of recombining two-single chromosomes in nature. Hence, the GA's crossover operation creates two new individuals, known as offspring in terms of GA, which have a high probability of exhibiting better fitness values than their parents. In order to generate P number of new offspring, $P/2$ number of crossover operations are required. A new pair of parents is selected from the mating pool for each crossover operation. The newly created offspring will form the basis of the next-generation population.

Crossover probability refers to the relative frequency of how often crossovers will be performed. If there is no crossover, the offspring are the exact copies of their parents. However, if there is a crossover, the offspring are constituted by bit-sequents of both parents' chromosome.

A range of various types of crossovers can be found in the literature, but we will only consider three crossover types in this section, namely the single-point crossover of Section 3.3.2.4.1, the two-point crossover of Section 3.3.2.4.2 and the uniform crossover regime of Section 3.3.2.4.3.

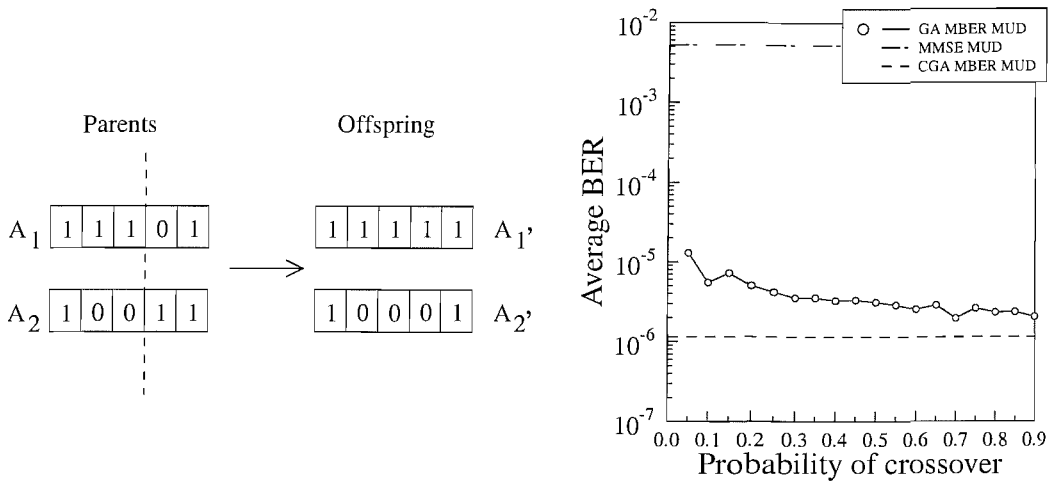

(a) One-point crossover

(b) Average BER versus probability of crossover

Figure 3.9: An example of the single-point crossover is portrayed in (a) while (b) shows the achievable average BER when varying the probability of crossover for the single-point crossover method invoked for User 1 at SNR = 15 dB. The remaining parameters are specified in Table 3.2.

3.3.2.4.1 Single-point crossover The single-point crossover constitutes the simplest type of crossover operation, which was also used by Holland in deriving his schema[2] theorem [231]. For the single-point crossover, a single cross-over point is chosen in the middle of an individual, and any bits beyond this point of the individual will be swapped between the parents, as depicted in Figure 3.9(a). However, adopting the single-point crossover has several disadvantages. Firstly, the single-point crossover is more likely to destroy a schemata of long defining lengths [231]. In other words, schemata that can be created or destroyed by opting for a single-point crossover depends strongly on the location of the cross-over point bits in the individual. Secondly, the single-point crossover cannot combine all possible schemata. The achievable BER performance when varying the crossover probability of the single-point crossover scenario is shown in Figure 3.9(b). The remaining parameters are summarised in Table 3.2. It can be seen that the achievable BER improves slightly, as the crossover probability increases.

[2]Holland [231] introduced the notion of a so-called *schema* (plural, *schemata*), in order to explain how GAs search for regions of high fitness. A schema H is a similarity template, defined over the alphabet 0,1,*, where 0 and 1 are referred to as *defined bits*, while * denotes a *don't care* symbol.

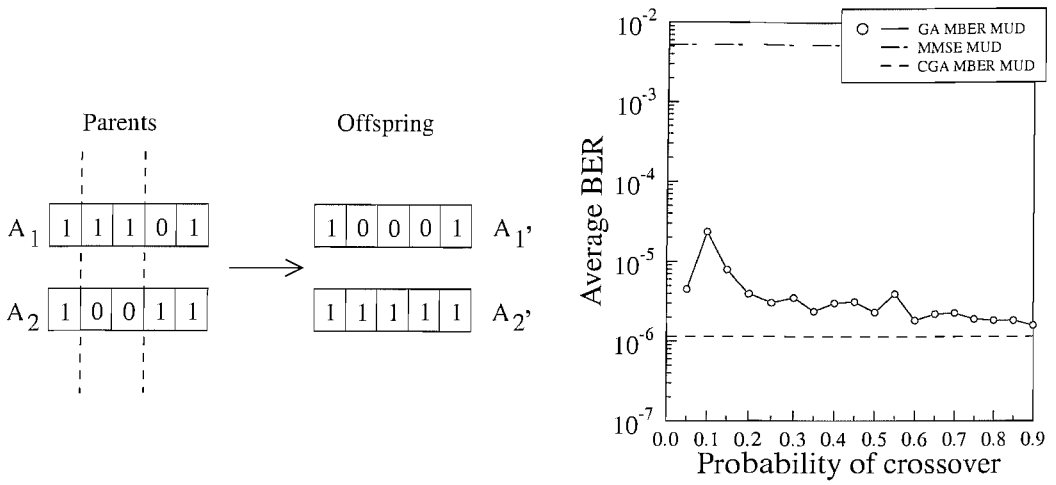

(a) Two-point crossover

(b) Average BER versus probability of crossover

Figure 3.10: An example of the two-point crossover is portrayed in (a) while (b) shows the achievable average BER when varying the probability of crossover for the two-point crossover method invoked for User 1 at SNR = 15 dB. The remaining parameters are specified in Table 3.2.

3.3.2.4.2 Two-point crossover Unlike the single-point crossover, a two-point crossover operation uses two randomly chosen crossover points, as portrayed in Figure 3.10(a). The binary string sequents of the decision variable that fall between these crossover points are then exchanged between the parents. Experimented evidence shows that a two-point crossover is less likely to destroy schemata that have a high defining length, and they are capable of combining more schemata than the single-point crossover [230]. However, there are still certain schemata that the two-point crossover is incapable of combining. The achievable BER of the two-point crossover is shown in Figure 3.10(b), when varying the probability of crossover. From the figure we can see that the two-point crossover is more sensitive to the change in the probability of crossover compared to the single-point crossover. However, at the highest possible probability of crossover, the performance of the two-point crossover is slightly better than that of the single-point crossover.

3.3.2.4.3 Uniform crossover The third type of crossover considered here is constituted by the uniform crossover, which was popularised by Syswerda [254] in 1989. In a uniform crossover operation a so-called crossover mask is invoked instead of a crossover point,

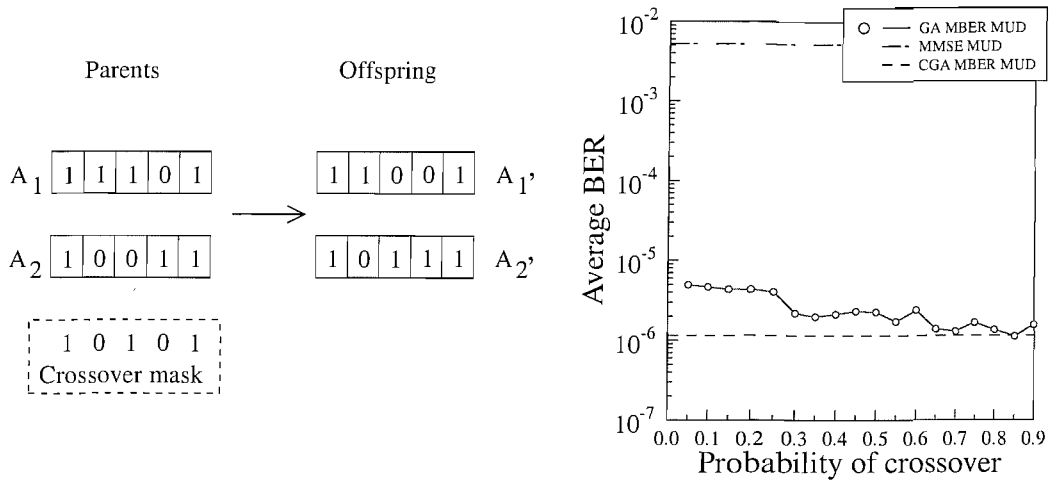

(a) Uniform crossover

(b) Average BER versus probability of crossover

Figure 3.11: An example of the uniform crossover is portrayed in (a) while (b) shows the achievable average BER when varying the probability of crossover for the uniform crossover method invoked for User 1 at SNR = 15 dB. The remaining parameters are specified in Table 3.2.

as can be seen in Figure 3.11(a). The crossover mask is a vector consisting of randomly generated 1s and 0s of equal probability, having a length equal to that of the individuals. Bits are exchanged between the selected pair of parents at locations corresponding to a 1 in the crossover mask. While it was shown in [255] that the uniform crossover operation has a higher probability of destroying a schema, it is also capable of creating new schemata. Figure 3.11(b) shows the achievable BER of User 1 at SNR = 15 dB, when employing the uniform crossover. The figure shows that the achievable BER is slightly better than that achieved, when using either a single-point crossover or the two-point crossover. Moreover, at a high probability of crossover, the achievable BER of the GA-assisted MBER invoking the uniform crossover approaches that of the CG MBER MUD.

3.3.2.5 The effects of the mutation probability

In this section, we will investigate the effects of varying the probability of mutation in the context of our GA-aided search method. Following the production of the offspring with the aid of the crossover operation, each component of the offspring will be mutated with a probability of p_m, where again, the mutation probability refers to the relative frequency of

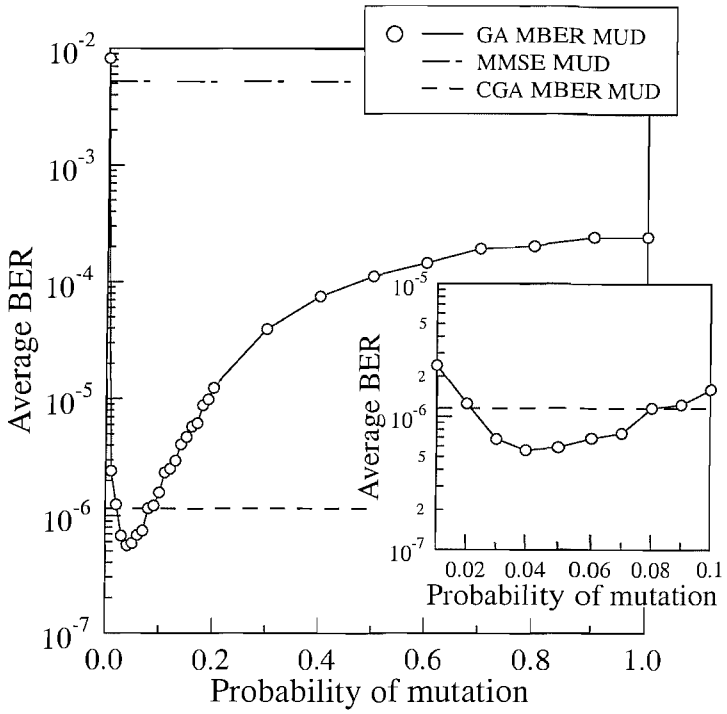

Figure 3.12: The achievable average BER of the GA-assisted MBER MUD upon varying the probability of mutation for User 1 at SNR = 15 dB. The remaining parameters are outlined in Table 3.2.

how often the bits of an individual will be mutated. Since we are only using binary decision variables, there are only two possible values for each binary decision variable hosted by an individual. Hence, when mutation is invoked for a particular bit, the value of the bit is toggled to its other possible value, i.e. a bit of logical '1' is changed to a logical '0' and vice versa.

The mutation operation is invoked, in order to ensure that sufficient diversity is maintained in the population so as to protect it against getting-trapped in local extremetes and low premature convergence. If there is no mutation, the offspring are generated directly after the crossover operation or are directly copied without any change. By contrast, if mutation is performed, one or more parts of a chromosome are changed. Moreover, if the mutation probability is 100%, the whole chromosome is changed. A high probability of mutation may prevent the survival of high-fitness values and hence may lead to suboptimal solutions. On the other hand, a low probability of mutation may result in premature convergence and to sub-optimum solutions due to the lack of diversity in the population. However, mutation should not occur too often, because then the GA would be degenerated

to a random search.

Numerous studies have been carried out for determining the optimum value of p_m. Schaffer *et al.* [256] suggested that the value of p_m should lie in the range between 0.005 and 0.01, Grefenstette [257] recommended the choice of $p_m \approx 0.01$, while Bäck [258] claimed that $p_m = 1/l$, is the most useful choice for unimodal functions, where l is the length of the individual. Adaptive mutation rates that change during the search process have also been proposed by Bäck [259]. The BER results characterising the effects of the mutation probability are shown in Figure 3.12. Using the parameters summarised in Table 3.2. We can see from Figure 3.12 that for our specific problem the optimum p_m was around the value of 0.04.

3.4 Complexity comparisons

The advantage of using GAs compared to the CG method [2] for determining the MBER MUD's weight values is that the GA does not necessarily require a good initial weight guess for exhibiting rapid convergence. In this section, we will compare the estimated complexity of the two methods. In this report, the complexity refers to the number objective function evaluations or gradient evaluations for the GA and the CG methods, respectively.

The complexity of the CG algorithm is proportional to the number of iterations used for finding the MBER solution on the BER surface. In each iteration the gradient of Equation 2.39 will have to be calculated and the SDMA-MUD weight values will be updated accordingly. Therefore the complexity of the CG method can be estimated as:

$$compl\{CG\} \simeq \text{Maximum number of objective function evaluations.} \quad (3.6)$$

On the other hand, if we used the maximum number of generations as the termination criterion in the GA, each generation of the population contains a certain number of individuals, thus the complexity of the GA aided MUD is proportional to the product of the population size and the number of generations used, which is given by:

$$\begin{aligned} compl\{GA\} &\simeq \text{Population size} \times \text{Generation} \\ &= \text{Total number of objective functions evaluation.} \end{aligned} \quad (3.7)$$

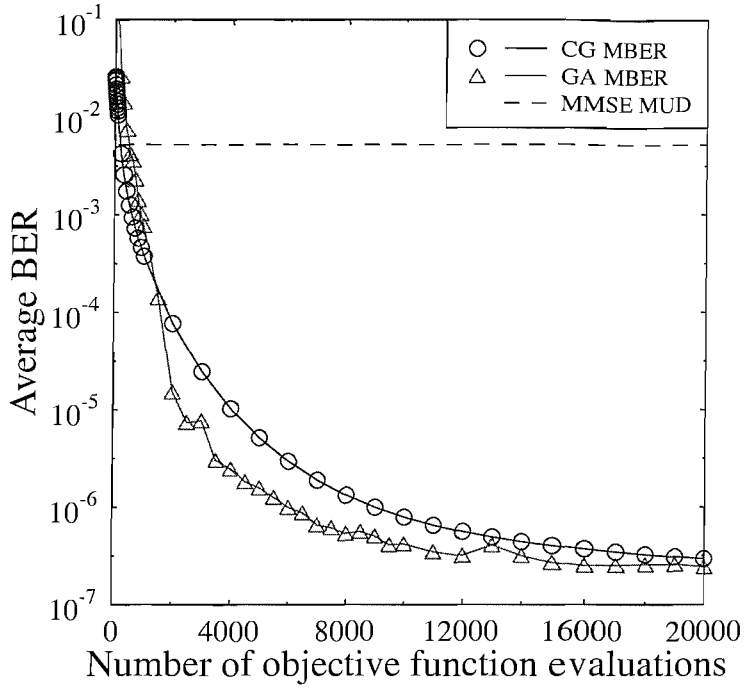

Figure 3.13: The achievable BER performance of User 1 versus the number of iterations imposed by the evaluating the objective function of GA and CG MBER MUD invoked in the OFDM/SDMA system employing P = 4, L = 4 and 128-subcarrier OFDM for communicating over the symbol-invariant SWATM [8 p.476] channel at SNR = 15 dB. The complexity calculations were described in Section 3.4. These curves were evaluated from Equation 2.33.

By using Equation 3.6 and Equation 3.7, we can compare the complexity of the two methods. Figure 3.13 shows the probability of error experienced by User 1 at SNR = 15 dB for the P = 4 and L = 4 system configuration. We can see from the figure that the GA-aided SDMA-MUD will approach the minimum BER at a lower complexity compared to the CG method.

3.5 Overloaded scenario

We will now continue our discussion by characterising the achievable performance, when supporting more users than the number of antennas at the base station. In Section 2.4.3.2 we have seen that the CG-based exact MBER MUD equipped with four receiver antennas is capable of supporting more than four users. By contrast, the MMSE MUD is only capable of supporting up to four users. Figure 3.14 characterises the achievable BER performance

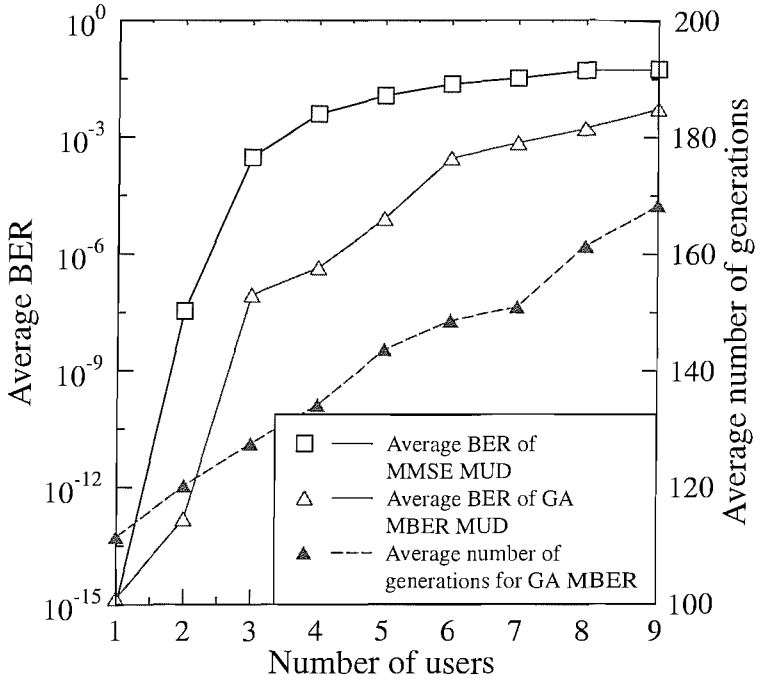

Figure 3.14: The achievable average BER and the number of generations required for User 1 of the P = 4 antenna system when varying the number of users at SNR = 15 dB. The remaining parameters are specified in Table 3.2. These curves were evaluated from Equation 2.33.

of the GA-based exact MBER MUD when employing four receiver antennas and supporting various number of users at SNR = 15 dB. The GA-aided iterations were terminated upon approaching the MBER solution sufficiently closely as described in Section 3.3.2.1.2. We can see that for a high number of users the GA-based MBER MUD particularly outperforms the MMSE MUD. However, we have to note that as the number of users increases, the number of generations required for sufficiently accurate convergence to the optimum solution also increases. This is because as more users are supported by the system, the search problem to be solved becomes more complex thus a higher complexity GA search has to be initiated.

3.6 Conclusion

In summary, this chapter has explored the novel idea of using GAs for finding the optimised MBER MUD weight value, namely those that are capable of satisfying the minimum BER criterion in the context of the OFDM SDMA based system. Unlike the conjugate gradient

search method used in Chapter 2, the GA method does not require an accurate initial value of the weights, yet it is more likely to reach the globally optimum solution.

We commenced the chapter with a brief overview of GAs in Section 3.1. In particular, we have introduced the family of GAs in Section 3.1.1 as a type of search algorithm that mimics the rule of evolution and survival in nature. We have also briefly characterised the processes that are involved in GAs in Section 3.1.2. In Section 3.1.3 we discussed how the family of GAs is related to traditional search methods, namely to *calculus-based*, *enumerative* and *random* search algorithms.

The proposed GA-aided MBER MUD employed in an SDMA OFDM system was introduced in Section 3.2, while in Section 3.3 the achievable performance of the proposed system was characterised. Firstly, the BER performance of the different users in a four-user four-receiver antenna system was portrayed in Section 3.3.1. Our simulation results showed that by using the default parameter values outlined in Table 3.3, the achievable BER performance of the GA-aided system is as good as that of the CG-base MBER MUD of Chapter 2.

We continued our performance related discussions to quantify the effects of varying the different parameters of the GA-aided search method in Section 3.3.2. The first algorithm feature investigated in Section 3.3.2.1 was the termination criterion. By using different types of termination criteria, different average BERs may be achieved at the cost of a different implementational complexity. The GA search method may be terminated by either fixing the number of generations, or when the best individual in the population achieves a sufficiently accurate convergence. Alternatively, the search may be terminated when the average fitness of all the individuals in a generation is within an acceptable range, as explained in Sections 3.3.2.1.1, 3.3.2.1.2 and 3.3.2.1.3, respectively. By using termination at a fixed number of generations, the associated implementational complexity may be calculated and fixed beforehand, but with the disadvantage that the achievable BER might not be sufficiently close to the optimum solution. By contrast, the convergence-based termination criterion will allow the GA-aided search method to continue, until the best solution is found at the cost of having an unpredictable implementational complexity. Therefore, the convergence-based termination might require an excessive number of generations, thus increasing the associated implementational complexity.

In Section 3.3.2.2, we portrayed a number of different types of GA individual representations, namely that of binary encoding in Section 3.3.2.2.1 and Gray encoding in Section 3.3.2.2.2. These discussions were followed in Section 3.3.2.3 by quantifying the effects of varying the population size of the GA. It was shown that as expected, the achievable average BER improves, as the population size increases.

Another algorithmic feature investigated was the GA's crossover which was the topic of Section 3.3.2.4. We explored three different types of crossovers, namely the single-point crossover, the two-point crossover and the uniform crossover in Section 3.3.2.4.1, Section 3.3.2.4.2 and Section 3.3.2.4.3, respectively. This discourse was followed by characterising another important element of the GA, namely that of the mutation probability, which was optimised in Section 3.3.2.5.

Having characterised the achievable system performance, the chapter continued with a complexity comparison of the GA-aided search to the conjugate gradient method in Chapter 2. It was shown in Section 3.4, that the GA was capable of approaching the optimum weight values of the MBER MUD in the context of the OFDM SDMA system at a lower complexity in comparison to the CG method. Finally, in Section 3.5 we studied the scenario, where the number of users was higher than the number of receiver antennas. Our simulation results recorded for the four-antenna scenario shows that just like for the CG MBER-MUD, the GA-based MBER MUD is also capable of supporting more users than the number of receiver antennas compared to the MMSE-MUD. However, as the number of users increases, the complexity of the GA-aided search algorithm required for approaching convergence also had to be increased.

In conclusion, the proposed GA-based MBER MUD is capable of achieving a similar performance to that of the CG-based MBER MUD at a lower complexity. Moreover, the GA-based MUD is capable of circumventing most of the MBER MUD parameter-optimisation problems, regardless of the choice of initial conditions and the step-size, rendering it more flexible than the CG based method. Moreover, in Chapter 2 and Chapter 3, we have assumed that the knowledge of the CIR is available, although this is not necessarily the case in a practical application. Hence, in the following chapter we will investigate the employment of the family of adaptive MBER MUDs in the context of the OFDM SDMA system investigated, where this assumption is eliminated.

Chapter 4

Adaptive MBER MUD

In our previous discourse of Chapters 2 and 3, we have assumed that the CIR or FDCHTF is perfectly known. In reality, they are unknown and have to be predicted. This can be achieved by using the FD pilot-assisted channel estimation techniques of Section 1.2.4 or the more complex interference-cancellation aided decision-directed methods of [5]. In this chapter, we will use a different training sequence in conjunction with adaptive methods designed for estimating the SDMA MUD's optimised weight values that will tend towards the minimum bit error rate criterion. We will commence with a brief introduction to the philosophy of adaptive MBER MUDs in Section 4.1. This is followed by Section 4.2, which describes the so-called block adaptive MBER algorithm, while the stochastic adaptive MBER algorithm is discussed in Section 4.3. In Section 4.4, we will invoke the GA search method to assist the block adaptive MBER MUD. Finally, Section 4.5 provides our conclusions.

4.1 Introduction

We will commence our chracterisation of the unknown channel by describing the philosophy of adaptive SDMA MUDs, where a set of consecutive known OFDM symbols is transmitted through the channel, rather than embedding a given percentage of FD pilots in each OFDM symbol. At the receiver, the weights of the multiuser detector are approximated by comparing the received OFDM symbols and the original OFDM training symbols. A number of adaptive algorithms can be found in the literature that are based on the MBER

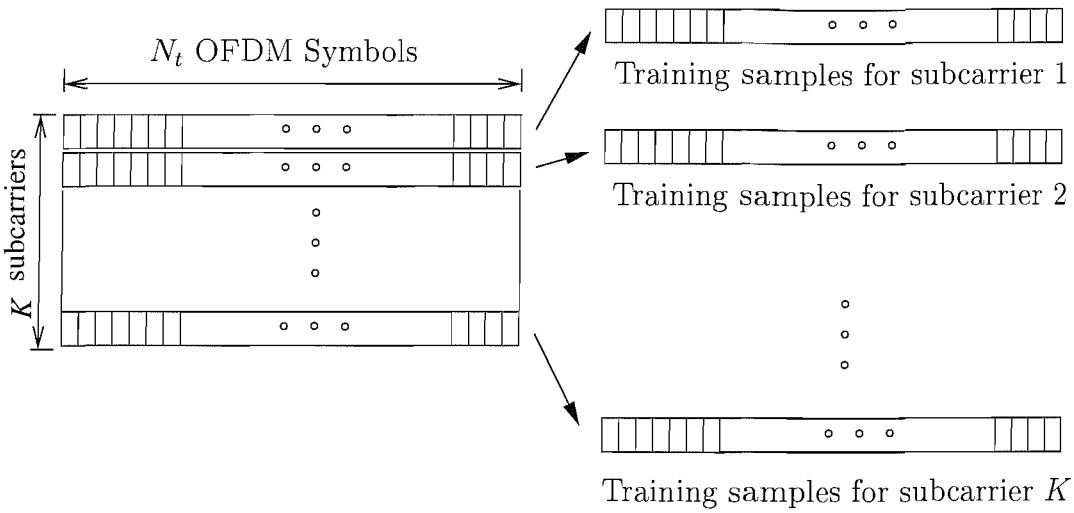

Figure 4.1: The training block composition showing how the training samples are arranged in N_t consecutive OFDM symbols each having K subcarriers.

criterion [209,213,221,223,228,229]. Two of these techniques will be discussed in this chapter, namely the block adaptive conjugate gradient (BACG) MBER technique and the Least Bit Error Rate (LBER) algorithm, which is sample-by-sample adaptation method. In the next section, we will elaborate on how the BER is estimated in a BPSK system based on a specific training sequence.

4.1.1 Estimated BER for BPSK

Before we proceed with our discussions on the MBER SDMA MUD's weight adjustment methods, we would like to clarify that as in the case of the exact MBER MUD of Chapter 2, in this chapter the weight calculations will also be considered on a subcarrier-by-subcarrier basis. Figure 4.1 depicts the arrangement of the training symbols invoked by the adaptive methods considered. Therefore, the training samples in the forthcoming discussions will be referring specifically to the training samples conveyed by a particular subcarrier.

In Section 2.4.1, we have shown that the probability of error $P_E(\mathbf{w})$ expressed as a function of the MUD's weight vector $\mathbf{w}$ can be derived by integrating the PDF of the signed decision variable given by Equation 2.30 over the negative half-plane of the PDF. The PDF can be estimated by employing Kernel Density Estimation (KDE)[1] [260, 261] techniques using a

[1]KDE was developed by Parzen [260] in 1962. The kernel density estimator can be considered as the superposition of specific kernel functions positioned at the observed data, where the shape of the kernels is determined by the choice of the kernel function and the associated kernel widths are determined by the KDE's window width. On the other hand, window width is the width of the kernel function positioned at

set of training symbols. In this section, we will derive the estimated probability of error $\hat{P}_E$ as a function of the SDMA detector's weight vector $\mathbf{w}$. The estimated BER can be derived by using the approach outlined in Section 2.4.1 for attaining an analytical expression for the BER. The only difference is that in deriving the estimated BER, we invoked a KDE for approximating the PDF, $p_y(y_s)$ of the MUD's signed decision variable.

We use complex-valued notation for representing the system model of the uplink SDMA OFDM system. In the case of BPSK, however, only the real part of the transmitted symbol actually carries the corresponding information bits. Let us define the estimated PDF produced by the KDE with the aid of N_t training symbols as follows:

$$\hat{p}_{z_l,R}(z_l;\mathbf{w}) = \frac{1}{N_t\sqrt{2\pi}\rho_n\sqrt{\mathbf{w}^H\mathbf{w}}}\sum_{i=1}^{N_t}\exp\left(-\frac{\{z_l-\mathrm{sgn}(b_l[i])\cdot s_{l,R}[i;\mathbf{w}]\}^2}{2\rho_n^2\mathbf{w}^H\mathbf{w}}\right), \quad (4.1)$$

where a Gaussian kernel was invoked and the so-called radius parameter, ρ_n is related to the noise standard deviation, σ_n.

As mentioned in [261], the kernel density estimator constructs the PDF estimates with the aid of N_t number of individual kernel functions - which is Gaussian in this case - centered at the signed decision variable values z_l associated with the N_t training data samples. The width of the kernel density functions, which is determined by the radius parameter or kernel-width, ρ_n signifies the range of z_l where the value of the kernel function is significant, i.e. where it contributes significantly to the PDF estimated. The selection of the kernel density function and the smoothing parameter $h = \rho_n\sqrt{\mathbf{w}^H\mathbf{w}}$ are intuitive since the conditional PDF of the signed decision variable corresponding to a particular combination of the L users' transmitted bits is Gaussian, having a standard deviation which is determined by that of the noise samples, weighted by the magnitude of the SDMA detector's weighting coefficients [261].

The estimated probability of error, $\hat{P}_{E,BPSK}(\mathbf{w})$ is evaluated by integrating the PDF estimate $\hat{p}_{z_l,R}(z_l;\mathbf{w})$ of Equation 4.1 over the negative abscissa interval $(-\infty,0)$, corresponding to an erroneous decision, as shown in the following equation:

$$\begin{aligned}\hat{P}_{E,BPSK}(\mathbf{w}) &= \int_{-\infty}^{0}\hat{p}_{z_l,R}(z_l;\mathbf{w})dz_l \\ &= \frac{1}{N_t}\sum_{i=1}^{N_t}Q(\hat{f}_R[i;\mathbf{w}]), \end{aligned} \quad (4.2)$$

each training data samples.

where $Q(x)$ is given by Equation 1.7 and $\hat{f}_R[i;\mathbf{w}]$ is given by:

$$\begin{aligned}\hat{f}_R[i;\mathbf{w}] &= \frac{\mathrm{sgn}(b_l[i])\cdot\hat{s}_{l,R}[i;\mathbf{w}]}{\rho_n\sqrt{\mathbf{w}^H\mathbf{w}}} \\ &= \frac{\mathrm{sgn}(b_l[i])\cdot\Re\{\mathbf{w}^H\mathbf{x}[i]\}}{\rho_n\sqrt{\mathbf{w}^H\mathbf{w}}},\end{aligned} \tag{4.3}$$

where $\hat{f}_R[i;\mathbf{w}]$ can be physically interpreted as the estimated signed decision variable introduced in Section 2.4.1.

Note that $\Re\{\mathbf{w}^H\mathbf{x}[i]\}$ can be expanded in the following form:

$$\Re\{\mathbf{w}^H\mathbf{x}[i]\} = \mathbf{w}_R^T\mathbf{x}_R[i] + \mathbf{w}_I^T\mathbf{x}_I[i], \tag{4.4}$$

where the vectors $\mathbf{w}_R$ and $\mathbf{w}_I$ denote the real and imaginary components of the SDMA MUD's weight vector. Likewise, $\mathbf{x}_R[i]$ and $\mathbf{x}_I[i]$ represent the real and imaginary components of the received signal at symbol index i. Having briefly described the derivation of the estimated BER function, we will now embark on discussing the first type of the adaptive MBER MUDs considered, which is the block adaptive algorithm in the next section.

4.2 Block adaptive MBER algorithm

The expression seen in Equation 4.2 is referred to as the block-based estimate of the BER. From this BER expression, we can derive the BER gradient with respect to the MUD's weight vector $\mathbf{w}$ and iteratively update them using the simplified conjugate gradient (CG) algorithm, as described earlier in Section 2.4.2, for the sake of attaining the MBER MUD weight solution as close to the MBER value as possible. This implies that the block adaptive algorithm is updating the MUD's weight vector $\mathbf{w}$ based on the entire block of training symbols in each subsequent iteration. The block adaptive MBER algorithm utilising the conjugate gradient algorithm of Equation 2.44 for updating the MUD's weight vector $\mathbf{w}$ is referred to as the Block Adaptive Conjugate Gradient (BACG) algorithm. The following section will describe the BACG MBER algorithm in more detail.

4.2.1 Block adaptive conjugate gradient MBER algorithm

The schematic of the block-based BACG MBER algorithm is depicted in Figure 4.2. A block of N_t subcarrier training symbols of the N_t consecutive OFDM symbols of user l is

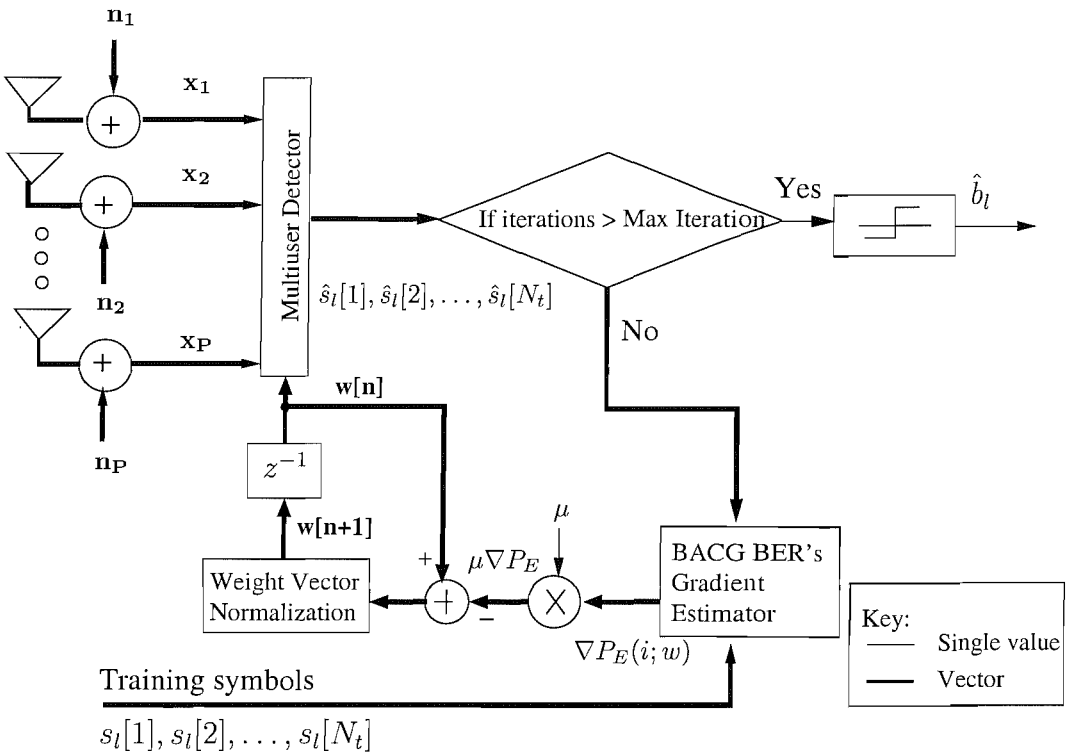

Figure 4.2: Signal flow diagram of the BACG MBER algorithm utilising the classic conjugate gradient method of Equation 2.44 at the receiver of the OFDM SDMA system for User l, $l \in 1, 2, \ldots, L$. The variable $\mathbf{x_p}$, where $x_p[i], i = 1, 2, \ldots, N_t$ and $\mathbf{n_p}$, where $n_p[i], i = 1, 2, \ldots, N_t$ represent the N_t received multiuser signals and the AWGN noise at receiver antenna p, $p \in 1, 2, \ldots, P$, respectively.

used for estimating the gradient of the BER on a subcarrier-by-subcarrier basis with the aid of the kernel density estimator. These training symbols are assumed to be known at the receiver. The vector $\mathbf{x}[i]$, $i = 1, 2, \ldots, N_t$, seen in Figure 4.2 hosts N_t number of the $(P \times 1)$-dimensional received multiuser signal components, where each $(P \times 1)$-dimensional received multiuser signal $\mathbf{x}[i]$ is associated with the corresponding training symbol $s_l[i]$. These received multiuser signal components $\mathbf{x}[i]$ are detected with the aid of a linear MUD, where the resultant N_t consecutive soft outputs of the MUD associated with a specific subcarrier index are grouped together in a vector denoted by $\mathbf{s}_l[n; \mathbf{w}]$, with the lower case n representing the iteration index. As seen in Figure 4.2, the soft outputs before the decision stage of the MUD and the knowledge of the actual transmitted symbols are used for estimating the gradient $\nabla \hat{P}_E(n; \mathbf{w})$ of the bit error probability. Again, as portrayed in Figure 4.2, this resultant block-based estimate of the BER's gradient is then multiplied by the adaptive step-size μ in order to provide an update factor to be used by the conjugate-gradient algorithm of Equation 2.44. The updated weight vector $\mathbf{w}[n+1]$ is normalised for

the sake of having a unity magnitude before being used in the next SDMA MUD weight updating process.

The OFDM subcarrier-related gradient $\nabla \hat{P}_{E,BPSK}(n;\mathbf{w})$ of the bit error probability given by Equation 4.2 at the n-th iteration can be attained by exploiting Equation 4.2, resulting in:

$$\nabla \hat{P}_{E,R}(n;\mathbf{w}) = \frac{1}{N_t\sqrt{2\pi}} \sum_{i=1}^{N_t} \left\{ \exp\left(-\frac{\{-\text{sgn}(b_l[i]) \cdot s_{l,R}[i;n;\mathbf{w}]\}^2}{2\rho_n^2 \mathbf{w}^H[n]\mathbf{w}[n]} \right) \cdot \nabla \hat{f}_R[i;n;\mathbf{w}] \right\}, \quad (4.5)$$

where the term $\nabla \hat{f}_R[i;n;\mathbf{w}]$ is given by:

$$\nabla \hat{f}_R[i;n;\mathbf{w}] = \frac{\text{sgn}(b_l[i])}{\rho_n \sqrt{\mathbf{w}^H[n]\mathbf{w}[n]}} \cdot \left(s_{l,R}[i;n;\mathbf{w}] \cdot \frac{\mathbf{w}[n]}{\mathbf{w}^H[n]\mathbf{w}} \right), \quad (4.6)$$

and where it was also taken into account that in case of BPSK modulation we have $\hat{P}_{E,BPSK}(\mathbf{w}) = \hat{P}_{E,R}(\mathbf{w})$. Note that in Equation 4.6 a new notation $s_{l,R}[i;n;\mathbf{w}]$ is used for representing the soft multiuser equalised output associated with the i-th transmitted bit $b_l[i]$ of a specific subcarrier at the n-th iteration.

After employing the weight normalization process of Equation 2.40 for the sake of ensuring that we have $\overline{\mathbf{w}}^H[n]\overline{\mathbf{w}}[n] = 1$, Equation 4.5 can be expressed as:

$$\nabla \hat{P}_{E,R}(n;\mathbf{w}) = \frac{1}{N_t\sqrt{2\pi}} \sum_{i=1}^{N_t} \left\{ exp\left(-\frac{\{s_{l,R}[i;n;\mathbf{w}]\}^2}{2\rho_n^2} \right) \cdot \hat{\mathbf{z}}_R[i;n;\mathbf{w}] \right\}, \quad (4.7)$$

where $\hat{\mathbf{z}}_R[i;n;\mathbf{w}]$ is given by:

$$\hat{\mathbf{z}}_R[i;n;\mathbf{w}] = \text{sgn}(b_l[i]) \cdot (s_{l,R}[i;n;\overline{\mathbf{w}}] \cdot \overline{\mathbf{w}}[n] - \mathbf{x}[i]), \quad (4.8)$$

while $\overline{\mathbf{w}}$ is the MUD's weight vector having a unity magnitude.

By using the gradient expression of Equation 4.7, the BACG algorithm may be defined for the BPSK system considered. Again, in the context of the BPSK system, the estimated BER's gradient $\nabla \hat{P}_{E,BPSK}(n;\mathbf{w})$ at the n-th iteration is unambiguously described by $\nabla \hat{P}_{E,R}(n;\mathbf{w})$ in Equation 4.7, because the BPSK symbols are real-valued. Thus, the gradient of the block-estimated BER for the BPSK-modulated OFDM system is given by:

$$\nabla \hat{P}_{E,BPSK}(n;\mathbf{w}) = \nabla \hat{P}_{E,R}(n;\mathbf{w}). \quad (4.9)$$

Notice that the gradient calculation of the block adaptive MBER algorithms is similar to that of the exact MBER algorithm highlighted in the context of Section 2.4.2. In this case,

Parameter	Value or type
BACG MBER	
Step size, μ	0.1
Kernel width, ρ_n	1
Training symbol length, N_t	100
Initialization	MMSE Initialization
Number of iterations	1000
OFDM	
Number of subcarriers	128
Number of cyclic prefix samples	32
Others	
Channel	3-path dispersive AWGN Channel

Table 4.1: Default parameters for the BACG MBER investigations.

the noisy received signal constellation points associated with the N_t known transmitted subcarrier symbols of the N_t consecutive OFDM symbols are used for driving the BACG algorithm towards the MBER solution instead of the perfectly known noiseless received signal's constellation points, where the latter was assumed in Section 2.4.2.

In the forthcoming sections we will study the effects of varying the parameter values of the BACG algorithm introduced above, namely the effects of varying the step-size, μ, the KDE's kernel-width, ρ_n, and the training sequence length, N_t in Sections 4.2.1.1, 4.2.1.2, and 4.2.1.3, respectively. For our simulations, we used the parameters specified in Table 4.1, except for the specific values that are studied.

4.2.1.1 The effects of varying the step-size

Firstly, we will study the effects of varying the step-size, μ, in our investigations of the BACG algorithm. Since SDMA OFDM detection was carried out on a subcarrier-by-subcarrier basis and each OFDM subcarrier experienced a different channel transfer factor, therefore each subcarrier will be affected differently by the step-size value. Figure 4.3 shows our simulation results for different values of μ, while the remaining parameters are fixed as summarised in Table 4.1. More specifically, the achievable BER at the different iterations related to a specific subcarrier at an SNR value of 15dB is shown for the case of $P = 2$, $L = 2$ as well as for $P = 4$, $L = 4$ in Figures 4.3(a) and 4.3(c), respectively. We have selected subcarrier 40 for the $P = 2$, $L = 2$ case and subcarrier 104 for the $P = 4$, $L = 4$ scenario as an example in order to show the achievable BER for every iteration at a specific subcarrier.

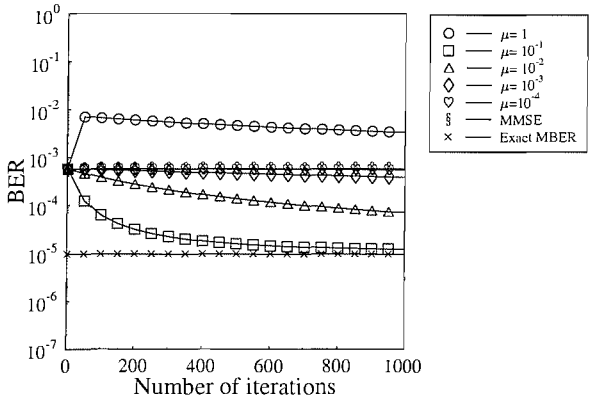

(a) P=2, L=2 for subcarrier 40 at SNR=15dB

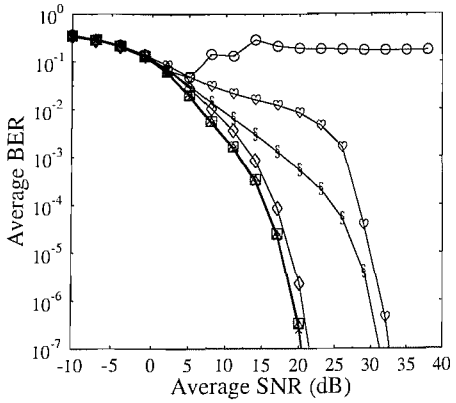

(b) P=2, L=2 for all SNRs

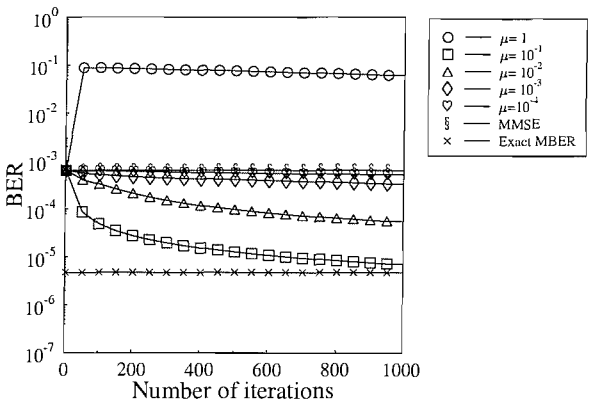

(c) P=4, L=4 for subcarrier 104 at SNR=15dB

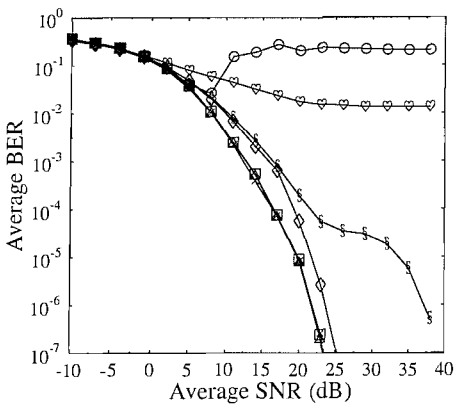

(d) P=4, L=4 for all SNRs

Figure 4.3: BER results of User 1, characterising the effects of the different values of the step-size, μ for the BACG MBER MUD for the case of a) $P = 2$, $L = 2$ at SNR=15dB for subcarrier 40, b) $P = 2$, $L = 2$ for all SNRs after 1000 iterations taken as average of all subcarriers, c) $P = 4$, $L = 4$ at SNR=15dB for subcarrier 104, and d) $P = 4$, $L = 4$ for all SNRs after 1000 iterations taken as average of all subcarriers. All other simulation parameters are summarised in Table 4.1. Note that for b) and d) the achievable BER curve for the exact MBER algorithm is exactly the same as for the curves associated with $\mu = 10^{-1}$ as well as $\mu = 10^{-2}$.

On the other hand, Figures 4.3(b) and 4.3(d) are depicting the achievable BERs for all SNRs and for different values of μ for the case of $P = 2,\ L = 2$ and $P = 4,\ L = 4$, respectively.

We can see from Figure 4.3 that the ideal value of μ for the two cases investigated is 10^{-1}. For a μ value that is higher than 10^{-1}, say for example $\mu = 1$, the BACG MBER MUD is incapable of reaching the BER of the exact MBER solution. By contrast, a μ value that is lower than 10^{-1} will converge at a slower pace and hence will require more iterations before the exact MBER solution is reached. Moreover, the value of μ is dependent on the shape of the BER surface and as we have seen in Figure 2.3 of Section 2.4.2, the BER surface varies between the subcarriers. For the simplified BACG algorithm, we assumed that a fixed value of μ is used for all subcarriers and SNRs.

4.2.1.2 The effects of varying the kernel-width

Let us now investigate the effects the kernel-width, ρ_n on the achievable BER of the BACG MBER MUD. Figure 4.4 shows our simulation results for various values of ρ_n with the other system parameters fixed as summarised in Table 4.1. In particular, Figures 4.4(a) and 4.4(c) depict the achievable BER at different iterations at two specific subcarriers and at SNR=15dB for the $P = 2,\ L = 2$ and $P = 4,\ L = 4$ scenarios, respectively, while Figures 4.4(b) and 4.4(d) show the achievable BER results for all SNRs of User 1 for the $P = 2,\ L = 2$ and $P = 4,\ L = 4$ scenarios, respectively.

The choice of the kernel width ρ_n determines the smoothness of the estimated PDF. This is why in the literature this parameter is also known as the *smoothening parameter* [260]. As argued in [261], too low a value of the kernel width would lead to an undersmoothed PDF estimate, which in turn renders the estimated BER surface bumpy, with many local minima. Note that these local minima may or may not correspond to the actual local BER minima. Operating the adaptive algorithm under this condition is likely to result in convergence to a local rather than global minimum. On the other hand, too high a kernel width will produce an over-smoothed PDF estimate, which fails to accurately resolve the detailed structure of the actual PDF. Therefore the minimum solution(s) associated with this over-smoothed estimate may be significantly different from the actual one. Moreover, choosing a kernel width ρ_n in between these two extremes is crucial, but once this range is found, the block adaptive algorithm is expected to be less sensitive to its variation. From

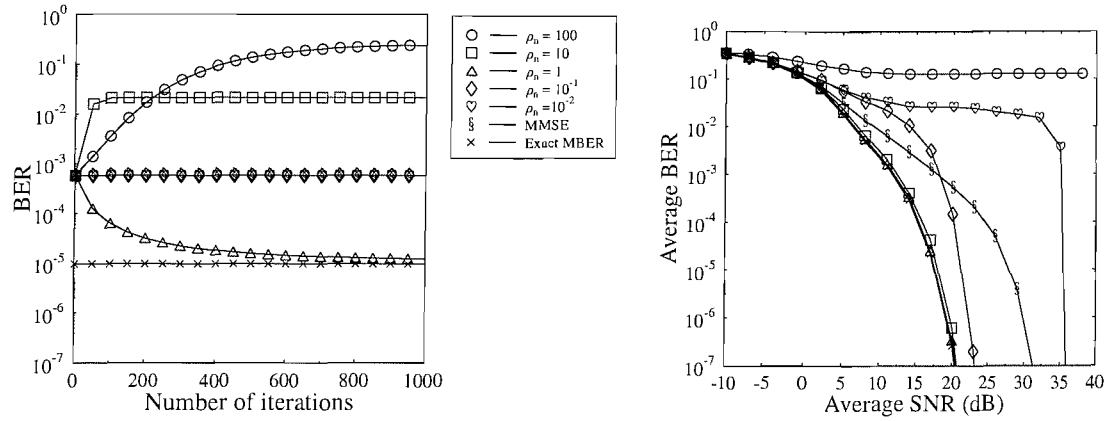

(a) P=2, L=2 for subcarrier 40 at SNR=15dB

(b) P=2, L=2 for all SNRs

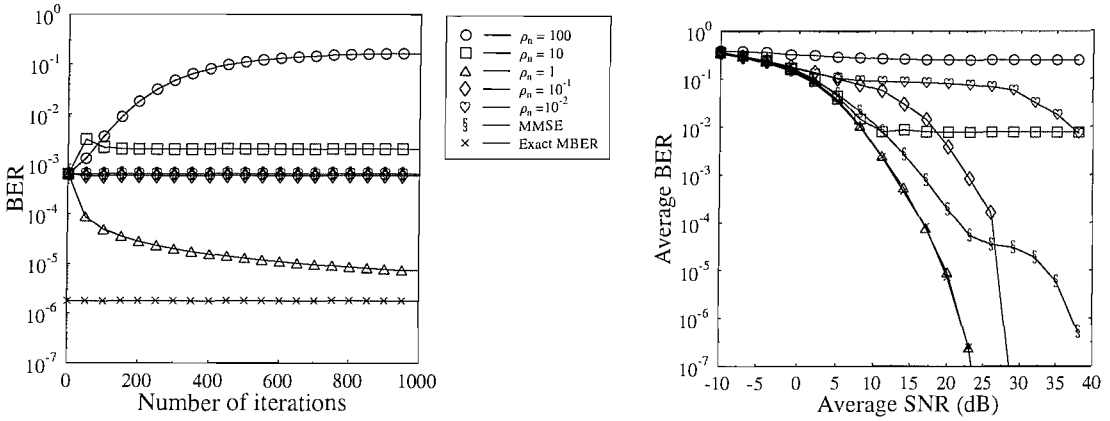

(c) P=4, L=4 for subcarrier 104 at SNR=15dB

(d) P=4, L=4 for all SNRs

Figure 4.4: BER results of User 1, characterising the effects of the different values of the kernel-width, ρ_n for the BACG MBER MUD for the case of a) P=2, L=2 at SNR=15dB for subcarrier 40, b) $P = 2$, $L = 2$ for all SNRs after 1000 iterations taken as average of all subcarriers, c) $P = 4$, $L = 4$ at SNR=15dB for subcarrier 104, and d) $P = 4$, $L = 4$ for all SNRs after 1000 iterations taken as average of all subcarriers. All other simulation parameters are summarised in Table 4.1. Note that for b) and d) the achievable BER curve for the exact MBER algorithm is exactly the same as for the curve associated with $\rho_n = 1$.

the results seen in Figure 4.4, we can see that the best value of ρ_n for the two cases that we studied, namely the $P = 2,\ L = 2$ and $P = 4,\ L = 4$ scenarios, which can achieve the closest BER value to that of the exact MBER solution is when ρ_n is equal to one.

4.2.1.3 The effects of varying the training block size

We will now continue our discussions by considering the effects of different training block sizes on the performance of the BACG MBER algorithm. The simulation parameters are summarised in Table 4.1, except for the training block length, N_t which is varied. Figure 4.5(a) depicts the achievable BER versus the number of iterations for the different values of N_t at SNR=15dB for a specific subcarrier in the $P = 2,\ L = 2$ scenario, while Figure 4.5(b) shows the results for all SNRs in the same scenario. Similar results were recorded for the $P = 4,\ L = 4$ scenario in Figures 4.5(c) and 4.5(d) for a specific subcarrier at SNR=15dB and for the average of all the subcarriers in the OFDM symbols at all SNRs, respectively.

We can see from the figures that a relatively small value of N_t is required for approaching the optimum MBER solution in the $P = 2,\ L = 2$ case. However, for the more complex scenario of $P = 4,\ L = 4$, if the number of training symbol is too low, the attainable performance of the BACG MBER algorithm may even become worse than that of the MMSE solution, as observed for example for $N_t = 10$ in Figure 4.5(c). Moreover, if the same number of training symbols is employed, the number of iterations required to reach the optimum MBER solution is also higher in a more complex system. We can also see that as expected, upon increasing the number of training symbols, the BACG algorithm will converge closer to the exact MBER solution. However, as we increase the number of training symbols, we are reducing the system's effective throughput. Therefore, we have to strike a good compromise between using a longer training that will result in a better steady-state performance but reduces the effective throughput or having a shorter training associated with a poorer BER performance but higher effective throughput.

In the following section, we will embark on investigating another type of adaptive MBER MUD which is the so-called stochastic adaptive MBER algorithm.

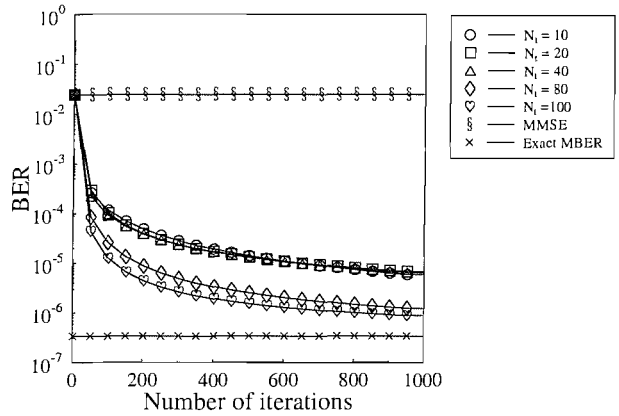

(a) P=2, L=2 for subcarrier 82 at SNR=15dB

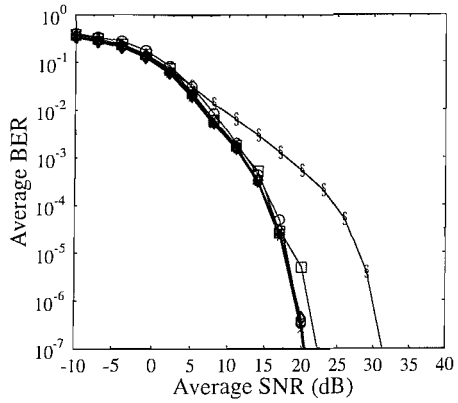

(b) P=2, L=2 for all SNRs

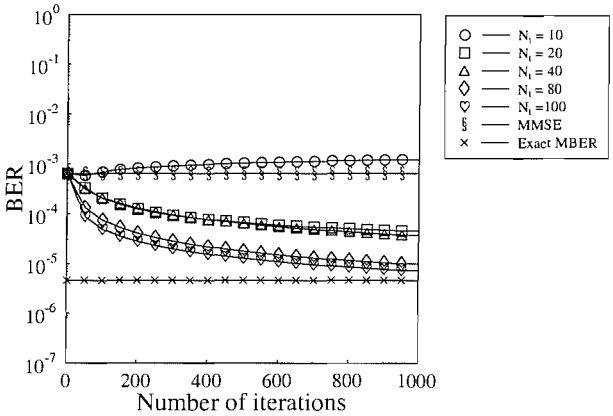

(c) P=4, L=4 for subcarrier 104 at SNR=15dB

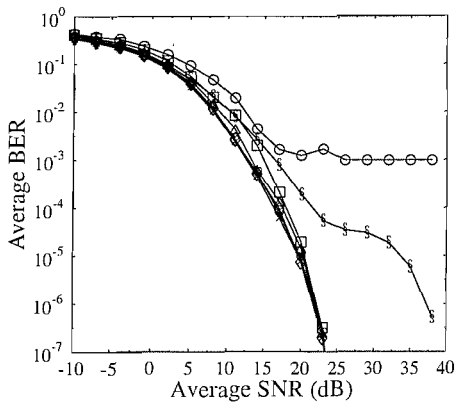

(d) P=4, L=4 for all SNRs

Figure 4.5: BER results of User 1, characterising the effects of the different length of the training symbols, N_t for the BACG MBER MUD for the case of a) $P = 2$, $L = 2$ at SNR=15dB for subcarrier 40, b) $P = 2$, $L = 2$ for all SNRs after 1000 iterations taken as average of all subcarriers, c) $P = 4$, $L = 4$ at SNR=15dB for subcarrier 104, and d) $P = 4$, $L = 4$ for all SNRs after 1000 iterations taken as average of all subcarriers. All other simulation parameters are summarised in Table 4.1.

4.3 Stochastic adaptive MBER algorithm

Let us now continue our investigations by considering another type of adaptive MBER MUDs, which is referred to as the stochastic adaptive MBER algorithm. The stochastic adaptive algorithm may be readily developed from the block adaptive algorithm of Section 4.2, which has a number of attractive properties. Instead of using a block of training symbols, this type of adaptive procedure utilises a single training symbol for estimating the PDF, $\hat{p}_y(i; y_s)$ of the signed decision variable of Equation 4.1, which allows us to derive the expression of the BER $\hat{P}_E(i; \mathbf{w})$ as well as the gradient $\nabla \hat{P}_E(i; \mathbf{w})$ of the estimated BER. Consequently, the MUD's weight vector $\mathbf{w}$ can be updated according to a factor given by the gradient of the estimated BER multiplied by the adaptive step size μ.

As suggested by the terminology, the stochastic adaptive MBER algorithm updates the MUD's weight vector $\mathbf{w}$ stochastically, such that a different training symbol is used in each updating operation, unlike in the context of the block adaptive MBER algorithm, which utilises all the training symbols in every iteration for its weight-update procedure.

Invoking all training symbols for estimating the BER's gradient requires a buffer to be constructed for storing the associated MUD's soft outputs. Furthermore, the performance of the block-adaptive MBER algorithm may become more dependent on the specific choice of the adaptive parameters and employing time-variant adaptive parameters is less straightforward, since the entire set of training symbols is used repeatedly in every iteration. On the other hand, the stochastic adaptive MBER algorithm may be able to respond to the instantaneous channel variations in a more prompt fashion. This adaptive method does not require a large buffer for storing the MUD's soft outputs, since it uses a single training symbol at a time. Moreover, the adaptive parameters may be chosen to suit the instantaneous channel conditions encountered by the system upon employing time-variant adaptive parameters. In addition to these characteristics, the decision-directed adaptation mode can be directly incorporated into the stochastic adaptive MBER algorithm by using the previously detected symbols for training, provided that the prevalent BER is sufficiently low, otherwise serious error-propagation effects would be inflicted. A number of stochastic adaptive algorithms have been investigated in [261], but we will only discuss one of them, namely the least bit error rate (LBER) algorithm in the following section.

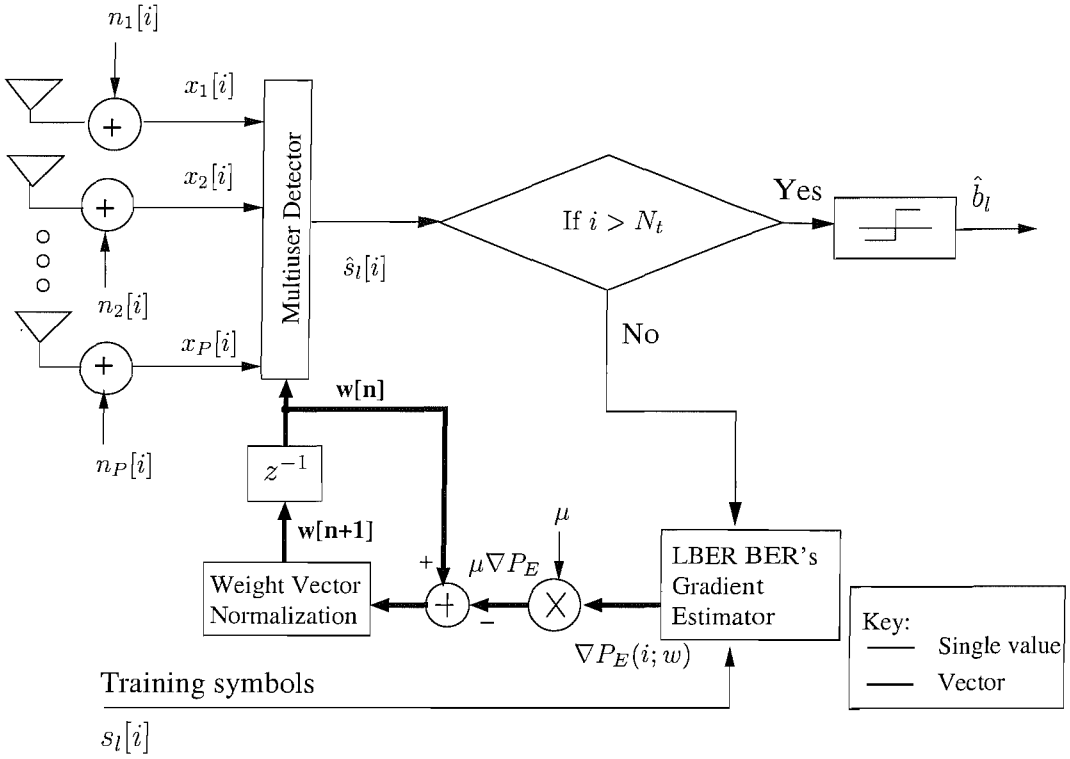

Figure 4.6: Signal flow diagram of the LBER MBER algorithm utilising the classic conjugate gradient method of Equation 2.44 at the receiver of the OFDM SDMA system for User l, $l \in 1, 2, \ldots, L$. In the figure, i is the training symbol index. This flow diagram is similar to that of the BACG algorithm seen in Figure 4.2, except for the LBER algorithm's BER-gradient estimator outlined in Section 4.3.1.

4.3.1 The least bit error rate algorithm

The single-symbol based PDF estimates are generated by setting $N_t = 1$ in the PDF estimates of Equation 4.1. Thus for the i-th OFDM symbol, the instantaneous PDF estimates can be written as:

$$\hat{p}_{z_l,R}(z_l; i; \mathbf{w}) = \frac{1}{\sqrt{2\pi}\rho_n\sqrt{\mathbf{w}^H[i]\mathbf{w}[i]}} \exp\left(-\frac{\{z_l - \text{sgn}(b_l[i]) \cdot s_{l,R}[i;\mathbf{w}]\}^2}{2\rho_n^2 \mathbf{w}^H[i]\mathbf{w}[i]}\right), \quad (4.10)$$

where all variables used in Equation 4.10 are similar to the variables used in conjunction with Equation 4.1.

As exploited in Equation 4.2 of Section 4.1.1, the instantaneous BER estimate - namely the $\hat{P}_{E,BPSK}(\mathbf{w})$ - can be derived by integrating the PDF estimate of Equation 4.10 over the negative half-value. Recall that the BER expression of the BPSK system is fully defined by the BER associated with the real component of the transmitted symbol. Then, the gradient $\nabla\hat{P}_{E,R}(i;\mathbf{w})$ of the instantaneous BER estimate can be calculated with the aid of

Equation 4.10, and after the weight normalisation according to $\overline{\mathbf{w}}^H[i]\overline{\mathbf{w}}[i] = 1$ we have:

$$\nabla \hat{P}_{E,R}(i;\overline{\mathbf{w}}) = \frac{1}{\sqrt{2\pi}} \exp\left(-\frac{\{s_{l,R}[i;\overline{\mathbf{w}}]\}^2}{2\rho_n^2}\right) \cdot \text{sgn}(b_l[i]) \cdot (s_{l,R}[i;\overline{\mathbf{w}}] \cdot \overline{\mathbf{w}}[i] - \mathbf{x}[i]). \quad (4.11)$$

Therefore, the gradient $\nabla \hat{P}_{E,BPSK}(i;\overline{\mathbf{w}})$ of the instantaneous BER estimate of the BPSK system is given by:

$$\nabla \hat{P}_{E,BPSK}(i;\overline{\mathbf{w}}) = \nabla \hat{P}_{E,R}(i;\overline{\mathbf{w}}), \quad (4.12)$$

where $\nabla \hat{P}_{E,R}(i;\overline{\mathbf{w}})$ was formulated in Equation 4.11.

A stochastic adaptive MBER algorithm based on the conjugate gradient method of Equation 2.44 can be formulated with the aid of the stochastic gradient expression of Equation 4.12. The resultant algorithm is referred to as the Least Bit Error Rate (LBER) [228] algorithm, because it updates the MUD's weights in a symbol-by-symbol adaptive manner, until all training data have been used. Note that the LBER algorithm requires the weight normalization operation of Equation 2.40 after every weight updating step for the sake of ensuring that the magnitude of the resultant weight vector becomes unity. This normalization is required for simplifying the mathematical description of the algorithm. One might argue that the instantaneous PDF estimate used for deriving the LBER algorithm is inaccurate and therefore the algorithm will be unable to converge to the MBER solution. However, this argument is not entirely true since a similar approach has been used for deriving the classic Least Mean Square (LMS) algorithm [261], where the Mean Square Error (MSE) is estimated based on a single training symbol. Despite this seemingly inaccurate PDF estimate, the LMS algorithm has been shown to converge fairly accurately to the MMSE solution, subject to a small misadjustment for a sufficiently large training data and to the appropriate choice of the adaptive step-size μ. Therefore, the LBER algorithm derived in this section may also be expected to converge towards the MBER solution, provided that the adaptive parameters, namely the step-size μ and the radius ρ_n, are chosen appropriately. However, there will always be a small misadjustment between the solution achieved by the LBER algorithm and the exact MBER solution due to the fact that all non-parametric PDF estimation techniques, including the KDE, are biased [261].

In the following sections we will investigate the effects of the adaptive parameters on the LBER MBER MUD system, namely the effects of the step-size μ and the radius ρ_n,

Parameter	Value or type
LBER MBER	
Step size, μ	10^{-2}
Kernel width, ρ_n	1
Training symbol length, N_t	100
Initialization	MMSE Initialization
OFDM	
Number of subcarriers	128
Number of cyclic prefix samples	32
Others	
Channel	3-path dispersive AWGN Channel

Table 4.2: Default parameters for the LBER MBER simulations.

in Sections 4.3.1.1 and 4.3.1.2, respectively. For the LBER simulations we employed the parameters summarised in Table 4.2, except for the specific parameter values that are varied.

4.3.1.1 The effects of varying the step-size

In this section, we will study the impact of varying the step-size μ imposed on the achievable BER performance of the LBER algorithm. Our simulation results are portrayed in Figure 4.7. More specifically, Figures 4.7(a) and 4.7(c) show the achievable BER versus the index of the training symbols for a specific subcarrier at SNR=15dB for the case of $P = 2,\ L = 2$ and $P = 4,\ L = 4$, respectively. On the other hand, Figures 4.7(b) and 4.7(d) depict the corresponding average BER results for all SNRs for the same two cases.

From Figures 4.7(a) and 4.7(c) we can see that the LBER algorithm is more sensitive to the value of μ compared to the BACG algorithm characterised in Figures 4.3(a) and 4.3(c). This is because the updating of the SDMA MUD's weight is carried out based on the prediction of the PDF using only a single training symbol at a time. Therefore, a μ value that is too high will result in a high BER fluctuation between the consecutive subcarrier symbols hosted by the consecutive OFDM symbols. By contrast, if the μ value is too small, then the weight value is not updated by a sufficiently large amount and thus will result in a small BER difference between the consecutive symbols. We can also see from the results of Figures 4.7(b) and 4.7(d) that the most suitable μ value that can approach the exact MBER MUD's BER for the cases that we investigated, namely for the $P = 2,\ L = 2$ and $P = 4,\ L = 4$ scenarios, is when we have $\mu = 10^{-2}$.

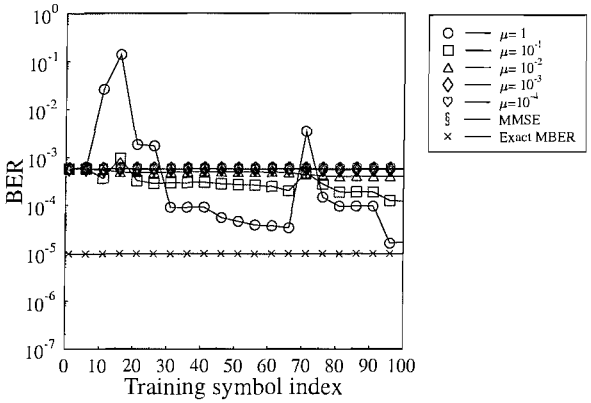

(a) $P = 2,\ L = 2$ for subcarrier 40 at SNR=15dB

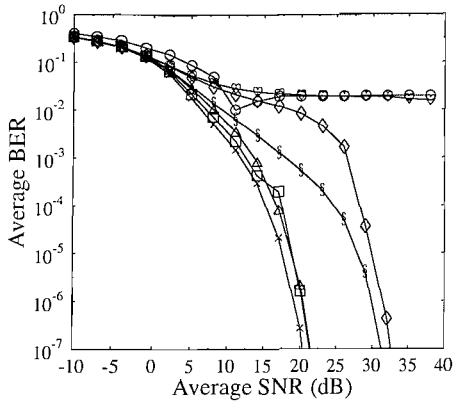

(b) $P = 2,\ L = 2$ for all SNRs

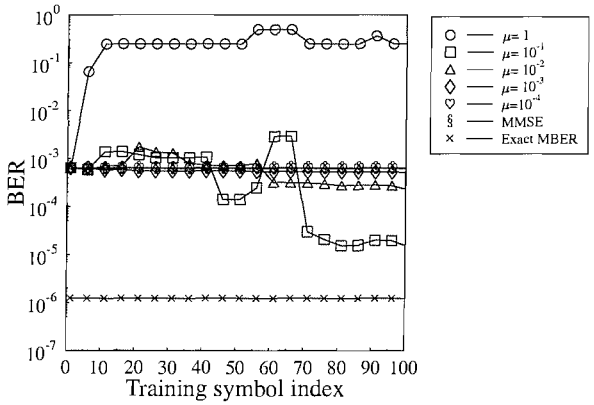

(c) $P = 4,\ L = 4$ for subcarrier 104 at SNR=15dB

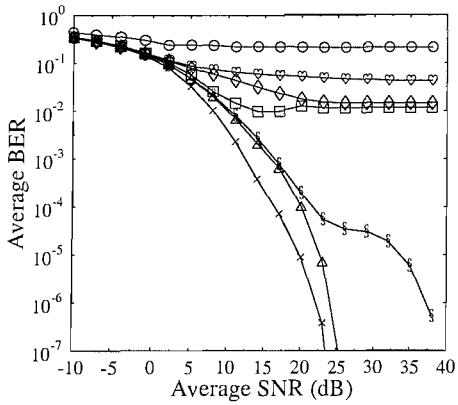

(d) $P = 4,\ L = 4$ for all SNRs

Figure 4.7: BER results of User 1, characterising the effects of the different values of the step-size, μ for the LBER MBER MUD for the case of a) $P = 2,\ L = 2$ at SNR=15dB for subcarrier 40, b) $P = 2,\ L = 2$ for all SNRs after 100 training OFDM symbols taken as average of all subcarriers, c) $P = 4,\ L = 4$ at SNR=15dB for subcarrier 104, and d) $P = 4,\ L = 4$ for all SNRs after 100 training OFDM symbols taken as average of all subcarriers. All other simulation parameters are summarised in Table 4.2.

In the next section, we will investigate the influence of another adaptive parameter that will impact on the LBER MBER MUD performance, which is the kernel-width ρ_n.

4.3.1.2 The effects of varying the kernel-width

Let us now commence our investigation of the effect of having different kernel widths ρ_n in the context of the LBER algorithm. Our related simulation results are depicted in Figure 4.8. Figure 4.8(a) shows the achievable BER versus the training symbol index when employing different values of ρ_n for the LBER algorithm for a specific subcarrier in the case of $P = 2$, $L = 2$. A similar comparison is shown in Figure 4.8(c) for the $P = 4$, $L = 4$ scenario. By contrast, Figures 4.8(b) and 4.8(d) show the achievable BER results for a range of SNRs, when using different values of ρ_n for the two previously mentioned cases.

Just as we have seen for the BACG algorithm in Section 4.2.1.2, the LBER algorithm is also dependent on the choice of the kernel width. However, unlike the BACG algorithm, the curves recorded for the LBER algorithm, as seen in Figures 4.8(a) and 4.8(c), are not as smooth as those of the BACG algorithms portrayed in Figures 4.8(a) and 4.8(c). Again, this is because the LBER algorithm predicts the PDF based on a single symbol, whereas the BACG algorithm's prediction is based on a block of training symbols. Moreover, the specific choice of ρ_n will determine the smoothness of the PDF estimation, as argued earlier in Section 4.2.1.2. From our results plotted in Figure 4.8, we can see that the best possible value of ρ_n for the LBER algorithm is the one that approaches the exact MBER most closely which is achieved when the value of ρ_n is 1.

4.4 GA assisted block adaptive MBER algorithm

Although the previously characterised BACG and LBER algorithms are capable of achieving a BER performance close to that of the exact MBER MUD's performance, the convergence rate of both algorithms is quite sensitive to the parameters selected, namely the step-size and kernel-width. Moreover, the algorithms also had to be carefully initialized for the sake of ensuring that the weights of the MBER MUD converge to the optimum weight value. In our investigations, we have used the MMSE SDMA MUD weight solution for the algorithm's initialization, but even with this choice of initialization convergence to the MBER solution is

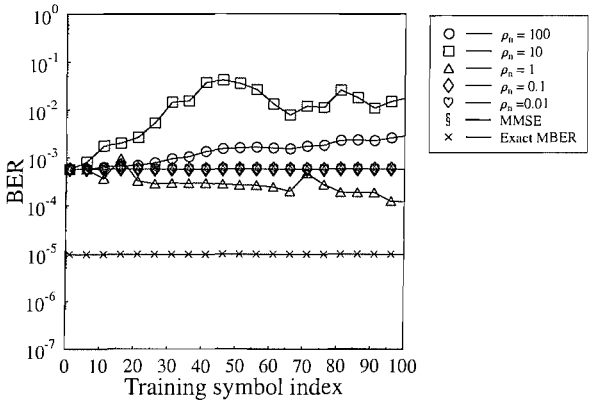

(a) P=2, L=2 for subcarrier 40 at SNR=15dB

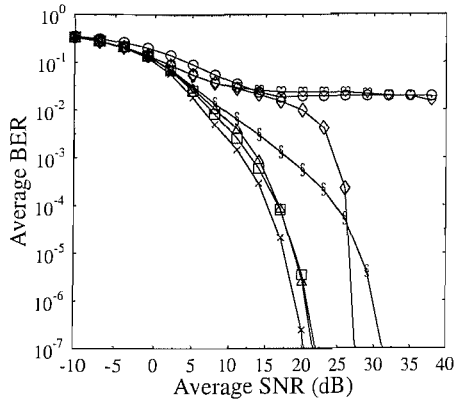

(b) P=2, L=2 for all SNRs

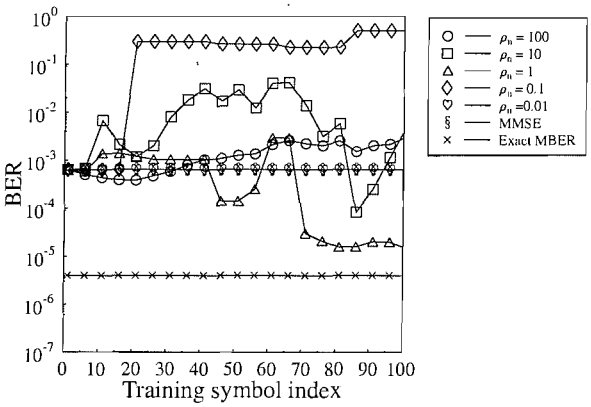

(c) P=4, L=4 for subcarrier 104 at SNR=15dB

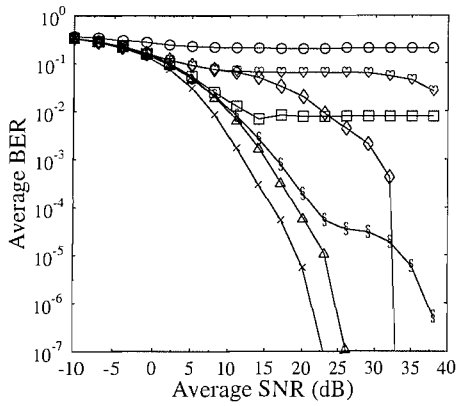

(d) P=4, L=4 for all SNRs

Figure 4.8: BER results of User 1, characterising the effects of the different values of the kernel-width, ρ_n for the LBER MBER MUD for the case of a) $P = 2$, $L = 2$ at SNR=15dB for subcarrier 40, b) $P = 2$, $L = 2$ for all SNRs after 100 training OFDM symbols taken as average of all subcarriers, c) $P = 4$, $L = 4$ at SNR=15dB for subcarrier 104, and d) $P = 4$, $L = 4$ for all SNRs after 100 training OFDM symbols taken as average of all subcarriers. All other simulation parameters are summarised in Table 4.2.

not guaranteed. In order to circumvent the algorithm's dependency on these requirements, we may employ the GA-aided search method, as we have done in the context of the exact MBER MUD in Chapter 3. We will commence this section by outlining the proposed GA-aided block adaptive (GABA) MBER MUD implementation in Section 4.4.1. This is then followed by the presentation of our simulation results in Section 4.4.2.

4.4.1 GA-aided block adaptive implementation

In this section, we will invoke a GA for finding the MBER MUD's weight values based on the block adaptive algorithm. The first thing that we have to do is to set the objective function of the GA to the probability of error as a function of the weight values. By using Equation 4.2 and Equation 4.3, the probability of error for the block adaptive algorithm can be written as:

$$\hat{P}_{E,BPSK}(\mathbf{w}) = \frac{1}{N_t}\sum_{i=1}^{N_t} Q\left(\frac{\mathrm{sgn}(b_l[i])\cdot\Re\{\mathbf{w}^H\mathbf{x}[i]\}}{\rho_n\sqrt{\mathbf{w}^H\mathbf{w}}}\right), \tag{4.13}$$

where, as previously defined, N_t is the number of training samples in the block, $\mathbf{w}$ is the current SDMA MUD weight vector, $b_l[i], i \in 1,\ldots,N_t$ is the i-th bit of l-th user, ρ_n is the kernel-width, and $\mathbf{x}[i], i \in 1,\ldots,N_t$ is the i-th received vector at the receiver antenna.

Using the same technique as in Chapter 3, we will again employ binary strings for representing the real and imaginary parts of the weight values. However, this time we will have to choose a specific fixed value for the kernel-width, ρ_n, that is well suited to the scenario we are investigating. We will explore the algorithm's dependence on this ρ_n value in further detail later in Section 4.4.2.1. We will refer to this solution as a static GA configuration [245].

As in Section 3.2, the fitness, f_i of an individual is again quantified as:

$$f_i = -\log_{10}(\hat{P}_E(\mathbf{w})), \tag{4.14}$$

where $\hat{P}_E(\mathbf{w})$ is the estimated probability of error given by Equation 4.13. As mentioned in Section 3.2, the employment of the logarithm of $\hat{P}_E(\mathbf{w})$ in the objective function has significantly improved the convergence behaviour of the GA, since the logarithmic function expands the most-important low-BER range. There are various ways of defining the fitness function, but for the context of the MBER MUD the fitness function of Equation 4.14

Parameter	Value or type
Adaptive parameters	
Kernel width, ρ_n	1
Training symbol length, N_t	100
OFDM	
Number of subcarriers	128
Number of cyclic prefix	32
BACG	
Kernel-width, ρ_n	1
GA	
GA type	Non-overlapping
Population size	30
Numbers of generation	100
Mutation type	Flip mutator
Probability of mutation	0.01
Crossover type	One-point crossover
Probability of crossover	0.6
Scaling	Sigma truncation
Genome type	Binary string
Initialisation	Uniform
Comparison	Bit comparator
Encoding/decoding	Binary encoding and decoding
Selection	Roulette wheel
Elitism	On
p-convergence	0.99
n-convergence	50
Others	
MBER	Exact MBER
Channel	3-path SWATM frame-invariant

Table 4.3: Default parameters for the GABA MBER MUD simulations.

constitutes a plausible choice. We will now continue our discussions by characterising the achievable performance of the proposed GABA MBER MUD.

4.4.2 Simulation results

Let us now present our simulation results for the proposed GABA MBER MUD of Section 4.4.1. We have used the parameters summarised in Table 4.3. Our investigations will commence by studying the effects of varying the kernel-width, ρ_n in Section 4.4.2.1, followed by the effects of varying the training block size, N_t in Section 4.4.2.2.

4.4.2.1 The effects of varying the kernel-width

Figure 4.9 shows our simulation results for different values of the kernel width, ρ_n. In particular, Figure 4.9(a) depicts the effects of the different ρ_n values for the GA-aided adaptive MBER MUD for the $P = 2$, $L = 2$ scenario, while Figure 4.9(c) represents the corresponding results for the $P = 4$, $L = 4$ case. We have also included the results of Figures 4.4(b) and 4.4(d) of the BACG algorithm from Section 4.2.1.2 for the sake of comparison. The two figures are now presented as Figures 4.9(b) and 4.9(d) for the case of $P = 2$, $L = 2$ and $P = 4$, $L = 4$, respectively.

From Figure 4.9 we can see that the effects of the different values of ρ_n on the GA-aided block adaptive algorithm are similar to those of the BACG algorithm, although at extreme ρ_n values, namely at $\rho_n = 100$ and $\rho_n = 0.01$, the GA-aided system performs better than the BACG algorithm. This is because in the BACG algorithm we used a fix value of the step-size μ, which also affects the performance of the BACG system. By contrast, the GA-aided system does not depend on the μ value and is capable of circumventing this problem. Morever, for the more complex scenario of $P = 4$, $L = 4$ we can see in Figures 4.9(c) and 4.9(d) that the GA-aided system is less affected by the choice of the ρ_n value.

In the next section, we will study the effects of employing different number of training OFDM symbols in the GA-aided block adaptive MBER MUD.

4.4.2.2 The effects of varying the training block size

Let us now continue our discourse with the investigation of varying the block size of the GA-aided adaptive system. Our simulation results are depicted in Figure 4.10. More specifically, Figure 4.10(a) portrays the effects of different training block sizes for the case of $P = 2$, $L = 2$ while Figure 4.10(c) characterises the GA-aided system associated with $P = 4$, $L = 4$. Similar to Section 4.4.2.1, the results recorded for the different training block sizes for the BACG algorithm of Section 4.2.1.3 are also presented for comparison as Figures 4.10(b) and 4.10(d) for the $P = 2$, $L = 2$ and $P = 4$, $L = 4$ scenarios, respectively.

We can observe in Figure 4.10 that for the $P = 2$, $L = 2$ case, the achievable BER of the $P = 2$, $L = 2$ scenario plotted for the different training sequence lengths is the same for both the GA-aided block adaptive system and for the one employing the BACG MBER

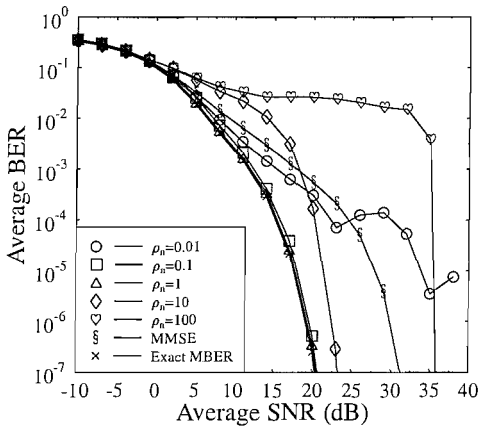

(a) GA-aided block adaptive for P=2, L=2

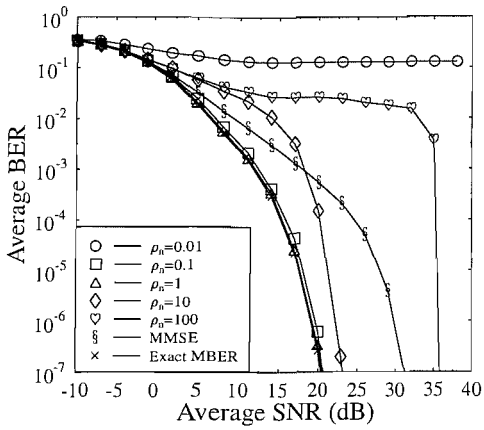

(b) BACG MBER MUD for P=2, L=2

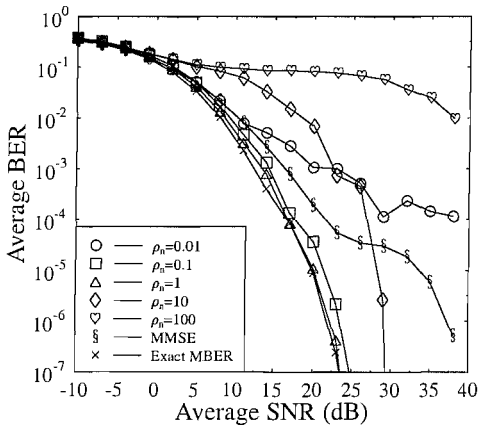

(c) GA-aided block adaptive for P=4, L=4

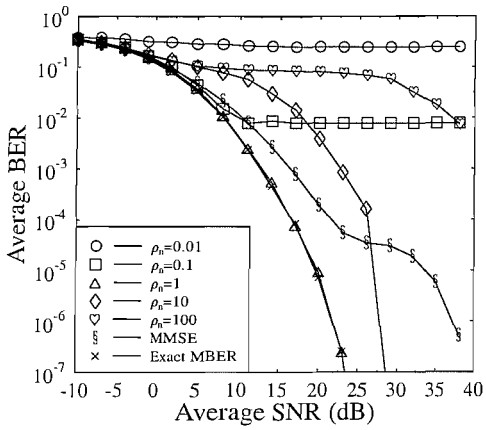

(d) BACG MBER MUD for P=4, L=4

Figure 4.9: Average BER results of all subcarriers for User 1, characterising the effects of the different values of the kernel-width, ρ_n for the MBER MUD for the case of a) $P = 2$, $L = 2$ employing the GA-aided block adaptive MBER, b) $P = 2$, $L = 2$ employing the BACG MBER MUD, c) $P = 4$, $L = 4$ employing GA-aided block adaptive MBER, and d) $P = 4$, $L = 4$ employing BACG MBER MUD. All other simulation parameters are summarised in Table 4.3.

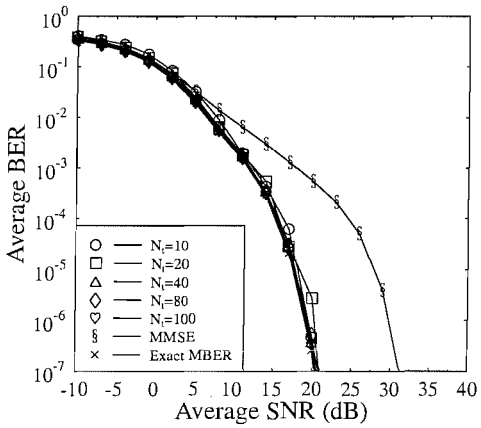

(a) GA-aided block adaptive for P=2, L=2

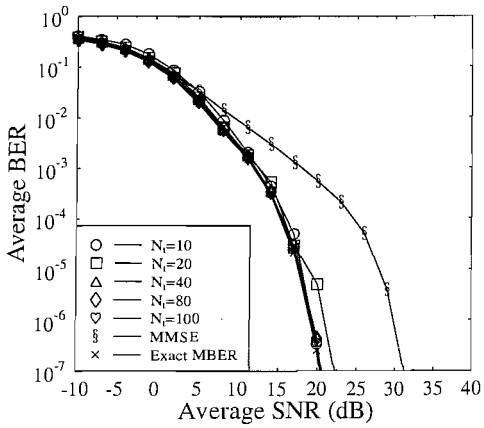

(b) BACG MBER MUD for P=2, L=2

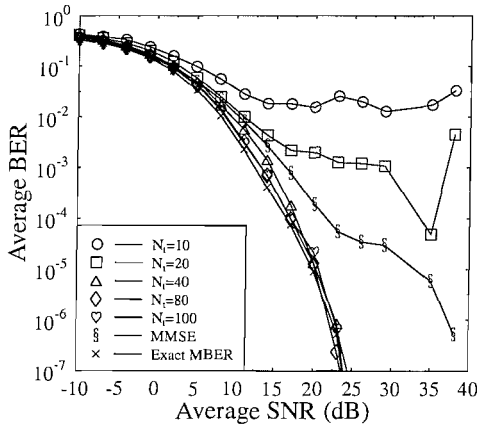

(c) GA-aided block adaptive for P=4, L=4

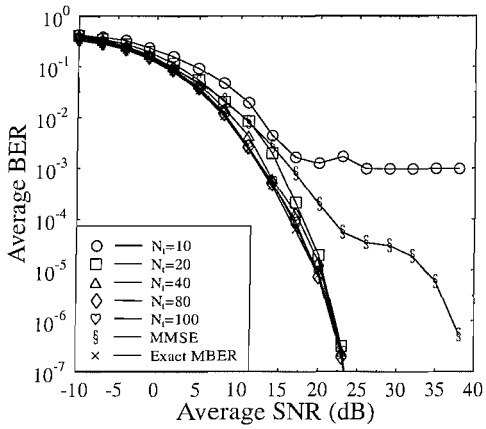

(d) BACG MBER MUD for P=4, L=4

Figure 4.10: Average BER results of all subcarriers for User 1, characterising the effects of the different number of training samples, N_t for the MBER MUD for the case of a) $P = 2$, $L = 2$ employing the GA-aided block adaptive MBER, b) $P = 2$, $L = 2$ employing the BACG MBER MUD, c) $P = 4$, $L = 4$ employing the GA-aided block adaptive MBER, and d) $P = 4$, $L = 4$ employing the BACG MBER MUD. All other simulation parameters are summarised in Table 4.3.

MUD. However, the GA-aided system is incapable of outperforming the BACG algorithm in the more complex scenario of $P = 4$, $L = 4$ for a shorter training sequence length, namely for $N_t = 10$ and $N_t = 20$. This observation suggests that the GA-aided system is more sensitive to the length of the training sequence compared to the BACG system.

4.5 Chapter conclusion

In Chapter 4, we have explored the design trade-offs of the adaptive MBER MUD. Using this method, a set of training samples is invoked for determining the weights of the MUD based on the MBER criterion in an unknown channel. The chapter commenced with an introduction to the adaptive MBER MUD in Section 4.1. More specifically, the calculation of the estimated BER for a BPSK modulated OFDM SDMA system was shown in Section 4.1.1.

There are numerous types of adaptive MBER algorithms in the literature [261], but only two of them were discussed in this chapter. The first one is the block adaptive MBER algorithm of Section 4.2. We have provided simulation results for characterising the effects of the various parameters of the BACG algorithm, namely the effects of varying the fixed step-size μ in Section 4.2.1.1, the effects of varying the kernel-width ρ_n in Section 4.2.1.2 and the impact of varying the training block size N_t in Section 4.2.1.3.

The second type of adaptive MBER MUD that we have studied was the stochastic adaptive MBER MUD of Section 4.3. In Section 4.3.1, more specifically the LBER algorithm. Similary to the BACG algorithm, we have also investigated the effects of varying the fixed step-size μ and the kernel-width ρ_n for the LBER algorithm in Sections 4.3.1.1 and 4.3.1.2, respectively.

Based on our experience in Chapter 3, in Section 4.4.1, we have incorporated the GA-aided method in the block adaptive algorithm for the sake of searching for the weight values of the MBER MUD. Our related simulation results were displayed in Section 4.4.2. More specifically, we have shown the effects of varying the kernel-width of the GA-aided block adaptive MBER MUD in Section 4.4.2.1, and the effects of varying the training block size in Section 4.4.2.2. While it was shown that the GA-aided block adaptive system is less susceptible to the suboptimum values of ρ_n, it has the disadvantage of requiring a longer

training sequence compared to the BACG algorithm.

In summary, the adaptive MBER MUD is providing an attractive design alternative for the MBER MUD in an environment, where the channel transfer function is unknown in the first place. Moreover, instead of using the classic conjugate-gradient based search method, the GA-aided system can be employed to assist in searching for the MBER MUD weights as well. However, as we have seen from the simulation results of Sections 4.2.1, 4.3.1 and 4.4.2, the BACG, LBER and GABA techniques require a substantial number of OFDM symbols for training purposes. This may be considered as ineffective owing to the associated effective throughput reduction. A more effective training technique may be the employment of multiuser channel estimation methods using pilots, or the employment of blind detection as well as decision-directed algorithms, which have been extensively studied for example in [5, 262].

Chapter 5

Conclusions and Future Research

In this thesis, we have investigated the application of MBER multiuser detection in an uplink OFDM SDMA environment. The proposed MBER MUD is not only capable of outperforming the classical MMSE MUD in terms of the achievable BER, but also capable of supporting more users than the number of receiver antennas at the base-station. In Section 5.1, we will summarise our findings. This will be followed by some suggestions for future research that can be explored for the sake of further enhancing the achievable performance of the MBER MUD detector in Section 5.2.

5.1 Summary and conclusion

In recent years, OFDM has played a major role in numerous applications in the field of wireless communications. Its achievable effective throughput and/or integrity may be further improved with the aid of multiple antennas and this report considered the benefits of employing the MBER MUD in an uplink OFDM SDMA system.

In **Chapter 1**, we have provided a brief overview of OFDM systems. We began the chapter with a brief historical background of OFDM systems in Section 1.1. This was followed by a discussion on the basic OFDM system components in Section 1.2. The basic OFDM concepts were presented in Section 1.2.1, followed by the performance characterisation of OFDM transmissions over Gaussian channels in Section 1.2.2. From the simulation results in Figure 1.5, it can be seen that these results closely match the theoretical BER performance

of classic serial systems. We introduced the wideband channels that were used throughout the report in Section 1.2.3. Specifically, the two wideband channels that were used are the two-path Rayleigh fading channel and the wireless asynchronous transfer mode (WATM) channel, which were highlighted in Section 1.2.3.1 and Section 1.2.3.2. In Section 1.2.4, a number of channel transfer function estimation techniques were presented, namely the perfect channel estimation scenario of Section 1.2.4.1, pilot symbol assisted channel estimation in Section 1.2.4.2, decision-directed channel estimation in Section 1.2.4.3 and blind channel estimation in Section 1.2.4.4. Another issue discussed was that of the OFDM signal amplitude PDFs in Section 1.2.5. We have briefly characterised the performance of the clipping amplifier in Section 1.2.5.1, focusing on its BER performance in Section 1.2.5.2.

We then continued with a discussion on some advanced OFDM systems that have been studied by other researchers in Section 1.3. The first advanced system of interest was the adaptive single-user OFDM scheme of Section 1.3.1. This adaptive algorithm can be implemented by using either the fixed threshold adaptation algorithm, the subband-BER estimator based algorithm or the constant-throughput adaptive algorithm of Section 1.3.1.1, Section 1.3.1.2 and Section 1.3.1.3, respectively. Another scheme capable of enhancing an OFDM system was channel coding. In Section 1.3.2, two of the most powerful FECs were highlighted, namely the turbo convolutional codes of Section 1.3.2.1 and the low-density parity-check codes of Section 1.3.2.2. The final advanced system that was discussed was based on exploiting both space and time diversity in Section 1.3.3. After introducing the STBC OFDM system in Section 1.3.3.1, we continued our discourse with the characterisation of an LDPC-based STBC OFDM system in Section 1.3.3.2. In particular, we investigated the effects of various coding rates, the impact of the code length and the influence of the number of iterations in Section 1.3.3.2.1, Section 1.3.3.2.2 and Section 1.3.3.2.3, respectively. We also estimated the decoding complexity of an LDPC-based STBC OFDM system and compared it to the TC-based STBC OFDM system in Section 1.3.3.3. It was shown that the LDPC assisted system is capable of performing as well as the TC-based system in terms of the achievable BER and FER, at a potentially lower implementational complexity.

We continued our discourse in **Chapter 2**, where we have investigated the advantages of using multiple antennas for multiuser detection in an OFDM system. The so-called SDMA system exploits the unique user-specific channel impulse responses for distinguishing the

different users, not unlike the spreading codes of a CDMA system differentiate the users.

The chapter commenced with a brief introduction to the various applications of smart antennas in Section 2.1. One of the smart antenna aided systems, namely the SDMA system was further investigated in this chapter. The SDMA system model was presented in Section 2.2.1, followed by a comparison of the SDMA model to the well-known CDMA system model in Section 2.2.2. In Section 2.3, linear multiuser detection techniques designed for the SDMA systems were introduced. We have specifically discussed one of the most famous classic linear detection techniques, namely MMSE MUD in further detailed in Section 2.3.1. We have also described the soft-output calculations procedure designed for the SDMA system to be used in conjunction with forward error correction coding in Section 2.3.2.

Our discussions then continued in Section 2.4 with the proposal of a novel MBER multiuser detector contrived for SDMA systems. We first interpreted the corresponding error probability expressions in the context of BPSK system in Section 2.4.1, followed by the derivation of the exact MBER MUD in Section 2.4.2. We later presented our simulation results in Section 2.4.3. The simulations were conducted in the context of two, four and eight receiver antennas and the corresponding results were discussed in Sections 2.4.3.1, 2.4.3.2 and 2.4.3.3, respectively. Moreover, we showed in Section 2.4.3.2 that unlike the MMSE MUD, the MBER MUD is capable of supporting more users than the number of receiver antennas at the base station. We also presented our results characterising the effects of different number of receiver antennas, while fixing the number of users to two in Section 2.4.3.4.

These discussions were then followed by studying the effects of varying the different parameters of the CG algorithm in Section 2.4.4. In particular, we have characterised the impact of varying the step-size μ in Section 2.4.4.1, the effects of varying the maximum number of iterations in Section 2.4.4.2 and the ramifications of varying the termination scalar β in Section 2.4.4.3. In Section 2.4.5, LDPC channel coding was employed by the OFDM SDMA system, in order to investigate the performance of the MBER MUD with the assistance of the LDPC code.

In summary, from **Chapter 2** we can say that the MBER MUD performs better in terms of the attainable BER compared to the classic MMSE MUD in all investigated cases. This

is because the MBER MUD directly minimises the BER, while the MMSE MUD attempts to minimise the MSE. Moreover, it was shown that the MMSE MUD is only capable of supporting the same number of users as the number of receiver antennas, whereas the MBER MUD is capable of supporting more users than the number of receiver antennas. However, the advantage of the MBER MUD over the MMSE MUD varies across the different users due to the fact that different users experience different combinations of the CIRs at the receiver antennas, hence resulting in a different system matrix **H**.

In **Chapter 3**, we have explored the novel idea of using GAs for finding the optimised MBER MUD weight value, namely those that are capable of satisfying the minimum BER criterion in the context of the OFDM SDMA based system. Unlike the conjugate gradient search method used in Chapter 2, the GA method does not require an accurate initial value of the weights, yet it is more likely to reach the globally optimum solution.

We commenced the chapter with a brief overview of GAs in Section 3.1. In particular, we have introduced the family of GAs in Section 3.1.1 as a type of search algorithm that mimics the rule of evolution and survival in nature. We have also briefly characterised the processes that are involved in GAs in Section 3.1.2. In Section 3.1.3 we discussed how the family of GAs is related to traditional search methods, namely to *calculus-based*, *enumerative* and *random* search algorithms.

The proposed GA-aided MBER MUD employed in an SDMA OFDM system was introduced in Section 3.2, while in Section 3.3 the achievable performance of the proposed system was characterised. Firstly, the BER performance of the different users in a four-user four-receiver antenna system was portrayed in Section 3.3.1. Our simulation results showed that by using the default parameter values outlined in Table 3.3, the achievable BER performance of the GA-aided system is as good as that of the CG-base MBER MUD of Chapter 2.

We continued our performance related discussions to quantify the effects of varying the different parameters of the GA-aided search method in Section 3.3.2. The first algorithm feature investigated in Section 3.3.2.1 was the termination criterion. By using different types of termination criteria, different average BERs may be achieved at the cost of a different implementational complexity. The GA search method may be terminated by either fixing

the number of generations, or when the best individual in the population achieved a sufficiently accurate convergence, as explained in Sections 3.3.2.1.1 and 3.3.2.1.2, respectively. Alternatively, the iterations may be halted when the average fitness of all the individuals in a generation is within an acceptable range, as explained in Section 3.3.2.1.3. By using the termination based on a fixed number of generations, the associated implementational complexity may be calculated and fixed beforehand, but with the disadvantage that the achievable BER might not be sufficiently close to the optimum MBER solution. By contrast, the convergence based termination criterion will allow the GA search method to continue, until the best solution is found, although this is achieved at the cost of having an unpredictable implementational complexity. Therefore, for a very complex system, the convergence-based termination might require an excessive number of generations.

In Section 3.3.2.2, we portrayed a number of different types of GA individual representations, namely that of binary encoding in Section 3.3.2.2.1 and Gray encoding in Section 3.3.2.2.2. These discussions were followed in Section 3.3.2.3 by quantifying the effects of varying the population size of the GA. It was shown that as expected, the achievable average BER improves, as the population size increases.

Another algorithmic feature investigated was the GA's crossover which was the topic of Section 3.3.2.4. We explored three different types of crossovers, namely the single-point crossover, the two-point crossover and the uniform crossover in Sections 3.3.2.4.1, 3.3.2.4.2 and 3.3.2.4.3, respectively. This discourse was followed by characterising another important element of the GA, namely that of the mutation probability, which was optimised in Section 3.3.2.5.

Having characterised the achievable system performance, the chapter continued with a complexity comparison of the GA-aided search to the conjugate gradient method in Chapter 2. It was shown in Section 3.4, that the GA was capable of approaching the optimum weight values of the MBER MUD in the context of the OFDM SDMA system at a lower complexity in comparison to the CG method. Finally, in Section 3.5 we studied the scenario, where the number of users was higher than the number of receiver antennas. Our simulation results recorded for the four-antenna scenario shows that just like for the CG MBER-MUD, the GA-based MBER MUD is also capable of supporting more users than the number of receiver antennas compared to the MMSE-MUD. However, as the number of

users increases, the complexity of the GA-aided search algorithm required for approaching convergence also had to be increased.

From **Chapter 3**, we can conclude that the proposed GA-based MBER MUD is capable of achieving a similar performance to that of the CG-based MBER MUD at a lower complexity. Moreover, the GA-based MUD is capable of circumventing most of the MBER MUD parameter-optimisation problems, regardless of the choice of initial conditions and the step-size, rendering it more flexible than the CG based method.

Our discussions then continued in **Chapter 4**, where we have investigated two different adaptive MBER MUDs. Using this method, a set of training samples was used to determine the weights of the MUD based on the MBER criterion in an unknown channel. The chapter commenced with an introduction of the adaptive MBER MUD in Section 4.1. More specifically, the calculation of the estimated BER of a BPSK modulated OFDM SDMA system was outlined in Section 4.1.1.

There are many types of adaptive methods that may be found in the literature, but only two of them are discussed in this chapter. The first one is the block adaptive MBER algorithm. This method was discussed in further detail in Section 4.2. In particular, we have chosen to elaborate on the block adaptive conjugate gradient (BACG) MBER algorithm in Section 4.2.1. We have characterised the effects of varying the various parameters of the BACG algorithm, namely the effects of varying the fixed step-size μ in Section 4.2.1.1, the effects of varying the kernel-width ρ_n in Section 4.2.1.2 and the effects of varying the training block size N_t in Section 4.2.1.3.

The second type of adaptive MBER MUD that we have studied is the stochastic adaptive MBER MUD of Section 4.3. In Section 4.3.1, we have opted for exploring the LBER algorithm. Just as we did for the BACG algorithm, we have also investigated the effects of varying the fixed step-size μ and the kernel-width ρ_n of the LBER algorithm in Sections 4.3.1.1 and 4.3.1.2, respectively.

Based on our experience in Chapter 3, in Section 4.4.1, we have incorporated the GA-aided technique in the block adaptive algorithm for the sake of finding the weight values of the MBER MUD. Our simulation results were displayed in Section 4.4.2. More specifically, we have shown the effects of varying the kernel-width in the GA-aided block adaptive MBER

MUD in Section 4.4.2.1, and the effects of varying the training block size in Section 4.4.2.2. While it was shown that the GA-aided block adaptive system is less susceptible to the variation of ρ_n, it has a disadvantage of requiring more training samples compared to the BACG algorithm.

In **Chapter 4**, we concluded that the adaptive MBER MUDs are capable of finding the weights of the MBER MUD in an environment, where the channel's transfer function is unknown. Moreover, instead of using the classic conjugate-gradient search method, the GA-aided system may be employed for searching for the MBER MUD solution as well. However, as we have seen from the simulation results, the adaptive methods in general require a substantial number of OFDM symbols for training purposes. This may be considered as ineffective. A more effective channel solving technique is constituted by employing multiuser channel estimation methods using pilots, blind detection or decision-directed algorithms, which have been extensively studied for example in [5, 262].

5.2 Suggestions for future research

The following subsections will briefly outline a few ideas that will be explored for the sake of improving the performance of various OFDM systems in multiuser scenarios. We will begin with a discussion on some of the further research that will be carried out in the context of the MBER MUD in Section 5.2.1. This will be followed by Section 5.2.2, where we will highlight other promising multiple antenna systems that can be used for enhancing the achievable system performance.

5.2.1 Advanced research on MBER MUD

The MBER MUD had achieved promising results, as we have seen in Section 2.4.3, demonstrating that MBER MUDs have the potential of outperforming the family of MMSE MUDs. This is because the MBER detector directly minimises the BER rather than the MSE. Minimising the MSE does not necessarily guarantee that the BER of the system is also minimised. Therefore, further research may be conducted to further improve the MBER MUD to be more implementable in real world applications. In Section 5.2.1.1, we will convey our suggestion on joint channel estimation and multiuser detection employing the MBER

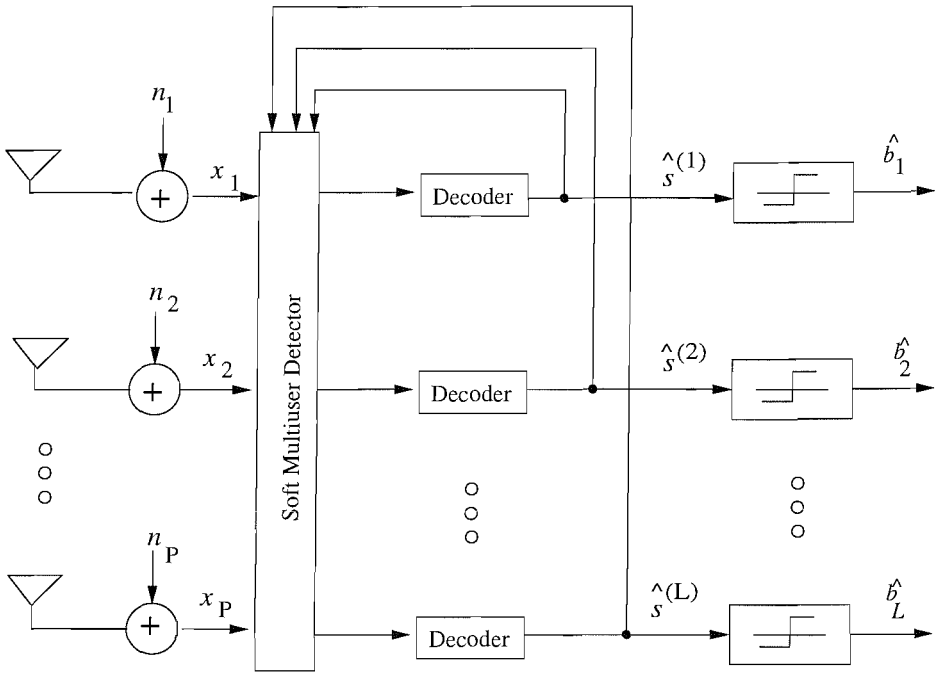

Figure 5.1: Iterative receiver structure for a multiuser SDMA OFDM system.

criterion, while in Section 5.2.1.2 we will highlight the principle of an iterative LDPC-coded MBER MUD.

5.2.1.1 Joint channel estimation and multiuser detection employing the MBER criterion

In most of the investigated scenarios, we have assumed that the channel is known. We have also used the two different adaptive MBER methods, but their effective throughput was reduced due to the substantial number of training samples required. One of the promising research approach is to estimate the channel as well as detecting the received symbol in the multiuser scenario based on the MBER criterion within the same process. It has been shown, for example in [238], that the two methods can be jointly optimised in the context of a synchronous CDMA system, which is likely to be applicable also to the MBER method.

5.2.1.2 Iterative LDPC-coded MBER MUD

In recent years iterative receivers have attracted considerable attention owing to their successful applications in various areas of coding and signal processing [67]. The basic idea behind iterative processing is that of iteratively exchanging the so-called extrinsic information among all the receiver modules in order to achieve an improved performance. In [40], Lu *et. al* have proposed iterative receiver structures for joint detection and decoding in multiuser STC systems. More recently, Lu *et al.* have also proposed a turbo receiver based on the maximum *a posteriori expectation maximisation* (EM) algorithm for STBC-OFDM systems employing an outer channel coding scheme in [41]. During the iterations, extrinsic information is computed and exchanged between a soft-MUD and a bank of channel decoders for the sake of generating successively refined estimates of the users' signals. It was shown that the proposed iterative receivers are capable of significantly outperforming the conventional non-iterative multiuser receivers. Other related work on the iterative multiuser receivers can also be found in [263].

The same iterative processing principles can also be applied to the SDMA MUDs presented in Chapter 2. The iterative MUD structure to be used is shown in Figure 5.1. It consists of a soft-MUD followed by L parallel channel decoders. The soft-MUD takes as its input the received signals from the P receiver antennas plus the *a priori* value provided by the channel decoder. It will then compute and output the *a posteriori* value for the channel decoder to process. This process is then repeated until the affordable number of iterations is exhausted. Most of the previous proposals employ MMSE type filtering at the soft-MUD. Since we have shown in Section 2.4.3 that the MBER MUD can outperform the MMSE MUD, the MBER MUD will replace the MMSE MUD at the soft-MUD. Another way of carrying out iterative-MUD is to employ LDPC channel coding, since it has been shown that LDPC coding is capable of approaching the Shannonian performance limits at a low computational complexity [264]. Besides the LDPC coded, other channel code can be implemented for example the Trellis Coded Modulation (TCM) or Turbo Trellis Coded Modulation (TTCM) [240].

5.2.2 Other MIMO-OFDM systems

Besides the space-time coding schemes of Section 1.3.3 and the SDMA multiuser system of Section 2.2, there are also other systems employing multiple antennas as highlighted in the following sections. In particular we will see the various types of layered space-time OFDM system in Section 5.2.2.1. We will also see another type of multiple antenna employment called beamforming in Section 5.2.2.2. If time permits, these systems will be implemented in the multiuser OFDM environment with the aid of the MBER MUD.

5.2.2.1 Layered space-time OFDM

In Section 1.3.3, STBC has been used for the multiple antenna at the transmitter system. Another type of space-time architecture that has been proposed by Foschini [200] is the so-called layered space-time (LST) that can attain a tight lower bound on the MIMO channel capacity. The distinguishing feature of this architecture is that it allows processing of multidimensional signals in the space domain by one-dimensional processing steps. The method relies on powerful signal processing techniques at the receiver and conventional one-dimensional channel codes.

There is a number of LST architectures, depending on whether error control coding is used or not and on the way the modulated symbols are assigned to transmit antennas [94]. An uncoded LST structure, known as *vertical layered space-time* (VLST) [265] or *vertical Bell Laboratories layered space-time* (VBLAST) scheme [265] is illustrated in Figure 5.2(a). Vertical structuring refers to transmitting a sequence of matrix columns in the space-time domain. This simple transmission process can be combined with conventional block or convolutional one-dimensional codes to improve the performance of the system.

In the *horizontal layered space-time* (HLST) architecture [200], shown in Figure 5.2(b), the information sequence is first encoded by a channel code and subsequently demultiplexed into n_T streams, where n_T is the number of antennas at the transmitter. Each sub-stream is modulated, interleaved and assigned to a transmit antenna. An HLST architecture can also be implemented by splitting the information sequence into n_T sub-streams, as shown in Figure 5.2(c). Each sub-stream is encoded independently by a channel encoder, interleaved, modulated and then transmitted by a particular transmit antenna. It is assumed that

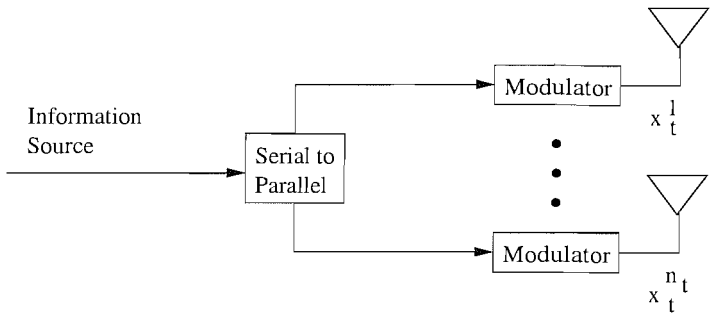

(a) A VLST architecture

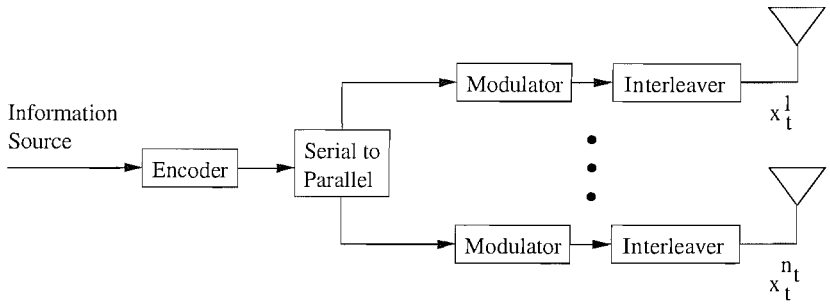

(b) HLST architecture with a single code

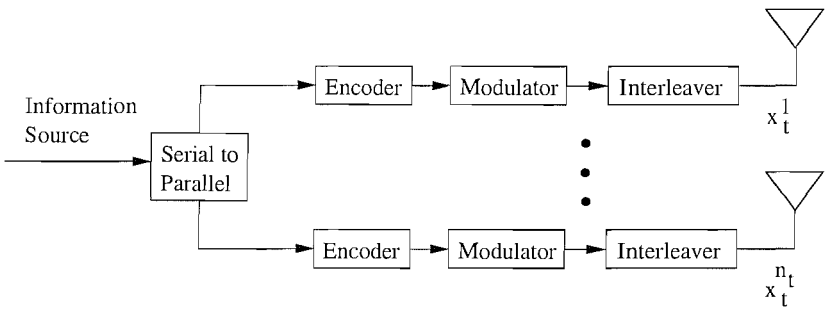

(c) HLST architecture with separate codes in each layer

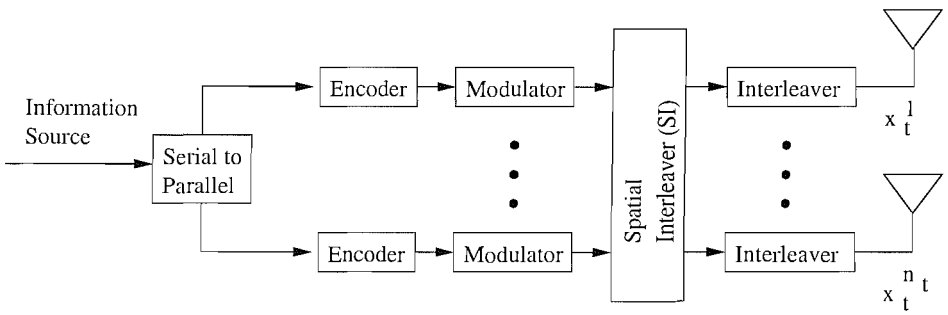

(d) DLST and TLST architectures

Figure 5.2: LST transmitter architectures for (a) VLST, (b) HLST with a single code, (c) HLST with separate codes in each layer, and (d) DLST and TLST.

channel encoder for various layers are identical. However, different coding in each sub-stream can be used.

A better performance is achieved by a *diagonal layered space-time* (DLST) [200] architecture, in which a modulated codeword of each encoder is distributed among the n_T antennas along the diagonal of the transmission array. The diagonal layering introduces space diversity and thus achieves a better performance than the horizontal one. It is important to note, however, that there is a spectral efficiency loss in DLST, since a portion of its transmission matrix is padded with zeros.

A *threaded layered space-time* (TLST) [200] structure is obtained form the HLST by introducing a spatial interleaver, SI, prior to the time interleavers, as shown in Figure 5.2(d). The spatial interleaver of the TLST can be represented by a cyclic-shift interleaver.

LSTs using OFDM have been studied for example in [34, 266–270]. However, in all the previous studies, the methods used to decouple and detect the LST signals at the receiver are mainly based on Zero Forcing (ZF), MMSE or iterative cancellation techniques. Since we have seen in Section 2.4.3 that a promising method of achieving a better BER performance is by using the MBER algorithm, there is a potential of applying the same scheme for the LST receivers. Moreover, LDPC codes or coded modulation [67] can be studied for employment in the HLST architectures.

5.2.2.2 Adaptive beamforming OFDM

As seen in Chapter 2, multiple antennas at the receiver can be used to distinguish the different users. This is done by assuming that the separation of the antennas is far enough that they do not interfere with each other's signals and there is a unique channel impulse response at each receiver antennas for each user. This particular system is also sometime known as the 'dumb antenna' because the antenna arrays are basically fix at one position only.

Another method to differentiate different users is by exploiting the fact that users are physically separated by providing the receiver with an antenna whose radiation pattern is not omni-directional. Likewise, directive antennas can concentrate transmitted power in the direction of the intended receiver [199]. This system is known commonly as beamforming or

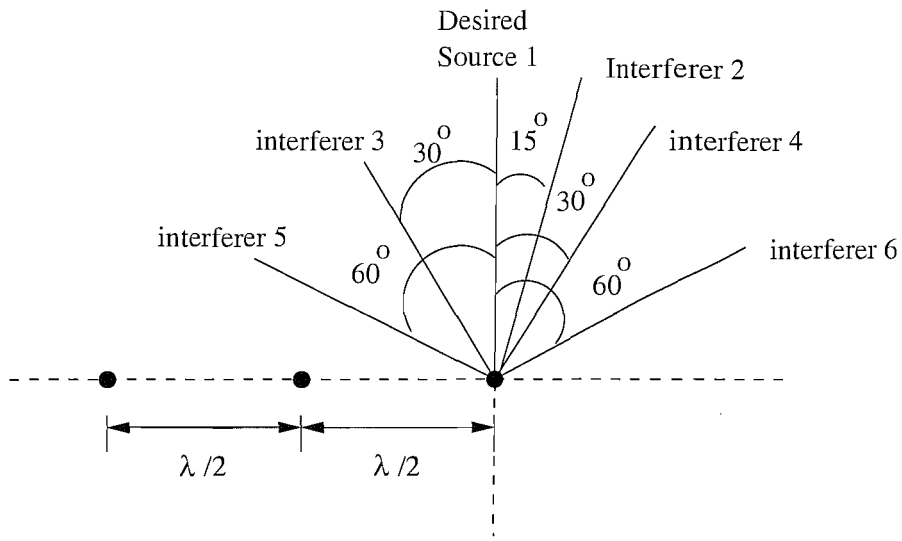

Figure 5.3: Example of a beamforming antenna array where the locations of the desired source and the interfering sources with respect to the three-element linear array with $\lambda/2$ element spacing with λ being the wavelength.

sometimes even called 'smart antennas'. At a given location in space, the received signals depend not only on time but also on the angle of arrival.

The simplest single-element antenna has an omni-directional radiation pattern. Linear arrays of equispread omnidirectional antennas are the most common approach to beamforming. The number of antennas in the array determines the achievable angle discrimination, in much the same way that the spreading codes length to a CDMA system. Once the number of elements in the array and their distances are fixed, the resulting antenna pattern depends on how the output of the elements are combined.

By combining beamforming and OFDM, a further enhancement can be achieved especially in the multipath fading environment. Beamforming OFDM has been investigated for example in [271–273]. Furthermore, the beamforming processing, which combines the signals received by the different elements of an antenna array to form a single output is classically done by minimising the mean square error between the desired and actual array outputs. However, in [211] that by using MBER algorithm, the BER can be minimised further. Therefore, a further research using the MBER in beamforming OFDM might result in a great enhancement as well.

List of Symbols

General notation

- Capital letters in boldface represent matrices, for instance $\mathbf{X}$.
- Column vectors are presented in lowercase letters, for instance $\mathbf{x}$.
- The superscript $(*)$ is used to indicate complex conjugation. Therefore, a^* represents the complex conjugate of the variable a.
- The subscript R and I indicate the real component and the imaginary component of a complex-valued variable, vector or matrix, respectively. For instance, $\mathbf{x}_R$ represents the vector of the real components of the complex-valued vector $\mathbf{x}$.
- The subscript l of a variable, vector or matrix implies that the variable, vector or matrix belongs to the l-th user.
- The superscript (T) of a matrix or a vector implies the transpose of the matrix or the vector. Therefore, $\mathbf{X}^T$ represents the transpose of the matrix $\mathbf{X}$, while $\mathbf{x}^T$ denotes the transpose of the vector $\mathbf{x}$.
- The notation $\mathbf{X}^H$ is used to represent the complex conjugate and transposed matrix of $\mathbf{X}$, i.e. $\mathbf{X}^H = \mathbf{X}^{*T}$, which is also referred to as the Hermitian matrix of $\mathbf{X}$. Likewise, the notation $\mathbf{x}^H$ denotes the complex conjugate and transposed vector of $\mathbf{x}$.
- The notation $\mathbf{X}^{-1}$ corresponds to the inverse of the matrix $\mathbf{X}$.
- The notation diag($\mathbf{X}$) is used for representing a diagonal matrix, where only the diagonal elements of the matrix $\mathbf{X}$ contain non-zero values.

- The notation $\overline{\mathbf{X}}$ denotes a matrix that is constituted by a set of column vectors $\overline{\mathbf{x}}$ of unity magnitude, hence the sum of the squared values of the elements in the column vectors $\overline{\mathbf{x}}$ is equal to unity.
- The matrix $\mathbf{I}$ and $\mathbf{0}$ represent the identity matrix and the null matrix, respectively.
- The notation $\hat{x}$ represents the estimate of the quantity x. This is also applied in the context of matrices and vectors.
- By default, the letters l and p are used for indexing the users and the receiver antennas at the base-station, respectively, unless stated otherwise.

Special symbols

A_l: The amplitude of the transmitted signal of user l.

A_l^2: The transmit power of the signal of user l.

$\mathbf{A}$: The $(L \times L)$-dimensional diagonal matrix of the users' transmit signal amplitude, where L is the number of simultaneous users.

B_D: Doppler spread of the channel: $B_D = 2f_D$.

c: Speed of light.

$compl\{\cdot\}$: The complexity calculation of a function.

$\mathbf{C}$: LDPC parity-check matrix.

$\mathbf{d}[n]$: The search direction vector associated with the steepest-descent algorithm at the n-th iteration.

f_c: OFDM carrier frequency.

f_d: Any frequency of the Doppler spectrum.

f_D: Maximum Doppler frequency.

f_i: The fitness of an individual in the GA search algorithm.

f_s: OFDM sampling frequency: $f_s = 1/T_s$.

F_D: OFDM symbol duration normalised Doppler frequency: $F_D = f_D T_f$.

$g_n(t)$: The complex-valued Rayleigh fading process for propagation path n.

G: The number of generations in the GA search algorithm.

$\mathbf{G_2}$: Alamouti's twin-transmitter based space-time block code as depicted by Figure 1.26 on page 38.

$h(t, \tau)$: Time-variant channel impulse response (CIR) at time instant t and multipath delay τ, as given by Equation 1.8.

$H(t, f)$: Time-variant channel transfer function: $H(t, f) = \underset{\tau \to f}{\mathcal{FT}}\{h(t, \tau)\}$.

$\mathbf{H}$:	The $(P \times L)$-dimensional system matrix of the SDMA system.
k:	OFDM subcarrier index.
K:	Number of OFDM subcarriers.
K_c:	Constraint length of the turbo convolutional channel code.
K_g:	Number of OFDM guard interval samples.
L:	The total number of simultaneous SDMA users that shares the same transmission bandwidth.
$L(b\|\mathbf{y})$:	The Log-Likelihood Ratio (LLR) of the users' transmitted bit b, given the noisy received signal $\mathbf{y}$ at the receiver.
M_m:	The modulation mode employed in the adaptive modulation, where m is the number of data bits associated with the data symbol of each mode.
MSE(x):	The Mean-Square Error (MSE) function of the symbol x, as used for example in Equation 2.17 on page 64.
n:	OFDM symbol index.
$n(t)$:	The continuous-time additive white Gaussian noise.
$\mathbf{n}[n]$:	The vector of noise samples that are corrupting the received signal at the n-th symbol instance.
N_b:	Number of equiprobable combinations of the binary vectors of the L users.
N_t:	The number of training samples used for the adaptive algorithm.
p_m:	Probability of mutation in the GA.
$p_y(y_s;\mathbf{w})$:	The probability density function (PDF) of the signed decison function.
P:	Number of receiver antennas at the base-station of the SDMA system.
$P_E(\mathbf{w})$:	The probability of error as a function of the multiuser detector's weights.
$P_E(n;\mathbf{w})$:	The probability of error as a function of the multiuser detector's weights, evaluated at the n-th iteration.

$P_{E,I}(\mathbf{w})$: The probability of error associated with the imaginary component of the transmitted symbol.

$P_{E,I}(n;\mathbf{w})$: The probability of error associated with the imaginary component of the transmitted symbol, evaluated at the n-th iteration.

$P_{E,R}(\mathbf{w})$: The probability of error associated with the real component of the transmitted symbol.

$P_{E,R}(n;\mathbf{w})$: The probability of error associated with the real component of the transmitted symbol, evaluated at the n-th iteration.

$\mathbf{Pr}\{b|\mathbf{y}\}$: The *a posteriori* probability of a binary information bit b, given the received coded bit sequence of $\mathbf{y}$.

$Q(\cdot)$: The Gaussian Q-function as defined in Equation 1.7 on page 11.

$r(t)$: Noisy time-domain received multiuser signal at the output of the channel.

R: Coding rate of the channel encoder.

$\mathbf{R}$: Auto-correlation matrix.

$\Re$: The notation used for representing the real part of a variable, vector or matrix.

$s_k[i]$: The i-th transmitted symbol of user k.

$\mathbf{s}[n]$: The vector of the users' symbols, transmitted during the n-th symbol instance.

$\text{sgn}(x)$: The sign or the signum function denotes the sign of the independent variable x and is defined as 1 for $x > 0$, -1 for $x < 0$ and 0 if x is 0 [48].

T_s: OFDM sampling period duration: $T_s = 1/f_s$.

T_f: OFDM symbol duration: $T_f = (K + K_g)T_s$.

$u(t)$: Information bit.

v: Vehicular speed.

$\mathbf{W}$:	The complex-valued multiuser detector's weight matrix.
$\mathbf{x}$:	Received signals at the SDMA base-station receiver antennas.
Y:	The number of individuals in a population, also known as the population size, in the GA-aided search method.
z_l:	The signed decision variable, as defined by Equation 2.29.
$\alpha_n(t)$:	Time-variant attenuation factor of the n-th CIR component.
$\alpha_t(s)$:	Forward recursion in TC, as given by Equation 1.15.
β:	The termination scalar in the conjugate-gradient search method.
$\beta_{t-1}(\grave{s})$:	Backward recursion in TC, as given by Equation 1.16.
$\gamma_t(\grave{s}, s)$:	Branch transition metric, as given by Equation 1.17.
$\delta(t)$:	Dirac impulse function.
Δf:	Subcarrier spacing of the OFDM symbol: $\Delta f = \frac{1}{KT_s}$.
$(\Delta f)_c$:	Coherence bandwidth of the channel: $(\Delta f)_c \approx \frac{1}{T_m}$.
Δp:	Spectral distance between consecutive pilot subcarriers.
$(\Delta t)_c$:	Coherence time of the channel: $(\Delta t)_c \approx \frac{1}{B_D}$.
$\nabla P_E(\mathbf{w})$:	The gradient vector of the probability of bit error as a function of the detector's weights.
$\eta_t(\grave{s}, s)$:	The legitimate transmitted coded bits corresponding to the information bit, when a state transition from the previous trellis state $\grave{s}$ to the present state s occurred, as seen in Equation 1.18 on page 49.
λ:	The eigenvalue of the auto-correlation matrix $\mathbf{R}$.
μ:	The step size used in gradient-based adaptive algorithms.
Π_{t,u_t}:	A priori information regarding the information bit u_t.
ρ:	Reciprocal of the signal to noise ratio: $\rho = \sigma_n^2/\sigma_s^2$.

ρ_n: The width of the kernel function employed for the adaptive algorithm.

σ_l^2: The variance of data signal of the l-th user.

σ_n: The standard deviation of the noise samples.

σ_n^2: The variance of the noise samples.

σ_s^2: The variance of the transmitted symbol.

τ: Time delay component.

$\tau_n(t)$: Time-variant delay of the n-th CIR component.

$\phi[n]$: The ratio of the current gradient of the probability of bit error over the previous one, which is used for weighting the previous search direction in the context of the simplified conjugate gradient algorithm.

ω_D: Doppler angular velocity: $\omega_D = 2\pi f_D$.

$\lfloor\rfloor$: Largest integer that is not greater than the argument in brackets.

$\lceil\rceil$: Smallest integer that is not less than the argument in brackets.

$||.||_2^2$: Euclidean norm of a vector.

Glossary

ADSL	Asymmetric Digital Subscriber Line which enables users to transmit both speech and data via the same telephone connection at the same time. ADSL is well suited for Internet access, since the transmission speed from the telephone exchange to the user is significantly higher than from the user to the network
AOFDM	Adaptive Orthogonal Frequency Division Mulplexing constitutes an OFDM scheme employing adaptive modulation in the frequency domain as well as in the time domain, resulting in so-called two-dimensional adaptive modulation or frequency-time processing
AWGN	Additive White Gaussian Noise
BACG	Block Adaptive Conjugate Gradient algorithm used in MBER MUDs
BER	Bit Error Ratio, the ratio of the number of bits received incorrectly to the total number of received bits
BPS	Bits Per Symbol, the number of bits conveyed by a modulated symbol
BPSK	Binary Phase Shift Keying, a PSK modulation type associated with two constellation points that are separated from each other by 180^o, *see also* PSK
BS	A common abbreviation for Base Station
CDF	Cumulative Distribution Function, the integral of the Probability Density Function (PDF), *see also* PDF

CDMA	Code Division Multiple Access, a multiple access technique where each user is provided with an individual user-specific spreading code
CG	The Conjugate Gradient algorithm is the gradient-driven iterative optimisation technique invoked for example for finding the optimum MBER MUD weights
CIR	Channel Impulse Response
DAB	Digital Audio Broadcasting
DFT	Discrete Fourier Transform, a discrete time version of the Fourier transform, which converts a time-domain signal into the corresponding frequency-domain signal
FDCHTF	Frequency Domain Channel Transfer Function
FFT	Fast Fourier Transform, a computationally efficient version of the DFT, *see also* DFT
FIR	Finite Impulse Response
GA	Genetic Algorithm
GABA	GA-aided Block Adaptive algorithm invoked for finding the optimum MBER MUD weights, *see also* GA
HDSL	High-bit-rate Digital Subscriber Line
HDTV	High-definition Digital TV
HIPERLAN	High Performance Local Area Network, a high-speed local area network for data transmission.
HLST	Horizontal Layered Space-Time
IEEE	Institute of Electrical and Electronics Engineers
IFFT	Inverse Fast Fourier Transform, the inverse of the FFT
ISI	Inter Symbol Interference

KDE	Kernel Density Estimation
LBER	Least Bit Error Rate
LDPC	Low Density Parity-Check error correction codes
LST	Layered Space-Time
MBER	Minimum Bit Error Rate
MC-CDMA	A version of Multi-Carrier CDMA, which spreads an information symbol over several subcarriers and uses the OFDM structure to transmit the signal, also known as OFDM-CDMA
MIMO	Multiple Input Multiple Output
ML	Maximum Likelihood
MMAC	Multimedia Mobile Access Communication
MMSE	Minimum Mean Square Error
MSE	Mean Square Error
MUD	Multiuser Detector
OFDM	Orthogonal Frequency Division Multiplex
PDF	Probability Density Function
PSAM	Pilot Symbol Assisted Modulation, a technique where known symbols (pilots) are transmitted regularly and the effect of channel fading on all symbols can then be estimated by interpolating between the pilots
PSK	Phase Shift Keying
QAM	Quadrature Amplitude Modulation
QPSK	Quadrature Phase Shift Keying
RF	Radio Frequency

SDG	Steepest Descent Gradient
SDMA	Space Division Multiple Access
SINR	Signal to Interference plus Noise ratio, same as signal to noise ratio (SNR), when there is no interference
SIR	Signal to Interference Ratio
SNR	Signal to Noise Ratio, the ratio of the signal energy to the noise power
STBC	Space-time Block Code
SWATM	Short Wireless Asynchronous Transfer Mode channel
TC	Turbo Codes
TDD	Time Division Duplex
VBLAST	Vertical Bell Laboratory Layered Space-Time, *see also* VLST
VDSL	Very-high-speed Digital Subscriber Line
VLSI	Very-Large Scale Integration
VLST	Vertical Layered Space-Time, *see also* VBLAST
WATM	Wireless Asynchronous Transfer Mode
WLAN	Wireless Local Area Network

Bibliography

[1] M. Y. Alias, A. K. Samingan, S. Chen, and L. Hanzo, "Minimum Bit Error Rate Multiuser Detection in Multiple Antenna Aided OFDM," in *8th International OFDM-Workshop*, (Hamburg, Germany), pp. 16–20, 24-25 September 2003.

[2] M. Y. Alias, A. K. Samingan, S. Chen, and L. Hanzo, "Multiple Antenna Aided OFDM Employing Minimum Bit Error Rate Multiuser Detection," *IEE Electronics Letters*, vol. 39, no. 24, pp. 1769–1770, 27 November 2003.

[3] M. Y. Alias, S. Chen, and L. Hanzo, "Genetic Algorithm Assisted Minimum Bit Error Rate Multiuser Detection in Multiple Antenna Aided OFDM," in *Proceedings of IEEE Vehicular Technology Conference (VTC-Fall)*, (Los Angeles, California, USA), p. To be published, September 2004.

[4] L. Hanzo, W. Webb, and T. Keller, *Single and Multi-carrier Quadrature Amplitude Modulation.* New York: John Wiley, 2000.

[5] L. Hanzo, M. Münster, B. J. Choi, and T. Keller, *OFDM and MC-CDMA.* West Sussex, England: John Wiley and IEEE Press, 2003.

[6] R. van Nee and R. Prasad, *OFDM for Wireless Multimedia Communications.* Boston, London: Artech House Publishers, 2000.

[7] J. L. Holsinger, "Digital Communications over Fixed Time-continuous Channels with Memory," *Lincoln Laboratory Technical Report*, vol. 366, October 1966.

[8] R. W. Chang, "Synthesis of Band Limited Orthogonal Signals for Multichannel Data Transmission," *Bell System Technical Journal*, vol. 45, no. 11, pp. 1775–1796, December 1966.

[9] B. R. Salzberg, "Performance of an Efficient Parallel Data Transmission System," *IEEE Transactions on Communication Technology*, vol. COM-15, no. 6, pp. 805–813, December 1967.

[10] R. W. Chang, "Orthogonal Frequency Division Multiplexing." US Patent No. 3, 488,4555. filed November 14, 1966, issued January 6, 1970.

[11] S. B. Weinstein and P. M. Ebert, "Data Transmission by Frequency Division Multiplexing Using the Discrete Fourier Transform," *IEEE Transactions on Communication Technology*, vol. COM-19, no. 5, pp. 628–634, October 1971.

[12] W. E. Keasler and D. L. Bitzer, "High-speed Modem Suitable for Operation with a Switched Network." US Patent. 4,206,320, June 1980.

[13] ANSI, "TR-28: A Technical Report on High-bit Rate Digital Subscriber Lines," *Committee T1-Telecommunications*, February 1994.

[14] J. M. Cioffi, "A Multicarrier Primer," *T1E1.4/91-157*, November 1991.

[15] J. M. Cioffi, "VDSL System Requirements," *T1E1.4/98-043R1*, 1998.

[16] ETSI, "Very High Speed Digital Subscriber Line (VDSL); Part 1: Functional Requirements," *TS101 270-1*, November 1998.

[17] ETSI, "Digital Audio Broadcasting to Mobile and Fixed Receivers," *European Telecommunication Standard ETS 300 401*, February 1995.

[18] ETSI, "Digital Video Broadcasting: Framing Structure, Channel Coding, and Modulation for Digital Terestrial Television ," *European Telecommunication Standard ETS 300 744*, March 1997.

[19] "IEEE 802.11, IEEE Standard for Wireless LAN Medium Access Control (MAC) and Physical Layer (PHY) Specifications," November 1997.

[20] ETSI, "Radio Equipment and Systems, HIgh PErformance Radio Local Area Network (HIPERLAN) Type 1," *European Telecommunication Standard, ETS 300-652*, October 1996.

[21] J. A. C. Bingham, "Multicarrier Modulation for Data Transmission: An Idea Whose Time Has Come," *IEEE Communication Magazine*, pp. 5–14, May 1990.

[22] B. Hirosaki, "An Orthogonally Multiplexed QAM System Using the Discrete Fourier Transform," *IEEE Transactions on Communications*, vol. COM-29, no. 7, pp. 982–989, July 1981.

[23] B. Hirosaki, S. Hasegawa, and A. Sabato, "Advanced Group-band Modem Using Orthogonally Multiplexed QAM Technique," *IEEE Transactions on Communications*, vol. COM-34, no. 6, pp. 587–592, June 1986.

[24] R. Steele and L. Hanzo, *Mobile Radio Communications (Second Edition): Second and Third Generation Cellular and WATM Systems.* New York: John Wiley and Sons Ltd., 1999.

[25] T. S. Rappaport, *Wireless Communications: Principles and Practice.* New Jersey: Prentice-Hall, 1996.

[26] Y. Li, L. J. Cimini, and N. R. Sollenberger, "Robust Channel Estimation for OFDM Systems with Rapid Dispersive Fading Channels," *IEEE Transactions on Communications*, vol. 46, no. 7, pp. 902–915, July 1998.

[27] X. Li and L. J. Cimini, "Effects of Clipping and Filtering on the Performance of OFDM," *IEEE Communications Letters*, vol. 2, pp. 131–133, May 1998.

[28] L. Lin, L. J. Cimini, and J. C.-J. Chuang, "Comparison of Convolutional and Turbo Codes for OFDM with Antenna Diversity in High-Bit-Rate Wireless Applications," *IEEE Communication Letter*, vol. 4, no. 9, pp. 277–279, September 2000.

[29] Y. Li and N. R. Sollenberger, "Adaptive Antenna Arrays for OFDM Systems with Cochannel Interference," *IEEE Transactions on Communications*, vol. 47, pp. 217–229, February 1999.

[30] R. S. Blum, Y. G. Li, J. H. Winters, and Q. Yan, "Improved Space-time Coding for MIMO-OFDM Wireless Communications," *IEEE Transactions on Communications*, vol. 49, no. 11, pp. 1873–1878, November 2001.

[31] C. Y. Wong, R. S. Cheng, K. B. Letaief, and R. D. Murch, "Multiuser Subcarrier Allocation for OFDM Transmission Using Adaptive Modulation," in *Proceedings of IEEE Vehicular Technology Conference (VTC-Spring)*, vol. 1, (Houston, Texas, USA), pp. 479–483, 16-20 May 1999.

[32] J. Li, K. B. Letaief, R. S. Cheng, and Z. Cao, "Co-Channel Interference Cancellation for Space-time Coded OFDM Systems," in *Proceedings of International Conference on Communications (ICC)*, vol. 6, (Helsinki, Finland), pp. 1638–1642, 11-14 May 2001.

[33] J. Li, K. B. Letaief, R. S. Cheng, and Z. Cao, "Multi-stage Low Complexity Maximum Likelihood Detection for OFDM/SDMA Wireless LANs," in *Proceedings of International Conference on Communications (ICC)*, vol. 4, (Helsinki, Finland), pp. 1152–1156, May 2001.

[34] N. Boubaker, K. B. Letaief, and R. D. Murch, "A Layered Space-time Coded Wideband OFDM Architecture for Dispersive Wireless Links," in *Proceedings of Sixth IEEE Symposium on Computers and Communications*, (Hammamet), pp. 518–523, 3-5 July 2001.

[35] C. Y. Wong, R. S. Cheng, K. B. Letaief, and R. D. Murch, "Multiuser OFDM with Adaptive Subcarrier, Bit, and Power Allocation," *IEEE Journal on Selected Areas in Communications*, vol. 17, no. 10, pp. 1747–1758, October 1999.

[36] T. May, H. Rohling, and V. Engels, "Performance Analysis of Viterbi Decoding for 64-DAPSK and 64-QAM Modulated Signals," *IEEE Transactions on Communications*, vol. 46, no. 2, pp. 182–190, February 1998.

[37] Z. Jianhua, H. Rohling, and Z. Ping, "Analysis of ICI Cancellation Scheme in OFDM Systems With Phase Noise," *IEEE Transactions on Broadcasting*, vol. 50, no. 2, pp. 97–106, June 2004.

[38] H. Bölcskei, D. Gesbert, and A. J. Paulraj, "On The Capacity of OFDM-Based Spatial Multiplexing Systems," *IEEE Transactions on Communications*, vol. 50, no. 2, pp. 225–234, February 2002.

[39] M. C. Necker and G. L. Stüber, "Totally Blind Channel Estimation for OFDM over Fast Varying Mobile Channels," in *Proceedings of International Conference on Communications (ICC)*, vol. 1, (New York, USA), pp. 421–425, 28 April-2 May 2002.

[40] B. Lu and X. Wang, "Iterative Receivers for Multiuser Space-Time Coding Systems," *IEEE Journal on Selected Areas in Communications*, vol. 18, no. 11, pp. 2322–2335, November 2000.

[41] B. Lu, X. Wang, and Y. Li, "Iterative Receivers for Space-time Block-coded OFDM Systems in Dispersive Fading Channels," *IEEE Transactions on Wireless Communications*, vol. 1, no. 2, pp. 213–225, April 2002.

[42] B. Lu, X. Wang, and K. R. Narayanan, "LDPC-based Space-time Coded OFDM Systems Over Correlated Fading Channels: Performance Analysis and Receiver Design," *IEEE Transactions on Communications*, vol. 50, no. 1, pp. 74–88, January 2002.

[43] J. Lindner, "MC-CDMA and Its Relation to General Multiuser/Multisubchannel Transmission Systems," in *Proceedings of IEEE 4th International Symposium on Spread Spectrum Tecniques and Applications*, vol. 1, (Mainz, Germany), pp. 115–121, 22-25 September 1996.

[44] A. Bury and J. Lindner, "Comparison of Amplitude Distributions for Hadamard Spreading and Fourier Spreading in Multi-carrier Code Division Multiplexing," in *Proceedings of IEEE Global Telecommunications Conference (GLOBECOM)*, vol. 2, (San Fransisco, USA), pp. 857–860, 27 November-1 December 2000.

[45] H. Schmidt and K.-D. Kammeyer, "Reducing the Peak to Average Power Ratio of Multicarrier Signals by Adaptive Subcarrier Selection," in *Proceedings of IEEE International Conference on Universal Personal Communications (ICUPC)*, vol. 2, (Florence, Italy), pp. 933–937, 5-9 October 1998.

[46] A. Dekorsky, V. Kuhn and K.-D. Kammeyer, "Exploiting Time and Frequency Diversity by Iterative Decoding in OFDM-CDMA Systems," in *Proceedings of IEEE Global Telecommunications Conference (GLOBECOM)*, vol. 5, (Rio de Jeneiro, Brazil), pp. 2576–2580, 5-9 December 1999.

[47] T. Petermann, S. Vogeler, K.-D. Kammeyer, and D. Boss, "Blind Turbo Channel Estimation in OFDM Receivers," in *Conference Record of the Thirty-Fifth Asilomar Conference on Signals, Systems and Computers*, vol. 2, (Pacific Grove, USA), pp. 1489–1493, 4-7 November 2001.

[48] J. G. Proakis and M. Salehi, *Communication Systems Engineering.* New Jersey: Prentice-Hall, 1994.

[49] J. G. Proakis, *Digital Communications, Third Edition.* New York: McGraw-Hill, 1995.

[50] W. C. Jakes, *Microwave Mobile Communications.* Piscataway, New Jersey, USA: IEEE Press, 1993.

[51] J. K. Cavers, "An Analysis of Pilot Symbol Assisted Modulation for Rayleigh Fading Channels," *IEEE Transactions on Vehicular Technology*, vol. 40, no. 4, pp. 686–693, November 1991.

[52] P. Frenger and A. Svensson, "Decision Directed Coherent Detection in Multicarrier Systems on Rayleigh Fading Channels," *IEEE Transactions on Vehicular Technology*, vol. 48, no. 2, pp. 490–498, March 1999.

[53] B. Muquet, "Subspace-Based Blind and Semi-Blind Channel Estimation for OFDM Systems," *IEEE Transactions on Signal Processing*, vol. 50, no. 7, pp. 1699–1722, July 2002.

[54] M. Luise, R. Reggiannini, and G. M. Vitetta, "Blind Equalization/Detection for OFDM Signals over Frequency-Selective Channels," *IEEE Journal on Selected Areas in Communications*, vol. 16, no. 8, pp. 1568–1578, October 1998.

[55] W. T. Webb and R. Steele, "Variable Rate QAM for Mobile Radio," *IEEE Transactions on Communications*, vol. 43, no. 7, pp. 2223–2230, July 1995.

[56] T. Keller, *Adaptive Multi-carrier Techniques for Cellular and Local Area Networks.* PhD thesis, University of Southampton, United Kingdom, Department of Electronics and Computer Science, August 1999.

[57] J. M. Torrance, *Adaptive Full Response Digital Modulation for Wireless Communications Systems.* PhD thesis, University of Southampton, United Kingdom, Department of Electronics and Computer Science, 1997.

[58] J. M. Torrance and L. Hanzo, "Optimisation of Switching Levels for Adaptive Modulation in Slow Rayleigh Fading," *IEE Electronics Letters*, vol. 32, no. 13, pp. 1167–1169, 20 June 1996.

[59] B. Chen and C.-E. W. Sundberg, "Complementary Punctured-Pair Convolutional Codes for Digital Audio Broadcasting," *IEEE Transactions on Communications*, vol. 48, no. 11, pp. 1829–1839, November 2000.

[60] J. L. Laneman and C.-E. W. Sundberg, "Reed-Solomon Decoding Algorithm for Digital Audio Broadcasting," *IEEE Transactions on Broadcasting*, vol. 47, no. 2, pp. 115–122, June 2001.

[61] Y. H. Kim, I. Song, H. G. Kim, T. Chang, and H. M. Kim, "Performance Analysis of a Coded OFDM System in Time-Varying Multipath Rayleigh Fading Channels,"

IEEE Transactions on Vehicular Technology, vol. 48, no. 5, pp. 1610–1615, September 1999.

[62] T. Keller, M. Münster, and L. Hanzo, "A Turbo-coded Burst-By-Burst Adaptive Wide-band Speech Tranceivers," *IEEE Journal on Selected Areas in Communications*, vol. 18, no. 11, pp. 2363–2372, November 2000.

[63] J. Yang, M. H. Lee, M. Q. Jiang, and J. Y. Park, "Robust Wireless Image Transmission Based on Turbo-coded OFDM," *IEEE Transactions on Consumer Electronics*, vol. 48, no. 3, pp. 724–731, August 2002.

[64] C. Berrou, A. Glavieux, and P. Thitimajshima, "Near Shannon Limit Error-correcting Coding and Decoding: Turbo-codes," in *Proceedings of International Conference on Communications (ICC)*, vol. 2, (Geneva, Switzerland), pp. 1064–1070, 23-26 May 1993.

[65] S. A. Barbulescu and S. S. Pietrobon, "TURBO CODES: A Tutorial on a New Class of Powerful Error Correcting Coding Schemes," *Journal of Electrical and Electronics Engineering, Australia*, vol. 19, no. 3, pp. 143–152, September 1999.

[66] O. Acikel and W. Ryan, "Punctured Turbo-codes for BPSK/QPSK Channels," *IEEE Transactions on Communications*, vol. 47, no. 9, pp. 1315–1323, September 1999.

[67] L. Hanzo, T. H. Liew, and B. L. Yeap, *Turbo Coding, Turbo Equalisation and Space Time Coding for Transmission over Wireless Channels*. West Sussex, England: John Willy and IEEE Press, 2002.

[68] R. G. Gallagher, "Low Density Parity Check Codes," *I R E Transactions on Information Theory*, vol. IT-8, pp. 21–28, January 1962.

[69] D. J. C. MacKay and R. M. Neal, "Near Shannon Limit Performance of Low Density Parity Check Codes," *IEE Electronics Letters*, vol. 32, no. 18, pp. 1645–1646, 29 August 1996.

[70] H. Futaki and T. Ohtsuki, "Low-Density Parity-Check (LDPC) Coded OFDM Systems," in *Proceedings of IEEE Vehicular Technology Conference (VTC-Fall)*, vol. 1, (New Jersey, USA), pp. 82–86, 7-11 October 2001.

[71] L. Ping and W. K. Leung, "Decoding Low Density Parity Check Codes wih Finite Quantization Bits," *IEEE Communications Letters*, vol. 4, no. 2, pp. 62–64, February 2000.

[72] H. Futaki and T. Ohtsuki, "Low-Density Parity-Check (LDPC) Coded OFDM Systems with M-FSK," in *Proceedings of IEEE Vehicular Technology Conference (VTC-Spring)*, vol. 2, (Alabama, USA), pp. 1035–1039, 6-9 May 2002.

[73] H. Futaki and T. Ohtsuki, "Performance of Low-Density Parity-Check (LDPC) Coded OFDM Systems," in *IEEE International Conference on Communications (ICC)*, vol. 3, (New York, USA), pp. 1696–1700, 28 April-2 May 2002.

[74] D. M. Gruenbacher and A. Serener, "Performance of Coded OFDM in a Fading Environment Using High Rate Low-Density Parity Check Codes," in *Proceedings of IEEE Global Telecommunication Conference (GLOBECOM)*, vol. 1, (San Antonio, Texas, USA), pp. 504–508, 25-29 November 2001.

[75] D. M. Gruenbacher and A. Serener, "High Rate Coded OFDM with Channel Equalization," in *The 2002 45th Midwest Symposium on Circuits and Systems (MWSCAS)*, vol. 3, (Tulsa, Oklahoma, USA), pp. 111445–111448, 4-7 August 2002.

[76] Y. Li and J. Moon, "Increasing Data Rates Through Iterative Coding and Antenna Diversity in OFDM-based Wireless Communication," in *Proceedings of IEEE Global Telecommunication Conference (GLOBECOM)*, vol. 5, (San Antonio, Texas, USA), pp. 3130–3134, 25-29 November 2001.

[77] N. Yoshimochi, T. Hiramoto, A. Mizuki, C.-J. Ahn, and I. Sasase, "LDPC Coded Unitary Space-time Modulated OFDM System in Broadband Mobile Channel," *IEE Electronics Letters*, vol. 39, no. 13, pp. 994–995, 26 June 2003.

[78] H. Niu, M. Shen, J. A. Ritcey, and H. Liu, "Performance of Clustered OFDM with Low Density Parity Check Codes over Dispersive Channels," in *Conference Record of the Thrity-Sixth Asilomar Conference on Signals, Systems and Computers*, vol. 2, (Pacific Groove, California, USA), pp. 1852–1856, 3-6 November 2002.

[79] V. Mannoni, D. Declereq, and G. Gelle, "Optimized Irregular Gallager Codes for OFDM Transmission," in *Proceedings of IEEE International Symposium on Personal Indoor and Mobile Radio Communications (PIMRC)*, vol. 1, (Lisbon, Portugal), pp. 222–226, 15-18 September 2002.

[80] A. Paulraj, R. Nabar, and D. Gore, *Introduction to Space-time Wireless Communications*. UK: Cambridge University Press, 2003.

[81] S. M. Alamouti, "A Simple Transmit Diversity Technique for Wireless Communications," *IEEE Journal on Selected Areas in Communications*, vol. 16, no. 8, pp. 1451–1458, October 1998.

[82] D. Agrawal, V. Tarokh, A. Naguib, and N. Seshadri, "Space-time Coded OFDM for High Data-rate Wireless Communication Over Wideband Channels," in *Proceedings of IEEE Vehicular Technology Conference (VTC)*, (Ottawa, Canada), pp. 2232–2236, 18-21 May 1998.

[83] M. Uysal, N. Al-Dhahir, and C. N. Georghiades, "A Space-Time Block-Coded OFDM Scheme for Unknown Frequency Selective Fading Channels," *IEEE Communications Letters*, vol. 5, no. 10, pp. 393–395, October 2001.

[84] V. Tarokh, H. Jafarkhani, and A. R. Calderbank, "Space-time Block Coding for Wireless Communications: Performance Results," *IEEE Journal on Selected Areas in Communications*, vol. 17, no. 5, pp. 451–460, May 1999.

[85] V. Tarokh, H. Jafarkhani, and A. R. Calderbank, "Space-time Block Codes from Orthogonal Designs," *IEEE Transactions on Information Theory*, vol. 45, no. 5, pp. 1456–1467, July 1999.

[86] V. Tarokh, H. Jafarkhani, and A. R. Calderbank, "Space-time Codes for High Data Rate Wireless Communication: Performance Criterion and Code Construction," *IEEE Transactions on Information Theory*, vol. 44, no. 2, pp. 744–765, March 1998.

[87] R. S. Blum, Q. Yan, Y. Li, and J. H. Winters, "Improved Techniques for 4 Transmit and 4 Receive Antenna MIMO-OFDM for Wireless Communications," in *Proceedings of IEEE Vehicular Technology Conference (VTC-Spring)*, vol. 2, (Rhodes, Greece), pp. 1298–1302, 6-9 May 2001.

[88] Y. Li, J. H. Winters, and N. R. Sollenberger, "Signal Detection for MIMO-OFDM Wireless Communications," in *Proceedings of IEEE International Conference on Communications (ICC)*, vol. 10, (Helsinki, Finland), pp. 3077–3081, 11-14 June 2001.

[89] T. H. Liew and L. Hanzo, "Space-time Block Coded Adaptive Modulation Aided OFDM," in *Proceedings of IEEE Global Telecommunications Conference (GLOBECOM)*, vol. 1, (San Antonio, Texas, USA), pp. 136–140, 25-29 November 2001.

[90] K. F. Lee and D. B. Williams, "Bandwidth Efficient OFDM Transmitter Diversity Techniques," in *IEEE International Conference on Acoustics, Speech, and Signal Processing (ICASSP)*, (Orlando, Florida, USA), pp. 2325–2328, 13-17 May 2002.

[91] J. Yue and J. D. Gibson, "Performance of a Space-time Block-coded OFDM System," in *Conference Record of the Thirty-Sixth Asilomar Conference on Signals, Systems and Computers*, vol. 2, (Pacific Groove, California, USA), pp. 1862–1866, 3-6 November 2002.

[92] K. Suto and T. Ohtsuki, "Performance Evaluation of Space-time-frequency Block Codes Over Frequency Selective Fading Channels," in *Proceedings of Vehicular Technology Conference (VTC-Fall)*, vol. 3, (Vancouver, Canada), pp. 1466–1470, 24-28 September 2002.

[93] E. Panayirci and H. A. Cirpan, "Channel Estimation for Space-time Block-coded OFDM Systems in the Presence of Multipath Fading," in *Proceedings of IEEE Global Telecommunications Conference (GLOBECOM)*, (Taipei, Taiwan), pp. 1157–1161, 17-21 November 2002.

[94] B. Vucetic and J. Yuan, *Space-Time Coding*. West Sussex, England: John Wiley & Sons Ltd, 2003.

[95] S. Liang and W. Wu, "Channel Estimation Based on Pilot Subcarriers in Space-time Block-coded OFDM System," in *Proceedings of International Conference on Communications Technology (ICCT)*, vol. 2, (Beijing, China), pp. 1795–1798, 9-11 April 2003.

[96] M. Torabi and M. R. Soleymani, "Adaptive Bit Allocation for Space-time Block Coded OFDM System," in *Proceedings of IEEE International Conference on Acoustics, Speech and Signal Processing (ICASSP)*, vol. 4, (Hong Kong, China), pp. 409–412, 6-10 April 2003.

[97] T. H. Liew, B. J. Choi, and L. Hanzo, "Comparative Study of Concatenated Turbo Coded and Space-time Trellis Coded OFDM," in *Proceedings of IEEE Vehicular Technology Conference (VTC-Spring)*, vol. 2, (Rhodes, Greece), pp. 781–785, 6-9 May 2001.

[98] P. Robertson, E. Villebrun, and P. Höher, "A Comparison of Optimal and Sub-Optimal MAP Decoding Algorithms Operating in the Log Domain," in *Proceedings*

of IEEE International Conference on Communications (ICC), (Seattle, Washington, USA), pp. 1009–1013, 18-22 June 1995.

[99] F. Guo, S. X. Ng, and L. Hanzo, "LDPC Assisted Block Coded Modulation for Transmission over Rayleigh Fading Channels ," in *Proceedings of IEEE Vehicular Technology Conference (VTC-Spring)*, (Jeju, Korea), pp. 1867–1871, 22-25 April 2003.

[100] R. Zhang, T. T. Tjhung, H. J. Hu, and P. He, "Window Function and Interpolation Algorithm for OFDM Frequency-offset Correction," *IEEE Transactions on Vehicular Technology*, vol. 52, no. 3, pp. 654–670, May 2003.

[101] P. Ciblat and L. Vandendorpe, "Blind Carrier Frequency Offset Estimation for Noncircular Constellation-based Transmissions," *IEEE Transactions on Signal Processing*, vol. 51, no. 5, pp. 1378–1389, May 2003.

[102] R. Narasimhan, "Performance of Diversity Schemes for OFDM Systems with Frequency Offset, Phase Noise, and Channel Estimation Errors," *IEEE Transactions on Communications*, vol. 50, no. 10, pp. 1561–1565, October 2002.

[103] R. Negi and J. M. Cioffi, "Blind OFDM Symbol Synchronization in ISI Channels," *IEEE Transactions on Communications*, vol. 50, no. 9, pp. 1525–1534, September 2002.

[104] P. Ciblat and E. Serpedin, "A Fine Blind Frequency Offset Estimator for OFDM/OQAM Systems," *IEEE Transactions on Signal Processing*, vol. 52, no. 1, pp. 291–296, January 2004.

[105] U. Tureli, P. J. Honan, and H. Liu, "Low-complexity Nonlinear Least Squares Carrier Offset Estimator for OFDM: Identifiability, Diversity and Performance," *IEEE Transactions on Signal Processing*, vol. 52, no. 9, pp. 2441–2452, September 2004.

[106] M. Morelli, "Timing and Frequency Synchronization for the Uplink of an OFDMA System," *IEEE Transactions on Communications*, vol. 52, no. 2, pp. 296–306, February 2004.

[107] J. Lei and T.-S. Ng, "A Consistent OFDM Carrier Frequency Offset Estimator Based on Distinctively Spaced Pilot Tones," *IEEE Transactions on Wireless Communications*, vol. 3, no. 2, pp. 588–599, March 2004.

[108] M. Luise, M. Marselli, and R. Reggiannini, "Low-complexity Blind Carrier Frequency Recovery for OFDM Signals Over Frequency-selective Radio Channels," *IEEE Transactions on Communications*, vol. 50, no. 7, pp. 1182–1188, July 2002.

[109] G. Leus and M. Moonen, "Per-tone Equalization for MIMO OFDM Systems," *IEEE Transactions on Signal Processing*, vol. 51, no. 11, pp. 2965–2975, November 2003.

[110] H. Bölcskei, R. W. Heath Jr., and A. J. Paulraj, "Blind Channel Identification and Equalization in OFDM-based Multiantenna System," *IEEE Transactions on Signal Processing*, vol. 50, no. 1, pp. 96–109, January 2002.

[111] Y. Ding, T. N. Davidson, Z.-Q. Luo, and K. M. Wong, "Minimum BER Block Precoders for Zero-forcing Equalization," *IEEE Transactions on Signal Processing*, vol. 51, no. 9, pp. 2410–2423, September 2003.

[112] C. Tepedelenlioglu, "Maximum Multipath Diversity with Linear Equalization in Precoded OFDM Systems," *IEEE Transactions on Information Theory*, vol. 50, no. 1, pp. 232–235, January 2004.

[113] P. Schniter, "Low-complexity Equalization of OFDM in Doubly Selective Channels," *IEEE Transactions on Signal Processing*, vol. 52, no. 4, pp. 1002–1011, April 2004.

[114] M.-X. Chang and Y. T. Su, "Performance Analysis of Equalized OFDM Systems in Rayleigh Fading," *IEEE Transactions on Wireless Communications*, vol. 1, no. 4, pp. 721–732, October 2002.

[115] B. Farhang-Boroujeny, "Multicarrier Modulation with Blind Detection Capability Using Cosine Modulated Filter Banks," *IEEE Transactions on Communications*, vol. 51, no. 12, pp. 2057–2070, December 2003.

[116] N. Benvenuto and S. Tomasin, "On the Comparison Between OFDM and Single Carrier Modulation with a DFE Using a Frequency-domain Feedforward Filter," *IEEE Transactions on Communications*, vol. 50, no. 6, pp. 947–955, June 2002.

[117] P. Siohan, C. Siclet, and N. Lacaille, "Analysis and Design of OFDM/OQAM Systems Based on Filterbank Theory," *IEEE Transactions on Signal Processing*, vol. 50, no. 5, pp. 1170–1183, May 2002.

[118] V. G. S. Prasad and K. V. S. Hari, "Interleaved Orthogonal Frequency Division Multiplexing (IOFDM) System," *IEEE Transactions on Signal Processing*, vol. 52, no. 6, pp. 1711–1721, June 2004.

[119] L. Sai-Weng and V. K. N. Lau, "Performance Analysis of Adaptive Interleaving for OFDM Systems," *IEEE Transactions on Vehicular Technology*, vol. 51, no. 3, pp. 435–444, May 2002.

[120] E. Hass and S. Kaiser, "Two-dimensional Differential Demodulation for OFDM," *IEEE Transactions on Communications*, vol. 51, no. 4, pp. 580–586, April 2003.

[121] F. Xiong, "M-ary Amplitude Shift Keying OFDM Systems," *IEEE Transactions on Communications*, vol. 51, no. 10, pp. 1638–1642, October 2003.

[122] D. L. Goeckel and G. Anathaswamy, "On the Design of Multidimensional Signal Sets for OFDM Systems," *IEEE Transactions on Communications*, vol. 50, no. 3, pp. 442–452, March 2002.

[123] C. V. Chong, R. Venkataramani, and V. Tarokh, "A New Construction of 16-QAM Golay Complementary Sequences," *IEEE Transactions on Information Theory*, vol. 49, no. 11, pp. 2953–2959, November 2003.

[124] M.-X. Chang and Y. T. Su, "Blind and Semiblind Detections on OFDM Signals in Fading Channels," *IEEE Transactions on Communications*, vol. 52, no. 5, pp. 744–754, May 2004.

[125] K. Zhong, T. T. Tjhung, and F. Adachi, "A General SER Formula for an OFDM System with MDPSK in Frequency Domain over Rayleigh Fading Channels," *IEEE Transactions on Communications*, vol. 52, no. 4, pp. 584–594, April 2004.

[126] B. Chen and H. Wang, "Blind Estimation of OFDM Carrier Frequency Offset via Oversampling," *IEEE Transactions on Signal Processing*, vol. 52, no. 7, pp. 2047–2057, July 2004.

[127] B. Muquet, M. de Courville, P. Duhamel, G. B. Giannakis, and P. Magniez, "Turbo Demodulation of Zero-padded OFDM Transmissions," *IEEE Transactions on Communications*, vol. 50, no. 11, pp. 1725–1728, November 2002.

[128] A. Al-Dweik and F. Xiong, "Frequency-hopped Multiple-access Communications with Noncoherent M-ary OFDM-ASK," *IEEE Transactions on Communications*, vol. 51, no. 1, pp. 33–36, January 2003.

[129] D. A. Wiegandt, Z. Wu, and C. R. Nassar, "High-throughput, High-performance OFDM via Pseudo-orthogonal Carrier Interferometry Spreading Codes," *IEEE Transactions on Communications*, vol. 51, no. 7, pp. 1123–1134, July 2003.

[130] S. Kaiser, "OFDM Code-division Multiplexing in Fading Channels," *IEEE Transactions on Communications*, vol. 50, no. 8, pp. 1266–1273, August 2002.

[131] X. Chai and G. B. Giannakis, "Bounding Performance and Suppressing Intercarrier Interference in Wireless Mobile OFDM," *IEEE Transactions on Communications*, vol. 51, no. 12, pp. 2047–2056, December 2003.

[132] D. Zhang, P. Fan, and Z. Cao, "Interference Cancellation for OFDM Systems in Presence of Overlapped Narrow Band Transmission System," *IEEE Transactions on Consumer Electronics*, vol. 50, no. 1, pp. 108–114, February 2004.

[133] R. Nilsson, F. Sjoberg, and J. P. LeBlanc, "A Rank-reduced LMMSE Canceller for Narrowband Interference Suppression in OFDM-based Systems," *IEEE Transactions on Communications*, vol. 51, no. 12, pp. 2126–2140, December 2003.

[134] P. Banelli, "Theoretical Analysis and Performance of OFDM Signals in Nonlinear Fading Channels," *IEEE Transactions on Wireless Communications*, vol. 2, no. 2, pp. 284–293, March 2003.

[135] Y.-P. Lin and S.-M. Phoong, "OFDM Transmitters: Analog Representation and DFT-based Implementation," *IEEE Transactions on Signal Processing*, vol. 51, no. 9, pp. 2450–2453, September 2003.

[136] T. Strohmer and S. Beaver, "Optimal OFDM Design for Time-frequency Dispersive Channels," *IEEE Transactions on Communications*, vol. 51, no. 7, pp. 1111–1122, July 2003.

[137] X. Ma, G. B. Giannakis, and S. Ohno, "Optimal Training for Block Transmission Over Doubly Selective Wireless Fading Channels," *IEEE Transactions on Signal Processing*, vol. 51, no. 5, pp. 1351–1366, May 2003.

[138] T. H. Meng, B. McFarland, D. Su, and J. Thompson, "Design and Implementation of an All-CMOS 802.11a Wireless LAN Chipset," *IEEE Communications Magazine*, vol. 41, no. 8, pp. 160–168, August 2003.

[139] A. Polydros, J. Rautio, G. Razzano, H. Bogucka, D. Ragazzi, A. Mammela, M. Benedix, M. Lobeira, and L. Agarossi, "WIND-FLEX: Developing a Novel Testbed for Exploring Flexible Radio Concepts in an Indoor Environment," *IEEE Communications Magazine*, vol. 41, no. 7, pp. 116–122, July 2003.

[140] B. Canpolat and Y. Tanik, "Performance Analysis of Adaptive Loading OFDM Under Rayleigh Fading," *IEEE Transactions on Vehicular Technology*, vol. 53, no. 4, pp. 1105–1115, July 2004.

[141] L. Ding, G. T. Zhou, D. R. Morgan, Z. Ma, J. S. Kenney, J. Kim, and C. R. Giardina, "A Robust Digital Baseband Predistorter Constructed Using Memory Polynomials," *IEEE Transactions on Communications*, vol. 52, no. 1, pp. 159–165, January 2004.

[142] B. Muquet, Z. Wang, G. B. Giannakis, M. de Courville, and P. Duhamel, "Cyclic Prefixing or Zero Padding for Wireless Multicarrier Transmissions?," *IEEE Transactions on Communications*, vol. 50, no. 12, pp. 2136–2148, December 2002.

[143] J. Jang and K. B. Lee, "Transmit Power Adaptation for Multiuser OFDM Systems," *IEEE Journal on Selected Areas of Communications*, vol. 21, no. 2, pp. 171–178, February 2003.

[144] H. Ochiai and H. Imai, "Performance Analysis of Deliberately Clipped OFDM Signals," *IEEE Transactions on Communications*, vol. 50, no. 1, pp. 89–101, January 2002.

[145] E. Costa and S. Pupolin, "M-QAM-OFDM System Performance in the Presence of a Nonlinear Amplifier and Phase Noise," *IEEE Transactions on Communications*, vol. 50, no. 3, pp. 356–367, March 2002.

[146] M. Sharif, M. Gharavi-Alkhansari, and B. H. Khalaj, "On the Peak-to-average Power of OFDM Signals Based on Oversampling," *IEEE Transactions on Communications*, vol. 51, no. 1, pp. 72–78, January 2003.

[147] G. Wunder and H. Boche, "Upper Bounds on the Statistical Distribution of the Crest-factor in OFDM Transmission," *IEEE Transactions on Information Theory*, vol. 49, no. 2, pp. 488–494, February 2003.

[148] G. Wunder and H. Boche, "Peak Value Estimation of Bandlimited Signals from Their Samples, Noise Enhancement, and a Local Characterization in the Neighborhood of an Extremum," *IEEE Transactions on Signal Processing*, vol. 51, no. 3, pp. 771–780, March 2003.

[149] H. Ochiai, "Performance Analysis of Peak Power and Band-limited OFDM System with Linear Scaling," *IEEE Transactions on Wireless Communications*, vol. 2, no. 5, pp. 1055–1065, September 2003.

[150] X. Wang, T. T. Tjhung, and Y. Wu, "On the SER and Spectral Analyses of A-law Companded Multicarrier Modulation," *IEEE Transactions on Vehicular Technology*, vol. 52, no. 5, pp. 1408–1412, September 2003.

[151] K. R. Panta and J. Armstrong, "Effects of Clipping on the Error Performance of OFDM in Frequency Selective Fading Channels," *IEEE Transactions on Wireless Communications*, vol. 3, no. 2, pp. 668–671, March 2004.

[152] B. S. Krongold and D. L. Jones, "An Active-set Approach for OFDM PAR Reduction via Tone Reservation," *IEEE Transactions on Signal Processing*, vol. 52, no. 2, pp. 495–509, February 2004.

[153] A. Pascual-Iserte, A. I. Perez-Neira, and M. A. Lagunas, "On Power Allocation Strategies for Maximum Signal to Noise and Interference Ratio in an OFDM-MIMO System," *IEEE Transactions on Wireless Communications*, vol. 3, no. 3, pp. 808–820, May 2004.

[154] L. Goldfeld, V. Lyandres, and D. Wulich, "Minimum BER Power Loading for OFDM in Fading Channel," *IEEE Transactions on Communications*, vol. 50, no. 11, pp. 1729–1733, November 2002.

[155] O. Simone, Y. Bar-Ness, and U. Spagnolini, "Pilot-based Channel Estimation for OFDM Systems by Tracking the Delay-subspace," *IEEE Transactions on Wireless Communications*, vol. 3, no. 1, pp. 315–325, January 2004.

[156] S. Ohno and G. B. Giannakis, "Capacity Maximizing MMSE-Optimal Pilots for Wireless OFDM Over Frequency-selective Block Rayleigh-fading Channels," *IEEE Transactions on Information Theory*, vol. 50, no. 9, pp. 2138–2145, September 2004.

[157] X. Chai and G. B. Giannakis, "Error Probability Minimizing Pilots for OFDM with M-PSK Modulation over Rayleigh-fading Channels," *IEEE Transactions on Vehicular Technology*, vol. 53, no. 1, pp. 146–155, January 2004.

[158] S. Adireddy, L. Tong, and H. Viswanathan, "Optimal Placement of Training for Frequency-selective Block-fading Channels," *IEEE Transactions on Information Theory*, vol. 48, no. 8, pp. 2338–2353, August 2002.

[159] A. Dekorsky, V. Kuehn, and K.-D. Kammeyer, "Low-rate Channel Coding with Complex-valued Block Codes," *IEEE Transactions on Communications*, vol. 51, no. 5, pp. 800–809, May 2003.

[160] Y.-P. Lin and S.-M. Phoong, "BER Minimized OFDM Systems with Channel Independent Precoders," *IEEE Transactions on Signal Processing*, vol. 51, no. 9, pp. 2369–2380, September 2003.

[161] Z. Wang and G. B. Giannakis, "Complex-field Coding for OFDM over Fading Wireless Channels," *IEEE Transactions on Information Theory*, vol. 49, no. 3, pp. 707–720, March 2003.

[162] P. J. Cherriman, T. Keller, and L. Hanzo, "Subband-adaptive Turbo-coded OFDM-based Interactive Video Telephony," *IEEE Transactions on Circuit and Systems for Video Telephony*, vol. 12, no. 10, pp. 829–839, October 2002.

[163] H. Zheng and Y. Li, "Optimum Frequency-domain Partial Response Encoding in OFDM System," *IEEE Transactions on Communications*, vol. 51, no. 7, pp. 1064–1068, July 2003.

[164] J. Haring and A. J. H. Vinck, "Iterative Decoding of Codes Over Complex Numbers for Impulsive Noise Channels," *IEEE Transactions on Information Theory*, vol. 49, no. 5, pp. 1251–1260, May 2003.

[165] B. Lu, G. Yue, and X. Wang, "Performance Analysis and Design Optimization of LDPC-coded MIMO OFDM Systems," *IEEE Transactions on Signal Processing*, vol. 52, no. 2, pp. 348–361, February 2004.

[166] J. H. Manton, "The Convex Geometry of Subchannel Attenuation in Linearly Precoded OFDM Systems," *IEEE Transactions on Information Theory*, vol. 48, no. 5, pp. 1203–1206, May 2002.

[167] Y. Xie and C. N. Georghiades, "Two EM-type Channel Estimation Algorithms for OFDM with Transmitter Diversity," *IEEE Transactions on Communications*, vol. 51, no. 1, pp. 106–115, January 2003.

[168] X. Zhou and X. Wang, "Channel Estimation for OFDM System Using Adaptive Radial Basis Function Networks," *IEEE Transactions on Vehicular Technology*, vol. 52, no. 1, pp. 48–59, January 2003.

[169] H. Wang, Y. Lin, and B. Chen, "Data-efficient Blind OFDM Channel Estimation Using Receiver Diversity," *IEEE Transactions on Signal Processing*, vol. 51, no. 10, pp. 2613–2623, October 2003.

[170] C. Li and S. Roy, "Subspace-based Blind Channel Estimation for OFDM by Exploiting Virtual Carriers," *IEEE Transactions on Wireless Communications*, vol. 2, no. 1, pp. 141–150, January 2003.

[171] Y. Li, "Simplified Channel Estimation for OFDM Systems with Multiple Transmit Antennas," *IEEE Transactions on Wireless Communications*, vol. 1, no. 1, pp. 67–75, January 2002.

[172] S. Roy and L. Chengyang, "A Subspace Blind Channel Estimation Method for OFDM Systems Without Cyclic Prefix," *IEEE Transactions on Wireless Communications*, vol. 1, no. 4, pp. 572–579, October 2002.

[173] B. Muquet, M. de Courville, and P. Duhamel, "Subspace-based Blind and Semi-blind Channel Estimation for OFDM Systems," *IEEE Transactions on Signal Processing*, vol. 50, no. 7, pp. 1699–1712, July 2002.

[174] Y. Gong and K. B. Letaief, "Low Complexity Channel Estimation for Space-time Coded Wideband OFDM Systems," *IEEE Transactions on Wireless Communications*, vol. 2, no. 5, pp. 876–882, September 2003.

[175] F. Shu, J. Lee, L.-N. Wu, and G.-L. Zhao, "Time-frequency Channel Estimation for Digital Amplitude Modulation Broadcasting Systems based on OFDM," *IEE Proceedings-Communications*, vol. 150, no. 4, pp. 259–264, 12 August 2003.

[176] A. Petropulu, R. Zhang, and R. Lin, "Blind OFDM Channel Estimation Through Simple Linear Precoding," *IEEE Transactions on Wireless Communications*, vol. 3, no. 3, pp. 647–655, March 2004.

[177] H. Minn, D. I. Kim, and V. K. Bhargava, "A Reduced Complexity Channel Estimation for OFDM Systems with Transmit Diversity in Mobile Wireless Channels," *IEEE Transactions on Communications*, vol. 50, no. 5, pp. 799–807, May 2002.

[178] H. Bölcskei, M. Borgmann, and A. J. Paulraj, "Impact of the Propagation Environment on the Performance of Space-fequency Coded MIMO OFDM," *IEEE Journal on Selected Areas of Communications*, vol. 21, no. 3, pp. 96–109, April 2003.

[179] S. Weifeng, Z. Safar, M. Olfat, and K. J. R. Liu, "Obtaining Full-diversity Space-frequency Codes from Space-time Codes via Mapping," *IEEE Transactions on Signal Processing*, vol. 51, no. 11, pp. 2905–2916, November 2003.

[180] I. Barhumi, G. Leus, and M. Moonen, "Optimal Training Design for MIMO OFDM Systems in Mobile Wireless Channels," *IEEE Transactions on Signal Processing*, vol. 51, no. 6, pp. 1615–1624, June 2003.

[181] S. Thoen, L. Van der Perre, M. Engels, and H. D. Man, "Constrained Least Squares Detector for OFDM/SDMA-based Wireless Networks," *IEEE Transactions on Wireless Communications*, vol. 2, no. 1, pp. 129–140, January 2003.

[182] Y. Gong and K. B. Letaief, "An Efficient Space-frequency Coded OFDM System for Broadband Wireless Communications," *IEEE Transactions on Communications*, vol. 51, no. 12, pp. 2019–2029, December 2003.

[183] Y. G. Li, J. H. Winters, and N. R. Sollenberger, "MIMO-OFDM for Wireless Communications: Signal Detection with Enhanced Channel Estimation," *IEEE Transactions on Communications*, vol. 50, no. 9, pp. 1471–1477, September 2002.

[184] H. Sampath, S. Talwar, J. Tellado, V. Erceg, and A. Paulraj, "A Fourth-generation MIMO-OFDM Broadband Wireless System: Design, Performance, and Field Trial Results," *IEEE Communications Magazine*, vol. 40, no. 9, pp. 143–149, September 2002.

[185] A. Stamoulis, S. N. Diggavi, and N. Al-Dhahir, "Intercarrier Interference in MIMO OFDM," *IEEE Transactions on Signal Processing*, vol. 50, no. 10, pp. 2451–2464, October 2002.

[186] S. H. Muller-Weinfurtner, "Coding Approaches for Multiple Antenna Transmission in Fast Fading and OFDM," *IEEE Transactions on Signal Processing*, vol. 50, no. 10, pp. 2422–2450, October 2002.

[187] S. Thoen, L. Van der Perre, M. Engels, and H. De Man, "Adaptive Loading for OFDM/SDMA-based Wireless Networks," *IEEE Transactions on Communications*, vol. 50, no. 11, pp. 1798–1810, November 2002.

[188] S.-Y. Kung, Y. Wu, and X. Zhang, "Bezout Space-time Precoders and Equalizers for MIMO Channels," *IEEE Transactions on Signal Processing*, vol. 50, no. 10, pp. 2499–2514, October 2002.

[189] J. Li, K. B. Letaief, and Z. Cao, "Co-channel Interference Cancellation for Space-time Coded OFDM Systems," *IEEE Transactions on Wireless Communications*, vol. 2, no. 1, pp. 41–49, January 2003.

[190] P. Xia, S. Zhou, and G. B. Giannakis, "Adaptive MIMO/OFDM Based on Partial Channel State Information," *IEEE Transactions on Signal Processing*, vol. 52, no. 1, pp. 202–213, January 2004.

[191] D. Huang, K. B. Letaief, and J. Liu, "A Receive Space Diversity Architecture for OFDM Systems Using Orthogonal Designs," *IEEE Transactions on Wireless Communications*, vol. 3, no. 3, pp. 992–1002, May 2004.

[192] G. L. Stuber, J. R. Barry, S. W. McLaughlin, Y. Li, M. A. Ingram, and T. G. Pratt, "Broadband MIMO-OFDM Wireless Communications," *Proceeedings of the IEEE*, vol. 92, no. 2, pp. 271–294, February 2004.

[193] M. Budsabathon, Y. Hara, and S. Hara, "Optimum Beamforming for Pre-FFT OFDM Adaptive Antenna Array," *IEEE Transactions on Vehicular Technology*, vol. 53, no. 4, pp. 945–955, July 2004.

[194] A. van Zelst and T. C. W. Schenk, "Implementation of a MIMO OFDM-based Wireless LAN System," *IEEE Transactions on Signal Processing*, vol. 52, no. 2, pp. 483–494, February 2004.

[195] D. Huang and K. B. Letaief, "Symbol-based Space Diversity for Coded OFDM Systems," *IEEE Transactions on Wireless Communications*, vol. 3, no. 1, pp. 117–127, January 2004.

[196] I. Lee, A. M. Chan, and C.-E. W. Sundberg, "Space-time Bit-interleaved Coded Modulation for OFDM Systems," *IEEE Transactions on Signal Processing*, vol. 52, no. 3, pp. 820–825, March 2004.

[197] L.-U. Choi and R. D. Murch, "A Pre-BLAST-DFE Technique for the Downlink of Frequency-selective Fading MIMO Channels," *IEEE Transactions on Communications*, vol. 52, no. 5, pp. 737–743, May 2004.

[198] Z. Liu, Y. Xin, and G. B. Giannakis, "Space-time Frequency Coded OFDM Over Frequency-selective Fading Channels," *IEEE Transactions on Signal Processing*, vol. 50, no. 10, pp. 2465–2476, October 2002.

[199] J. Blogh and L. Hanzo, *3G Systems and Intelligent Networking*. John Wiley and IEEE Press, 2002.

[200] G. Foschini, "Layered Space-time Architecture for Wireless Communication in a Fading Environment when Using a Multi-element Antennas," *Bell Labs Technical Journal*, vol. 10, pp. 41–59, Autumn 1996.

[201] J.H. Winters, "Smart Antennas for Wireless Systems," *IEEE Personal Communications*, vol. 5, no. 1, pp. 23–27, February 1998.

[202] R. T. Derryberry, S. D. Gray, D. M. Ionescu, G. Mandyam, and B. Raghothaman, "Transmit Diversity in 3G CDMA Systems," *IEEE Communications Magazine*, vol. 40, pp. 68–75, April 2002.

[203] B. Suard, G. Xu, H. Liu, and T. Kailath, "Uplink Channel Capacity of Space-Division-Multiple-Access Scheme," *IEEE Transactions on Information Theory*, vol. 44, no. 4, pp. 1468–1476, July 1998.

[204] P. Vandenameele, L. Van Der Perre, M. G. E. Engels, B. Gyselinckx, and H. J. D. Man, "A Combined OFDM/SDMA Approach," *IEEE Journal on Selected Areas in Communications*, vol. 18, no. 11, pp. 2312–2321, November 2000.

[205] M. Münster and L. Hanzo, "Co-channel Interference Cancellation Techniques for Antenna Array Assisted Multiuser OFDM Systems," in *3G-2000*, (London, UK), pp. 256–260, 27-29 March 2000.

[206] L. Hanzo, L.-L. Yang, E.-L. Kuan, and K. Yen, *Single- and Multi-Carrier DS-CDMA: Multi-User Detection, Space-Time Spreading, Synchronisation, Networking and Standards*. West Sussex, England: John Wiley and Sons, 2002.

[207] L. Hanzo, C. H. Wong, and M. S. Yee, *Adaptive Wireless Tranceivers*. West Sussex, England: John Wiley and Sons, 2002.

[208] A. K. Samingan, S. Chen, and L. Hanzo, "Adaptive Minimum Symbol Error Rate CDMA Multiuser Detection for Pulse Amplitude Modulation," in *Proceedings of IEEE Vehicular Technology Conference (VTC-Spring)*, (Jeju, Korea), pp. 2812–2816, 22-25 April 2003.

[209] X. Wang, W.-S. Lu, and A. Antoniou, "Constrained Minimum-BER Multiuser Detection," *IEEE Transactions on Signal Processing*, vol. 48, no. 10, pp. 2903–2909, October 2000.

[210] R. C. de Lamare and R. Sampaio-Neto, "Adaptive MBER Decision Feedback Multiuser Receivers in Frequency Selective Fading Channels," *IEEE Communications Letters*, vol. 7, no. 2, pp. 73–75, February 2003.

[211] S. Chen, L. Hanzo, and N. N. Ahmad, "Adaptive Minimum Bit Error Rate Beamforming Assisted Receiver for Wireless Communications," in *Proceedings of IEEE International Conference of Acoustics, Speech and Signal Processing (ICASSP)*, vol. IV, (Hong Kong, China), pp. 640–643, 6-10 April 2003.

[212] B. Mulgrew and S. Chen, "Adaptive Minimum-BER Decision Feedback Equalizers for Binary Signalling," *EURASIP Signal Processing Journal*, vol. 81, no. 7, pp. 1479–1489, 2001.

[213] C.-C. Yeh and J. R. Barry, "Adaptive Minimum Bit-Error Rate Equalization for Binary Signalling," *IEEE Transactions on Communications*, vol. 48, no. 7, pp. 1226–1235, July 2000.

[214] M. R. Aaron and D. W. Tufts, "Intersymbol Interference and Error Probability," *IEEE Transactions on Information Theory*, vol. IT-12, pp. 26–34, January 1966.

[215] E. Shamash and K. Yao, "On the Structure and Performance of a Linear Decision Feedback Equalizer Based on the Minimum Error Probability Criterion," in *Proceedings of the International Conference on Communications (ICC)*, (Minneapolis, Minnesota, USA), pp. 25F1–25F5, 17-19 June 1974.

[216] S. Chen, E. Chng, B. Mulgrew, and G. Gibson, "Minimum-BER Linear-Combiner DFE," in *Proceedings of International Conference on Communications (ICC)*, (Dallas, Texas, USA), pp. 1173–1177, 23-27 June 1996.

[217] C. C. Yeh and J. R. Barry, "Approximate Minimum Bit-Error Rate Equalization for Binary Signaling," in *Proceedings of International Conference on Communications (ICC)*, vol. 1, (Montreal, Canada), pp. 1095–1099, 8-12 June 1997.

[218] N. B. Mandayam and B. Aazhang, "Gradient Estimation for Sensitivity Analysis and Adaptive Multiuser Interference Rejection in Code-Division Multiple-Access Systems," *IEEE Transactions on Communications*, vol. 45, no. 6, pp. 848–858, July 1997.

[219] C. C. Yeh and J. R. Barry, "Approximate Minimum Bit-Error Rate Equalization for Pulse-Amplitude and Quadrature Amplitude Modulation," in *Proceedings of International Conference on Communications (ICC)*, vol. 1, (Atlanta, Georgia, USA),

pp. 16–20, 7-11 June 1998.

[220] C. C. Yeh, R. R. Lopes, and J. R. Barry, "Approximate Minimum Bit-Error Rate Multiuser Detection," in *Proceedings of IEEE Global Telecommunications Conference (GLOBECOM)*, vol. 1, (Sydney, Australia), pp. 3590–3595, 8-12 November 1998.

[221] S. Chen, B. Mulgrew, E. S. Chng, and G. Gibson, "Space Translation Properties and the minimum-BER Linear-Combiner DFE," *IEE Proceedings on Communications*, vol. 145, no. 5, pp. 316–322, October 1998.

[222] S. Chen and B. Mulgrew, "The Minimum-SER Linear-Combiner Decision Feedback Equalizer," *IEE Proceedings on Communications*, vol. 146, no. 6, pp. 347–353, December 1999.

[223] I. N. Psaromiligkos, S. N. Batalama, and D. A. Pados, "On Adaptive Minimum Probability of Error Linear Filter Receivers for DS-CDMA Channels," *IEEE Transactions on Communications*, vol. 47, no. 7, pp. 1092–1102, July 1999.

[224] B. Mulgrew and S. Chen, "Stochastic Gradient Minimum-BER Decision Feedback Equalisers," in *Proceedings of IEEE Symposium on Adaptive Systems for Signal Processing, Communication and Control*, (Lake Louise, Alberta, Canada), pp. 93–98, 1-4 October 2000.

[225] S. Chen, A. K. Samingan, B. Mulgrew, and L. Hanzo, "Adaptive Minimum-BER Linear Multiuser Detection," in *Proceedings of IEEE International Conference of Acoustics, Speech and Signal Processing (ICASSP)*, (Salt-Lake City, Utah, USA), pp. 2253–2256, 7-11 May 2001.

[226] S. Chen, A. K. Samingan, B. Mulgrew, and L. Hanzo, "Adaptive Minimum-BER Linear Multiuser Detection for DS-CDMA Signals in Multipath Channels," *IEEE Transactions on Signal Processing*, vol. 49, no. 6, pp. 1240–1247, June 2001.

[227] A. K. Samingan, S. Chen, and L. Hanzo, "Adaptive Minimum-BER Linear Multiuser Detection for CDMA Signals in Multipath Channels with 4-QAM Constellation," *IEE Electronics Letters*, vol. 37, no. 11, pp. 721–723, 24 May 2001.

[228] S. Chen, B. Mulgrew, and L. Hanzo, "Least Bit Error Rate Adaptive Nonlinear Equalizers for Binary Signalling," *IEE Proceedings Communications*, vol. 150, no. 1, pp. 29–36, February 2003.

[229] D. Gesbert, "Robust Linear MIMO Receivers: A Minimum Error-Rate Approach," *IEEE Transactions on Signal Processing*, vol. 51, no. 11, pp. 2863–2871, November 2003.

[230] D. E. Goldberg, *Genetic Algorithms in Search, Optimization, and Machine Learning.* Reading, Massachusetts: Addison-Wesley, 1989.

[231] J. Holland, *Adaptation in Natural and Artificial Systems.* Ann Arbor, Michigan: University of Michigan Press, 1975.

[232] M. Mitchell, *An Introduction to Genetic Algorithm.* Cambridge, Massachusetts: MIT Press, 1996.

[233] D. Whitley, "A Genetic Algorithm Tutorial," *Statistics and Computing*, vol. 4, pp. 65–85, June 1994.

[234] K. Yen, *Genetic Algorithm Assisted CDMA Multiuser Detection.* PhD thesis, University of Southampton, United Kingdom, Department of Electronics and Computer Science, December 2000.

[235] M. J. Juntti, T. Schlosser, and J. O. Lilleberg, "Genetic Algorithms for Multiuser Detection in Synchronous CDMA," in *Proceedings of IEEE Symposium on Information Theory*, (Ulm, Germany), p. 492, 29 June-4 July 1997.

[236] X. F. Wang, W.-S. Lu, and A. Antoniou, "Genetic-algorithm-based Multiuser Detector for Multiple-access Communications," in *Proceedings of IEEE International Symposium on Circuits and Systems*, vol. 4, (Monterey, CA, USA), pp. 534–537, 31 May-3 June 1998.

[237] C. Ergun and K. Hacioglu, "Multiuser Detection Using a Genetic Algorithm in CDMA Communications Systems," *IEEE Transactions on Communications*, vol. 48, no. 8, pp. 1374–1383, August 2000.

[238] K. Yen and L. Hanzo, "Genetic Algorithm Assisted Joint Multiuser Detection and Fading Channel Estimation for Synchronous CDMA Systems," *IEEE Journal on Selected Areas in Communications*, vol. 19, no. 6, pp. 985–998, June 2001.

[239] S. Abedi and R. Tafazolli, "A New CDMA Multiuser Detection Technique Using an Evolutionary Algorithm," *IEE Proceedings: Communications*, vol. 148, no. 6, pp. 393–399, December 2001.

[240] S. X. Ng, K. Yen, and L. Hanzo, "TTCM Assisted Genetic-algorithm Aided Reduced-Complexity Multiuser Detection," *Electronics Letters*, vol. 38, no. 14, pp. 722–724, 4 July 2002.

[241] C.-T. Chiang and C.-Y. Chang, "An Improved Genetic Algorithm Based on Eugenic Population for Multiuser Detection in DS-CDMA Systems," in *Proceedings of IEEE Region 10 Annual International Conference (TENCON)*, vol. 2, (Beijing, China), pp. 984–987, 28-31 October 2002.

[242] M. G. Shayesteh, M. B. Menhaj, and B. G. Nobary, "A Modified Genetic Algorithm for Multiuser Detection in DS/CDMA," *IEICE Transactions on Communications*, vol. E86-B, no. 8, pp. 2377–2388, August 2003.

[243] K. Yen and L. Hanzo, "Antenna-diversity-assisted Genetic-algorithm-based Multiuser Detection Schemes for Synchronous CDMA Systems," *IEEE Transactions on Communications*, vol. 51, no. 3, pp. 366–370, March 2003.

[244] Y. Du and K. T. Chan, "Feasibility of Applying Genetic Algorithms in Space-time Block Coding Multiuser Detection Systems," in *Proceedings of the IASTED International Conference on Wireless and Optical Communications*, vol. 3, (Banff, Canada), pp. 469–473, 2-4 July 2003.

[245] A. Wolfgang, N. N. Ahmad, S. Chen, and L. Hanzo, "Genetic Algorithm Assisted Minimum Bit Error Rate Beamforming," in *Proceedings of IEEE Vehicular Technology Conference (VTC-Spring)*, (Milan, Italy), pp. CD–ROM, 17-19 May 2004.

[246] J. J. Grefenstette, *Genetic Algorithms for Machine Learning.* Kluwer academic Publishers, 1993.

[247] H. Adeli and S. L. Hung, *Machine Learning: Neural Networks, Genetic Algorithms and Fuzzy Systems.* John Wiley & Sons Inc., 1994.

[248] S. K. Pal and P. P. Wong, *Genetic Algorithms for Pattern Recognition.* CRC Press, 1996.

[249] M. D. Vose, *The Simple Genetic Algorithm: Foundations and Theory (Complex Adaptive Systems).* Cambridge, Massachusetts: MIT Press, 1999.

[250] H. Dawid, *Adaptive Learning by Genetic Algorithms: Analytical Results and Applications to Economic Models (lecture Notes in Economics and Mathematical Systems).* Springer-Verlay Berlin and Heidelberg GmbH & Co. KG, 1996.

[251] M. Gen and R. Cheng, *Genetic Algorithms and Engineering Optimisation (Wiley Series in Engineering Design & Automation)*. John Wiley & Sons Inc., 2000.

[252] T. K. Moon and W. C. Stirling, *Mathematical Methods and Algorithms for Signal Processing*. New Jersey: Prentice-Hall, 2000.

[253] J. T. Alander, "On Optimal Population Size of Genetic Algorithms," in *Proceedings of Computer Systems and Software Engineering (CompEuro '92)*, (The Hague, Netherlands), pp. 65–70, 4-8 May 1992.

[254] G. Syswerda, "Uniform Crossover in Genetic Algorithms," in *Proceedings of the Third International Conference on Genetic Algorithms*, pp. 2–9, 1989.

[255] E. Falkenauer, "The Worth of Uniform," in *Proceedings of the 1999 Congress on Evolutionary Computation (CEC 99)*, vol. 1, (Washington, DC, USA), pp. 776–782, 6-9 July 1999.

[256] J. D. Schaffer, R. A. Caruana, L. J. Eshelman, and R. Das, "A Study of Control Parameters Affecting Online Performance of Genetic Algorithms for Function Optimization," in *Proceedings of the Third International Conference on Genetic Algorithms*, (California, USA), pp. 51–60, 1989.

[257] J. J. Grefenstette, "Optimization of Control Parameters for Genetic Algorithm," *IEEE Transactions on Systems, Man and Cybernetics*, vol. SMC-16, pp. 122–128, January 1986.

[258] T. Bäck, "Optimal Mutation Rates in Genetic Search," in *Proceedings of the Fifth International Conference on Genetic Algorithms*, (California, USA), pp. 2–8, 1993.

[259] T. Bäck, "Self Adaptation in Genetic Algorithms," in *Proceedings of the First European Conference on Artificial Life*, (Massachusetts, USA), pp. 263–271, 1993.

[260] E. Parzen, "On Estimation of a Probability Density Function and Mode," *The Annals of Mathematical Statistics*, vol. 33, pp. 1066–1076, September 1962.

[261] A. K. Samingan, *Minimum Bit Error Rate Multiuser Detection Techniques for DS-CDMA*. PhD thesis, University of Southampton, United Kingdom, School of Electronics and Computer Science, September 2003.

[262] Y. Zeng and T.-S. Ng, "A Semi-blind Channel Estimation Method for Multiuser Multiantenna OFDM Systems," *IEEE Transactions on Signal Processing*, vol. 52, no. 5, pp. 1419–1429, May 2004.

[263] M. C. Reed, C. B. Schlegel, P. D. Alexander, and J. A. Asentorfer, "Iterative Multiuser Detection for CDMA with FEC: Near Single User Performance," *IEEE Transactions on Communications*, vol. 46, no. 12, pp. 1693–1699, December 1999.

[264] M. Y. Alias, F. Guo, S. X. Ng, T. H. Liew, and L. Hanzo, "LDPC and Turbo Coding Assisted Space-time Block Coded OFDM," in *Proceedings of IEEE Vehicular Technology Conference (VTC-Spring)*, vol. 4, (Jeju, Korea), pp. 2309–2313, 22-25 April 2003.

[265] G. D. Golden, G. J. Foschini, R. A. Valenzuela, and P. W. Wolniansky, "Detection Algorithm and Initial Laboratory Results Using the V-BLAST Space-time Communication Architecture," *IEE Electronics Letters*, vol. 35, no. 1, pp. 14–16, 7 January 1999.

[266] Y. Xin and G. B. Giannakis, "High-rate Space-time Layered OFDM," *IEEE Communications Letters*, vol. 6, no. 5, pp. 187–189, May 2002.

[267] N. Boubaker, K. B. Letaief, and R. D. Murch, "A Low Complexity Multicarrier BLAST Architecture for Realizing High Data Rates Over Dispersive Fading Channels," in *Proceedings of IEEE Vehicular Technology Conference (VTC-Spring)*, vol. 2, (Rhodes, Greece), pp. 800–804, 6-9 May 2001.

[268] O. Border, L. Collins, G. Burel, and P. Rostaing, "Digital Transmission Combining BLAST and OFDM Concepts: Experimentation on the UHF COST 207 Channel," in *Proceedings of Global Telecommunications Conference (GLOBECOM)*, vol. 1, (San Antonio, Texas, USA), pp. 141–145, 25-29 November 2001.

[269] D. K. C. So and R. S. Cheng, "Layered Maximum Likelihood Detection for V-BLAST in Frequency Selective Fading Channels," in *Proceedings of IEEE Vehicular Technology Conference (VTC-Spring)*, vol. 1, (Birmingham, Alabama, USA), pp. 135–139, 6-9 May 2002.

[270] L. Wang, Y. Ren, and X. Shan, "Effect of Carrier Frequency Offset on Performance of BLAST-OFDM Systems," *IEE Electronics Letters*, vol. 38, no. 14, pp. 747–748, 4 July 2002.

[271] C. K. Kim, S. Choi, and Y. S. Cho, "Adaptive Beamforming for an OFDM System," in *Proceedings of IEEE Vehicular Technology Conference (VTC-Spring)*, vol. 1, (Houston, Texas, USA), pp. 484–488, 16-20 May 1999.

[272] D. Bartlomé and A. I. Pérez-Neira, "MMSE Techniques for Space Diversity Receivers in OFDM-Based Wireless LANs," *IEEE Journal on Selected Areas in Communications*, vol. 21, no. 2, pp. 151–160, February 2003.

[273] S. Hara, A. Nishikawa, and Y. Hara, "A Novel OFDM Adaptive Antenna Array for Delayed Signal and Doppler-Shifted Signal Suppression," in *Proceedings of IEEE International Conference on Communications (ICC)*, vol. 7, (Helsinki, Finland), pp. 2302–2306, 11-14 June 2001.

Index

Symbols

802.11 6

A

a posteriori 66
a-priori 106
adaptive modulation 29
    constant-throughput 33
    fixed threshold algorithm 30
    subband-BER estimator 32
ADSL 5
amplifier
    back-off 27
    clipping 27
    non-linear 27
AWGN 10

B

BACG 131, 133
backward recursion 49
base-station 57
beamforming 56
branch transition metric 49

C

CDMA 60
channel
    two-path 11
    WATM 12
channel estimation 14
    blind 21
    decision-directed 21
    perfect 16
    pilot symbol assisted 17
closed-form 69
Conjugate Gradient 72
cost function 70
crossover 106
cyclic prefix 9

D

DAB 5
delay spread 9
detector
    MBER 67
    MMSE 63
DFT 4

E

equiprobable 67, 69
Euclidean 60, 62
expectation maximisation 164

F

FFT 5
FIR 11

fitness 106
forward error correction 63
forward recursion 49
forward-error correction 34
frequency selective fading 11

G

GA 103
Gauss-Newton 72
gradient 70, 71

H

HDSL 5
HDTV 5

I

IEEE 6
individuals 105
interpolation
    linear 17
    lowpass 19
ISI 9
iterative 70
iterative receivers 164

K

KDE 131

L

LBER 131
least-square 72
Log Likelihood Ratio 49
log-likelihood ratio 66
Log-MAP 49
Low-density parity-check 36
LST 165

M

MAP decoder 49
MIMO 57
MMAC 6
MSE 66
MUD 60
mutate 103
mutation 106

O

objective function 105

P

PDF 67
population 105
Probability Density Function 67

S

SDMA 56
search methods
    calculus-based 106
    enumerative 107
    random 107
SIR 63
smart antennas 55
SNR 63
soft-bit 66
soft-MUD 164
soft-output 66
space-time block code 38
space-time trellis 56
spatial diversity 56

steepest-descent 70, 72
step-size 70

T

time dispersive 11
trellis transitions 49
Turbo codes 34

V

VDSL 5
vectorial 70

W

WLAN 6

Author Index

A

Aaron [214] 68
Aazhang [218] 68
Abedi [239] 104
Acikel [66] 35, 44
Adachi [125] 52
Adeli [247] 103
Adireddy [158] 53
Agarossi [139] 53
Agrawal [82] 37–39
Ahmad [245] 104, 105, 149
Ahmad [211] 66, 68, 168
Ahn [77] 37
Al-Dhahir [185] 53
Al-Dhahir [83] 37, 39
Al-Dweik [128] 52
Alamouti [81] 37–40
Alander [253] 119
Alexander [263] 164
Alias [2] 2, 68
Alias [1] 2
Alias [264] 164
Alias [3] 2, 104
Anathaswamy [122] 52
ANSI [13] 5
Antoniou [236] 104
Antoniou [209] 66, 68, 131
Armstrong [151] 53
Asentorfer [263] 164

B

Bäck [258] 125
Bäck [259] 125
Bölcskei [38] 7, 57
Bölcskei [178] 53
Bölcskei [110] 52
Banelli [134] 53
Bar-Ness [155] 53
Barbulescu [65] 35, 36
Barhumi [180] 53
Barry [213] 67, 68, 131
Barry [217] 68
Barry [219] 68
Barry [220] 68
Barry [192] 53
Bartlomé [272] 168
Batalama [223] 68, 131
Beaver [136] 53
Benedix [139] 53
Benvenuto [116] 52
Berrou [64] 34, 40
Bhargava [177] 53
Bingham [21] 5, 7
Bitzer [12] 5

Blogh [199] 55, 56, 167
Blum [87] 39
Blum [30] 7, 37, 39
Boche [148] 53
Boche [147] 53
Bogucka [139] 53
Border [268] 167
Borgmann [178] 53
Boss [47] 7
Boubaker [267] 167
Boubaker [34] 7, 167
Budsabathon [193] 53
Burel [268] 167
Bury [44] 7

C

Calderbank [85] 39
Calderbank [84] 39
Calderbank [86] 39
Canpolat [140] 53
Cao [132] 52
Cao [32] 7, 38
Cao [33] 7
Cao [189] 53
Caruana [256] 125
Cavers [51] 17
Chai [131] 52
Chai [157] 53
Chan [196] 53
Chan [244] 104
Chang [241] 104
Chang [124] 52
Chang [114] 52
Chang [10] 4, 5, 7
Chang [8] 4, 5, 7
Chang [61] 34
Chen [227] 68
Chen [208] 66
Chen [245] 104, 105, 149
Chen [59] 34
Chen [126] 52
Chen [212] 67, 68
Chen [224] 68
Chen [169] 53
Chen [2] 2, 68
Chen [1] 2
Chen [3] 2, 104
Chen [225] 68
Chen [226] 67–72
Chen [222] 68
Chen [221] 68, 131
Chen [228] 68, 131, 144
Chen [216] 68
Chen [211] 66, 68, 168
Cheng [35] 7, 29
Cheng [31] 7, 29
Cheng [269] 167
Cheng [32] 7, 38
Cheng [33] 7
Cheng [251] 105
Chengyang [172] 53
Cherriman [162] 53
Chiang [241] 104
Chng [221] 68, 131
Chng [216] 68

Cho [271] 168
Choi [271] 168
Choi [5] .. 3, 4, 7–9, 14, 17, 21, 24, 26, 29, 33, 55, 56, 58, 59, 62, 63, 65, 66, 109, 130, 155, 162
Choi [197] 53
Choi [97] 40
Chong [123] 52
Chuang [28] 7, 34
Ciblat [104] 52
Ciblat [101] 52
Cimini [28] 7, 34
Cimini [27] 7
Cimini [26] 7
Cioffi [14] 5, 7
Cioffi [15] 5, 7
Cioffi [103] 52
Cirpan [93] 39
Collins [268] 167
Costa [145] 53
Courville [173] 53
Courville [127] 52
Courville [142] 53

D

Das [256] 125
Davidson [111] 52
Dawid [250] 105
Declereq [79] 37
Dekorsky [46] 7
Dekorsky [159] 53
Derryberry [202] 56
Diggavi [185] 53
Ding [141] 53
Ding [111] 52
Du [244] 104
Duhamel [173] 53
Duhamel [127] 52
Duhamel [142] 53

E

Ebert [11] 4, 5, 7, 8
Engels [204] 57, 66
Engels [187] 53
Engels [181] 53
Engels [36] 7
Erceg [184] 53
Ergun [237] 104
Eshelman [256] 125
ETSI [17] 5
ETSI [18] 5
ETSI [20] 5, 6
ETSI [16] 5

F

Falkenauer [255] 123
Fan [132] 52
Farhang-Boroujeny [115] 52
Foschini [265] 165
Foschini [200] 55, 57, 165, 167
Frenger [52] 21
Futaki [70] 36, 37
Futaki [72] 37
Futaki [73] 37

G

Gallagher [68] 36

Gelle [79] 37
Gen [251] 105
Georghiades [83] 37, 39
Georghiades [167] 53
Gesbert [229] 68, 131
Gesbert [38] 7, 57
Gharavi-Alkhansari [146] 53
Giannakis [127] 52
Giannakis [142] 53
Giannakis [198] 53
Giannakis [190] 53
Giannakis [156] 53
Giannakis [131] 52
Giannakis [157] 53
Giannakis [137] 53
Giannakis [266] 167
Giannakis [161] 53
Giardina [141] 53
Gibson [91] 39
Gibson [221] 68, 131
Gibson [216] 68
Glavieux [64] 34, 40
Goeckel [122] 52
Goldberg [230] 102–107, 114, 116, 122
Golden [265] 165
Goldfeld [154] 53
Gong [182] 53
Gong [174] 53
Gore [80] 37, 39
Gray [202] 56
Grefenstette [246] 103
Grefenstette [257] 125
Gruenbacher [75] 37
Gruenbacher [74] 37
Guo [99] 51
Guo [264] 164
Gyselinckx [204] 57, 66

H

Höher [98] 50
Hacioglu [237] 104
Hanzo [227] 68
Hanzo [208] 66
Hanzo [245] 104, 105, 149
Hanzo [99] 51
Hanzo [199] 55, 56, 167
Hanzo [58] 30
Hanzo [243] 104
Hanzo [238] 104, 163
Hanzo [67] .. 35, 37, 39, 40, 42–44, 49, 55, 164, 167
Hanzo [207] 60
Hanzo [206] 60, 102, 105
Hanzo [5] 3, 4, 7–9, 14, 17, 21, 24, 26, 29, 33, 55, 56, 58, 59, 62, 63, 65, 66, 109, 130, 155, 162
Hanzo [4] 3, 4, 11, 12, 19, 33, 76
Hanzo [205] 58
Hanzo [2] 2, 68
Hanzo [1] 2
Hanzo [264] 164
Hanzo [3] 2, 104
Hanzo [162] 53
Hanzo [24] 5
Hanzo [225] 68

Hanzo [226] 67–72
Hanzo [228] 68, 131, 144
Hanzo [211] 66, 68, 168
Hanzo [240] 104, 164
Hanzo [89] 39
Hanzo [97] 40
Hanzo [62] 34, 35
Hara [193] 53
Hara [273] 168
Hari [118] 52
Haring [164] 53
Hasegawa [23] 4, 5, 7
Hass [120] 52
He [100] 52
Hiramoto [77] 37
Hirosaki [22] 4, 5, 7
Hirosaki [23] 4, 5, 7
Holland [231] 103–105, 116, 121
Holsinger [7] 4, 5, 7
Honan [105] 52
Hu [100] 52
Huang [195] 53
Huang [191] 53
Hung [247] 103

I

Imai [144] 53
Ingram [192] 53
Ionescu [202] 56

J

Jafarkhani [85] 39
Jafarkhani [84] 39
Jafarkhani [86] 39
Jakes [50] 11, 42
Jang [143] 53
Jiang [63] 34, 35
Jianhua [37] 7
Jones [152] 53
Jr. [110] 52
Juntti [235] 104

K

Kailath [203] 57, 58
Kaiser [120] 52
Kaiser [130] 52
Kammeyer [46] 7
Kammeyer [159] 53
Kammeyer [45] 7
Kammeyer [47] 7
Keasler [12] 5
Keller [5] 3, 4, 7–9, 14, 17, 21, 24, 26, 29, 33, 55, 56, 58, 59, 62, 63, 65, 66, 109, 130, 155, 162
Keller [4] 3, 4, 11, 12, 19, 33, 76
Keller [162] 53
Keller [56] 29
Keller [62] 34, 35
Kenney [141] 53
Khalaj [146] 53
Kim [271] 168
Kim [177] 53
Kim [141] 53
Kim [61] 34
Krongold [152] 53
Kuan [206] 60, 102, 105

Kuehn [159] 53
Kuhn [46] 7
Kung [188] 53

L

Lacaille [117] 52
Lagunas [153] 53
Lamare [210] 66, 68
Laneman [60] 34, 40
Lau [119] 52
LeBlanc [133] 52
Lee [175] 53
Lee [196] 53
Lee [143] 53
Lee [63] 34, 35
Lee [90] 39
Lei [107] 52
Letaief [35] 7, 29
Letaief [31] 7, 29
Letaief [195] 53
Letaief [191] 53
Letaief [32] 7, 38
Letaief [33] 7
Letaief [189] 53
Letaief [267] 167
Letaief [34] 7, 167
Letaief [182] 53
Letaief [174] 53
Leung [71] 36
Leus [109] 52
Leus [180] 53
Li [41] 7, 39, 164
Li [170] 53
Li [192] 53
Li [163] 53
Li [32] 7, 38
Li [33] 7
Li [189] 53
Li [87] 39
Li [30] 7, 37, 39
Li [27] 7
Li [183] 53
Li [88] 39
Li [171] 53
Li [76] 37
Li [26] 7
Li [29] 7
Liang [95] 39
Liew [67] 35, 37, 39, 40, 42–44, 49, 55, 164, 167
Liew [264] 164
Liew [89] 39
Liew [97] 40
Lilleberg [235] 104
Lin [176] 53
Lin [169] 53
Lin [28] 7, 34
Lin [160] 53
Lin [135] 53
Lindner [44] 7
Lindner [43] 7
Liu [203] 57, 58
Liu [191] 53
Liu [78] 37
Liu [198] 53

Liu [179] 53
Liu [105] 52
Lobeira [139] 53
Lopes [220] 68
Lu [165] 53
Lu [40] 7, 164
Lu [42] 7, 37
Lu [41] 7, 39, 164
Lu [236] 104
Lu [209] 66, 68, 131
Luise [108] 52
Luise [54] 24
Luo [111] 52
Lyandres [154] 53

M

Münster [5] .. 3, 4, 7–9, 14, 17, 21, 24, 26, 29, 33, 55, 56, 58, 59, 62, 63, 65, 66, 109, 130, 155, 162
Münster [205] 58
Münster [62] 34, 35
Ma [141] 53
Ma [137] 53
MacKay [69] 36
Magniez [127] 52
Mammela [139] 53
Man [204] 57, 66
Man [187] 53
Man [181] 53
Mandayam [218] 68
Mandyam [202] 56
Mannoni [79] 37
Manton [166] 53
Marselli [108] 52
May [36] 7
McFarland [138] 53
McLaughlin [192] 53
Meng [138] 53
Menhaj [242] 104
Minn [177] 53
Mitchell [232] 103, 104, 117, 118
Mizuki [77] 37
Moon [252] 107
Moon [76] 37
Moonen [109] 52
Moonen [180] 53
Morelli [106] 52
Morgan [141] 53
Mulgrew [212] 67, 68
Mulgrew [224] 68
Mulgrew [225] 68
Mulgrew [226] 67–72
Mulgrew [222] 68
Mulgrew [221] 68, 131
Mulgrew [228] 68, 131, 144
Mulgrew [216] 68
Muller-Weinfurtner [186] 53
Muquet [53] 24
Muquet [173] 53
Muquet [127] 52
Muquet [142] 53
Murch [35] 7, 29
Murch [31] 7, 29
Murch [267] 167
Murch [34] 7, 167

N

Nabar [80] 37, 39
Naguib [82] 37–39
Narasimhan [102] 52
Narayanan [42] 7, 37
Nassar [129] 52
Neal [69] 36
Necker [39] 7, 24
Nee [6] 3, 4, 7
Negi [103] 52
Ng [99] 51
Ng [107] 52
Ng [264] 164
Ng [240] 104, 164
Ng [262] 155, 162
Nilsson [133] 52
Nishikawa [273] 168
Niu [78] 37
Nobary [242] 104

O

Ochiai [149] 53
Ochiai [144] 53
Ohno [156] 53
Ohno [137] 53
Ohtsuki [70] 36, 37
Ohtsuki [72] 37
Ohtsuki [73] 37
Ohtsuki [92] 39
Olfat [179] 53

P

Pérez-Neira [272] 168
Pados [223] 68, 131
Pal [248] 103
Panayirci [93] 39
Panta [151] 53
Park [63] 34, 35
Parzen [260] 131, 138
Pascual-Iserte [153] 53
Paulraj [80] 37, 39
Paulraj [38] 7, 57
Paulraj [178] 53
Paulraj [110] 52
Paulraj [184] 53
Perez-Neira [153] 53
Perre [204] 57, 66
Perre [187] 53
Perre [181] 53
Petermann [47] 7
Petropulu [176] 53
Phoong [160] 53
Phoong [135] 53
Pietrobon [65] 35, 36
Ping [71] 36
Ping [37] 7
Polydros [139] 53
Prasad [6] 3, 4, 7
Prasad [118] 52
Pratt [192] 53
Proakis [49] 10
Proakis [48] 10, 173
Psaromiligkos [223] 68, 131
Pupolin [145] 53

R

R. D. Murch [197] 53
Ragazzi [139] 53
Raghothaman [202] 56
Rappaport [25] 5
Rautio [139] 53
Razzano [139] 53
Reed [263] 164
Reggiannini [108] 52
Reggiannini [54] 24
Ren [270] 167
Ritcey [78] 37
Robertson [98] 50
Rohling [36] 7
Rohling [37] 7
Rostaing [268] 167
Roy [170] 53
Roy [172] 53
Ryan [66] 35, 44

S

Sabato [23] 4, 5, 7
Safar [179] 53
Sai-Weng [119] 52
Salehi [48] 10, 173
Salzberg [9] 4, 5, 7
Samingan [261] .. 131, 132, 138, 142, 144, 154
Samingan [227] 68
Samingan [208] 66
Samingan [2] 2, 68
Samingan [1] 2
Samingan [225] 68
Samingan [226] 67–72
Sampaio-Neto [210] 66, 68
Sampath [184] 53
Sasase [77] 37
Schaffer [256] 125
Schenk [194] 53
Schlegel [263] 164
Schlosser [235] 104
Schmidt [45] 7
Schniter [113] 52
Serener [75] 37
Serener [74] 37
Serpedin [104] 52
Seshadri [82] 37–39
Shamash [215] 68
Shan [270] 167
Sharif [146] 53
Shayesteh [242] 104
Shen [78] 37
Shu [175] 53
Siclet [117] 52
Simone [155] 53
Siohan [117] 52
Sjoberg [133] 52
So [269] 167
Soleymani [96] 39
Sollenberger [183] 53
Sollenberger [88] 39
Sollenberger [26] 7
Sollenberger [29] 7
Song [61] 34
Spagnolini [155] 53

Stüber [39] 7, 24
Stamoulis [185] 53
Steele [24] 5
Steele [55] 29
Stirling [252] 107
Strohmer [136] 53
Stuber [192] 53
Su [124] 52
Su [114] 52
Su [138] 53
Suard [203] 57, 58
Sundberg [59] 34
Sundberg [196] 53
Sundberg [60] 34, 40
Suto [92] 39
Svensson [52] 21
Syswerda [254] 122

T

Tafazolli [239] 104
Talwar [184] 53
Tanik [140] 53
Tarokh [123] 52
Tarokh [82] 37–39
Tarokh [85] 39
Tarokh [84] 39
Tarokh [86] 39
Tellado [184] 53
Tepedelenlioglu [112] 52
Thitimajshima [64] 34, 40
Thoen [187] 53
Thoen [181] 53
Thompson [138] 53
Tjhung [125] 52
Tjhung [100] 52
Tjhung [150] 53
Tomasin [116] 52
Tong [158] 53
Torabi [96] 39
Torrance [58] 30
Torrance [57] 30
Tufts [214] 68
Tureli [105] 52

U

Uysal [83] 37, 39

V

Valenzuela [265] 165
Vandenameele [204] 57, 66
Vandendorpe [101] 52
Venkataramani [123] 52
Villebrun [98] 50
Vinck [164] 53
Viswanathan [158] 53
Vitetta [54] 24
Vogeler [47] 7
Vose [249] 105
Vucetic [94] 39, 40, 165

W

Wang [126] 52
Wang [165] 53
Wang [40] 7, 164
Wang [42] 7, 37
Wang [41] 7, 39, 164
Wang [142] 53

Wang [169] 53
Wang [270] 167
Wang [236] 104
Wang [150] 53
Wang [209] 66, 68, 131
Wang [168] 53
Wang [161] 53
Webb [4] 3, 4, 11, 12, 19, 33, 76
Webb [55] 29
Weifeng [179] 53
Weinstein [11] 4, 5, 7, 8
Whitley [233] 103, 107
Wiegandt [129] 52
Williams [90] 39
Winters [201] 55, 56
Winters [87] 39
Winters [30] 7, 37, 39
Winters [183] 53
Winters [88] 39
Wolfgang [245] 104, 105, 149
Wolniansky [265] 165
Wong [35] 7, 29
Wong [31] 7, 29
Wong [207] 60
Wong [248] 103
Wong [111] 52
Wu [129] 52
Wu [175] 53
Wu [95] 39
Wu [188] 53
Wu [150] 53
Wulich [154] 53
Wunder [148] 53
Wunder [147] 53

X

Xia [190] 53
Xie [167] 53
Xin [198] 53
Xin [266] 167
Xiong [128] 52
Xiong [121] 52
Xu [203] 57, 58

Y

Yan [87] 39
Yan [30] 7, 37, 39
Yang [63] 34, 35
Yang [206] 60, 102, 105
Yao [215] 68
Yeap [67] ... 35, 37, 39, 40, 42–44, 49, 55, 164, 167
Yee [207] 60
Yeh [213] 67, 68, 131
Yeh [217] 68
Yeh [219] 68
Yeh [220] 68
Yen [234] 103, 105
Yen [243] 104
Yen [238] 104, 163
Yen [206] 60, 102, 105
Yen [240] 104, 164
Yoshimochi [77] 37
Yuan [94] 39, 40, 165
Yue [165] 53

Yue [91] 39

Z

Zelst [194] 53
Zeng [262] 155, 162
Zhang [176] 53
Zhang [132] 52
Zhang [100] 52
Zhang [188] 53
Zhao [175] 53
Zheng [163] 53
Zhong [125] 52
Zhou [141] 53
Zhou [190] 53
Zhou [168] 53